



UNIVERSITY OF
CAMBRIDGE

Functional analysis of the F-box protein Fbxl17

Bethany Jane Mason



Clare College

December 2019

This dissertation is submitted for the degree of
Doctor of Philosophy



Declaration

This dissertation is the result of my own work and includes nothing which is the outcome of work done in collaboration except where specified in the text.

It is not substantially the same as any work that has already been submitted before for any degree or other qualification at the University of Cambridge or any other University or similar institution.

This dissertation does not exceed the prescribed word limit of 60,000 words.

Bethany Jane Mason

Abstract

Advances in DNA sequencing technology have allowed detailed characterisation of cancer genomes and has highlighted the contribution of somatic structural variations to the mutational landscape of epithelial tumours. However, our understanding of the functional consequences of such genome rearrangements remains rudimentary. By surveying the METABRIC dataset, consisting of segmented array-CGH copy number data, and paired-end whole-genome DNA and RNA sequencing data from primary breast tumours, we found that the F-box protein encoded by *FBXL17* is frequently rearranged in breast cancer.

F-box proteins are the substrate-recognition components of Skp1-cullin 1-F-box protein (SCF) E3 ligases. As essential components of the ubiquitin proteasome system (UPS) they are responsible for directing target proteins for ubiquitination. Fbxl17 is a relatively understudied member of the FBXL family of F-box proteins and, in breast cancers, is disrupted in the region of the gene that encodes its substrate-binding leucine rich repeat (LRR) domain. Truncating Fbxl17 LRRs impaired its association with the other SCF holoenzyme subunits Skp1, Cul1 and Rbx1, and decreased its ubiquitination activity. Loss of the LRRs also affected Fbxl17 binding to its targets. Thus, genomic rearrangements in *FBXL17* are likely to disrupt SCF^{Fbxl17}-regulated networks in cancer cells.

To investigate the functional effect of these rearrangements, we performed a yeast two-hybrid screen to identify Fbxl17-interacting proteins. Among the 37 binding partners Uap1, an enzyme involved in *O*-GlcNAcylation of proteins was identified most frequently. We demonstrate that Fbxl17 binds to UAP1 directly and inhibits its phosphorylation, which we propose regulates UAP1 activity. Knockdown of Fbxl17 expression elevated *O*-GlcNAcylation in breast cancer cells, arguing for a functional role for Fbxl17 in this metabolic pathway.

To identify further interacting partners of Fbxl17, we performed a mass spectrometry analysis of purified Fbxl17 SCF E3 ubiquitin ligases. Co-immunoprecipitates were enriched for DNA damage/ DNA repair proteins suggesting a novel role for Fbxl17 in the DNA damage response (DDR). We have demonstrated that Fbxl17 is recruited to DNA damage sites rapidly upon double-strand break (DSB) induction and knockdown of Fbxl17 protein expression sensitises cells to the DNA damaging agent Camptothecin. Furthermore, Fbxl17 can ubiquitinate the tandem BRCT domain of the well-known DDR protein 53BP1, which we propose targets 53BP1 for proteasomal degradation.

In conclusion, we have identified two regulatory networks of Fbxl17 which provide an insight into the role of Fbxl17 in breast cancer pathogenesis. These pathways may be amenable to therapeutic targeting in the future for the treatment of breast cancers rearranged in *FBXL17*.

Acknowledgements

Thanks must first go to my supervisor Dr Heike Laman, for her unwavering support and guidance throughout my PhD. You are a true champion of women in science and it has been an absolute joy working in the lab these last four years.

To the past and present members of the Laman lab, thank you for always being on hand to answer questions and offer support when I needed it. It would have been a lonely journey without you all there to make the failed experiments seem that little less disappointing. A special thanks to my colleague and friend Dr Suzie Randle, still offering her support and answering my questions even after leaving the lab for pastures new.

I would like to thank Dr Paul Edwards for his continued encouragement throughout this PhD and for his bioinformatics expertise. Thank you for all your help in extracting the *FBXL17* primary tumour data and of course to Professor Carlos Caldas and his lab for access to the primary tumour data before it has been published. In addition, thank you to Dr Edwards and Dr Susanne Flach for their initial work on Fbxl17 and their contributions to our published manuscript.

Many thanks to Dr Yaron Galanty and the Jackson lab, at the Gurdon Institute, Cambridge, for their help with all things DNA damage. I am hugely grateful for your assistance with experiments and generous donation of reagents. I would also like to acknowledge and thank Dr Robin Antrobus, for performing the mass spectrometry analysis of Fbxl17, Dr Christian Frezza and lab members for their LC-MS expertise and Drs Vincenzo D'Angiolella and Svetlana Khoronenkova for reagents.

To my friends in Cambridge, thank you for four fun-filled years. Adam, you are my still point in an ever-turning world. Thanks for looking after me and always knowing when I need food.

Finally, I would like to thank my amazing parents, you believe in me even when I doubt myself and I hope I have made you both proud.

Not bad for a Yorkshire lass in the South.

Table of Contents

Declaration	1
Abstract	2
Acknowledgements	3
Table of Contents	4
List of Figures.....	8
List of Tables.....	11
Abbreviations	12
CHAPTER 1 - Introduction	16
1.1 Breast Cancer	16
1.1.1 Stratification of breast cancers	16
1.1.2 Genomic rearrangements in breast cancer	17
1.2 The Hexosamine Biosynthetic Pathway.....	20
1.2.1 O-GlcNAcylation in cancer.....	23
1.2.2 Uap1	24
1.2.2.1 Uap1 in cancer.....	26
1.3 DNA double-strand break repair	28
1.3.1 DNA end resection	29
1.3.2 Non-homologous end-joining	32
1.3.3 53BP1.....	33
1.3.4 BRCA1	36
1.3.5 BRCA1 antagonises 53BP1.....	36
1.4 The Ubiquitin Proteasome System (UPS)	40
1.4.1 SCF-type E3 ubiquitin ligases.....	41
1.4.2 F-box proteins	43
1.4.3 F-box proteins in cancer	43
1.4.4 Fbxl17	45
1.4.5 Fbxl17 is recurrently rearranged in breast cancer	48
1.5 Aims of this thesis	50
1.5.1 Investigating the functional consequences of <i>FBXL17</i> rearrangements	50
1.5.2 Identifying and verifying new target substrates of Fbxl17	50
CHAPTER 2- Materials and methods	52

2.1 CELL CULTURE AND ANALYSIS	52
2.1.1 Cell line maintenance	52
2.1.2 Transfection of adherent cells.....	52
2.1.3 Retroviral infection of adherent cells.....	52
2.1.4 Cell fractionation	54
2.1.5 siRNA transfection.....	54
2.1.6 shRNA knockdown of Fbxl17 expression	55
2.1.7 Cell cycle analysis- propidium iodide staining.....	55
2.1.8 Annexin V staining.....	55
2.2 MOLECULAR BIOLOGY METHODS.....	56
2.2.1 Polymerase chain reaction	56
2.2.2 Two-step mutagenesis PCR	57
2.2.3 Agarose gel electrophoresis	58
2.2.4 Cloning.....	58
2.2.4.1 Plasmids.....	58
2.2.4.2 Gel purification of DNA fragments.....	58
2.2.4.3 Restriction enzyme digests of DNA	58
2.2.4.4 Ligation	61
2.2.4.5 Transformation of bacteria with plasmid DNA	61
2.2.4.6 Preparation of plasmid DNA	61
2.3 BIOCHEMISTRY.....	62
2.3.1 Protein extraction and quantification	62
2.3.2 Western blotting	62
2.3.2.1 Gradient gels	63
2.3.3 GST protein purification	63
2.3.4 GST pull-down assay.....	63
2.3.5 Co-Immunoprecipitation	64
2.3.6 E3 ligase production	65
2.3.7 <i>In vitro</i> ubiquitination assay	65
2.3.8 <i>In vivo</i> ubiquitination assay.....	65
2.3.9 Metabolites extraction and LC-MS analysis	66
2.4 MICROSCOPY	67

2.4.1 Immunofluorescence.....	67
2.4.2 Laser micro-irradiation	67
2.6 ANTIBODIES	68
2.7 SOLUTIONS.....	70
CHAPTER 3 - Characterising breast cancer-associated rearrangements of <i>FBXL17</i>	73
3. INTRODUCTION.....	73
3. RESULTS	75
3.1 Fbxl17 is rearranged in primary breast tumours	75
3.2 WT and mutant Fbxl17 expression and localisation	79
3.2.1 Truncation of Fbxl17 LRRs enhances protein expression	79
3.2.2 Deletion of the F-box domain of Fbxl17 abolishes Skp1 binding.....	80
3.2.3 Fbxl17 mutant constructs show wild-type localisation	81
3.3 WT and mutant SCF ^{Fbxl17} purification and characterisation.....	83
3.3.1 Deletion of LRRs impairs SCF subunit recruitment	83
3.3.2 Auto-ubiquitination assays.....	86
3.3.3 Ubiquitination of the Fbxl17 target substrate Sufu	88
3.4 Fbxl17 protein structure prediction	89
3.4.1 The N-terminus of Fbxl17 is highly disordered	89
3.4.2 The LRRs of Fbxl17 are highly structured helical repeats	89
3.4.3 Loss of LRRs changes the predicted 3D structure of Fbxl17	90
3. DISCUSSION	96
CHAPTER 4- Fbxl17 as a regulator of the Hexosamine Biosynthetic Pathway	100
4. Introduction	100
4. Results.....	102
4.1 Fbxl17 interacts with Uap1 in human cells in vivo.....	102
4.2 Fbxl17 binds Uap1 directly via its LRRs	103
4.3 Overexpression of Fbxl17 does not increase Uap1 turnover.....	105
4.4 Fbxl17 does not ubiquitinate Uap1 <i>in vitro</i>	106
4.5 Fbxl17 inhibits the phosphorylation of Uap1.....	107
4.6 Fbxl17 knockdown inhibits UDP-GlcNAc production.....	110
4.7 Fbxl17 knockdown results in increased levels of O-GlcNAcylation.	112
4.8 Fbxl17 knockdown results in decreased OGA expression.....	114

4. Discussion	115
CHAPTER 5 - Role of Fbx17 in DNA damage repair	120
5. Introduction	120
5. Results.....	122
5.1 Identifying Fbx17 interacting partners by mass spectrometry	122
5.1.1 Mass spectrometry analysis with DAVID	124
5.1.2 Co-immunoprecipitates of SCF ^{Fbx17} ligases are enriched for DNA damage/repair proteins	126
5.2 Fbx17 knockdown results in a decrease in cell colony size.....	131
5.3 Cell cycle analysis	133
5.4 Loss of Fbx17 sensitises cells to Camptothecin treatment	136
5.5 Fbx17 is recruited to DNA damage sites	139
5.6 Fbx17 overexpression decreases 53BP1 expression	142
5.7 Fbx17 ubiquitinates the BRCT domain of 53BP1.....	143
5.8 Loss of Fbx17 LRRs abolishes ubiquitination of 53BP1	148
5.9 Fbx17 interacts with DNA damage response proteins.....	149
5. Discussion	151
CHAPTER 6 - General Discussion	156
REFERENCES	161
APPENDIX A	176
APPENDIX B	180

List of Figures

CHAPTER 1 - Introduction

Figure 1. 1 - Types of genomic arrangements that can occur in DNA.	18
Figure 1. 2 - Hexosamine Biosynthetic Pathway.	21
Figure 1. 3 - High Uap1 expression levels correlate with reduced breast cancer survival	27
Figure 1. 4 - Bidirectional DNA end resection	29
Figure 1. 5 - Non-homologous end joining and homologous recombination.....	31
Figure 1. 6 - Schematic of wild-type 53BP1.....	34
Figure 1. 7 - Antagonistic relationship between 53BP1 and BRCA1	38
Figure 1. 8 - Schematic showing the SCF complex and ubiquitination of target proteins.	42
Figure 1. 9 - Schematic of an E3 SCF ligase complex with wild-type Fbx17.	46
Figure 1. 10 - SCF ^{Fbx17} -ubiquitination of Sufu regulates Hedgehog signalling and medulloblastoma	47

CHAPTER 2 - Materials and Methods

Figure 2. 1 - Two-step mutagenesis PCR strategy	57
---	----

CHAPTER 3 - Characterising the breast cancer-associated rearrangements in *FBXL17*

Figure 3. 1 - FBXL17 is rearranged in primary breast tumours.	76
Figure 3. 2 - FBXL17 is rearranged in primary breast tumours and mutations cluster in the LRRs of Fbx17.	77
Figure 3. 3 - Schematic of wild-type Fbx17 domains and mutant constructs.....	79
Figure 3. 4 - Expression of Fbx17 constructs and Δ Fbox Co-IP with Skp1.....	80
Figure 3. 5 - Cellular fractionation of endogenous Fbx17 and Fbx17 constructs.	81
Figure 3. 6 - Subcellular localisation of Fbx17 and Fbx17 constructs.	82
Figure 3. 7 - Co-immunoprecipitation of Fbx17 wild-type and mutant constructs with SCF ligase components.	83
Figure 3. 8 - Loss of Fbx17 LRRs impairs SCF subunit recruitment.....	85
Figure 3. 9 - E2 ligase activity screen for Fbx17.	86
Figure 3. 10 - Loss of Fbx17 LRRs impairs SCF ^{Fbx17} auto-ubiquitination activity.....	87
Figure 3. 11 - Loss of Fbx17 LRRs impairs ubiquitination of the Fbx17 substrate Sufu.	88
Figure 3. 12 - Fbx17 secondary structure predictions.....	92

Figure 3. 13 - 3D structure predictions for Fbxl17 using Robetta protein structure prediction service.....	93
Figure 3. 14 - 3D structure predictions for Fbxl17 Δ 3LRR using Robetta protein structure prediction service.	94
Figure 3. 15 - 3D structure predictions for Fbxl17 Δ 10LRR using Robetta protein structure prediction service.	95

CHAPTER 4 - Fbxl17 as a regulator of the Hexosamine biosynthetic pathway

Figure 4. 1 - Downstream steps of the Hexosamine Biosynthetic pathway	101
Figure 4. 2 - Deletion of ten LRRs ablates binding of Fbxl17 to Uap1.....	102
Figure 4. 3 - Fbxl17 binds Uap1 directly.	103
Figure 4. 4 - Fbxl17 does not target Uap1 for proteasomal degradation.	105
Figure 4. 5 - Fbxl17 does not ubiquitinate Uap1 in vitro.	106
Figure 4. 6 - Fbxl17 does not target Uap1 for ubiquitination.	107
Figure 4. 7 - Fbxl17 inhibits the phosphorylation of Uap1.....	108
Figure 4. 8 - Uap1 steady state levels are not altered following Fbxl17 knockdown	110
Figure 4. 9 - Knockdown of Fbxl17 inhibits UDP-GlcNAc production.	111
Figure 4. 10 - Knockdown of Fbxl17 increases global O-GlcNAcylation.....	112
Figure 4. 11 - Knockdown of Fbxl17 increases O-GlcNAcylation in breast cancer cells.....	113
Figure 4. 12 - Knockdown of Fbxl17 results in decreased OGA expression and activity	114
Figure 4. 13 - Model of interaction between Fbxl17 and Uap1.	116

CHAPTER 5 - Role of Fbxl17 in DNA damage repair

Figure 5. 1 - Total spectrum count of SCF subunits and published Fbxl17 substrates	122
Figure 5. 2 - Functional Annotation Clustering Chart.....	125
Figure 5. 3 - KEGG Pathway functional annotation chart	126
Figure 5. 4 - Fbxl17 co-immunoprecipitates are enriched for DNA damage/repair proteins	127
Figure 5. 5 - Total spectrum counts of DNA damage/repair proteins	128
Figure 5. 6 - STRING analysis of DNA damage/ repair proteins identified by DAVID	130
Figure 5. 7 - Fbxl17 knockdown does not affect clonogenic ability of U2OS cells.....	132
Figure 5. 8 - shRNA knockdown of Fbxl17 expression in MCF7 cells	133
Figure 5. 9 - Cell cycle analysis of Fbxl17 knockdown cells in response to IR.....	135

Figure 5. 10 - Knockdown of Fbxl17 protects cells from Camptothecin-induced apoptosis..	137
Figure 5. 11 - Fbxl17 knockdown sensitises cells to low concentrations of Camptothecin...	138
Figure 5. 12 - Fbxl17-Venus is not recruited to laser-induced DNA breaks.	139
Figure 5. 13 - Localisation of N-terminally GFP-tagged Fbxl17.	140
Figure 5. 14 - Fbxl17 is recruited to DNA damage sites	141
Figure 5. 15 - Fbxl17 overexpression decreases 53BP1 steady state levels.	142
Figure 5. 16 - Schematic of 53BP1 domains and truncated constructs.	144
Figure 5. 17 - WT Fbxl17 ubiquitinates the BRCT domain of 53BP1	145
Figure 5. 18 - Endogenous Fbxl17 co-immunoprecipitates with HA-53BP1 BRCT.....	146
Figure 5. 19 - WT Fbxl17 ubiquitinates the BRCT domain of 53BP1.	147
Figure 5. 20 - Loss of Fbxl17 LRRs impairs ubiquitination of 53BP1_BRCT.....	148
Figure 5. 21 - Co-immunoprecipitation of Fbxl17 with DDR proteins.....	150
Figure 5. 22 - Proposed model of interaction between Fbxl17 and 53BP1	154

CHAPTER 6 - General Discussion

Figure 6. 1 - Mutational patterns of the FBPs Fbxl17, Fbxw7 and Skp2	157
--	-----

List of Tables

Table 1 - Cell lines and culture conditions.	53
Table 2 - shRNA design – 21-mer shRNA sequences targeting FBXL17	55
Table 3 - Standard PCR Reaction volumes and concentrations	56
Table 4 - Standard PCR Cycling conditions	56
Table 5 - Two-step PCR cycling conditions	57
Table 6 - PCR primers for cloning and sequencing.....	59
Table 7 - Plasmids used in this dissertation	60
Table 8 - Primary antibodies used for immunoblotting.....	68
Table 9 - Secondary antibodies and normal IgG used for immunoblotting/ IP	69
Table 10 - Antibodies used for immunohistochemistry	69

Abbreviations

Δ3LRR	3 leucine-rich repeats deletion	DAPI	4', 6-diamidino-2-phenylindole
Δ10LRR	10 leucine-rich repeats deletion	DAVID	The Database for Annotation, Visualisation and Integrated Discovery
ΔF-box	F-box deletion	DDR	DNA damage response
53BP1	p53-binding protein 1	DMEM	Dulbecco's Modified Eagle Medium
aa	Amino acids	DMSO	Dimethyl sulfoxide
aCGH	Array comparative genomic hybridisation	dNTP	Deoxyribonucleotide triphosphate
AR	Androgen receptor	DNA	Deoxyribonucleic acid
ATCC	American Type Culture Collection	DSB	DNA double-strand break
ATM	Ataxia telangiectasia mutated protein kinase	ECL	Enhanced Chemiluminescence
bp	Base pairs	<i>E.coli</i>	<i>Escherichia coli</i>
BRCA	Breast Cancer susceptibility protein	EDTA	Ethylenediaminetetraacetic acid
BrdU	5-bromo-2'-deoxyuridine	ER	Oestrogen receptor
BSA	Bovine serum albumin	FACS	Fluorescence activated cell sorter
CNA	Copy number aberration	FBD	F-box domain
CNV	Copy number variant	FBP	F-box protein
CO₂	Carbon dioxide	FBS	Foetal bovine serum
CPT	Camptothecin	Fbxl17	F-box and leucine-rich repeat protein 17
CRL	Cullin-RING E3 ligase	GAPDH	Glyceraldehyde 3-phosphate dehydrogenase
CtIP	C-terminal binding protein interacting protein		
Cul1	Cullin 1		

GFAT	Glutamine fructose-6-phosphate amidotransferase	LPS	Lipopolysaccharide
GFP	Green fluorescent protein	LRR	Leucine-rich repeat
GlcNAc	N-acetylglucosamine	M	Molar
h	Hours	METABRIC	Molecular Taxonomy of Breast Cancer International Consortium
HBP	Hexosamine biosynthetic pathway	MG132	Carbobenzoxy-Leu-Leu- leucinal
HCC	Hepatocellular carcinoma	MgCl₂	Magnesium Chloride
HEK	Human embryonic kidney	min	Minutes
HER2	Human epidermal growth factor receptor 2	μl	Microlitre
HEPES	4-(2-hydroxyethyl)-1- piperazineethanesulfonic acid	ml	Millilitre
His	Histidine	mM	Millimolar
HR	Homologous recombination	NaCl	Sodium Chloride
IntClust	Integrative cluster	NaF	Sodium Fluoride
IP	Immunoprecipitation	Na₃VO₄	Sodium orthovanadate
IR	Ionising radiation	NEM	N-ethylmaleimide
IRES	Internal ribosomal entry site	NHEJ	Non-homologous end- joining
IVT	<i>in vitro</i> translation	NLS	Nuclear localisation signal
kb	Kilo base	OGA	O-GlcNAcase
kDa	Kilo Dalton	O-GlcNAc	O-linked N- acetylglucosamine
L	Litre	OGT	O-GlcNAc-transferase
LB	Lysogeny broth	PBS	Phosphate buffered saline
LC/MS	Liquid chromatography- mass spectrometry	PBS-T	Phosphate buffered saline with Tween-20
		PCR	Polymerase chain reaction
		PI	Propidium iodide

PMSF	Phenylmethanesulfonyl fluoride	siRNA	Short interfering ribonucleic acid
Polybrene	1,5-dimethyl-1,5-diazaundecamethylene polymethobromide	Skp1	S-phase kinase-associated protein 1
PR	Progesterone receptor	SNP	Single nucleotide polymorphism
P/S	Penicillin Streptomycin	ssDNA	single-stranded DNA
PugNAc	O-(2-Acetamido-2-deoxy-D-glucopyranosylidene) amino N-Phenylcarbamate	Sufu	Suppressor of fused
PVDF	Polyvinylidene fluoride	SV	Structural variation
RFP	Red fluorescent protein	TAE	Tris/Acetate/EDTA
ROS	Reactive oxygen species	Taq	<i>Thermus aquaticus</i>
RNA	Ribonucleic acid	TBS	Tris buffered saline
rpm	Revolutions per minute	TBS-T	Tris buffered saline with Tween-20
RPMI	Roswell Park Memorial Institute medium	TCGA	The Cancer Genome Atlas
RRM2	Ribonucleotide reductase subunit M2	Uap1	UDP-N-acetylglucosamine pyrophosphorylase
RT	Room temperature	Ub	Ubiquitin
s	Seconds	UDP-GlcNAc	Uridine diphosphate N-acetylglucosamine
SCF	Skp1/Cullin/F-box E3 Ubiquitin ligase complex	UPS	Ubiquitin proteasome system
SDS	Sodium dodecyl sulphate	UV	Ultraviolet
SDS-PAGE	Sodium dodecyl sulphate polyacrylamide gel electrophoresis	V	Volt
shRNA	Short hairpin ribonucleic acid	WT	Wild-type
		Y2H	Yeast two-hybrid

1 | INTRODUCTION

CHAPTER 1 - Introduction

1.1 Breast Cancer

Cancer is by definition a group of over 100 genetic diseases, characterised by uncontrolled proliferation of cells [1]. Cancer cells accumulate genetic changes over time through a multistep process. Hanahan and Weinberg initially described six key processes that cells must possess to become malignant: resisting cell death, sustaining proliferative signalling, evading growth suppressors, activating invasion and metastasis, enabling replicative immortality and inducing angiogenesis [2]. The hallmarks were updated in 2011 to include deregulating cellular energetics and avoiding immune destruction, which are involved in the pathogenesis of some if not all cancers. Aside from these hallmarks, Hanahan and Weinberg also described two enabling characteristics that underpin neoplasia: tumour-promoting inflammation and genomic instability and mutation [3].

Epithelial cancers represent 80-90% of all cancers diagnosed and of these breast cancers are among the most prevalent. In 2018 breast cancer was the second most common cancer diagnosed worldwide with an estimated 2.1 million new cases [4]. It remains the most common cancer in women and in the UK alone accounted for 31% of all female cancer cases in 2016 [5] and 7% of all cancer deaths from 2015-2017, despite significant improvements in survival over the last 25 years [6]. Breast cancer as with most other cancers is complex and its aetiology is still relatively unknown. The complexity of the disease is largely due to the heterogeneity exhibited by breast tumours [7]. Subpopulations of cells exist in tumours that can differ dramatically in both genotype and phenotype from their surrounding cells [8]. Breast cancers can therefore exhibit very distinct histopathological and biological features, which also differ in their response to therapeutic strategies. This makes diagnosis, classification and ultimately treatment of breast cancer very complicated and is one of the greatest challenges facing clinicians and researchers in this field.

1.1.1 Stratification of breast cancers

Classification of invasive breast cancer subtypes involves the assessment of immunohistochemical markers, namely the expression of hormone receptors (oestrogen (ER) and progesterone (PR)) and the overexpression and/or amplification of the human epidermal growth factor receptor 2 (HER2). This initial sub-classification alone has led to improved patient outcomes with the introduction of targeted therapies e.g. Tamoxifen for

hormone-receptor-positive cancers [9] and the HER2 targeted therapy Trastuzumab [10]. Increasingly, genomically-guided approaches are being used to stratify breast cancers even further [11]. In 2000, Perou et al. systematically investigated the gene expression patterns of human breast tumours and identified five subgroups into which breast cancers could be separated: luminal A, luminal B, HER2 overexpressing, basal-like and normal breast tissue-like, based on 496 genes [12]. This intrinsic classification was refined to just 50 genes and used to generate the PAM50 assay (Prosigna), which maps a tumour sample to one of the five groups through microarray and quantitative reverse transcriptase PCR techniques [13].

However, the true scale of genomic changes in breast cancers is not fully captured by histopathological or transcriptomic approaches. Previous technical limitations meant that genome-sequencing of cancers favoured the discovery of point mutations over genome rearrangement events, mainly due to the ease of analysis by PCR and array comparative genomic hybridisation (aCGH) [14]. Advances in sequencing technology however, have enabled analysis of tumour genomes at a much greater depth than was previously possible [15-17]. Whilst once believed to be confined largely to leukaemias and sarcomas, somatic rearrangements are now being shown to be prevalent in breast cancer and other epithelial cancers [18-21].

1.1.2 Genomic rearrangements in breast cancer

Genomic rearrangements are described as gross changes to DNA that can result in duplications, inversions, deletions or translocations (Figure 1. 1) [14]. These rearrangements affect whole chromosomes or parts of chromosomes and are often found recurring across tumour types [22]. This suggests they may have a significant role in tumour biology and cancer progression.

Breast cancers are well known for acquiring multiple genomic rearrangements during their development [23] as shown by karyotyping [24, 25]. Studying the spectrum of copy number alterations in breast cancer using aCGH has already proven to be useful for characterising breast cancers and identifying new subtypes [26]. To further understand the complex landscapes of rearrangements in breast cancer, Stephens et al. analysed 24 breast cancer genomes by paired-end sequencing [19]. Intrachromosomal rearrangements were much more prevalent than interchromosomal rearrangements and of these, tandem duplications were most commonly observed. Most striking perhaps was the large variation in

rearrangement frequency between genomes, with some harbouring almost no duplications and others containing hundreds. This could in part be attributed to breast cancer subtype, as cancers that were ER negative had comparatively more tandem duplications than ER positive subtypes. It was also shown that 50% of rearrangements fell within protein coding regions, compared to the 40% that would be predicted by chance. This apparent enrichment may be due to selection of rearrangements that are advantageous to the breast cancer cells.

Further analyses have also utilised next-generation sequencing to identify novel cancer genes that are recurrently mutated in breast cancer [27, 28]. The limitation of most of these early studies was the relatively modest numbers of samples analysed, making it difficult to

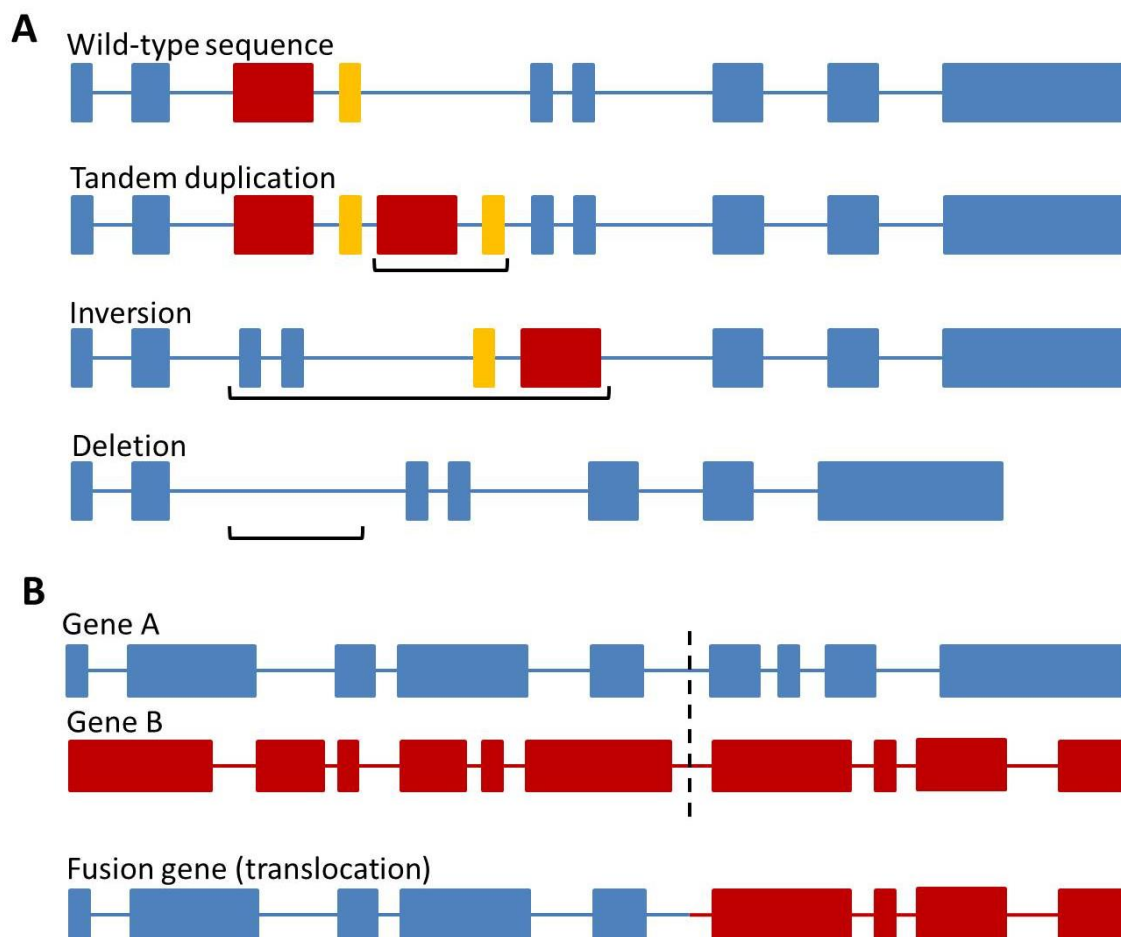


Figure 1.1 - Types of genomic arrangements that can occur in DNA.

(A) Genomic rearrangements can include tandem duplications, inversions and deletions, shown here for two exons (red and yellow boxes) in a single gene. Brackets indicate the region of rearrangement.

(B) Larger scale rearrangements can result in the fusion of two different genes (Gene A: blue, Gene B: red). This results in a fusion gene that can have different activity and function within the cell. Figure adapted from [21].

integrate this data with the histopathological and expression-based classifiers. To overcome this the METABRIC (Molecular Taxonomy of Breast Cancer International Consortium) dataset characterised the genomic and transcriptomic profiles of a discovery set of 997 primary breast tumours and a validation set of 995 tumours [29]. Analysis of inherited genomic variants; single nucleotide polymorphisms (SNPs) and copy number variants (CNVs), along with somatic genomic changes; copy number aberrations (CNAs), were found to be associated with alterations in gene expression. Clustering of the copy number and gene expression data revealed ten novel molecular subgroups of breast cancer. Each integrative cluster (IntClust 1-10) presented with distinct CNAs and clinical features that shed light on the potential molecular drivers and pathways underlying certain breast cancer subgroups [30]. The five distinct groups classified by PAM50 fall into several integrative clusters, for example IntClust 1 is predominantly luminal B tumours whereas IntClust 2 includes both luminal A and luminal B tumours. The IntClusters are characterised by distinct mutational landscapes which can stratify the five PAM50 classes even further.

The disruptive nature of genomic rearrangements, the frequency at which they occur and the variability between breast cancer subtypes has increased our understanding of how genomic rearrangements contribute to the aetiology of breast cancer and helped us better understand breast cancer heterogeneity. However, despite validating numerous novel rearrangements, determining if rearrangements are in fact true ‘driver’ mutations that are advantageous to cancer cells and are therefore positively selected, or simply passenger mutations acquired along the way, can be challenging [31-33]. A few common, large-scale rearrangements across cancer types have been known for some time, such as loss of the distal arm of 8p [34], 17p [35, 36] and 18q [37] and the amplification of ERBB2 in breast cancer [38], but many less frequently occurring aberrations remain to be characterised and may be diagnostically or therapeutically important. For example, the EML4-ALK fusion occurs in only approximately 5% of non-small cell lung cancer (NSCLC) but is a target for therapy [39, 40] and interest in therapeutically targeting Neuregulin-1 (NRG1) gene fusions is increasing, despite only occurring in 0.2% of a wide range of carcinomas [41]. Characterising genes that are recurrently disrupted in breast cancer is therefore biologically and therapeutically important.

1.2 The Hexosamine Biosynthetic Pathway

As discussed previously, cancer genotypes were originally described as the manifestation of six essential biological capabilities or 'hallmarks' acquired and exhibited by cells [2]. After over a decade of research, reprogramming of energy metabolism was highlighted as an additional hallmark of cancer [3]. The uncontrolled cell proliferation characteristic of neoplastic disease cannot be achieved without a compensatory change in the cellular energetics of a cell. Under normal aerobic conditions, cells primarily produce energy via mitochondrial oxidative phosphorylation (OXPHOS). In anaerobic conditions, cells instead catabolise glucose via the less efficient and oxygen-independent pathway glycolysis [42]. Cancer cells and other highly proliferative cells can utilise glycolysis even in the presence of oxygen (aerobic glycolysis), a phenomenon known as the Warburg effect [43-46]. To overcome the lower efficiency of glycolysis, cancer cells upregulate glucose transporters such as GLUT1 to significantly increase the flux of glucose into the cytoplasm [47, 48]. However, it is not just glycolysis and OXPHOS that utilise glucose. Glycolytic intermediates feed into various biosynthetic pathways and as such any changes in glucose flux are also likely to impact these pathways [49]. The Hexosamine Biosynthetic pathway (HBP), which utilises the glycolysis intermediate Fructose-6-phosphate (F6P), represents one such pathway (Figure 1. 2).

The HBP utilises glucose, glutamine, fatty acids and amino acids to produce the amino sugar uridine diphosphate N-acetylglucosamine (UDP-GlcNAc), which serves as the basis for glycosaminoglycans, proteoglycans and glycolipids. Of the glucose that enters a non-cancer cell, 2-5% is used by the HBP [50]. The HBP and glycolysis share the first two metabolic steps, whereby glucose is first phosphorylated by hexokinase (HK) to Glucose-6-phosphate and then converted to Fructose-6-phosphate (F6P) by phosphoglucose isomerase (GPI). It is here that the two pathways diverge, and glutamine fructose-6-phosphate amidotransferase (GFAT) converts F6P and glutamine, to glucosamine-6-phosphate and glutamate, to drive the HBP. GFAT activity is considered rate-limiting for the HBP [50, 51]. Glucosamine entering the cell can also be directly converted to glucosamine-6-phosphate by GNK (GlcNAc kinase) and feed into the HBP without the need for glycolysis or the rate-limiting GFAT. Glucosamine-6-phosphate and acetyl-coenzyme A (Ac-CoA); derived from free fatty acid oxidation, are then catalysed by glucosamine-phosphate N-acetyltransferase (GNPNAT) to generate N-

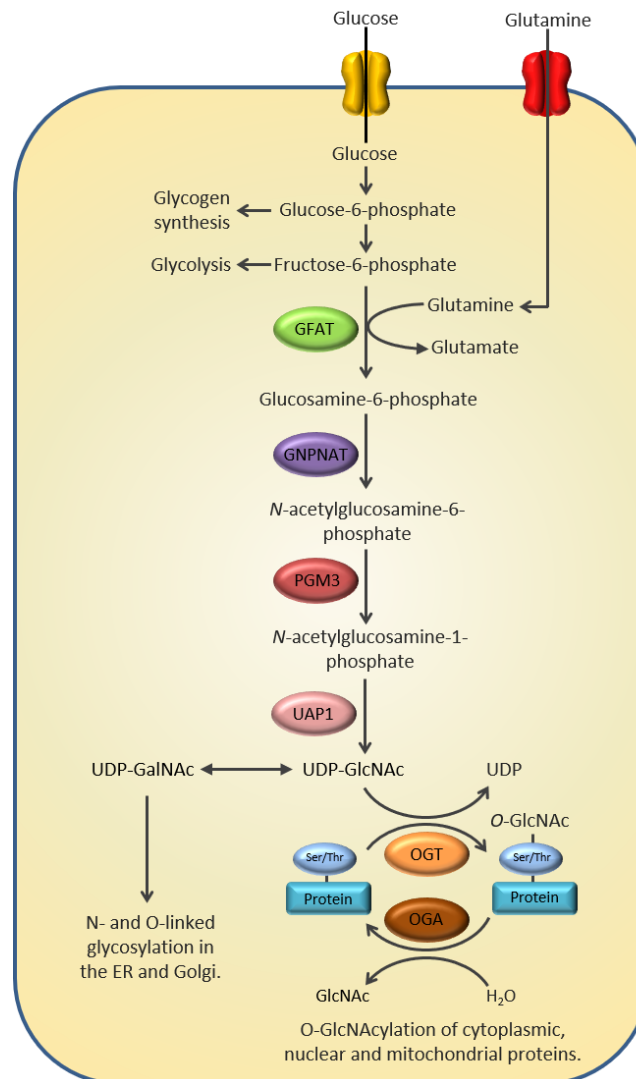


Figure 1. 2 - Hexosamine Biosynthetic Pathway.

Glucose enters the cells and is converted to Fructose-6-phosphate, after which 2-5% is directed to the Hexosamine Biosynthetic Pathway (HBP). The enzyme GFAT (glutamine fructose-6-phosphate amidotransferase) catalyses the first and rate-limiting step in the HBP, converting Fructose-6-phosphate and glutamine to Glucosamine-6-phosphate. Glucosamine entering the cell can also be directly converted to glucosamine-6-phosphate by GNK (GlcNAc kinase) and feed into the HBP. Glucosamine-6-phosphate and acetyl-coenzyme A (Ac-CoA) are then catalysed by glucosamine-phosphate N-acetyltransferase (GNPNAT) to generate N-acetylglucosamine-6-phosphate (GlcNAc-6-P). GlcNAc phosphomutase (PGM3)-mediated isomerisation produces GlcNAc-1-phosphate (GlcNAc-1-P) which along with uridine (UTP) is then rapidly converted to UDP-GlcNAc by the enzyme UDP-N-acetylglucosamine pyrophosphorylase 1 (Uap1). UDP-GlcNAc can then be used for N- and O-linked glycosylation in the ER and Golgi or for the O-GlcNAcylation of nuclear and cytoplasmic proteins. OGT (O-GlcNAc transferase) and OGA (O-GlcNAcase) catalyse the addition and removal of O-GlcNAc respectively. Figure adapted from [76].

acetylglucosamine-6-phosphate (GlcNAc-6-P). GlcNAc phosphomutase (PGM3)-mediated isomerisation produces GlcNAc-1-phosphate (GlcNAc-1-P), which along with uridine (UTP); produced during nucleotide metabolism, is then rapidly converted to UDP-GlcNAc by the enzyme UDP-N-acetylglucosamine pyrophosphorylase 1 (UAP1) [52-58] (Figure 1. 2). Since the HBP utilises nutrient-derived precursors e.g. carbohydrates, lipids and amino acids to produce UDP-GlcNAc, it is considered a nutrient sensor pathway [53, 59]. Levels of UDP-GlcNAc are therefore sensitive to the nutritional state of the cell. UDP-GlcNAc produced by the HBP has two fates, (1) *O*- and *N*-linked glycosylation of proteins in the endoplasmic reticulum (ER) and Golgi apparatus or (2) *O*-GlcNAcylation that takes place in the cytoplasm, nucleus and mitochondria.

N-linked glycosylation is the attachment of complex oligosaccharides or 'glycans' to an asparagine residue of target proteins and takes place in the ER. This type of glycosylation requires the synthesis of a precursor oligosaccharide which can be found attached to the membrane of the ER. Once formed, the precursor oligosaccharide is transferred to a nascent polypeptide in the lumen of the ER [60]. Once proteins have been folded, they can also be modified in the Golgi apparatus by the addition of *O*-linked *N*-acetylgalactosamine (*O*-GalNAc) to a serine or threonine residue. *O*-GalNAc sugars are common on membrane glycoproteins such as low-density lipoprotein receptor (LDL) and as such usually occur on proteins that will be secreted [61].

O-GlcNAcylation is the attachment of *O*-linked *N*-acetylglucosamine (*O*-GlcNAc) moieties to serine and threonine residues of nuclear and cytoplasmic proteins. *O*-GlcNAcylation of proteins is important in several cellular processes including cell signalling, gene regulation and metabolism [62-65] and in many respects is analogous to phosphorylation. It has been shown that *O*-GlcNAcylation and phosphorylation can compete for the same residues on proteins highlighting a complex cross-talk between these two modifications [66]. *O*-GlcNAcylation is a dynamic post-translational modification, which unlike *O*-glycosylation in the Golgi, can be added or removed from a protein several times. The addition and removal of *O*-GlcNAc is catalysed solely by *O*-GlcNAc-transferase (OGT) and *O*-GlcNAcase (OGA) respectively [55]. It has been proposed that there is an optimal level of global *O*-GlcNAcylation levels for cells to function and this is maintained by mutual regulation and balance of OGT and OGA expression and activity [59, 67]. Knockout of OGT expression

results in a rapid decrease in OGA protein expression in murine embryonic fibroblasts [68]. In hepatocytes, OGA overexpression triggers an increase in OGT mRNA levels [69] further highlighting the mutual regulation of these proteins.

O-GlcNAcylation is an important post translational modification on many intracellular proteins—including p53, RNA polymerase II, the polycomb complex and Phosphofructokinase 1 (Pfk1), the main regulator of glycolysis- and is essential for viability of several mammalian cell types [64, 70]. It is therefore unsurprising that disruption of *O*-GlcNAc homeostasis has been implicated in many human diseases including diabetes, neurodegeneration and cancer [71-75].

1.2.1 *O*-GlcNAcylation in cancer

There is already considerable evidence that GlcNAcylation is altered in cancer [76]. Increased protein *O*-GlcNAcylation and changes in OGT and/or OGA expression have been reported in different cancer types. Caldwell et al. found that breast cancer cells had increased *O*-GlcNAcylation and elevated OGT [77]. Knocking down OGT inhibited tumour growth, decreased cell cycle progression, increased expression of the cell cycle inhibitor p27Kip1, and decreased invasiveness [77]. High nuclear and cytoplasmic *O*-GlcNAc was also observed in breast cancer patients with increased relapse rates, increased sites of distant metastases and poor outcome [78]. Dahl et al. found that *MGEA5* expression, the gene encoding for OGA, was reduced by 56% in breast tumours [79]. In agreement with this, it was found that breast tumour tissues exhibit increased global *O*-GlcNAcylation and low OGA levels are linked to higher grade tumours and metastasis [80]. Treatment of breast cancer cells with PI3K or mTOR inhibitors reduced OGT expression and *O*-GlcNAcylation highlighting a role for the PI3K/mTOR/MYC signalling pathway in OGT elevation [81]. *O*-GlcNAcylation has also been shown to regulate cancer cell metabolic reprogramming by stabilising the transcription factor HIF-1 α , which upregulates GLUT1 therefore protecting cancer cells from metabolic stress [82].

In liver cancer, hepatocellular carcinoma (HCC) cells exhibit increased global *O*-GlcNAcylation levels, which is important for migration, invasion and viability [83]. Low OGA expression in HCC correlated with tumour recurrence suggesting it may be a useful marker to predict patient risk of recurrence [83]. Similarly, in prostate cancer, OGT is overexpressed and both OGT and *O*-GlcNAcylation are elevated in prostate carcinoma cell lines [84]. OGT can

regulate the stability of c-Myc, which modulates prostate cancer growth [85, 86]. Mi et al. have shown that human lung and colon cancer tissues show significantly elevated O-GlcNAcylation and OGT expression compared to adjacent tissues and this enhances growth and invasion [87].

1.2.2 Uap1

In contrast to OGT and OGA, upstream enzymes of the HBP, in particular Uap1, have received less attention with regards to their role in cancer pathogenesis. UDP-N-acetylglucosamine pyrophosphorylase 1 (Uap1) is the enzyme responsible for converting GlcNAc-1-P and UTP into UDP-GlcNAc. UDP-GlcNAc is an essential metabolite, which acts as the major cytoplasmic precursor of cell wall peptidoglycan in both Gram-positive and Gram-negative bacteria and is a precursor for the synthesis of lipid A required for lipopolysaccharide (LPS), the major component of the Gram-negative bacteria outer membrane [88]. UDP-GlcNAc is also a substrate of chitin synthase, whose product is essential for fungal cell wall formation [88]. Extensive studies of UDP-GlcNAc in bacteria identified the bifunctional GlcNAc-1-P uridyltransferase (also called UDP-GlcNAc pyrophosphorylase) GlmU as the enzyme responsible for UDP-GlcNAc production [89].

Discovery of the eukaryotic gene for UDP-GlcNAc pyrophosphorylase came from comparisons between the amino acid sequences of *E. coli* GlmU and *S. cerevisiae* UDP-Glc pyrophosphorylase (one of three enzymes in *S. cerevisiae* with UDP-sugar pyrophosphorylase activity but not responsible for UDP-GlcNAc formation). An amino acid motif, L(X)₂GXGTXM(X)₄PK where X represents any amino acid, was identified and used to search the yeast database for genes that could encode proteins with a sequence similar to the motif. YDL103C was one of two candidates that came out of the screen and thus was tested for UDP-GlcNAc pyrophosphorylase activity. Recombinant YDL103C fused to GST was expressed in *E. coli* and incubated with GlcNAc-1-P and UTP. YDL103C was able to produce UDP-GlcNAc *in vitro* in a dose-dependent manner and as such the gene was designated *ScUAP1* (*S. cerevisiae* UDP-GlcNAc pyrophosphorylase gene 1) [90].

ScUAP1 DNA was then used as a probe to identify the human homolog of *ScUAP1* by screening a human testis cDNA library. The resulting *HsUAP1* was cloned and sequenced and was shown to possess UDP-GlcNAc pyrophosphorylase activity *in vitro*. A null mutation in *ScUAP1* is lethal but can be rescued by overexpression of the human Uap1 enzyme, further

highlighting its evolutionary conservation [90]. Interestingly the cloned *HsUAP1* was identical to the previously reported *AGX1*, an antigen implicated in antibody-mediated human infertility [91]. Szumilo et al. successfully purified UDP-GlcNAc pyrophosphorylase from the soluble fraction of pig liver extracts and showed that the enzyme could synthesise UDP-GlcNAc [56]. They isolated three peptides of 64, 57 and 49kDa by SDS-PAGE, which all showed strong cross-reactivity with an antibody prepared against the 64kDa protein. It was therefore proposed that UDP-GlcNAc pyrophosphorylase functions as a homodimer of two 64kDa subunits [56]. Concurrent with Mio et al. the isolated peptides were later shown to be 100% identical to *AGX1* [57].

A second isoform of *AGX1* exists, *AGX2*, that is identical in sequence to *AGX1* except for an additional 17-amino acid insert near the carboxyl terminus. Wang-Gillam et al. therefore investigated whether *AGX2* also has pyrophosphorylase activity and showed that *AGX1* and *AGX2* differ in their preference for substrates. *AGX2* activity was around 8 times higher with GlcNAc-1-P than GalNAc-1-P highlighting a preference for UDP-GlcNAc pyrophosphorylase activity, whereas *AGX1* exhibited higher activity with GalNAc-1-P [57, 92]. *AGX1* and *AGX2* result from alternative splicing of *HsUAP1* and their expression varies across tissue types. *AGX1* is highly expressed in the testis and hence *HsUap1* is also alternatively named sperm-associated antigen 2 (*SPAG2*) [93] whereas *AGX2* is more abundant in somatic tissues [91].

The crystal structures of human *Uap1* isoforms *AGX1* and *AGX2* have been solved and revealed a dimeric arrangement for both proteins as predicted by Szumilo et al., however *AGX2* dimers were not observed in solution [94]. The 17 amino acid insert in *AGX2* appears to dictate oligomeric assembly, which can modify the active site of the protein and influence enzymatic activity. However, both isoforms could bind to UDP-GlcNAc and UDP-GalNAc and showed no significant change in substrate specificity contrary to previous studies in *AGX* proteins isolated from pigs [57, 94].

In summary, *Uap1* is the human UDP-GlcNAc pyrophosphorylase responsible for the production of the HBP end-product UDP-GlcNAc. Two isoforms of *Uap1*, *AGX1* and *AGX2* have been identified, which show variable expression in tissues and may differ in their preference for GlcNAc-1-P or GalNAc-1-P. *AGX2* seems to be the likely isoform driving UDP-GlcNAc production in mammalian cells.

1.2.2.1 Uap1 in cancer

There is increasing evidence that Uap1 is also implicated in the pathogenesis of cancer, namely prostate cancer [58, 95]. Itkonen et al. showed that Uap1 and the HBP rate-limiting enzyme GFAT are upregulated in localised prostate cancer and this upregulation is androgen receptor (AR) driven. Uap1 mRNA and protein levels were upregulated in AR-overexpressing prostate cancer cell lines LNCaP and VCaP whereas normal prostate epithelial cells RWPE-1, expressing wild-type AR, showed no changes in Uap1 expression after treatment with synthetic androgen [85].

Further research by Itkonen et al. went on to show that cell lines with high UAP1 expression have 10-fold higher UDP-GlcNAc and UDP-GalNAc levels. Inhibition of Uap1 by siRNA resulted in a significant decrease in UDP-GlcNAc levels but did not affect total *O*-GlcNAcylation levels. Uap1 overexpression was shown to protect cells against inhibitors of *N*-linked glycosylation. Knockdown of Uap1 in LNCaP cells sensitised cells to inhibitors of *N*-linked glycosylation and decreased their colony-forming ability. However, overexpression of Uap1 in RWPE-1 cells alone, was not sufficient to protect cells from inhibitors of *N*-linked glycosylation suggesting the combined overexpression of GFAT is also required [58].

Changes in Uap1 expression associated with prostate cancer have the potential to be used as predictive biomarkers for prostate cancer diagnosis. Gene expression levels of Uap1 in plasma and urine samples from 319 patients recommended for prostate biopsies were measured by qRT-PCR. Uap1 mRNA levels in plasma were significantly different in prostate cancer patients than post-prostatectomy control patients and urine Uap1 mRNA levels were statistically significant between cancer and non-cancer patient samples after normalisation to GAPDH [96].

One potential explanation for the overexpression of Uap1 in prostate cancer is the downregulation of microRNA (miR)-224-5p. *In silico* analysis revealed that miR-224-5p is downregulated in prostate adenocarcinoma and the prospective targets of miR-224-5p, which include Uap1, are highly expressed as a result. However further *in vivo* or *in vitro* experiments are required to confirm these findings [97].

Aside from prostate cancer, GISTIC (Genomic Identification of Significant Targets in Cancer) analysis [98] of Liposarcoma patient samples, identified a statistically significant

amplification of chromosome 1 in the region encoding Uap1 [99]. This suggests that Uap1 overexpression may also be involved in Liposarcoma pathogenesis.

In breast cancer, reduction of UDP-GlcNAc production through inhibition of PGM3, the enzyme acting just upstream of Uap1 causes breast cancer growth arrest and apoptosis [100]. Uap1 may therefore also represent a viable biological target for the treatment of breast cancer given it acts in the same pathway as PGM3. Whilst no such data implicating Uap1 directly in breast cancer pathogenesis currently exists, Kaplan Meier analysis of Uap1 using the KM Plotter (<http://www.kmplot.com>)[101] revealed that breast tumours with high Uap1 expression were associated with poorer survival in patients (Figure 1. 3).

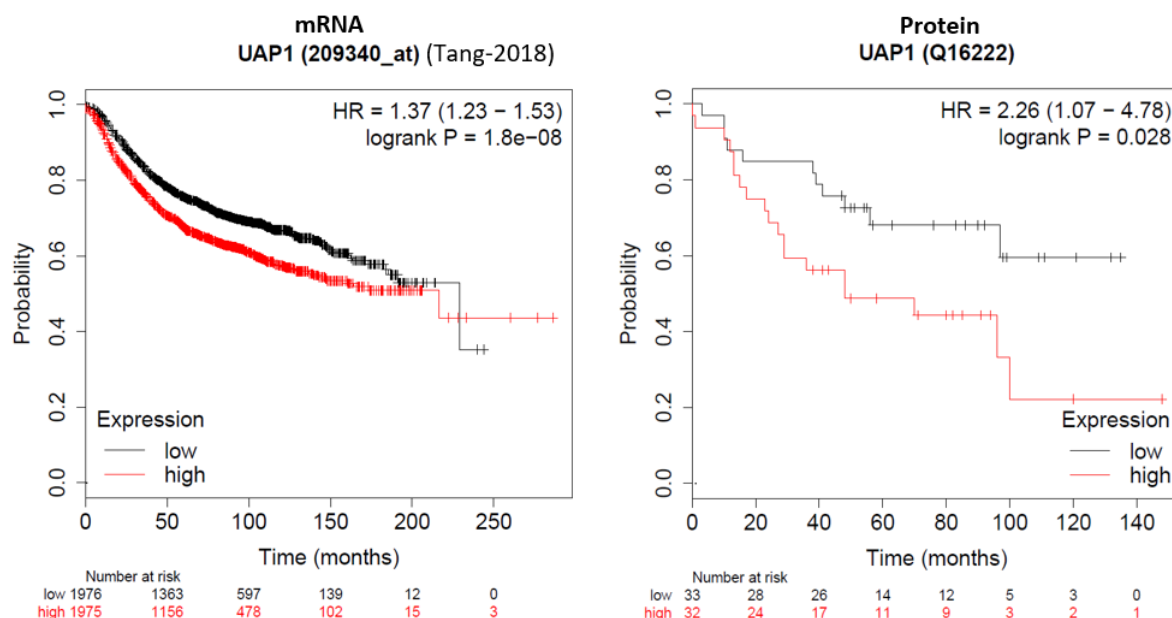


Figure 1. 3 - High Uap1 expression levels correlate with reduced breast cancer survival

Kaplan Meier curves for Uap1 mRNA (left panel) and protein (right panel) expression were generated using the KM Plotter analysis platform (<http://kmplot.com>) resource. Publicly available breast cancer tumour datasets were mined for Uap1 expression data in correlation with survival probabilities, JetSet best probe set selected for mRNA data analysis.

1.3 DNA double-strand break repair

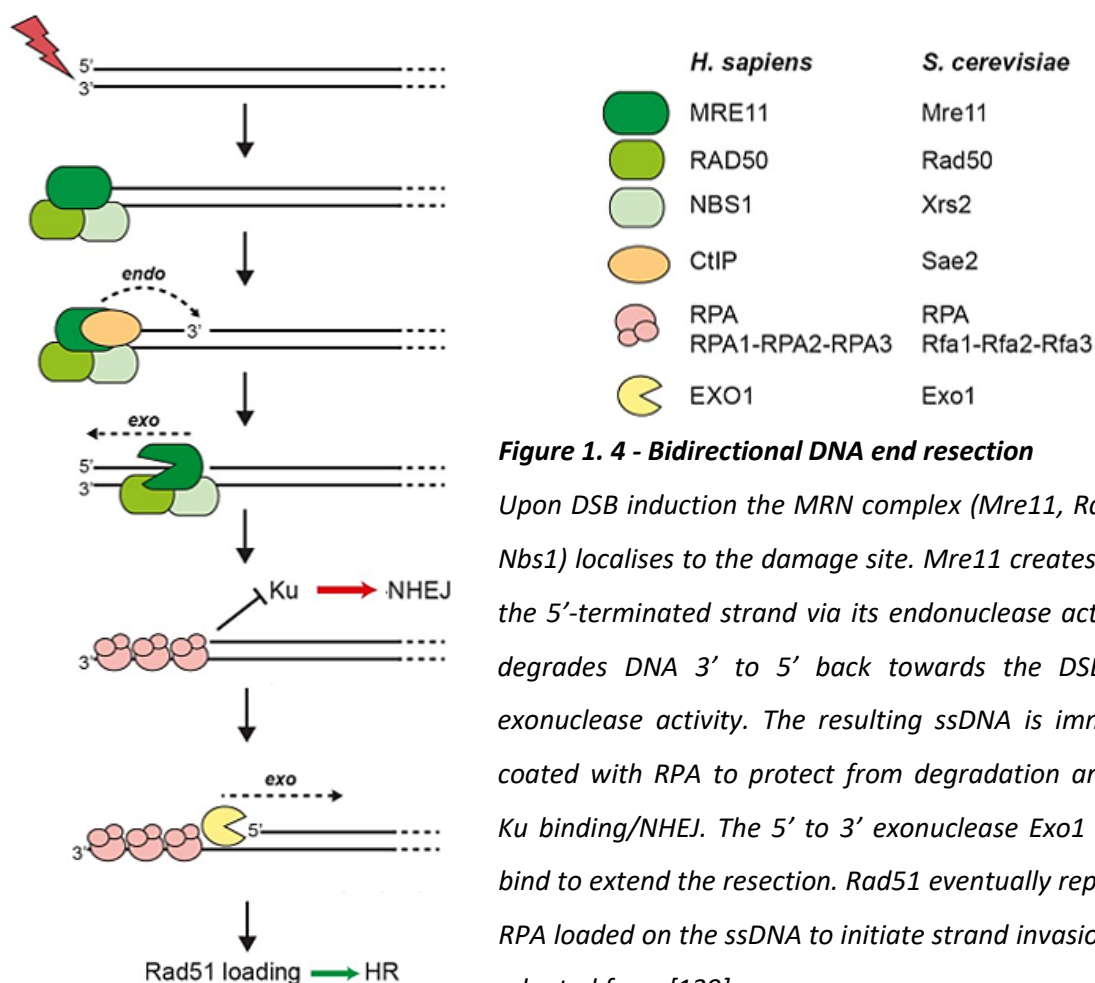
The DNA in our cells continually suffers damage from environmental and endogenous stimuli, including reactive oxygen species (ROS) and ionising radiation (IR) [102-104]. Such insults generate a variety of DNA lesions including DNA double-strand breaks (DSBs), whereby the sugar-phosphate backbones of both DNA strands are broken [105]. DSBs are among the most harmful lesions and failure to accurately repair just one of these breaks can trigger permanent growth arrest and cell death and induce gross chromosomal rearrangements [106]. DNA damage events have the potential to be highly mutagenic and can promote tumorigenesis [106]. Indeed, genomic instability is considered an enabling characteristic of cancer cells [3]. To cope with the continuous threat to genome integrity posed by DSBs, eukaryotic cells have evolved a complex DNA damage response (DDR), which coordinates several DNA repair pathways with cell-cycle checkpoint activation. The two major and most studied DNA damage repair pathways, homologous recombination (HR) and non-homologous end-joining (NHEJ), are largely distinct from one another [107]. HR uses an identical sister chromatid as a template ensuring accurate repair. The requirement of a sister chromatid restricts HR to phases S and G2 of the cell cycle [108]. Both HR and NHEJ are highly conserved pathways but the relative contribution to DNA repair differs from organism to organism [109]. Simple eukaryotes such as the yeasts *S. cerevisiae* and *S. pombe* rely mainly on HR to repair radiation-induced DSBs [110, 111]. In contrast, NHEJ is the favoured pathway for DSB repair in mammals [112, 113] with HR preferred for the repair of DSBs that arise during replication. NHEJ does not require a template but instead directly ligates broken DNA ends together. It is faster but potentially more mutagenic than HR and its activity is controlled throughout the cell cycle [114-119].

Choosing which repair pathway to adopt is vitally important to maintain genetic stability [120-122]. A number of factors are believed to influence the selection of repair pathway including direct competition for DSB ends. HR is the pathway of choice during S and G2 phases of the cell cycle. However, the canonical NHEJ factor DNA-dependent protein kinase (DNA-PK) consisting of the Ku70/80 (XRCC6/XRCC5) heterodimer (Ku) and the DNA-PK catalytic subunit (DNA-PKcs) can localise quickly and independently to DSBs during S phase and bind with high affinity to prevent HR and promote NHEJ. In this regard competition for binding to DSB ends is unlikely to dictate repair pathway choice, especially during S phase.

More sophisticated mechanisms must exist to drive DNA repair pathway choice. Indeed, CYREN (cell cycle regulator of NHEJ) has been shown to bind ku heterodimers to prevent NHEJ during S and G2 [119]. However, initial processing of the DNA ends at a DSB is considered the key process that stands at the crossroads between HR and NHEJ [107, 123].

1.3.1 DNA end resection

End resection is essential for HR-driven DSB repair and is considered the point at which cells are committed to repair by HR or not at all [123, 124]. DNA end resection only happens in phases S and G2 of the cell cycle where it can inhibit NHEJ and promote HR [125]. This is consistent with the fact that HR requires sister chromatids for accurate repair, which are also only present in S and G2 phase. During other cell cycle phases DNA end resection is actively inhibited or blocked by Ku heterodimers therefore only NHEJ can be initiated [126]. End resection catalyses the nucleolytic degradation of broken DNA ends in the 5' to 3' direction. This results in 3' single-stranded DNA (ssDNA) which provides a platform for the recruitment of proteins required for HR repair (Figure 1. 4).



End resection is initiated by the nuclease Mre11, the core component of the MRN complex [128]. The MRN complex, which comprises Mre11, Rad50 and nibrin (Nbs1), senses DSBs and binds DNA through its globular domain [127]. Mre11 exhibits a 3' to 5' exonuclease activity on dsDNA but 5' to 3' exonuclease activity is required for the generation of 3' overhangs. This necessitates the recruitment of an additional protein with 5' to 3' exonuclease activity, Exo1. Experiments in yeast and later in human fibroblasts identified a two-step bidirectional model for end resection, whereby the MRN complex rapidly localises to DSBs during S and G2 phases of the cell cycle (Figure 1. 4). Mre11, which possesses ssDNA endonuclease activity, generates a ssDNA nick in the 5'-terminated strand upstream from the DSB and degrades DNA in a 3' to 5' direction back towards the DSB via its exonuclease activity [129-131]. The resulting ssDNA is immediately coated by RPA to prevent degradation and becomes the preferred binding site for the 5' to 3' exonuclease Exo1, which can extend the resection to generate long 3' ssDNA tails [132, 133] (Figure 1. 4). The MRN complex can bind to DSBs even in the presence of Ku heterodimers but Ku removal is essential for Exo1 exonuclease activity to proceed [134]. Various potential Ku removal mechanisms have been proposed including ubiquitination of Ku by the E3 ubiquitin ligase RNF138 [135], phosphorylation of Ku70 [136] and CtIP (C-terminal binding protein (CtBP) interacting protein) endonuclease activity [137].

CtIP was first identified as a cofactor for the transcriptional repressor CtBP, but is now better known as an interacting partner of the MRN complex [138]. CtIP stimulates the endonuclease activity of Mre11 and is recruited to the MRN complex following cyclin-dependent kinase (CDK) dependent phosphorylation after which it binds to the MRN subunit Nbs1 via its FHA/BRCT domains [139]. CtIP itself possesses 5' flap endonuclease activity, which is required for the repair of more complex DNA lesions created by topoisomerase poisons or IR [140, 141]. The endonuclease activity of CtIP requires further phosphorylation of CtIP by ataxia telangiectasia mutated (ATM) protein kinase and is considered the crucial step for end resection initiation. Chanut et al. showed that the endonuclease activity of CtIP is also important for Ku removal at DSBs. CtIP depletion from human U2OS cells strongly impaired DNA resection and resulted in an accumulation of Ku foci following DNA damage. ATM-mediated phosphorylation of CtIP was required to inhibit Ku accumulation [137]. CtIP depletion can also impair cell survival when DSBs are generated in S phase but causes only weak hypersensitivity at other cell cycle stages highlighting its role in HR [142].

The final steps of HR sees breast cancer susceptibility gene 2 (BRCA2) mediate assembly of a Rad51 filament, which replaces RPA on ssDNA to initiate homology search and strand invasion (Figure 1. 5) [143, 144]. Rad51 binds to ssDNA in a ternary complex with ATP, binding to ATP but not ATP hydrolysis is required for stable Rad51-DNA binding. The transient interaction or ‘invasion’ of the Rad51 nucleoprotein filament with the template dsDNA leads to displacement of one of the template strands, and the presynaptic Rad51

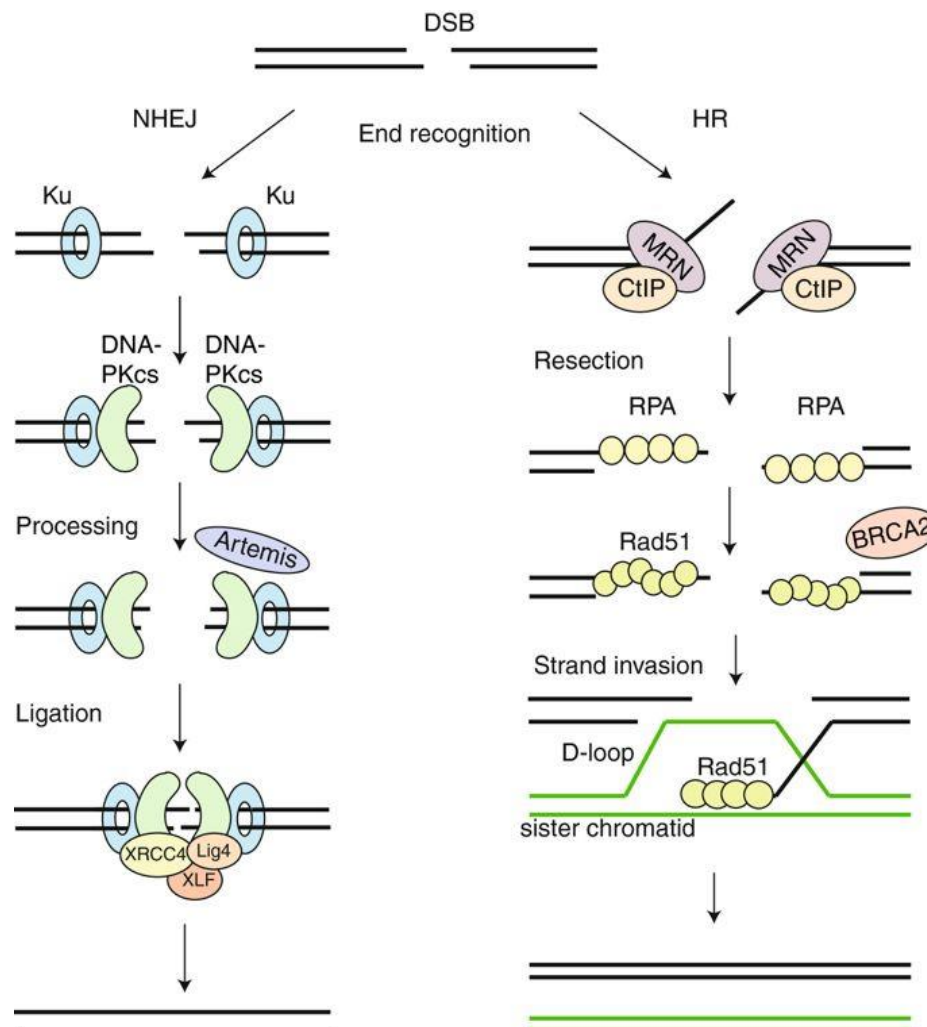


Figure 1. 5 - Non-homologous end joining and homologous recombination

NHEJ starts with recognition of DSB ends by the Ku70/80 heterodimer which recruits DNA-PKcs. If the ends are incompatible nucleases such as Artemis trim the ends and the XRCC4-DNA Ligase IV-XLF ligation complex seals the break. HR repair involves DNA end resection by the MRN-CtIP complex to generate single stranded DNA (ssDNA). At this point the break can only be repaired by HR. The ssDNA is coated by RPA and subsequently replaced by Rad51 aided by BRCA2. Rad51 nucleoprotein filaments mediate strand invasion of the homologous template forming a displacement loop (D-loop) for repair. Figure taken from [122].

filament binds its complementary sequence to form a displacement loop (D-loop). Rad51 is removed from the ssDNA strands by Rad54 to allow DNA synthesis by DNA polymerases δ (Pol δ) or DNA polymerase ϵ (Pol ϵ) [145, 146]. As a result, the initial DSB is repaired accurately ensuring no loss of genetic instability (Figure 1. 5).

1.3.2 Non-homologous end-joining

Outside S and G2 phases of the cell cycle, homology-directed repair is simply not feasible in a eukaryotic cell. DNA is condensed into highly-ordered chromatin structures, and thus homology searching, and strand invasion are extremely difficult. NHEJ becomes the markedly preferred DNA repair pathway of choice in this instance. DNA ends at break points are bound by Ku heterodimers in a sequence-independent manner. Ku has a toroidal, ring-shaped structure, and broken DNA ends can thread through the hole at the centre of Ku as though the eye of a needle [147]. Ku is considered the first protein to bind DSB breaks due to its high abundance in cells and strong binding affinity for duplex DNA ends. It does so at all cell cycle stages [114], where it acts as a scaffold to recruit the NHEJ machinery (Figure 1. 5). Recruitment is not in a step-wise manner but rather a dynamic assembly that can occur in any order. The phosphatidylinositol-3 kinase-like kinase family member DNA-PKcs is recruited rapidly to DSBs and results in translocation of Ku inwards on the dsDNA to allow DNA-PKcs direct access to the DSB end which activates DNA-PKcs kinase activity. If the DSB ends are incompatible, the NHEJ machinery can trim or fill in the DNA ends, as required. Artemis is the best established NHEJ nuclease and is regulated by DNA-PKcs. The Artemis/DNA-PKcs complex has a diverse range of nuclease activities and can endonucleolytically cut a variety of damaged DNA overhangs [117]. The DNA polymerases mu (Pol μ) and lambda (Pol λ) are both able to bind to Ku:DNA complexes to conduct template-independent synthesis of DNA at DSB ends [114]. These polymerases have no proofreading capability and so are error-prone. Once the required DNA end processing is complete the final step of NHEJ is the ligation of the broken DNA ends (Figure 1. 5). The DNA ligation complex consists of DNA Ligase IV and its co-factor, X-ray repair cross-complementing protein 4 (XRCC4). XRCC4 stimulates DNA Ligase IV activity by stabilising it and promoting its adenylation [117]. XLF also forms part of the ligation complex and facilitates the ligation of mismatched or non-cohesive ends by DNA Ligase IV. XRCC4 appears

to have functions independent of the terminal ligation step highlighting the versatility of the NHEJ pathway [114].

1.3.3 53BP1

Ku removal from DSB ends is essential for HR to progress, and CtIP-mediated DNA end resection is considered the key step after which cells are committed to DNA repair by HR. However, the post-translational regulation of CtIP is not the only control mechanism dictating repair pathway choice. During the non-replicative phases of the cell cycle i.e. M and G1, DNA end resectioning is actively inhibited, suppressing HR and promoting DNA repair by NHEJ. The tumour suppressor p53-binding protein 1 (53BP1) was identified as a key protein involved in the inhibition of end resectioning and therefore a key promotor of NHEJ in G1.

53BP1, as the name suggests, was first identified as a binding partner of the well-known tumour suppressor protein p53 [148] and can stimulate p53-mediated transcriptional activation [149, 150]. It is however, the p53-independent roles of 53BP1 that have received most attention, in particular the role of 53BP1 in the DDR. Schultz et al. showed that 53BP1 localised to distinct nuclear foci following treatment of cells with agents that specifically induce DSBs, suggesting a role for 53BP1 in DNA repair [151]. Further fluorescence microscopy experiments showed 53BP1 is recruited to DSBs at all stages of the cell cycle [152, 153]. The recruitment of 53BP1 to DSBs is well understood and requires the ubiquitination of histone 2A (H2A). ATM is recruited to the DSB by the MRN complex, and a signalling cascade is initiated by ATM-mediated phosphorylation of H2A variant H2AX (γ H2AX). Mediator of DNA damage checkpoint protein 1 (MDC1) binds to the modified histone (γ H2AX) and is subsequently phosphorylated by ATM. Phosphorylated MDC1 recruits the E3 ubiquitin ligase RNF8, which adds K63-linked ubiquitin chains to histone H1 (Ub-H1). This recruits a second E3 ligase, RNF168, that binds Ub-H1 with high affinity. RNF168 ubiquitinates H2A at lysine 13 or 15 (H2AK13Ub or H2AK15Ub), which leads to the stable recruitment of 53BP1 via its ubiquitylation-dependent recruitment (UDR) motif (Figure 1. 6). RNF168 can also recognise its own histone mark leading to an amplification of the Ub signal and therefore increased 53BP1 recruitment.

The ability of 53BP1 to recognise mono-methylated and di-methylated histone H4 (H4K20me2) is also vital, but not sufficient for 53BP1 recruitment to DSB sites. The tandem Tudor motif of 53BP1 binds to H4K20me1 and H4K20me2 (Figure 1. 6), but H3K20me2 is an

abundant histone mark, present in 80% of all nucleosomes and so the modification must be regulated to be selective for DNA damage sites [154]. In the absence of damage, H4K20me2 is masked by the binding of chromatin compaction factor L3MBTL1 and lysine demethylase JMJD2A to the modified histone mark. After DSB initiation, the E3 ubiquitin ligases RNF8 and RNF168 ubiquitinate L3MBTL1 and JMJD2A, which are evicted by the ATPase VCP or targeted for proteasomal degradation, respectively [155]. 53BP1 will only bind to nucleosomes that are both ubiquitinated at H2AK13/15 and methylated at H4K20.

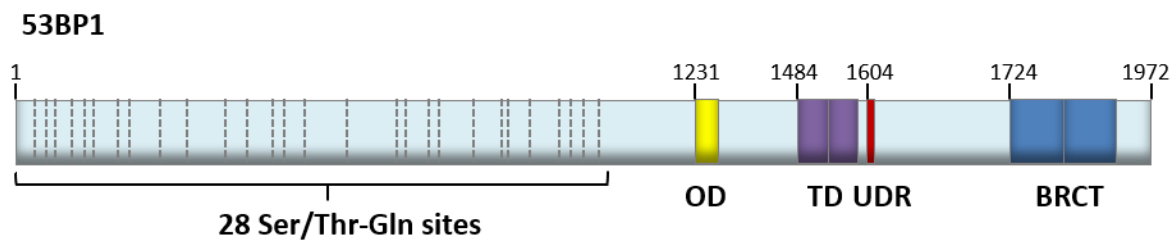


Figure 1. 6 - Schematic of wild-type 53BP1

p53 binding protein 1 (53BP1) contains 28 N-terminal Ser/Thr-Gln sites at which it can be phosphorylated by ataxia-telangiectasia mutase (ATM) kinase. ATM-mediated phosphorylation promotes the binding of Rif1 (Rap1-interacting factor 1) and PTIP (PAX transactivation activation domain-interacting protein). 53BP1 also contains an oligomerisation domain (OD), a tandem Tudor motif (TD) that binds to demethylated Lys20 of Histone 4 (H4K20me2) and a ubiquitylation-dependent recruitment (UDR) motif that interacts with H2AK15Ub. The C-terminus of 53BP1 contains tandem BRCT domains that bind most notably to p53.

53BP1 has no intrinsic enzymatic activity but rather acts to recruit other effector proteins, namely Rif1 and PTIP, which mediate inhibition of DNA end resection during the G1 stage of the cell cycle. Rif1 was first identified in yeast as an interacting partner of Rap1 and promotes telomere length homeostasis [156]. In vertebrates however, Rif1 does not accumulate at functional telomeres but instead shows a pattern of telomere association typical of DNA-damage response factors. Rif1 accumulates at damaged chromatin in a 53BP1- and ATM-dependent manner with depletion of either protein leading to loss of Rif1 foci in cells after DSB induction [157]. Rif1 is recruited to damaged chromatin by the N-terminal domain of 53BP1 which contains multiple ATM-phosphorylated Ser/Thr-Gln sites (Figure 1. 6) [158]. Mutation of all 28 of these phosphorylation sites (53BP1^{28A}), or inhibition of ATM, abolishes the 53BP1-Rif1 interaction and prevents recruitment of Rif1 to damaged

chromatin [159]. Furthermore, the 53BP1 mutant 53BP1^{15AQ}, which has the five most N-terminal S/TQ motifs intact and the following 15 motifs substituted for alanine, failed to recruit Rif1 into IR-induced foci (IRIF) [159]. Phospho-mutant 53BP1 can still accumulate at DSBs supporting the fact that 53BP1, but not Rif1, recognises DSBs. However, cells lacking Rif1 show a delayed resolution of DSB-induced 53BP1 foci, arguing that whilst Rif1 may be dispensable for recruitment of 53BP1 to damaged chromatin, it appears to be required for the repair function of 53BP1 [159]. The exact mechanism by which Rif1 and 53BP1 cooperate to inhibit resection is unclear, but Drané, et al. have shown Rif1 may also act prior to resection inhibition to dissociate a protein that binds to the tandem Tudor motif of 53BP1, thereby promoting binding to methylated H4K20. An uncharacterised protein, TIRR (Tudor Interacting DNA Repair Regulator) was identified that interacts directly with the Tudor domain of 53BP1 and prevents binding to chromatin at H4K20. Dissociation of the 53BP1-TIRR complex was impaired by the depletion of Rif1. Co-depletion of TIRR restored 53BP1 foci formation, suggesting the impact of Rif1 loss on 53BP1 is due to the sustained complex with TIRR [160].

PTIP appears to be a context-specific effector of 53BP1 which executes only a subset of 53BP1 functions. In contrast to 53BP1 and Rif1, PTIP depletion has no effect on class switch-recombination, a specialised form of NHEJ that occurs at DSBs generated by cytosine deamination in developing B cells [159, 161, 162]. PTIP contains BRCT repeats which also interact with 53BP1 (Ser25) in an ATM-dependent manner, but it is not clear whether 53BP1 is required for the focal accumulation of PTIP. In human cells, binding to 53BP1 was shown to be dispensable for PTIP recruitment at DSB sites [163]. However, Callen, et al. showed PTIP accumulation at DNA damage foci was diminished in the absence of 53BP1 [164].

Given that 53BP1 can be recruited to DSBs at all stages of the cell cycle [152, 153], it appears to be the default cellular response to DSBs. This suggests NHEJ is the repair pathway of choice in the cell. Indeed, it has been shown that NHEJ predominates even in G2 and occurs faster than HR [165]. How then do cells overcome this clear preference for 53BP1-driven NHEJ? The answer lies with Breast Cancer susceptibility protein 1 (BRCA1), a known antagonist to 53BP1 and a central effector of pathway choice.

1.3.4 BRCA1

BRCA1 is a known tumour suppressor protein with important checkpoint and DNA damage repair functions [166]. Mutations in *BRCA1* predispose carriers to an elevated risk of breast and ovarian cancer, and *BRCA1*-mutated tumours present with genomic instability as a consequence of impaired DNA repair [167]. The first indication that 53BP1 and BRCA1 were functionally interrelated came from the finding that loss of 53BP1 rescues the embryonic lethal phenotype of BRCA1 exon 11 deletion (*BRCA1*^{Δ11/Δ11}) by preventing premature senescence and apoptosis [168]. Unlike rescue by concomitant deletion of ATM, Chk1 or p53, the loss of 53BP1 in a *BRCA1*^{Δ11/Δ11} background did not lead to increased tumorigenesis and premature aging [168]. Bunting et al. explored this further and found that radial chromosome formation, characteristic of HR-defective cells, was present in *BRCA1*^{Δ11/Δ11} cells and was dependent on 53BP1. Loss of 53BP1 was therefore proposed to positively affect the residual capacity of cells to carry out HR. Indeed, this was found to be the case and the rescue was specific to 53BP1, as deletion of DNA Ligase IV and inhibition of DNA-PKcs, both of which are required for NHEJ, did not rescue the HR defect of *BRCA1*-deficient cells [169]. These data demonstrate that BRCA1 is not required for the promotion of resection but instead is critical to overcome the resection block imposed by 53BP1. DNA repair pathway choice is therefore controlled by the balance or mutual antagonism between 53BP1 and BRCA1 in the cell. Loss of BRCA1 promotes NHEJ as shown by the accumulation of Rif1 and 53BP1 at DSBs in S/G2 phases of the cell cycle, when repair by HR usually predominates [153, 159, 170]. Similarly, knockdown of 53BP1 induces ectopic BRCA1-containing nuclear foci in G1, indicating that the potential for BRCA1 recruitment exists in G1 but is blocked in a 53BP1-dependent manner [170]. The overexpression of BRCA1 can overcome the inhibition of DNA end resection enforced by 53BP1 and leads to increased resection at IR-induced DNA breaks [171].

1.3.5 BRCA1 antagonises 53BP1

The exact mechanism by which BRCA1 can overcome the end resection block imposed by 53BP1 is still somewhat unclear. It was shown by super-resolution microscopy that 53BP1 localised to IRIF, subnuclear aggregates containing numerous DNA-damage-responsive genes, most prominently in G0/G1 cell cycle stages, consistent with its role in NHEJ. BRCA1, on the other hand, accumulated as cells transitioned through S phase and was associated

with an exclusion of 53BP1 to the foci periphery in a BRCA1-dependent manner, and an IRIF core primed for DNA repair by HR [172]. RPA foci also form following 53BP1 repositioning suggesting end resectioning progresses following the removal of 53BP1 from DSB sites [173].

BRCA1 interacts with its N-terminal binding partner BRCA1-associated RING domain protein 1 (BARD1) to form an active E3 ubiquitin ligase. Several targets of the BRCA1-BARD1 E3 ligase have been identified including Histone H2A. H2A modification by ubiquitin has been implicated in the recruitment of the chromatin remodeller SMARCAD1 to DSBs, the ATPase activity of which is required for positioning of 53BP1 away from break sites and promotion of end resectioning [174]. Consistent with this model, it was found that the deubiquitinase (DUB) ubiquitin specific protease-48 (USP48) can remove ubiquitin from H2A at the specific BRCA1-BARD1 ubiquitination site and in doing so restricts resection. USP48 depletion results in a hyper-resection phenotype and positioning of 53BP1 further from the break site [175].

Feng et al. showed that BRCA1 can restrain the phosphorylation of 53BP1 by ATM in S/G2 with increased phosphorylation of 53BP1 observed following BRCA1 depletion. The phosphorylation of other ATM substrates was not affected, with the exception of Nbs1, but the mechanism for this was unclear. Feng, et al. went on to show that the C-terminus of 53BP1 can be ubiquitinated by BRCA1-BARD1 but not by the BRCA1 mutant C61G which contains a mutation in the RING domain; however, this could not be directly linked to the suppression of 53BP1 phosphorylation. They did, however, show that unlike WT BRCA1, re-introduction of BRCA1 C61G to BRCA1-depleted cells was unable to suppress PTIP foci formation in S/G2 cells, suggesting that the E3 ligase activity of BRCA1 is important for inhibiting 53BP1 phosphorylation, either directly or indirectly [153].

A cell-cycle dependent interaction between BRCA1 and CtIP may also be important for antagonising 53BP1. As cells enter S phase, CDK-mediated phosphorylation of CtIP at Ser327 mediates binding to BRCA1 which is reported to be required for end resectioning [142, 170, 176]. The inhibition of Rif1 at DSB break sites in chicken DT40 cells was impaired following CtIP depletion or re-introduction of the BRCA1 S1655A mutant, which disrupts CtIP binding, implicating the binding of BRCA1 to CtIP in Rif1 antagonism [170]. Whether this also holds true in mammalian cells is still debated with research suggesting the BRCA1-CtIP interaction is dispensable for end resection and proficient HR [177-179]. The BRCA1-CtIP interaction may instead be controlling the speed of resection. The CtIP S237A mutant, which cannot

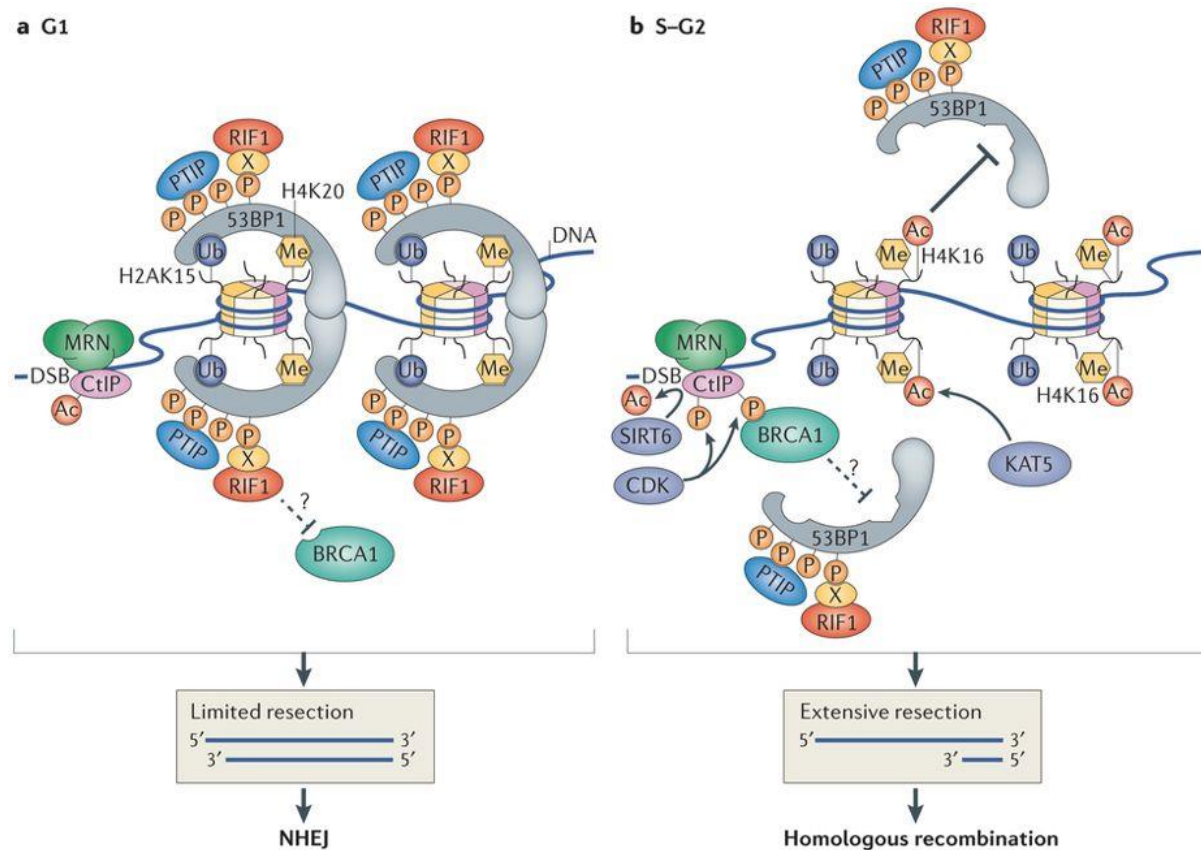


Figure 1. 7 - Antagonistic relationship between 53BP1 and BRCA1

a) During G1, oligomerised 53BP1 binds to H2AK13/15Ub and H4K20me2 and recruits its effector proteins Rif1 and PTIP following ATM-mediated phosphorylation at the amino terminus of 53BP1. Chromatin-bound 53BP1-Rif1 prevents association of BRCA1 with the MRN complex subunit CtIP through an unknown mechanism. The net outcome of this inhibition is to limit DNA end resection and thus enable NHEJ-mediated DSB repair. **b)** As cells enter S phase, CtIP is phosphorylated in a CDK-dependent manner which promotes its binding to BRCA1. This prevents the chromatin association of 53BP1-Rif1 and 53BP1-PTIP through unknown mechanisms. Acetylation of H4K16 further reduces 53BP1 binding to the K4K20me2 mark. Deacetylation of CtIP by Sirtuin 6 (SIRT6) upregulates the end resection activity of CtIP which enables 3' to 5' resection of the DNA end and commits cells to HR. Figure taken from [155], reprinted with permission.

bind BRCA1, exhibited slower resection than WT CtIP, potentially due to the role of BRCA1 in removing 53BP1-Rif1 complexes [180]. Alternatively, BRCA1-CtIP interactions may only be required for the repair of a subset of DNA breaks. Aparicio, et al. showed that whilst dispensable for resection of endonuclease-generated DSB ends, the interaction between BRCA1 and CtIP is required for resection of topoisomerase II (Top2)-adducted DSBs, and therefore resistance to the chemotherapeutic agent etoposide [181].

In summary, 53BP1 is a key regulator of NHEJ that recruits its effector proteins Rif1 and PTIP following ATM-mediated phosphorylation of N-terminal Ser/Thr-Gln sites. Rif1 and PTIP promote DNA end resection during G1 and thus inhibit HR. During S/G2 stages of the cell cycle, BRCA1 can counteract the block imposed by 53BP1 by an as yet indeterminate mechanism (Figure 1. 7). BRCA1 may inhibit the phosphorylation of 53BP1 by ATM or interact with CtIP to promote DNA end resection. What is clear, is that the relationship between 53BP1 and BRCA1 is vital for repair pathway choice and is highly regulated to ensure DSBs are repaired efficiently to maintain genomic stability.

1.4 The Ubiquitin Proteasome System (UPS)

A number of cellular processes including cell cycle progression, cell division and apoptosis require the rapid degradation of proteins. This rapid degradation is essential to allow protein levels to change quickly in response to external stimuli. In eukaryotic cells there are two major pathways controlling this degradation, lysosomal degradation/autophagy and the ubiquitin proteasome system (UPS). Lysosomal degradation involves the uptake of proteins by lysosomes, membrane-enclosed vesicles that contain proteases and other digestive enzymes [182]. This process can be non-selective and is primarily adopted during apoptosis or as a response to cellular stress such as infection or cell starvation. In contrast, the UPS is a highly regulated and selective pathway, whereby proteins are targeted for degradation upon covalent conjugation of a 76 amino acid ubiquitin peptide.

Addition of ubiquitin requires the combined action of E1 (ubiquitin activating), E2 (ubiquitin conjugating) and E3 (ubiquitin ligating) enzymes in an ATP-dependant cascade [182, 183]. First, the E1 enzyme forms a thio-ester bond with ubiquitin which activates the carboxyl-terminal glycine residue of ubiquitin. This allows the transfer of activated ubiquitin to a cysteine residue of an E2 enzyme. The E3 ubiquitin ligase is responsible for bringing substrates into close proximity with the E2 enzyme and for catalysing the transfer of ubiquitin to the amino group of a lysine residue on target proteins [184]. Proteins with multiple lysine residues can be mono-ubiquitinated (addition of a single ubiquitin moiety), on more than one lysine at once to become multi-mono-ubiquitinated. Ubiquitin itself can also be ubiquitinated on any of its seven internal lysines resulting in a polyubiquitin chain. These chains can be linear, homologous; consisting of one linkage type, heterogenous; consisting of multiple ubiquitin linkages in a single polymer or branched [185, 186]. The functions of some linkage types are well characterised but by no means exclusive, for example, K48 linkages are known to target proteins for proteasomal degradation at the 26S proteasome and are the most abundant linkage type identified in organisms, while K63-linked chains have non-proteolytic functions such as NF- κ B activation and re-localisation of proteins. The physiological consequences of the remaining atypical ubiquitin chain linkages (K6, K11, K27, K29 or K33) remain relatively uncharacterised despite their high abundance, but may all mediate protein degradation [187]. K11-linked ubiquitin chains are utilised by the anaphase promoting complex (APC/C) to target proteins for degradation [188], and K6

chains may regulate DNA repair [189].

1.4.1 SCF-type E3 ubiquitin ligases

The functional complexity of ubiquitination signalling is as a result of the large and diverse range of enzymes that catalyse ubiquitination reactions. The human genome encodes for two E1 enzymes, 38 E2 enzymes and approximately 600-1000 E3 ligases [190-192]. The combination of these enzymes enables a high degree of substrate specificity. The selectivity of the UPS is determined by the E3 ligases and the E2 enzymes they interact with. E3 ligases bind, and therefore select, the substrate to be ubiquitinated, but it is the E2 enzyme that determines the ubiquitin linkage specificity. For example, the E3 ligase BRCA1-BARD1 assembles K63-linked chains with the E2 UBE2N but K48-linked chains with UBE2K [193]. E3 enzymes can be subdivided into three different classes: the HECT (Homologous to E6-associated protein C-terminus)-domain type, RING (Really Interesting New Gene)-finger type and RBR (RING-in-between-RING) family [194]. HECT and RBR E3 ligases catalyse the transfer of ubiquitin to a substrate in two steps: first ubiquitin is transferred from the E2 to the E3, and then from the E3 to the substrate. In contrast, RING-finger type E3s catalyse the transfer of ubiquitin directly from the E2 enzyme to the substrate [195]. RING-finger type E3 enzymes can function as monomers, dimers or multi-subunit complexes. The largest family of this type is the Cullin-RING E3 ligase (CRL) complex family, with over 200 members [196].

The central scaffold of the CRL comprises one of seven cullin proteins which binds a RING-box protein (Rbx1 or Rbx2) at its C-terminus. CRL1 or SCF (S-phase kinase-associated protein 1 (Skp1)-Cullin 1-F-box protein) E3 ligases are the best characterised of the CRL ligases. In these ligases, the CRL scaffold Cullin 1 (Cul1) binds the adaptor Skp1 at its N-terminus and Rbx1 at its C-terminus, thereby bringing together two essential components required for E3 ligase activity. Skp1 binds to an F-box-domain containing protein (FBP); which acts as the substrate recognition component of the SCF ligase and Rbx1 binds the E2 enzyme conjugated to activated ubiquitin, thus enabling the direct transfer of ubiquitin to the substrate (Figure 1. 8). Skp1 binds to FBPs via their characteristic F-box domain, an approximately 50aa protein-protein interaction motif first identified in cyclin-F (Fbxo1) and conserved in FBPs. The FBP:Skp1 dimer is a switchable unit that docks the cullin scaffold and is actively dissociated by the protein Cand1 (Cullin-associated NEDD8-dissociated protein 1) to regulate levels of active E3 ligases in the cell [197].

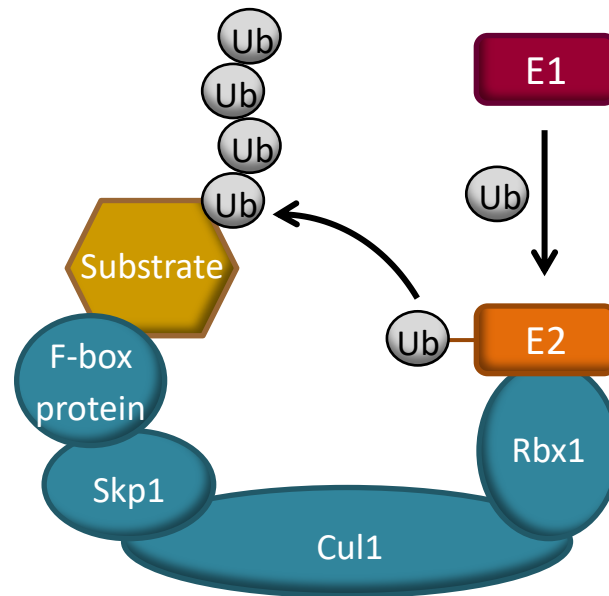


Figure 1. 8 - Schematic showing the SCF complex and ubiquitination of target proteins.

Ubiquitination of target substrates requires the combined action of E1 (red), E2 (orange) and E3 (blue) enzymes. The SCF E3 ubiquitin ligase is shown here in its characteristic horseshoe conformation. The scaffold protein Cul1 binds Rbx1 and Skp1. Skp1 binds the substrate determining component F-box protein which can recruit substrates. Sequential ATP-dependent reactions transfer ubiquitin molecules to lysine residues on the substrates recruited by the F-box protein.

It is worth noting that FBPs not engaged as part of active E3 ligases also have functions outside of the UPS [198]. FBPs compete for binding to cullin scaffolds and so it is unsurprising that many have functions that do not require the assembly of ligase complexes. In yeast FBP:Skp1 dimers have been identified with roles in centromere complex assembly and recycling of endosome components independent of an SCF complex [199]. It is not just yeast that utilise FBPs outside of the UPS, Emi1 (Fbxo5), a mammalian example of an FBP with SCF-independent roles, can stably bind and inhibit the APC/C complex to coordinate DNA replication and mitosis [200, 201]. Furthermore, some FBPs, despite being able to bind Skp1, utilise their F-box domains to bind proteins other than Skp1. For example, Fbxo38 uses its F-box domain to interact with the transcription factor Klf7 to act as a transcriptional cofactor [202].

1.4.2 F-box proteins

F-box proteins recruit target substrates to the SCF ligase complex via a variable protein-protein domain. The protein-binding domain present determines the nomenclature of FBP subfamilies, Fbx_{ws} contain WD40 repeats, 10 family members, Fbx_{ls} have leucine rich repeats, 21 family members and Fbx_{os} have other known binding domains such as proline rich regions, 38 family members [198]. There are 69 known FBPs in human, at least 42 of which have been shown to interact with Cul1 to form SCF-type E3 ubiquitin ligases complexes [203]. This allows for recognition of a diverse range of substrates and far-reaching roles within the cell. Most substrates require post-translational modification before they can be recognised and bound by FBPs. The canonical model of FBP substrate recruitment requires binding to short degradation motifs (known as degrons) which are often primed by phosphorylation on specific serine or threonine residues prior to FBP binding (known as phosphodegrons) [204]. In the absence of phosphorylation, a protein is stable, but upon phosphorylation at sites within the degron the protein can be ubiquitinated and degraded [205-207]. To increase stringency some degrons contain multiple phosphorylation sites or can require the combined activity of multiple kinases before recognition by an FBP [208]. Phosphorylation is not the only modification that facilitates FBP binding, Fbxo2 and Fbxo6 bind glycosylated proteins [209, 210] and the binding of Fbxl17 and Fbxo24 to target proteins is determined by the acetylation status of binding motifs (acetyl-degrons) within their substrates [211, 212]. Not all FBPs require modified degrons to bind substrates [213, 214], and in some cases post-translational-modification actually prevents binding [215, 216]. On the other hand, some FBPs require more than just post-translational modifications to recognise substrates and therefore utilise co-factors. For example, Skp2 (Fbxl1)-mediated degradation of p27 requires the accessory protein Cks1 (CDK regulatory subunit 1). It is in fact Cks1 that binds to the phosphodegron (Thr187) on p27, not Skp2, to recruit p27 to the SCF ligase complex as a substrate for ubiquitination [217-219]. Skp2 can still interact with p27 directly, but via an alternative interface [218].

1.4.3 F-box proteins in cancer

Many FBPs have already been implicated as tumour suppressors or oncogenes due to their ability to regulate the expression and activity of other oncogenic or tumour suppressive proteins. Dysregulation of F-box protein mediated proteolysis leads to human malignancies

and inhibition of FBPs has been shown to have potential as a therapeutic strategy [220]. Skp2 (Fbxl1) is perhaps the best characterised FBP and a known oncoprotein. First identified as a cell cycle regulator, Skp2 has been reported to be overexpressed in various human tumour samples including breast, lymphoma, non-small cell lung cancer and glioblastoma [221-223]. Transgenic mice overexpressing Skp2 show low-grade carcinoma but knock-out mice are resistant to sarcoma and lymphoma [221]. Skp2 exerts its oncogenic effect by ubiquitinating its substrates, many of which are tumour suppressors, most notably the cyclin-dependent kinase inhibitor, p27 [224-228]. Therefore understanding the target repertoire of F-box proteins is important for determining their mechanistic roles in cancer progression [229].

In contrast Fbxw7 is a well-established tumour suppressor that targets oncogenic proteins including cyclin E and c-myc for degradation [230]. Fbxw7 also targets mTOR (mammalian target of rapamycin) for degradation, and tumour cell lines containing Fbxw7 mutations are particularly sensitive to rapamycin treatment [231]. Approximately 6% of all primary human cancers have a mutation in *FBXW7* with the most frequent mutations identified in T cell acute lymphoblastic leukaemia (T-ALL: 30%) and cholangiocarcinomas (35%) [232]. Mouse models have been used to confirm its tumour suppressive role with bone-marrow specific Fbxw7-knockout mice developing T-ALL within 16 weeks, due in part to an accumulation of the Fbxw7 substrates c-myc and Notch1 [233].

β -TRCP1 and β -TRCP2 (Fbxw1 and Fbxw11) differ from Skp2 and Fbxw7 in that they show context-dependent roles in governing tumorigenesis and have been shown to possess both tumour suppressive and oncogenic properties dependent on the specific tumour type. β -TRCP1 is overexpressed in pancreatic [234] and colorectal cancer [235] with the latter associated with poor patient outcome, and β -TRCP2 is overexpressed in breast, prostate and gastric cancers [236, 237]. Targeted expression of β -TRCP1 in the mammary gland led to tumour formation, which supports the idea that β -TRCP1 is an oncogene [238]. However, β -TRCP1 and β -TRCP2 mutations have been identified in gastric cancer that result in loss of the E3 ligase activity of β -TRCP. The resulting stabilisation of the β -TRCP substrate β -catenin was associated with development of tumours in this setting, suggesting a tumour suppressive role for β -TRCP1 and β -TRCP2 [239].

F-box proteins and the dysregulation thereof have been implicated in almost all the hallmarks of cancer described by Hanahan and Weinberg [2, 3, 240]. For example, Fbxo31 is downregulated in gastric cancer and inhibits gastric cancer progression by suppressing the epithelial-mesenchymal transition (EMT) [241, 242]. Fbxo31 is also known to target Cyclin-D1 for degradation in response to DNA damage to activate the cell cycle arrest checkpoint. Loss of Fbxo31 is therefore also likely to sustain cell proliferation and promote uncontrolled cell cycle progression. Fbxo5 (Emi1) is overexpressed in ovarian tumours and is associated with poor outcome in in hepatocellular carcinoma [243, 244]. Emi1 stabilisation inhibits the APC/C complex which blocks APC/C-mediated degradation of Skp2 and promotes cell proliferation in chronic myeloid leukaemia cells [245]. Fbxo8 negatively regulates the small GTPase Arf6, a regulator of membrane trafficking and remodelling. Fbxo8 expression was lost in several breast tumour cell lines that require Arf6 for invasion, but this invasiveness could be suppressed with the forced expression of Fbxo8 [246]. There are undoubtedly further roles for FBPs in cancer and other diseases. Wang et al. identified Fbxo11, Fbxw8, Fbxl3, Fbxo1, Fbxo4 and Fbxo18 as emerging tumour suppressors further highlighting the role of F-box proteins in cancer pathogenesis [224].

1.4.4 Fbxl17

Fbxl17 is a relatively understudied member of the FBXL family of FBPs which binds to Skp1 via its F-box domain to assemble an SCF-type E3 ligase complex. The protein structure of Fbxl17 is characterised by its 11 C-terminal leucine rich repeats through which it can interact with target substrates (Figure 1. 9). LRRs are a repeating motif, 20-29 residues long that contain a conserved 11-residue consensus sequence (LxxLxLxx^N/c^xL, where x can be any amino acid and L can be occupied by leucine, valine, isoleucine or phenylalanine; amino acids with hydrophobic side chains) [247]. Proteins may also bind at the N-terminus of Fbxl17, but it is unclear whether these would also be targeted for ubiquitination. As Fbxl17 assembles into an SCF complex, its role is to bring substrates into close proximity with an E2 enzyme for the direct transfer of ubiquitin from the E2 to the target protein.

Whilst some substrates of Fbxl17 have been identified most remain widely unknown. Fbxl17 was first reported to stabilise ribonucleotide reductase subunit M2 (RRM2), promoting its overexpression in the breast cancer cell line MCF-7. RRM2 expression and activity has been associated with resistance to multiple drugs in human cancer and together with RRM1

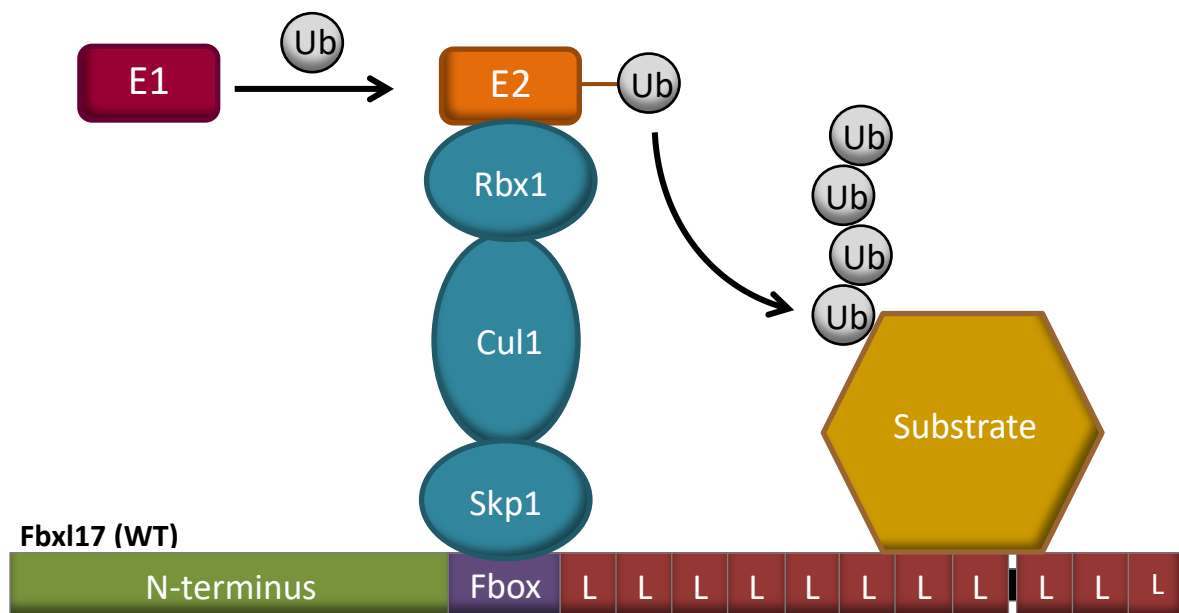


Figure 1. 9 - Schematic of an E3 SCF ligase complex with wild-type Fbx17.

Fbx17 binds to Skp1 via its Fbox domain (purple) to form the SCF complex. The leucine rich repeats (LRRs, red) of Fbx17 then interact with target substrates and bring them into close proximity with the E2 conjugating enzyme recruited by Rbx1 for subsequent transfer of ubiquitin molecules.

makes up the two subunits of human ribonucleotide reductase (RR). RR is an S-phase specific rate-limiting enzyme that mediates the synthesis of deoxyribonucleotides, DNA precursors. Patients less sensitive to the RR antisense oligonucleotide inhibitor GTI-2040 were shown by Xiao et al. to have high levels of Fbx17. However, the mechanism of this apparent stabilisation is unclear. They suggest that Fbx17 may therefore be a useful biomarker for breast cancer therapy [248].

In 2013, Tan, et al. identified the transcriptional repressor BACH1 as a substrate of Fbx17. Parallel adaptor capture (PAC) proteomics was used to systematically identify FBXL FBP substrates for 19 FBXL family members (all except Fbx16 and Fbx121). Fbx17 was found to associate with several BTB-domain containing proteins including BACH1 [249]. Further analysis showed that Fbx17 is important for turnover of BACH1 which promotes transcription of the NRF2 target HMOX1. HMOX1 encodes Heme oxygenase 1 which is important for the breakdown of free Heme. This has a cytoprotective role as an excess of free Heme sensitises cells to undergo apoptosis. The ubiquitination of BACH1 by Fbx17 provides one mechanism for controlling HMOX1 activation in response to oxidative stress.

Fbxl17 has also been shown to mediate the ubiquitination and degradation of Sufu (Suppressor of fused), a central regulator of Hedgehog (Hh) signalling. Sufu was identified as a candidate substrate by Tan, et al. [249], and further research by Raducu, et al. showed that Fbxl17 targets Sufu for proteolysis. Sufu sequesters Gli (Glioma-associated oncogene homolog) transcription factors to negatively regulate Hh signalling thus acting as a tumour suppressor (Figure 1. 10A). Polyubiquitination of Sufu by Fbxl17 is favoured by the presence of Gli1, bound to Sufu, and dephosphorylation of Sufu residues S342 and S346. Degradation of Sufu following ubiquitination by Fbxl17 releases Gli1 which can then activate the Hh pathway (Figure 1. 10B). This regulation by Fbxl17 is exploited in medulloblastoma cells to aberrantly amplify Hh signalling.

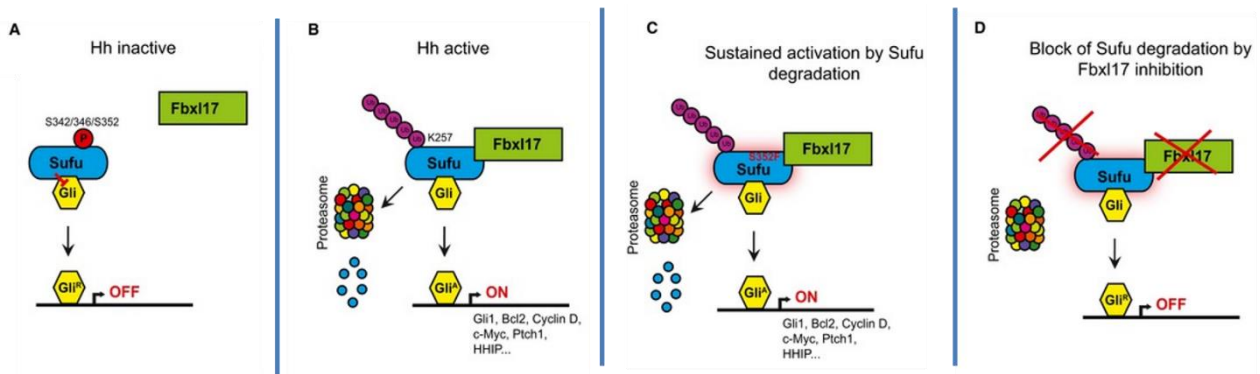


Figure 1. 10 - SCF^{Fbxl17}-ubiquitination of Sufu regulates Hedgehog signalling and medulloblastoma

(A) Phosphorylation of Sufu at S342 and S346 prevents Fbxl17 binding. Gli1 is sequestered by Sufu and so cannot activate the Hh pathway. **(B)** Dephosphorylation of Sufu initiates Fbxl17 polyubiquitination of Sufu at Lys257. Sufu is degraded which releases Gli1 to activate the Hh pathway. **(C)** In medulloblastoma, the Sufu substitution S352F abolishes Sufu phosphorylation and promotes Fbxl17 binding, resulting in sustained Hh pathway activation. **(D)** Inhibition of Fbxl17 blocks Sufu degradation and prevents medulloblastoma tumour growth. Figure adapted from [250].

In human medulloblastoma DAOY cells Fbxl17 depletion impaired proliferation suggesting that Fbxl17 mediates cancer cell proliferation. A naturally occurring mutation (S352F) found in medulloblastoma patients affected by Gorlin syndrome abolishes phosphorylation of Sufu at S352. This substitution increases Fbxl17 binding allowing for faster proteolysis of Sufu, amplified pathway activation and increased cell proliferation (Figure 1. 10C). Fbxl17 inhibition was able to rescue this sustained activation and prevent medulloblastoma tumour growth by blocking Sufu degradation (Figure 1. 10D). Therefore, the control of Sufu levels by

Fbxl17 in medulloblastoma is important for regulating Hh activation. This evidence suggests that targeting Fbxl17 and the UPS may be a useful therapy in the treatment of cancer [250].

In the case of Sufu, Fbxl17 binding could be inhibited by phosphorylation of Sufu highlighting the importance of post-translational modifications in substrate binding. There is now evidence that Fbxl17 can recognise and bind a tandem IK (Isoleucine, lysine) motif (IKxxxIK) within the histone modifying protein PRMT1 [212]. The lysine acetylation status of this motif or so called 'acetyldegron' determines Fbxl17 binding. The co-ordinately ordered activity of the deacetylase Sirt1 and the acetylase p300 prime this acetyldegron within PRMT1 for Fbxl17 binding. Fbxl17 can then dock and target PRMT1 for proteasomal degradation. Bronchial epithelial cells treated with pathogen-derived lipopolysaccharide (LPS) downregulated p300 and Sirt1 which protected PRMT1 from Fbxl17-mediated degradation and increased cell proliferation. This perhaps explains how bronchial epithelial overgrowth occurs in asthma. Identifying other proteins that contain the tandem IK motif identified in PRMT1 may be a means of identifying further Fbxl17 substrates.

Most recently, Fbxl17 has been shown to interact with BTB-domain containing proteins in a quality-control capacity [251]. In concurrence with Tan, et al. it was found that Fbxl17 can bind many BTB-domain-containing proteins and can recognise inactive BTB heterodimers which are consequently targeted for proteasomal degradation. This ensures only functional BTB dimers are present in cells. Interestingly these data demonstrate that Fbxl17 recognises domains shared by many proteins rather than simply targeting a specific substrate. Mena et al. showed that Fbxl17 preferentially recognises BTB heterodimers by recognising a degron within the dimer interface. These residues are only exposed and therefore accessible to Fbxl17 in nascent or mutant BTB proteins or aberrant heterodimers. Binding is dependent on a conserved cysteine residue (C627) of Fbxl17 and the somatic mutation C627R identified in breast cancer ablated the interaction of Fbxl17 with BTB proteins. The dimerization quality control (DQC) function of Fbxl17 was shown to be required for neural differentiation and function in *Xenopus laevis* embryos, highlighting the importance of DQC for specific BTB proteins [251].

1.4.5 Fbxl17 is recurrently rearranged in breast cancer

Data-mining of the METABRIC (Molecular Taxonomy of Breast Cancer International Consortium) dataset [29], consisting of segmented array-CGH copy number data from 1,992

primary breast tumours, was carried out by Dr Susanne Flach, a previous PhD student in the lab, to identify genes that are recurrently disrupted in cancers [252]. Many of the genes in the top 1000 most frequently broken genes, as derived by copy number changes, resided in common fragile sites (CFS). These are loci prone to breaks when cells are under replicative stress. Given the increased rate of breaks at these sites, it can be difficult to determine whether these rearrangements confer any advantage and are true driver mutations. After excluding genes in CFS, and cancer genes already described in the literature, we found that multiple family members of the F-box protein (FBP) family appeared in the top half of the frequently broken genes list. These identified proteins were both novel with regards to cancer involvement at the time of discovery and did not fall within CFS. By surveying the METABRIC dataset in more detail it was found that 135 (7%) tumours had at least one genomic break within the FBP *FBXL17*, often clustered around the LRR-encoding regions. These genomic alterations suggest the ability of Fbxl17 to recruit substrates for ubiquitination or to form part of an SCF complex may be compromised in breast cancers.

1.5 Aims of this thesis

1.5.1 Investigating the functional consequences of *FBXL17* rearrangements

As a result of the identified rearrangements of *FBXL17* in breast cancer, described above, the initial aim of this thesis was to determine the functional consequences of these mutations for Fbxl17. Many of the rearrangements observed previously, truncated Fbxl17, resulting in loss of LRRs. We therefore investigated the effect of loss of LRRs on SCF ligase assembly and function. By surveying paired-end whole-genome sequencing data from primary breast tumours, we also set out to identify further breast cancer-associated rearrangements in *FBXL17*.

1.5.2 Identifying and verifying new target substrates of Fbxl17

Only a few substrates of Fbxl17 are currently known, and so the second aim of this thesis was to identify and verify new potential binding partners of Fbxl17. Identifying the regulatory network of Fbxl17 will provide an insight into its role in breast cancer pathogenesis, which may then reveal pathways amenable to therapeutic targeting. To address this aim, we identified potential interacting partners of Fbxl17 by yeast two-hybrid and mass spectrometry approaches. The resulting aims were then to validate Fbxl17 binding partners, and to investigate the downstream effects of *FBXL17* mutations on its regulatory networks.

In summary, this thesis investigates the functional downstream effects of novel *FBXL17* rearrangements identified in breast cancer and identifies two distinct pathways that appear to be regulated by Fbxl17, providing mechanistic insight into the role of Fbxl17 in breast cancer.

2 | MATERIALS AND METHODS

CHAPTER 2- Materials and methods

2.1 CELL CULTURE AND ANALYSIS

2.1.1 Cell line maintenance

Frozen ampoules of cells were thawed at room temperature from -80°C and diluted in complete growth medium, centrifuged at 300G for 3 mins, washed once in PBS to remove traces of dimethyl sulfoxide (DMSO, Sigma D8418), centrifuged again and resuspended in 10ml complete growth medium. Complete medium for the cell lines grown are shown in Table 1. Cells were grown in 90mm tissue culture dishes, unless otherwise stated, at 37°C, 5% CO₂ humidified atmosphere. Confluent cells were washed with 5ml PBS after removal of growth medium and 2ml of trypsin was added. Cells were incubated at 37°C until no longer adhered to the dish and passaged as required. Fresh complete medium was then added to a total volume of 10ml.

Cells were frozen by trypsinising as above and pelleting the cells by centrifugation 300G 3 mins. Pellets were resuspended in freezing media (90% (v,v) FBS, 10% (v,v) DMSO), 1ml per 90mm dish and frozen slowly at -80°C before transfer to liquid nitrogen.

2.1.2 Transfection of adherent cells

24 hours prior to transfection cells were seeded in order to reach 50-80% confluency overnight, $\sim 2 \times 10^6$ cells for 90mm dishes and $\sim 2 \times 10^5$ cells for flat bottomed 6 well plates. For 90mm dishes a minimum of 5µg of DNA was added to 300µl OptiMEM® (Thermo Fisher Scientific, 51985026) and 15µl PEI (3µl/µg DNA) vortexed 10s and incubated room temperature (RT) for 15 minutes. For 6 well plates 1ug DNA was added to 50µl OptiMEM® and 3µl PEI. The entire volume was then added drop-wise to cells whilst gently rocking the plate to ensure an even distribution. Unless otherwise stated, cells were incubated for 48 h before assaying.

2.1.3 Retroviral infection of adherent cells

Viral packaging cell line Phoenix-ECO [253] were transfected as above (PEI mediated) with 3µg DNA of interest and 2µg viral envelope VSVG. Eight hours after transfection the media was changed to that of the target cells. 24h prior to infection 2×10^5 target cells were seeded in complete growth medium to flat bottomed 6 well plates and grown overnight to 50-80%

Table 1 - Cell lines and culture conditions.

Cell line	Medium	Supplements	Characteristics	Source
HB4a	RPMI-1640	10% (v/v) FBS, 1% (v/v) Pen/Strep, 5µg/ml Hydrocortisone, 5µg/ml Insulin	Epithelial, adherent	McKenzie ¹
HCC38	RPMI-1640	20% (v/v) FBS, 1% (v/v) Pen/Strep	Epithelial, adherent	ATCC
HCC1395	RPMI-1640	20% (v/v) FBS, 1% (v/v) Pen/Strep	Epithelial, adherent	ATCC
HEK293T	DMEM	10% (v/v) FBS, 1% (v/v) Pen/Strep	Epithelial, adherent	ATCC
MCF7	DMEM	10% (v/v) FBS, 1% (v/v) Pen/Strep	Epithelial, adherent	ATCC
U2OS	DMEM	10% (v/v) FBS, 1% (v/v) Pen/Strep	Epithelial, adherent	ATCC
U2OS_RFP-53BP1	DMEM	10% (v/v) FBS, 1% (v/v) Pen/Strep, µg/ml Geneticin	Epithelial, adherent	Jackson ²
U2OS_TLR	DMEM	10% (v/v) FBS, 1% (v/v) Pen/Strep, µg/ml puromycin	Epithelial, adherent	Jackson ²

¹HB4a cells were a kind gift from C. McKenzie (Department of Pathology, University of Cambridge, Cambridge, UK)²These cells lines were a kind gift from Yaron Galanty, Steve Jackson lab (Gurdon Institute, University of Cambridge, Cambridge, UK)

confluency. 24h after the initial transfection the conditioned media from the Phoenix-ECO cells containing virus was sterile filtered through a 0.45µm filter and collected in a Falcon tube. The cationic polymer Polybrene was added (1:1000) to increase the efficiency of infection as well as ~1ml of complete growth medium to replenish serum. Medium was removed from the target cells and 2ml of viral conditioned media was added per well, cells were then centrifuged at 2000rpm for 30-45 minutes and returned to incubate at 37°C, 5% CO₂. Fresh target cell complete growth medium was added to the Phoenix-ECO cells and they were returned to incubate. This process was repeated the following day or every other day depending on the cell line. After the final infection the Phoenix-ECO cells were disinfected with Virkon and discarded. Infected cells were trypsinised and a small sample was run through a flow cytometer to check infection efficiency.

2.1.4 Cell fractionation

3 x 10⁶ cells were resuspended in 75µl Buffer A (10mM Hepes pH7.9, 10mM KCl, 1.5mM MgCl₂, 0.34M Sucrose, 10% Glycerol, 1mM DTT, 0.1mM PMSF, protease inhibitors). Triton X-100 was added to a final concentration of 0.1%, lysates were then incubated on ice 5 min and centrifuged 4 min 3,500 rpm at 4°C. Supernatant was removed (cytoplasmic fraction) and clarified by centrifugation, 15 min, 13,000 rpm, 4°C. The remaining nuclear pellet was washed in Buffer A + Triton X-100 and lysed in Diehl Buffer with protease inhibitors, incubated on ice 5 min and centrifuged 13,000 rpm 15 min, 4°C (nuclear fraction).

2.1.5 siRNA transfection

U2OS cells were seeded at 5x10⁵ per 60mm dish in 2ml DMEM media containing 5% FBS without antibiotics (no P/S). Once cells were adhered (~6 hours), 250µl OptiMEM® was added to 10µl siRNA and 10µl Lipofectamine™ RNAiMAX (Thermo Fisher Scientific, 13778075) in separate Eppendorf tubes. After 5 mins at RT the two tubes were mixed and incubated at RT for a further 15 mins. siRNA mixes were then added dropwise to cells. A minimum of 12 hours later, media was replaced to DMEM + 10% FBS no antibiotics. 72 hours after siRNA transfection cells were harvested for analysis. siRNAs were purchased from Eurofins genomics and transfected at a final concentration of ~60nM. Sequences for the siRNAs were as follows:

siRNA1: GGAUUAUCAUGCAGGAAAA (targets exon 4)

siRNA2: GCAGAGAACUCAAGAUUAU (targets exon 4)

siRNA3: GGACAAACUCACUGAUGAA (targets exon 3)

2.1.6 shRNA knockdown of Fbxl17 expression

Short hairpin RNA sequences targeting *FBXL17* were taken from the RNAi Codex database (<http://codex.cshl.org>) [254]. shRNA vectors were generated by PCR amplification of a single mir30 template oligonucleotide containing restriction enzyme sites either side of the complete shRNA sequence, for subsequent cloning into the LMP vector (MSCV-LTRmir30-IRES-GFP). The 22-mer shRNA sequences chosen, and the region of *FBXL17* they target, are listed in Table 2. Vectors were sequenced to ensure correct amplification of the shRNA sequence. shRNA vectors were then used to retrovirally infect cells for Fbxl17 knockdown.

Table 2 - shRNA design – 21-mer shRNA sequences targeting FBXL17

<u>2.1.7 Cell analysis-propidium iodide staining</u>	Sequence	Target region	<u>cycle</u>
shRNA 1	CGGATAGTAACTGGTCAGGATA	3' UTR of <i>FBXL17</i>	
shRNA 2	CGCTTTCTGACACCTCTATTAT	exon 3 of <i>FBXL17</i>	
shRNA 3	CCCTGTAATCTTTAGATGGTTA	3' UTR of <i>FBXL17</i>	

For cell cycle analysis 2×10^5 cells were seeded to 6 well plates and irradiated (2Gy). Non-irradiated cells were used as a control. Cells were harvested at the indicated time points, washed in PBS, centrifuged and the pellet slowly resuspended in ice-cold 70% ethanol with vortexing to prevent clumping. Cells were fixed for at least 24h before propidium iodide (PI) staining. Prior to analysis by flow cytometry, cells were pelleted by centrifugation 2000rpm 5 mins, washed in PBS and resuspended in PI staining solution. Cells were incubated at 37°C for 30 mins and then analysed on a Cytex DXP8 Flow Cytometer with a minimum of 20,000 events collected per sample.

2.1.8 Annexin V staining

To assay apoptosis, supernatant was collected from cells, remaining adhered cells were trypsinised and added to the supernatant. Cells were spun down 300G, 3 min, washed in PBS and counted. Cells were spun down again, 300G 3min, and resuspended in 100µl/ 100,000 cells Annexin V buffer (10 mM HEPES, 140 mM NaCl, 2.5 mM CaCl₂, pH7.4). Annexin V- Alexa Fluor 647 (Invitrogen, A23204) (1µl/100µl) and propidium iodide (PI) (5µg/ml) were added to each sample. PI was used to discriminate live cells from dead cells. Cells were incubated at RT for 15 mins and then analysed on a Cytex DXP8 Flow Cytometer with a minimum of 15,000 events collected per sample.

2.2 MOLECULAR BIOLOGY METHODS

2.2.1 Polymerase chain reaction

All standard PCRs were carried out using Vent DNA polymerase (New England Biolabs, M0254S); primers were purchased from Sigma Aldrich and resuspended in nuclease free H₂O to give 100µM stock solutions. A typical PCR reaction was prepared as per Table 3 to a total of 50µl. PCR reactions were run on an MJ Research Tetrad PTC-225 Thermal Cycler; standard PCR cycling conditions are shown in Table 2.

Table 3 - Standard PCR Reaction volumes and concentrations

Component	Volume/Concentration
10x Thermo Pol Buffer	1x
Template	30ng (plasmid DNA)
Forward primer	1µM
Reverse primer	1µM
dNTPs	0.4mM
Vent Polymerase	1U
DMSO (if required)	10%
DEPC Water	up to 50µl

Table 4 - Standard PCR Cycling conditions

Standard PCR		
Step	Temperature	Time
1 Denature	95°C	5min
2 Denature	95°C	30s
3 Anneal	60°C	30s
4 Elongate	72°C	1min per Kb of template
Repeat steps 2-4 (35-40 times)		
5 Elongate	72°C	5min
6 Reaction end/hold	4°C	∞

2.2.2 Two-step mutagenesis PCR

Site-directed mutagenesis for the deletion of the FBD of Fbx;17 was achieved using the two-step PCR method. Two-step PCR mutagenesis required two rounds of amplification (Figure 2.1). The first round produced the 5' and 3' products using primers A/B and C/D respectively. Primers B and C spanned the FBD region to be deleted ($\Delta 324-358$ aa). Reactions were carried out as described previously. Fragments were resolved by gel electrophoresis and the DNA fragments purified from the gel. The second round of amplification allowed hybridisation of the 5' and 3' products before addition of primers A and D for extension of the mutated fragment (Figure 2.1). Cycling conditions for the 2nd step are shown in Table 5.

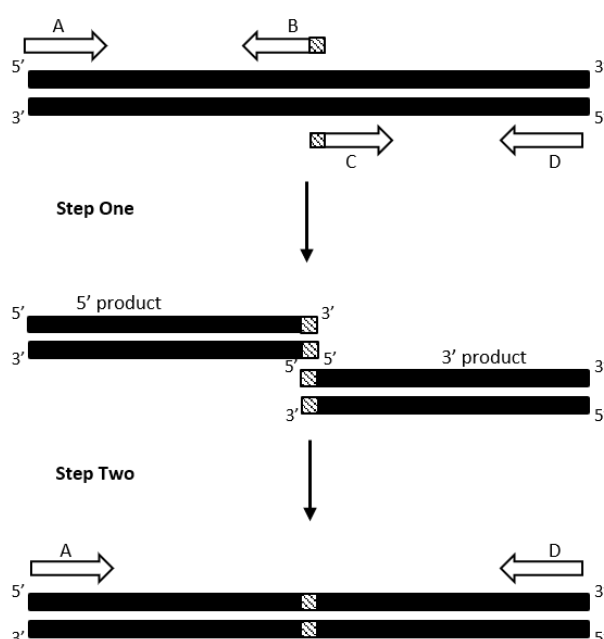


Figure 2.1 - Two-step mutagenesis PCR strategy

The first round of PCR produces a 5' and a 3' product. Primers B and C contain the mutation or span the region to be deleted. The 2nd PCR step requires hybridisation of the two products followed by extension with primers A and D.

Table 5 - Two-step PCR cycling conditions

Two-step PCR		
Step	Temperature	Time
1 Denature	95°C	5min
2 Denature	95°C	30s
3 Anneal	60°C	30s
4 Elongate	72°C	1min per Kb of template
Repeat steps 2-4 (10 times) without primers		
Add primers (A and B)		
5 Denature	95°C	30s
6 Anneal	60°C	30s
7 Elongate	72°C	1min per Kb of template
Repeat steps 5-7 (30 times)		
8 Elongate	72°C	5min
9 Reaction end/hold	4°C	∞

2.2.3 Agarose gel electrophoresis

DNA fragments and PCR products were resolved on 0.8% (w,v) agarose gels. Agarose (Bioline, BIO41025) was dissolved in 1x Tris-Acetic acid-EDTA (TAE) buffer by heating in a microwave to boiling point. Once cooled but prior to setting ethidium bromide or SYBR™ Safe (Thermo Fisher Scientific, S33102) was added (1:1000) to a final concentration of 0.5µg/ml and mixed in gently to avoid bubbles before being poured into a gel casting tray. Samples were loaded after addition of 6x DNA loading buffer (Thermo Fisher Scientific) and run alongside 10-15µl of molecular weight marker (GeneRuler 1kb Plus DNA Ladder, Thermo Fisher Scientific, SM1331) at 120V with 1x TAE as the running buffer. DNA was visualised under UV light using a ChemiDoc™ XRS+ imaging system or Syngene G:Box Chemi XRQ gel imaging system.

2.2.4 Cloning

2.2.4.1 Plasmids

Plasmids used are shown in Table 7 along with the restriction enzymes used to insert the fragments into the associated vector. Where the source states 'constructed' these plasmids were either subcloned or made by PCR for this project.

2.2.4.2 Gel purification of DNA fragments

DNA fragments were resolved by agarose gel electrophoresis (see 2.2.3) and the desired band excised from the gel using a sterile scalpel under UV visualisation. DNA was then extracted from the gel using the QIAquick gel extraction kit (Qiagen, 28706) to manufacturer's instructions. DNA was eluted in 30µl elution buffer (EB buffer) and stored at -20°C.

2.2.4.3 Restriction enzyme digests of DNA

For digestion reactions 1µg of the backbone vector DNA was digested in a 20µl reaction and the entire 30µl elution for the inserts was digested in a 50µl reaction. Glycerol concentrations of the final reactions were no more than 10%. Digests were carried out in a 37°C water bath for 1h. Double digests were performed sequentially; both enzymes were incubated for 1h at 37°C with a 20 min incubation using a heat block at 65°C to inactivate the first restriction enzyme before the second enzyme was added. Digestion of a vector backbone with a single restriction enzyme was followed by alkaline phosphatase, calf

intestinal (CIP, New England Biolabs, M0290S) treatment to prevent relegation of the vector to itself. Following digestion 0.2µl CIP was added and the reaction was incubated for a further 30min at 37°C. Digested (and treated) DNA fragments were then resolved by agarose gel electrophoresis and gel purified.

Table 6 - PCR primers for cloning and sequencing

Restriction endonuclease sites are underlined. Bases in italics and underlined constitute Fbxl17 specific shRNA segment.

PRIMERS	Sequence 5'-3'
Fbxl17 sequencing primers	
Fbxl17 seq F1	GAA GTC TCT TCC TGG CCA GCT TG
Fbxl17 seq F2	ACT GAT GAA GGA CTC AAG CAG CTG
Fbxl17 seq R1	TTC CGC TTG CAC ACC ATT TCG
Fbxl17 654 R	TGA CGA TCA TGC CTT CAT CT
Deletion of F-box domain	
ΔF box R1	CCA AAA CTG GAA CTG GTT GAT GTC TGG GGT TTC GGG
ΔF box F1	GAC ATC AAC CAG TTC CAG TTT TGG AAG CAG CTG GAT
XhoI kozak Flag F	CGTT <u>CTCGAG</u> CACC ATGGACTACAAGGACGACGAC
HpaI Fbxl17 aa701 Rev	CG <u>GTTAAC</u> CTA GGA GGA GGC GGC AGA CAT
Fbxl17 shRNA construction	
mir30 forward	CAG AAG GCT CGA GAA GGT ATA TTG CTG TTG AC AGT GAG CG
mir30 reverse	CTA AAG TAG CCC CTT GAA TTC CGA GGC AGT AGG CA
mir30 sequencing	CCA GGT TAA GAT CAA GGT CTT TTC ACC
Fbxl17 GFP fusion construction	
XhoI Fbxl17 F	CGTT <u>CTCGAG</u> CCA TGG GCC ACC TTC TCT CG
Fbxl17 EcoRI R	GGAC <u>GAATTC</u> GGG AGGA GGC GGC AGA CAT G
GST Fbxl17 from aa321	
EcoRI Fbxl17 Fbox F	CGG AAT TCA AAT GAT CAA CCA GCT GCC
Removing tag from Uap1	
BamHI Uap1 F	CGTT <u>GGATCC</u> ATG AAC ATT AAT GAC CTC AAA CTC ACG TTG TCC
UAP1 NotI R	CTTA <u>GCGGCCGC</u> TCA AAT ACC ATT TTT CAC CAG CTC ATG
Fbxl17 shRNA templates	
Fbxl17 shRNA1	TGCTGTTGACAGTGAGCG <u>CGGATAGTAACTGGTCAGGATATAGTGAAGCCACAGATGTATATCCTGACCAGTTACTATCCATGCCTACTGCCTCGGA</u>
Fbxl17 shRNA2	TGCTGTTGACAGTGAGCG <u>CGCTTTCTGACACCTCTATTATTAGTGAAGCCACAGATGTAA</u> <u>TAATAGAGGTGTCAGAAAGCTTGCCTACTGCCTCGGA</u>
Fbxl17 shRNA3	TGCTGTTGACAGTGAGCG <u>CCCTGTAATCTTTAGATGGTTATAGTGAAGCCACAGATGTA</u> <u>TAACCATCTAAAGATTACAGGTTGCCTACTGCCTCGGA</u>

Table 7 - Plasmids used in this dissertation

NAME	VECTOR	INSERT	SOURCE
pcDNA3 EV	pcDNA3	-	Invitrogen
pcDNA3 FLAG		FLAG	From Dr W. Breitwieser
pcDNA3 HA		HA	From Dr S. Flach
Fbxl17 WT		FLAG-Fbxl17 (1-701aa)	
Fbxl17 (Δ Fbox)		FLAG-Fbxl17 Δ F box (Δ 324-358)	See section 2.2.2
Fbxl17 (Δ 3LRR)		FLAG-Fbxl17- Δ 3LRR (1-586aa)	From Dr S. Flach
Fbxl17 (Δ 10LRR)		FLAG-Fbxl17- Δ 10LRR (1-384aa)	
Fbxl17 WT		HA-Fbxl17 (1-701aa)	Cloned from pcDNA3 FLAG Fbxl17 vector
Uap1		Uap1	PCR cloned from pcDNA3 HA Uap1 into pcDNA3
Uap1		HA-Uap1	From Dr S. Flach
Skp1		Skp1	Laman lab
Rbx1		Myc-Rbx1	Laman lab
Cullin 1		Cullin1	Laman lab
Sufu		HA-Sufu	From Dr V. D'Angiolella
DDB1		FLAG-DDB1	From Dr S. Khoronenkova
-	LMP-IRES-GFP	-	From Dr S. Lowe
Fbxl17 shRNA1		Fbxl17 shRNA1	See section 2.1.6
Fbxl17 shRNA2		Fbxl17 shRNA2	
Fbxl17 shRNA3		Fbxl17 shRNA3	
53BP1	pCMH6K	53BP1 (1-1972bp)	From Dr Y. Galanty [249]
53BP1 Δ BRCT		53BP1 Δ BRCT (1-1710bp)	
53BP1 N term.		NLS 53BP1-N terminus (1-1052bp)	
53BP1 C term.		53BP1 C-terminus (1052-1972bp)	
53BP1 BRCT		53BP1 BRCT only (1483-1972bp)	
53BP1 C term. Δ BRCT		53BP1 C-terminus Δ BRCT (1052-1710bp)	
Ubiquitin	pCMV	6xHis-Myc-Ubiquitin	Laman lab
Venus EV	pVenus-N1	-	Laman lab
Fbxl17 WT		Fbxl17 (1-701aa)	From Dr S. FLach
GFP EV	pEGFP-C1	-	From Dr. P D'Avino
Fbxl17 WT		GFP-FBXL17 (1-701aa)	Subcloned
Ku70 (XRCC6)		GFP-Ku70 (XRCC6)	From Dr Y. Galanty
Ku80 (XRCC5)		GFP-Ku80 (XRCC5)	
Fbxl17_Skp1	pGEX (KG)	GST-Fbxl17 (321-701aa) Fbox to end_IRES Skp1	Laman lab
Fbxl17 WT	pGEX-6P-2	GST-Fbxl17 (321-701aa) F-box to end	PCR cloned from pcDNA3 WT
Fbxl17 (Δ 10LRR)		GST-Fbxl17 (321-384aa) F-box to Δ 10	PCR cloned from pcDNA3 WT
Skp2		GST-Skp2 full-length	Laman lab

2.2.4.4 Ligation

Ligation reactions were carried out in a total of 20µl using 0.5µl T4 DNA ligase (New England Biolabs, M0202L) per reaction and 2µl T4 DNA ligase buffer (10x). Ligation reactions were incubated at room temperature (RT) for a minimum of 20 mins with a vector to insert ratio of 1:3 most commonly used as well as a no insert, vector only control to determine ligation efficiency.

2.2.4.5 Transformation of bacteria with plasmid DNA

To transform bacteria with plasmid DNA 50µl aliquots of chemically competent *E.coli* cells (Subcloning Efficiency™ DH5α™ Competent Cells, Thermo Fisher Scientific, 18265017) were thawed on ice from -80°C, one aliquot per ligation reaction. The entire 50µl of cells was added to the ligation reaction and mixed gently with the end of the pipette. The cells plus ligation mix were incubated on ice for at least 20 min, heat-shocked in a water bath at 42°C for 45 seconds then returned to ice for at least 2 min prior to plating on LB-Agar plates with added Ampicillin antibiotic (1µl/ml of stock: 100mg/ml) under sterile conditions. Plates were incubated at 37°C overnight (O/N). The following day colonies were isolated for preparation of plasmid DNA.

2.2.4.6 Preparation of plasmid DNA

Isolated bacteria colonies from a transformation plate were used to inoculate 3ml of 2xTY liquid culture media with added Ampicillin (1µl/ml of stock: 100mg/ml) and incubated O/N at 37°C with shaking. Around 16 hours later plasmid DNA was extracted using the QIAprep Spin Plasmid Kit (Qiagen, 27104) according to manufacturer's instructions. DNA was eluted in 50µl of EB buffer and 1µl was then taken for a test restriction enzyme digest and run on an agarose gel to check for the presence of the desired insert. Plasmids verified by the test digests were then sent for Sanger sequencing. 0.2µl of this plasmid DNA was used to transform bacteria (see 2.2.4.5), colonies were then used to inoculate 100ml of 2xTY (+ ampicillin, 100µl/ml) cultured O/N at 37°C with shaking. Plasmid DNA was then prepared using the QIAGEN Plasmid Midi Kit (Qiagen, 12143) according to manufacturer's instructions. DNA was eluted in 400µl EB buffer and DNA concentration was determined using a NanoDrop™ Lite Spectrophotometer (Thermo Fisher Scientific) before storing at -20°C.

2.3 BIOCHEMISTRY

2.3.1 Protein extraction and quantification

For western blots, cells were washed once in PBS after media had been removed and trypsinised as described previously. Cells were collected in 15ml Falcon tubes and spun down at 300G for 3min. Cells were washed once more in PBS and spun again and pellets resuspended in 50µl RIPA lysis buffer (25mM Tris-HCl pH7.6, 150mM NaCl, 1% NP-40, 1% sodium deoxycholate, 0.1% SDS) plus additional protease inhibitors (Protease inhibitor cocktail (Sigma, P8340) 1:100, 1mM Na₃VO₄, 10mM NaF, 1mM PMSF). Samples were vortexed briefly and then incubated on ice for 30min. Lysates spun again at 13000rpm for 15 mins to pellet cell debris, supernatant removed to fresh tube and protein concentration determined by BCA assay (Pierce™ BCA Protein Assay Kit, Thermo Fisher Scientific, 23227). Samples diluted in Laemmli buffer (125mM Tris pH 6.8, 4% SDS, 20% Glycerol, 10% β-mercaptoethanol, 0.02% Bromophenol Blue) and boiled 95°C 10min prior to loading.

2.3.2 Western blotting

Proteins were separated on the basis of molecular weight by sodium dodecyl sulphate polyacrylamide gel electrophoresis (SDS-PAGE) using a 30% (w,v) acrylamide/methylene bisacrylamide solution (37.5:1 ratio) (National diagnostics, EC890). Different percentage gels were run depending on the molecular weight of the proteins to be resolved. Gels were run in a 1x Tris-Glycine-SDS PAGE running buffer (National Diagnostics, B9-0032) at 60V until the protein had migrated through the stacking gel, and then at 120V until good separation was achieved. Proteins were then transferred onto polyvinylidene fluoride (PVDF) membrane using a Trans-Blot® SD Semi-Dry Transfer Cell system (BioRad). Blots were blocked for 1 hour in 5% dried skimmed milk powder in 1x PBS-T (1x PBS, 0.05% TWEEN® 20) or 3% BSA before probing overnight with primary antibody (Ab) diluted in 5% milk or 1% BSA, 4°C with rocking. The following day blots were washed 3 x 5min in 1x PBS-T on gyro rocker, incubated at RT with secondary Ab diluted in 5% milk for 1h and then washed a further 3 times in 1xPBS-T. Amersham enhanced chemiluminescence (ECL) Western Blotting Detection Reagent (GE Healthcare Life Sciences) and X-ray film (Konica) were used for signal detection.

2.3.2.1 Gradient gels

For the separation of 53BP1 constructs, samples were loaded on Novex™ 4-20% Tris-Glycine Mini Gels (ThermoFisher, XP04200BOX) and run in 1x Tris-Glycine-SDS as described above (2.3.2) using an XCell SureLock Mini-cell electrophoresis system (ThermoFisher). For optimum protein transfer, proteins were transferred to PVDF membrane using a wet/tank transfer method (BioRad), 250mA with stirring, 4°C, overnight. The following day membranes were blocked for 1 hour in 5% milk and incubated for a minimum of 3 hours in primary antibody before detection of proteins with secondary antibody conjugated to HRP.

2.3.3 GST protein purification

Chemically competent *E.coli* strain FB810 cells were transformed with GST DNA constructs by heat shock (42°C for 45s). Transformed cells were grown in 200ml cultures of 2xTY media containing ampicillin (100µg/ml) to log phase (~OD₆₀₀ 0.3-0.6) at 37°C. Once at the required density cultures were cooled on ice for 10 minutes. Recombinant protein expression was induced by addition of 1mM isopropyl-β-D-1-thiogalactopyranoside (IPTG) for 3 hours at 30°C. Bacteria were harvested by centrifugation (4500 rpm, 10 min) and resuspended in 5ml Tris buffered saline (TBS) plus protease inhibitors (cOmplete™ EDTA free protease inhibitor cocktail, Roche, 118733580001), lysozyme (from chicken egg white, Sigma, L6876) and 1mM PMSF. Cells were incubated on ice for 20 minutes followed by sonication (3 cycles of 15 seconds at 10 microns). 250µl Triton X-100 (VWR, 28817.295) was added and tubes inverted 4 times to mix. Cell debris was removed by centrifugation (18000 xg, 4°C, 30min) and the supernatant incubated with rotation, overnight at 4°C with 100µl of TBS/1% Triton X-100 and Glutathione-Sepharose 4B beads (GE Healthcare, 17075601) at a 50% slurry. Purified proteins, bound to beads, were harvested by centrifugation (1200 rpm, 4°C, 5min) and washed twice in TBS/1% Triton X-100 and twice in PBS, and resuspended in PBS as a 50% slurry. Ten microlitre samples were added to equal volumes of 2x Laemmli buffer and denatured at 95°C for 5mins. Proteins were resolved by SDS-PAGE and the gel stained with Quick Coomassie stain (Generon, GEN-QC-STAIN) to visualise proteins. Equal protein loads were estimated, and equivalent input volumes used in a GST pull-down assay.

2.3.4 GST pull-down assay

One microgram of pcDNA3 Uap1 (or empty pcDNA3 control) were used to express proteins *in vitro* using the TnT Quick Couple Transcription/Translation System (Promega, L1170)

according to manufacturer's instructions. The reticulocyte lysates were diluted in Alternative binding buffer (20mM Hepes-KOH pH7.6, 50mM KCl, 2.5mM MgCl₂, 10% glycerol, 0.02% NP-40, 1mM PMSF, 1mM DTT) to a final volume of 260µL. Diluted lysate was centrifuged (13,000 rpm, 15-30min, 4°C) and 50µL of diluted lysate was added to equal amounts of GST proteins bound to beads. Samples were rotated for 2h at 4°C. Beads were then washed five times with 10x volume of wash buffer, NET-N (50mM Tris pH7.5, 1mM EDTA, 1% NP-40, 150mM NaCl) and resuspended in 40µL 2x Laemmli buffer. Equal volumes of samples were then analysed by immunoblotting.

2.3.5 Co-Immunoprecipitation

2.3.5.1 FLAG Co-IP

Cells were transfected or infected as described previously and lysed in 500µl/90mm plate modified RIPA buffer (25mM Tris HCl pH 7.6, 150mM NaCl, 1% NP-40, 0.1% SDS) with additional protease inhibitors (see 2.3.2). Samples incubated on ice for 10mins with occasional vortexing. NaCl added to 150mM and incubated for a further 5min on ice. Lysates spun at 13,000rpm 15mins at 4°C. 50µl supernatant kept for total lysate sample, remainder added to 20µl/90mm plate ANTI-FLAG® M2 Affinity gel (Sigma, A2220) beads washed 3x with lysis buffer. Beads and lysates were incubated rotating at 4°C for 4hrs. Beads then washed 3x in lysis buffer, spinning down at low speed (2000rpm 1min) in between washes. 50µl Laemmli (1:1 ratio) added to total lysate sample and 40µl added to beads to elute proteins. Samples boiled 95°C for 3min prior to loading of equal volumes for western blot analysis.

2.3.5.2 Normal Co-IP

Lysates prepared as described above in modified RIPA buffer. After spinning at 13,000rpm 15min at 4°C 50µl supernatant kept for total lysate sample, remainder added to 20µl/90mm plate. Protein A/G PLUS agarose beads (Santa Cruz) washed 3x with lysis buffer. Beads and lysates incubated rotating at 4°C for 1hr to preclear lysates. Beads then spun down at low speed (2000rpm 1min) and lysate added to fresh Eppendorfs containing 2µg primary antibody (or species IgG control) for 2hrs rotating at 4°C. 20µl/90mm plate of washed Protein A/G PLUS agarose beads added to each tube and incubated for a further 2hrs 4° with rotation. Beads then washed 3x in lysis buffer spinning down at low speed (2000rpm 1min) in between washes 50µl Laemmli added to total lysate sample and 40µl added to beads to

elute proteins. Samples boiled 95°C for 3min prior to loading equal volumes for western blot analysis.

2.3.6 E3 ligase production

HEK293Ts were transfected (PEI mediated) with 5µg pcDNA3 Fbxl17 constructs and 1.7µg of each ligase component (Rbx1, Skp1, Cul1). 48h after transfection cells lysed and FLAG Co-IP performed as described previously. After 4h incubation beads washed 3x with lysis buffer and 2x with FLAG elution buffer (10mM Hepes, 225mM KCl, 1.5mM MgCl₂, 0.1% NP-40, protease inhibitors, phosphatase inhibitors). FLAG peptide (Sigma) diluted to 500µg/ml in FLAG elution buffer, 100µl added to beads and incubated 2h 4°C with rotation after removing buffer from washes. Beads pelleted and eluate recovered. Samples frozen in a final 15% Glycerol solution at -20°C.

2.3.7 *In vitro* ubiquitination assay

A screen of 10 different E2 enzymes determined that E2 UbcH5a enabled the most specific SCF^{Fbxl17} activity and was used in subsequent experiments. Purified SCF complexes at 12.5, 25, 50 and 100 nM were tested in the presence of a ubiquitin-mix (ubiquitin buffer, ubiquitin (20µM) E1 (UBE1,100nM), E2 (UbcH5a, 500nM) and Mg-ATP (2mM) (Boston Biochem) incubated at 30°C for 90min to determine ligase activity by auto ubiquitination. 50nM of the SCF was sufficient for ligase activity and used in subsequent experiments. To test substrate ubiquitination substrates were transfected into HEK293T cells and immunoprecipitated using their indicated epitope tags conjugated to agarose beads. The purified substrate was then eluted from the beads and added as a component of the ubiquitin-mix. HA-Sufu was kindly provided by Vincenzo D'Angiolella (CRUK/MRC Oxford Institute for Radiation Oncology, Oxford, UK). Ubiquitination was detected by probing for the substrate or HA tag (for Sufu).

2.3.8 *In vivo* ubiquitination assay

HEK293T cells were transfected with expression constructs of interest, including myc-ubiquitin, and treated with 10 µM MG132 (Sigma-Aldrich) 4 hr prior to lysis. UAP1 was then immunoprecipitated with Monoclonal Anti-HA-Agarose antibody (Sigma-Aldrich). Modified UAP1 was detected with an endogenous UAP1 antibody. To test for phosphorylation 10mM β-glycerophosphate was added to the LB or washed Anti-HA-Agarose beads were CIP treated, 15 min, 37°C.

2.3.9 Metabolites extraction and LC-MS analysis

Cells were washed three times with PBS prior to the extraction and 1 ml of extraction buffer (50% LC-MS grade methanol and 30% acetonitrile, 20% ultrapure water) was added per 1×10^6 cells. Cells were then incubated on dry ice for 15 min, collected, kept under vigorous shaking for 15 min at 4°C, and left for 1-hour incubation at 20°C. Samples were centrifuged at 13,000 rpm and supernatants were transferred to autosampler vials for LC-MS analysis. To avoid bias due to machine drift and processed blindly, samples were randomized. Q Exactive mass spectrometer (Thermo Fisher Scientific) coupled to a Dionex U3000 UHPLC (Thermo Fisher Scientific) system was used to perform the LC-MS analysis. Sequant ZIC-pHILIC column (150mm x 2.1 mm) and guard column (20mm x 2.1 mm) (Merck Millipore) were utilized for the chromatographic separation and the column oven temperature was maintained at 40°C. The mobile phase was composed of 20mM ammonium carbonate and 0.1% ammonium hydroxide in water (solvent A), and acetonitrile (solvent B). The flow rate was set at 200 ml/min and the gradient was programmed as follows: initially stayed at 20% of A and 80% of B for 2 min, then subjected to a linear increase to 80% of A and decrease to 20% of B in 15 min. Both solvents were then brought back to initial condition and stayed for 8 min. The mass spectrometer was operated in full MS and tSIM (targeted Single Ion Monitoring), in positive and negative mode. XCalibur Qual Browser and XCalibur Quan Browser software (Thermo Fisher Scientific) were used to acquire the spectra and analyse the data.

2.4 MICROSCOPY

2.4.1 Immunofluorescence

U2OS cells were seeded onto glass coverslips and transfected 24h later with FLAG-Fbx17 constructs. 48h post-transfection cells were washed in ice cold PBS, fixed in 4% PFA (in PBS) RT for 10min, permeabilised in 0.1% Triton X-100 (in PBS) RT for 10min and blocked in 0.2% fish skin gelatine (in PBS) for 30min. Endogenous Fbx17 was immunostained with anti-Fbx17 antibody and exogenous constructs with anti-FLAG antibody, both diluted in 0.2% fish skin gelatine. After 1h cells were stained with Alexa Fluor 488 conjugated secondary antibodies. Coverslips were then washed in PBS-T and ddH₂O and mounted using 50% glycerol (in PBS) containing 1µg/ml DAPI counterstain. Images were collected using a Zeiss Confocal LSM700 Laser Scanning Microscope and ZEN imaging software.

2.4.2 Laser micro-irradiation

U2OS cells stably expressing RFP-53BP1 were seeded onto glass bottomed plates (Mattek) and pre-sensitised with 10µM BrdU. 24h later, the cells were transfected with GFP-Fbx17 or GFP empty vector. 48h post transfection, fresh prewarmed, CO₂ adjusted media supplemented with 10% FBS and 1% pen/strep was added to the U2OS cells. Localised lines of DNA-damage were induced by laser micro-irradiation using a Zeiss Confocal LSM700 Laser Scanning Microscope equipped with a Solent heated environmental chamber. To induce localised DNA damage a stripe of 5-pixel width was irradiated with a 405nm laser diode (laser set to 100%, 50 iterations, pixel dwell time 12.61 µsec) on regions of interest in the nucleus. Cells were observed at regular time points after DNA damage (every 1min) or after 10min.

2.6 ANTIBODIES***Table 8 - Primary antibodies used for immunoblotting***

Antibody	Species	Company (ID)	Dilution
53BP1	Rabbit polyclonal	Novus (MB100-304)	1:5000
Actin	Rabbit polyclonal	Sigma (A2066)	1:5000
Cul1	Rabbit polyclonal	Santa Cruz (sc-11384)	1:1000
Fbxl17	Rabbit polyclonal	Genetex (GTX119211)	1:2000
Flag tag	Mouse monoclonal	Sigma (F3165)	1:5000
GAPDH	Rabbit polyclonal	Sigma (g9545)	1:5000
GFP	Mouse monoclonal	Santa Cruz (sc-9996)	1:1000
HA tag	Rabbit monoclonal	Cell Signaling (3724S)	1:1000
Histone H1	Mouse monoclonal	Santa Cruz (sc-8030)	1:1000
myc tag	Rabbit polyclonal	Cell Signaling (2272)	1:1000
OGA/MGEA5	Rabbit monoclonal	Abcam (ab124807)	1:5000
O-GlcNAc	Mouse Monoclonal	Covance (MMS-248R)	1:1000
OGT	Rabbit monoclonal	(Abcam) ab177941	1:1000
Skp1	Mouse monoclonal	BD (610530)	1:1000
Uap1	Rabbit polyclonal	Abcam (ab95949)	1:1000
Uap1	Rabbit polyclonal	Bethyl Laboratories (A305-643A-M)	1:1000
Ubiquitin	Mouse monoclonal	Santa Cruz (P4D1, sc8017)	1:1000

Table 9 - Secondary antibodies and normal IgG used for immunoblotting/ IP

Antibody	Species	Company (ID)	Dilution
Anti-mouse IgG HRP	donkey	Jackson ImmunoResearch (711-035-150)	1:5000
Anti-mouse IgG HRP	goat	Santa Cruz (sc-2055)	1:10,000
Anti-rabbit IgG HRP	donkey	Jackson ImmunoResearch (711-035-152)	1:5000
Anti-rabbit IgG HRP	donkey	Santa Cruz (sc-2313)	1:10,000
-	Mouse IgG	Santa Cruz (sc-2025)	N/A
-	Rabbit IgG	Santa Cruz (sc-2027)	N/A

Table 10 - Antibodies used for immunohistochemistry

Antibody	Species	Company (ID)	Dilution
Anti-mouse IgG AlexaFluor488	donkey	Invitrogen (A21206)	1:500
Anti-rabbit IgG AlexaFluor488	donkey	Invitrogen (A-21206)	1:500
Fbxl17	Rabbit polyclonal	Genetex (GTX119211)	1:100
Flag tag	Mouse monoclonal	Sigma (F3165)	1:100

2.7 SOLUTIONS

10x PBS

PBS-T

1x PBS, 0.05% Tween-20

TAE

40mM Tris pH8, 20mM glacial acetic acid, 1mM EDTA

TBS

50mM Tris pH7.6, 150mM NaCl

TBS-T

1x TBS, 0.1% Tween-20

NET-N (*for GST pull-down washes*)

50mM Tris pH7.5, 1mM EDTA, 1% NP-40, 150mM NaCl

2x Laemmli buffer

125mM Tris pH 6.8, 4% SDS, 20% Glycerol, 0.02% Bromophenol Blue, 10%, β -Mercaptoethanol

RIPA buffer (lysis)

25mM Tris-HCl pH7.6, 150mM NaCl, 1% NP-40, 1% Sodium deoxycholate, 0.1% SDS

Diehl buffer (lysis)

50mM Tris-HCl pH7.6, 150mM NaCl, 1% NP-40, 0.1% SDS

KCl buffer

50mM Tris HCl pH7.5, 225mM KCl, 1% NP-40

Elution buffer (*elution of immunoprecipitates from FLAG/HA beads*)

10mM Hepes, 225mM KCl, 1.5mM MgCl₂, 0.1% NP-40

Buffer A (*cell fractionation*)

10mM Hepes pH7.9, 10mM KCl, 1.5mM MgCl₂, 0.34M Sucrose, 10% Glycerol, 1mM DTT, 0.1mM PMSF

Annexin V binding buffer

10mM Hepes, 140mM NaCl, 2.5mM CaCl₂

Alternative binding buffer (for GST pull-down)

20mM Hepes pH7.6, 50mM KCl, 2.5mM MgCl₂, 10% Glycerol, 0.02% NP-40, 1mM DTT, 1mM PMSF

PI staining solution

1x PBS, 100 µg/ml RNase A, 50 µg/ml propidium iodide

Fixing/Staining solution (For Clonogenic assay)

1X PBS, 0.05% w/v Crystal Violet, 1% Formaldehyde, 1% Methanol

3

CHARACTERISING BREAST CANCER-ASSOCIATED REARRANGEMENTS OF FBXL17

CHAPTER 3 - Characterising breast cancer-associated rearrangements of *FBXL17*

3. INTRODUCTION

A vast amount of data regarding mutations in cancer genomes has been published. However, analysis of such data is laborious and in many cases much of the data remains uncharacterised. Massively-parallel paired-end sequencing has overcome this problem somewhat and whilst once believed to be confined largely to leukaemias and sarcomas, somatic rearrangements are now being shown to be prevalent in breast cancer and other epithelial cancers [18-21]. Genome-sequencing of cancers previously favoured point mutations over structural rearrangements due to ease of analysis by PCR and array CGH [14], but genomic rearrangements can now be resolved to much better resolution thanks to advances in sequencing techniques. A few common large-scale rearrangements have been known for some time, but many more aberrations found in 5-10% cases remain to be described and may be diagnostically or therapeutically important.

Previous work in the lab surveying the METABRIC (Molecular Taxonomy of Breast Cancer International Consortium) dataset, which contains array-CGH copy number data for 1,992 primary breast tumours, identified *FBXL17* as being highly rearranged in breast cancer [29]. 135 (7%) tumours had at least one genomic break within *FBXL17*, detected as a copy number step, distributed in various ways. The majority of copy number losses or gains identified in *FBXL17* occurred at the 3' end, with small deletions clustered around exon 4 and potential tandem duplications observed [255]. *FBXL17* encodes the 701 amino acid (aa) F-box protein, Fbxl17, which can function as a substrate-determining component of an SCF-type E3 ubiquitin ligase. It binds Skp1 via its characteristic F-box domain and recruits substrates for ubiquitination via its C-terminal leucine rich repeat domains (LRRs) (Figure 1. 9, Page 46). Given the LRRs of Fbxl17 are encoded from exon 3 onwards it is likely these protein-protein interacting domains are disrupted by such rearrangements.

In addition to breaks in tumours, array-CGH data showed breaks in *FBXL17* in four cancer cell lines, the breast carcinoma cell lines, BT-474, HCC38, and HCC1395, and the oesophageal/gastric cardia adenocarcinoma line OE-19 [32]. The breaks were verified by FISH, RT-PCR and paired-end sequencing and included an *FBXL17-PJA2* fusion transcript reported in [256] and an internal homozygous deletion in *FBXL17* between exons 6 and 9

[19, 32]. The *FBXL17-PJA2* fusion in HCC38 cells, which joins exon 1 of *FBXL17* to exon 2 of *PJA2*, is not in frame at the *PJA2* portion, and so would encode an Fbxl17 that retains most of the N-terminal domain (1-331aa) but only a partial F-box domain and no LRRs. Deletion of exons 7 and 8 in HCC1395 cells would truncate Fbxl17 at its C-terminus after LRR8, resulting in loss of 3 LRRs ($\Delta 583-655$ aa).

As demonstrated, at least some of these detected breaks truncate Fbxl17 at its C-terminus, removing some or all of the LRRs and sometimes also the F-box domain. I have identified further examples of *FBXL17* rearrangements in breast cancer, in paired-end whole-genome DNA and RNA sequencing data from primary breast tumours, which also seem to target the LRR domain. These genomic alterations suggest the ability of Fbxl17 to recruit substrates for ubiquitination or to form part of an SCF complex may be compromised. To study this further I have investigated the effect of loss of LRRs on Fbxl17 expression, localisation and ligase activity in order to characterise the functional consequences of these novel genomic rearrangements recurring in breast tumours and determine the role that they play in breast cancer. Some of the data in this chapter is included in a manuscript published in *Cellular and Molecular Life Sciences*, which can be found in Appendix B [255].

3. RESULTS

3.1 Fbxl17 is rearranged in primary breast tumours

The array-CGH data for *FBXL17* from the METABRIC dataset clearly demonstrated that *FBXL17* is highly rearranged in breast cancer. However, the exact consequences of the rearrangements could not be concluded due to the absence of paired-end next generation sequencing (NGS) data. Equally the cell line examples, despite mirroring the tumour data, may not accurately reflect the mutations that occur in primary tumours. We therefore looked for examples of *FBXL17* rearrangements in breast cancers, in paired-end whole-genome DNA sequencing data from 250 primary breast tumours of the Cambridge Personalised Breast Cancer Programme. Rearrangements ('Structural variants') in *FBXL17* were identified by collaborators in 5 of the tumours (Appendix A). Manual inspection of RNA sequences from these 5 tumours confirmed that 2 of the rearrangements were transcribed as predicted: a translocation joining exon 6 to an undocumented exon on chromosome 7 and a duplication of exon 6, respectively (Figure 3. 1A; Appendix A). A third case with a breakpoint in intron 6 showed unspliced transcription from exon 6 into intron 6, however, we cannot rule out that this was normal unspliced RNA. Serendipitously, a further RNA sample, inspected because it had a rearrangement which did not pass filtering, showed splicing from exon 6 into exon 4. This suggested the presence of a rearrangement, which was not detected by DNA sequencing in an additional tumour. The partial agreement we find between RNA and DNA sequencing is expected as both methods lack sensitivity to identify all rearrangements [257]. Thus, consistent with the cell line rearrangements, the breakpoints in the tumours fell within introns that would disrupt the expression of LRRs, with the majority (4/6) occurring in intron 6 (Figure 3. 1B).

There was no clear relationship between *FBXL17* rearrangement and any molecular classification [30] of the tumours and cell lines, although 5/6 tumours and the breast cell lines were *TP53* mutant (Figure 3. 2A, Appendix A). Of the tumours, three were oestrogen receptor (ER) positive, and three were ER-negative. One tumour and one cell line were ERBB2/HER2 positive (Figure 3. 2A, Appendix A). We also classified these tumours into the 11 IntClust sets [30], and they fell into three sets: clusters 4, 7 and 10. In addition, classifying these six cases using PAM50 breast cancer subtyping, gave four basal and two luminal A cases (Appendix A). Although the number of cases is small, these data suggest Fbxl17 is not rearranged in a particular cancer subtype.

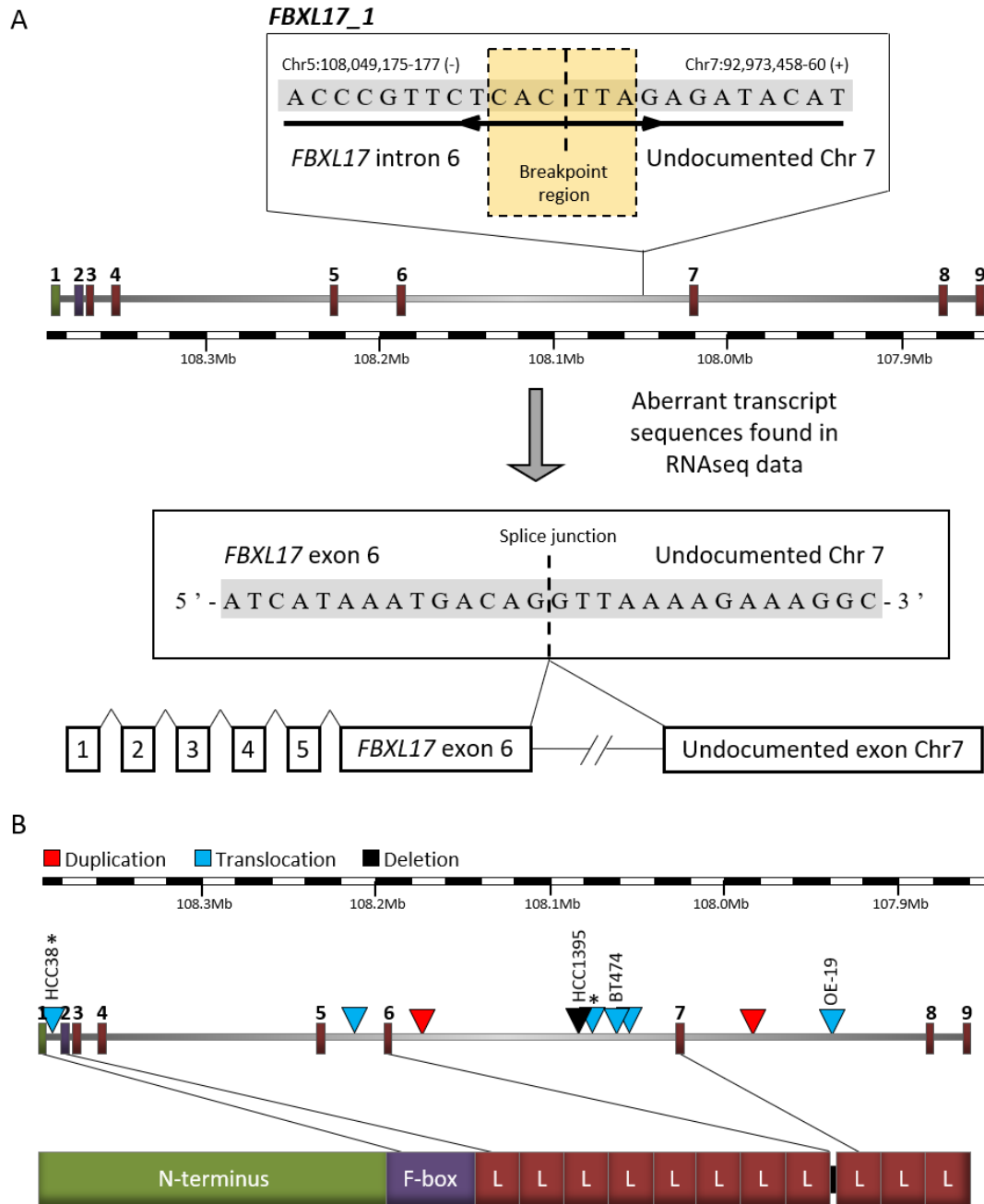


Figure 3. 1 - *FBXL17* is rearranged in primary breast tumours.

(A) Schematic of structural variant found in case *FBXL17_1* shows a breakpoint sequence between intron 6 of *FBXL17* and an undocumented region on chromosome 7. The corresponding spliced mRNA transcript sequence identified from paired RNAseq data shown below, indicates splicing from exon 6 of *FBXL17* to an undocumented exon on chromosome 7 resulting in a fusion protein of unknown length. **(B)** *FBXL17* exons from Ensembl transcript ENST00000542267.5 (Refseq NM_001163315.2, NP_001156787.2), chr5:107,859,045-108,382,098 in GRCh38/hg38. Triangles indicate breakpoints in *FBXL17* identified in cell lines (as labelled) or primary breast tumours (unlabelled), * indicates known fusion. Bottom, protein domains of *Fbx17* scaled to protein sequence. L, leucine-rich repeat.

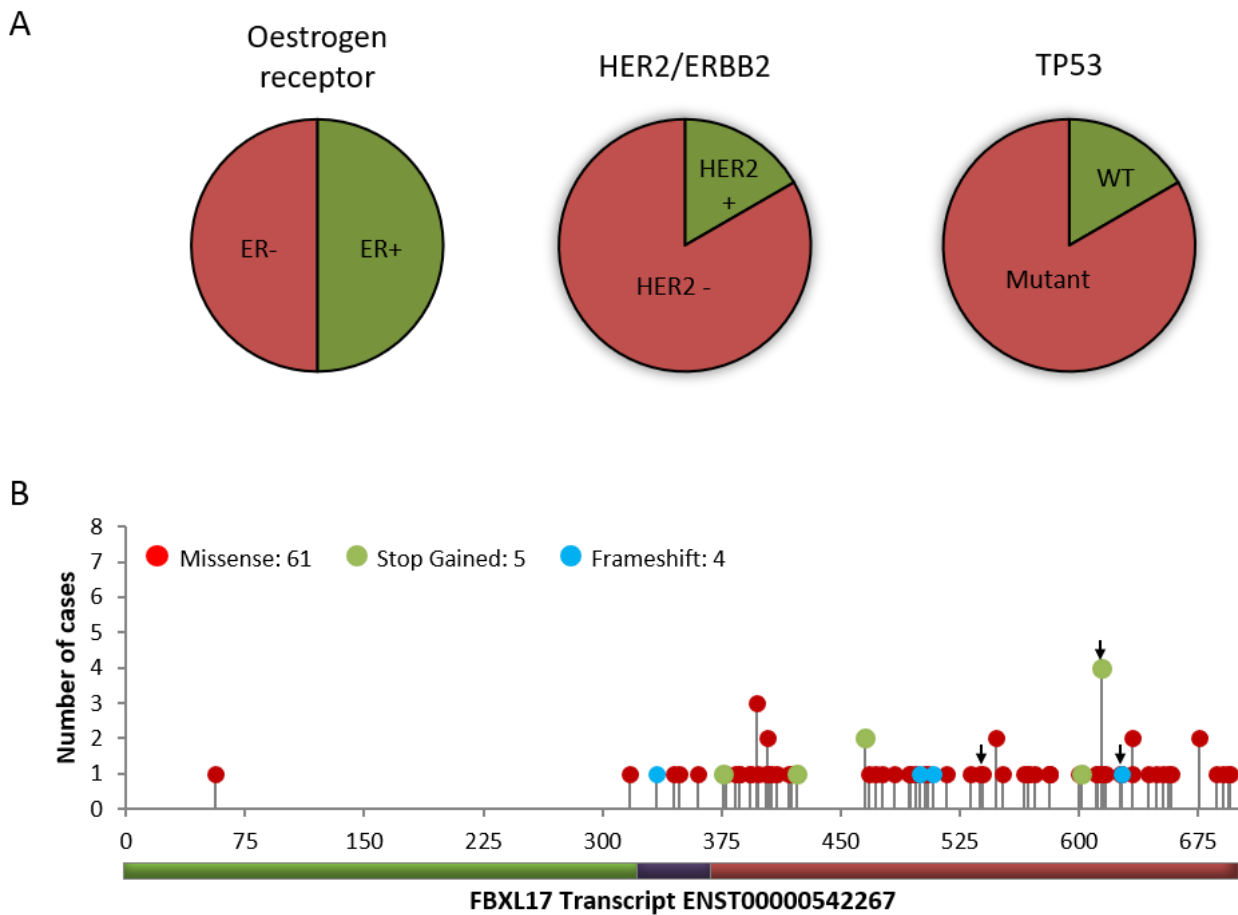


Figure 3. 2 - *FBXL17* is rearranged in primary breast tumours and mutations cluster in the LRRs of *Fbxl17*.

(A) Molecular classification of the primary breast tumours containing *FBXL17* rearrangements with regards to Oestrogen receptor (ER), HER2/ERBB2 expression and TP53 status (WT=wild-type), $n=6$. **(B)** Non-synonymous somatic mutations mapped to *Fbxl17* as reported by The Cancer Genome Atlas (TCGA), arrows indicate breast cancer associated mutations. Schematic underneath represents *Fbxl17* domains, green, N-terminus, purple, F-box domain, red, leucine-rich repeats.

Rearrangements of *FBXL17* have also been detected in other epithelial cancers including prostate [258] and oesophageal adenocarcinoma [259]. Many of these rearrangements are also predicted to truncate Fbxl17, resulting in loss of LRRs. TCGA (Cancer Genome Atlas project) data was mined for genomic alterations affecting *FBXL17* using the National Cancer Institute GDC Data portal (<https://portal.gdc.cancer.gov/>) [260, 261]. Perhaps most striking was the TCGA mapping of non-synonymous somatic *FBXL17* mutations. Mutations in *FBXL17* almost exclusively (68/70) target its C-terminus containing the FBD and LRRs; with five resulting in premature stop codons that would truncate the LRR domains of Fbxl17 (Figure 3.2B).

In summary, *FBXL17* was identified as being frequently rearranged in primary breast tumours and cancer cell lines by array-CGH and FISH analysis. I have identified further rearrangements in six primary breast tumours, which have been validated by paired DNA and/or RNA sequencing data. I have shown that at least some of the breaks truncate Fbxl17, resulting in loss of the LRRs and sometimes also the FBD. These genomic alterations suggest the ability of Fbxl17 to recruit substrates for ubiquitination may be altered or lost and the SCF activity of Fbxl17 may be compromised.

3.2 WT and mutant Fbxl17 expression and localisation

3.2.1 Truncation of Fbxl17 LRRs enhances protein expression

Full-length Fbxl17 (1-701aa) and two LRR-truncation constructs, Fbxl17 Δ 3LRR (1-586aa) and Fbxl17 Δ 10LRR (1-384aa), were cloned into pcDNA3 expression vectors with an N-terminal FLAG-tag by a previous graduate student S. Flach (Figure 3. 3). The Δ 3LRR mutant is representative of the *FBXL17* rearrangements observed in the breast cell line HCC1395 and primary breast tumours, i.e. deletion of exons 7 and 8 or breaks in intron 6, both of which would truncate Fbxl17 by 3LRRs. Fbxl17 Δ 10LRR is representative of the Fbxl17-PJA2 fusion observed in HCC38 cells. The fusion is not in frame and so would encode an Fbxl17 that retains most of the N-terminal domain but only a partial F-box domain and no LRRs. The first LRR of Fbxl17 overlaps slightly with the FBD and so, unlike in HCC38 cells, this was not removed in Fbxl17 Δ 10LRR to ensure the FBD remained intact. To be able to test the ubiquitin ligase activity of SCF^{Fbxl17} I also generated an Fbxl17 construct containing an internal F-box domain deletion (Δ 324-358aa) by two-step PCR to act as a negative control. The F-box domain binds to Skp1 to enable SCF holoenzyme assembly and so deletion should render Fbxl17 incapable of recruiting other components of the SCF complex. This construct was also cloned into pcDNA3 with an N-terminal FLAG-tag (Figure 3. 3).

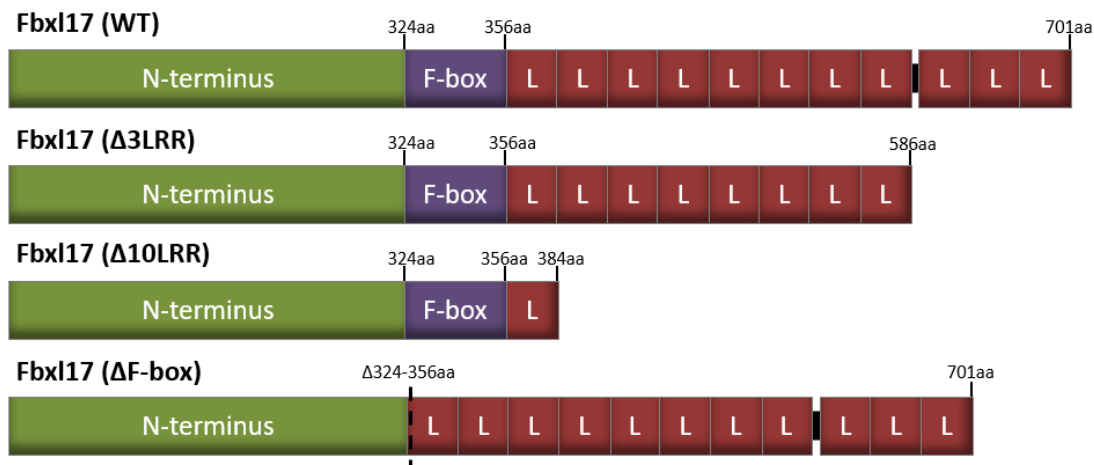


Figure 3. 3 - Schematic of wild-type Fbxl17 domains and mutant constructs.

Wild-type (WT) Fbxl17 contains an N-terminus (green) of mostly unknown function. The characteristic F-box domain (purple) binds Skp1 to enable the SCF holoenzyme formation. At its C-terminus, Fbxl17 contains 11 leucine rich repeats (LRRs, L, red) through which it binds target substrates. Fbxl17 Δ 3LRR contains the first eight LRRs and Fbxl17 Δ 10LRR just a single LRR. The Δ F-box mutant removes the F-box domain preventing SCF assembly. All constructs contain a FLAG tag at their N-terminus.

To test whether the Fbxl17 constructs could be expressed in mammalian cells, I transfected HEK293T cells with Fbxl17 WT, Δ Fbox, Δ 3LRR and Δ 10LRR. All constructs were expressed, and I noted truncation of LRRs resulted in increased expression of Fbxl17 (Figure 3. 4A). This increased expression appears to correlate with the number of LRRs lost. The higher molecular weight bands present in the Δ 10LRR lane are indicative of ubiquitination. This suggests the cells are targeting Fbxl17 Δ 10LRR for degradation.

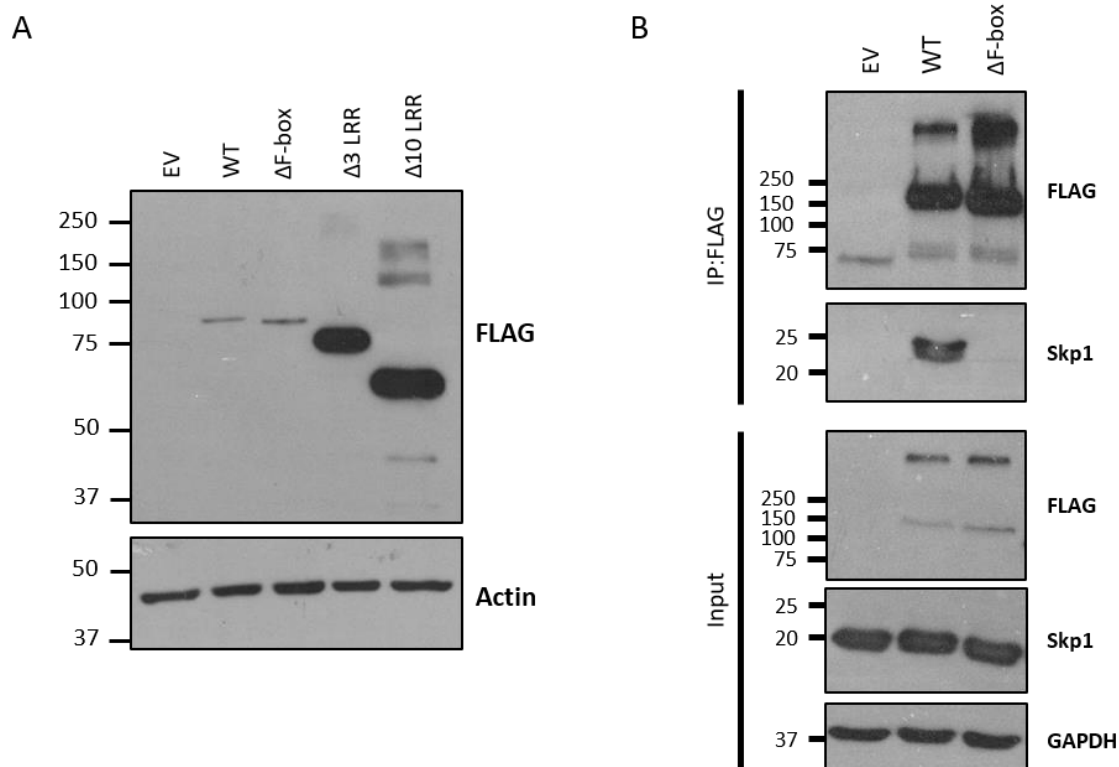


Figure 3. 4 - Expression of Fbxl17 constructs and Δ Fbox Co-IP with Skp1.

(A) Protein lysates from HEK293T cells transfected with the indicated Fbxl17 constructs resolved by SDS-PAGE and immunoblotted with the indicated antibodies. **(B)** Immunoprecipitates using anti-FLAG beads from HEK293T cells expressing FLAG-Fbxl17 or FLAG-Fbxl17 Δ Fbox, probed for Skp1 and FLAG.

3.2.2 Deletion of the F-box domain of Fbxl17 abolishes Skp1 binding

To test whether the Fbxl17 Δ Fbox construct binds Skp1, I performed a co-immunoprecipitation assay. HEK293T cells were transfected with Fbxl17WT, Fbxl17 Δ Fbox or an empty vector. Forty-eight hours post-transfection cells were lysed, immunoprecipitated with FLAG antibodies and blotted for endogenous Skp1. Whilst WT Fbxl17

immunoprecipitated endogenous Skp1, deletion of amino acids 324-358 of Fbxl17 abolished binding to Skp1 (Figure 3. 4B). Failure to bind Skp1 will prevent SCF complex assembly rendering Fbxl17 Δ Fbox enzymatically inactive.

3.2.3 Fbxl17 mutant constructs show wild-type localisation

Cellular fractionation and immunofluorescence assays were conducted in parallel to determine the distribution of WT and mutant Fbxl17 proteins in cells. Endogenous Fbxl17 was present in both cytoplasmic and nuclear fractions with greater expression observed in the nuclear fraction (Figure 3. 5). However, in the absence of a cytoplasmic marker we cannot be certain the fractionation is clean. Immunofluorescence showed all transfected Fbxl17 constructs showed a predominantly nuclear localisation as observed with endogenous Fbxl17 immunostaining and concurrent with the fractionation data (Figure 3. 6).

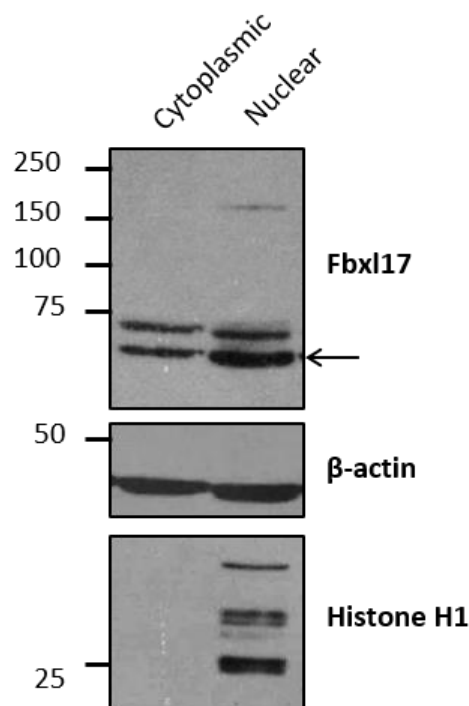


Figure 3. 5 - Cellular fractionation of endogenous Fbxl17 and Fbxl17 constructs.

Cellular fractionation of MCF7 cells immunoblotted for indicated proteins, n=2. Arrow represents bands corresponding to Fbxl17. Histone H1 used as a nuclear fraction marker, β-actin used a loading control.

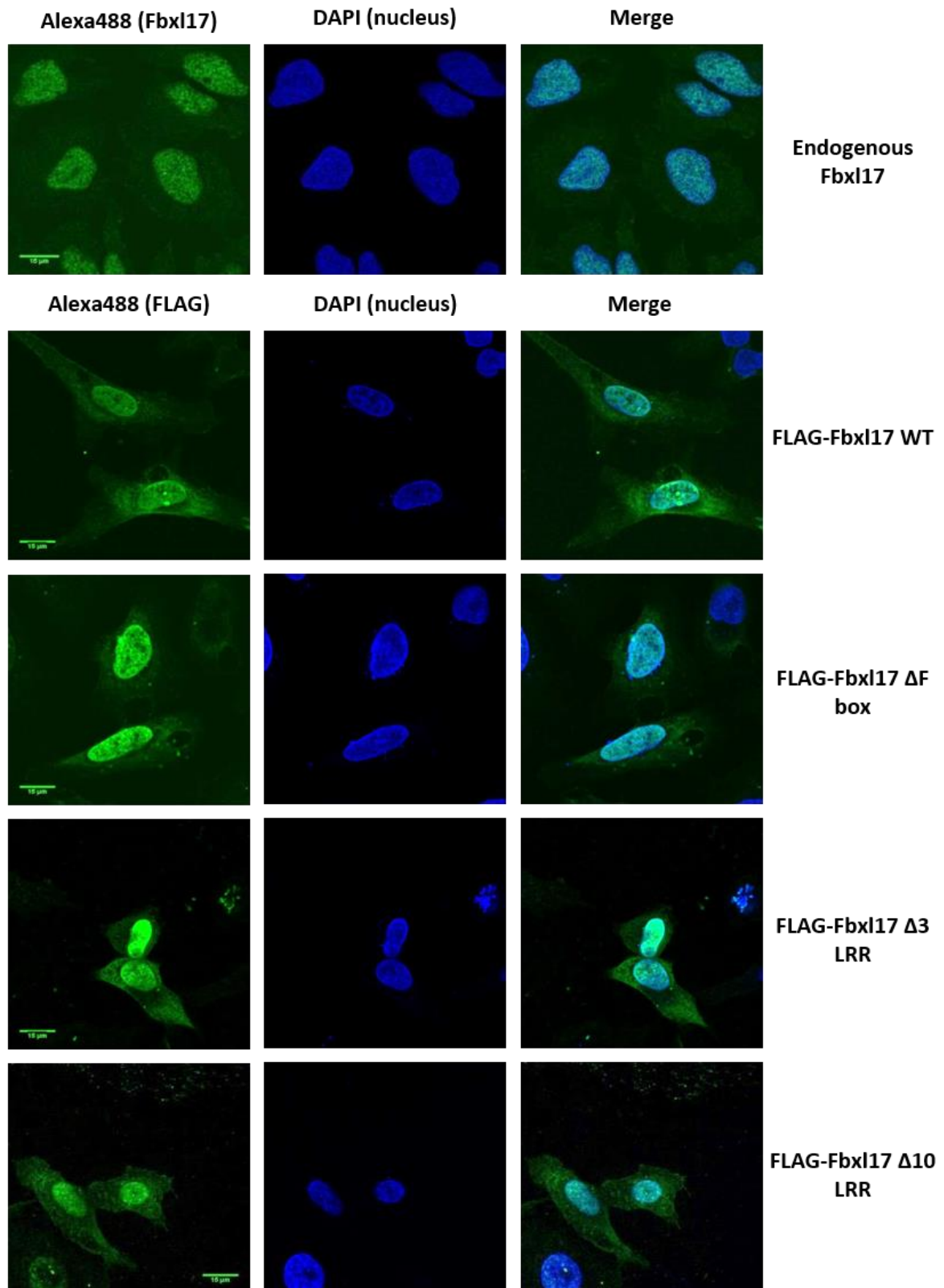


Figure 3. 6 - Subcellular localisation of Fbxl17 and Fbxl17 constructs.

Confocal microscopy images of endogenous Fbxl17 and indicated FLAG-Fbxl17 constructs using immunostaining with Fbxl17/FLAG antibodies and Alexa Fluor 488. DNA visualized with DAPI, scale bar is 15µm.

3.3 WT and mutant SCF^{Fbxl17} purification and characterisation

3.3.1 Deletion of LRRs impairs SCF subunit recruitment

To check the incorporation of Fbxl17, WT and mutant, into an SCF E3 ligase I used co-immunoprecipitation assays. HEK293T cells were transfected with N-terminally FLAG-tagged Fbxl17 constructs (WT, Δ Fbox, Δ 3LRR or Δ 10LRR) and also co-transfected with the SCF subunits, Skp1, Cullin1 and Rbx1. Forty-eight hours post transfection, cells were lysed, immunoprecipitated with FLAG antibodies, and blotted for the associated SCF subunits (Figure 3. 7). While Skp1, Rbx1 and Cullin1 co-immunoprecipitated efficiently with WT Fbxl17, these components were reduced in the immunoprecipitates of the truncation mutants when normalised to Fbxl17 expression. This was somewhat surprising given that

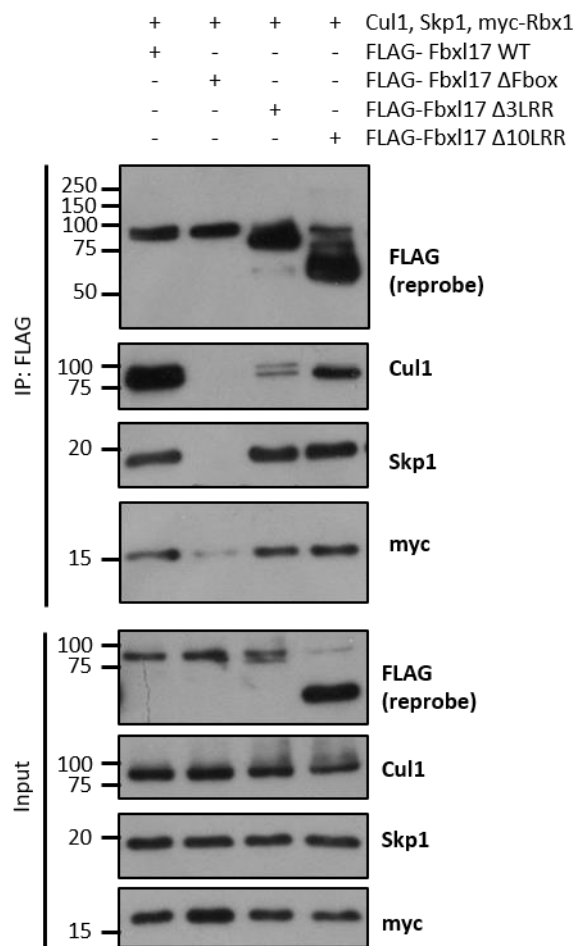


Figure 3. 7 - Co-immunoprecipitation of Fbxl17 wild-type and mutant constructs with SCF ligase components.

Immunoprecipitates using anti-FLAG beads from HEK293T cells expressing FLAG-Fbxl17, FLAG-Fbxl17 Δ Fbox, FLAG-Fbxl17 Δ 3LRR or FLAG-Fbxl17 Δ 10LRR, probed for Cul1, Skp1 and myc-tag (Rbx1).

Fbxl17 Δ 3LRR and Fbxl17 Δ 10LRR contained intact F-box domains. As expected, when the FBD was deleted in Fbxl17 Δ Fbox, Cul1 and Skp1 were not co-immunoprecipitated and binding to Rbx1 was significantly reduced. The faint myc-tag band present in the Δ Fbox lane could be an artefact as Cullin1 is responsible for recruiting Rbx1 to the SCF complex and was not co-immunoprecipitated with Fbxl17 Δ Fbox in this assay. It could also represent a direct interaction between the FBP and Rbx1. My data suggests the presence of unknown stabilising interactions between the LRRs and Cullin 1 and so Rbx1 may also have a cryptic binding site on Fbxl17.

Since these interaction data indicated differential capabilities of the Fbxl17 mutants to assemble the SCF enzyme, I next tested the Fbxl17 ligase activity *in vitro* by purifying SCF^{Fbxl17} ligase complexes from cells. As described above, I transfected HEK293T with the subunits of SCF ligases, Skp1, Cullin1, Rbx1, and the FLAG-tagged Fbxl17 constructs (WT, Δ Fbox, Δ 3LRR or Δ 10LRR). Forty-eight hours post-transfection, cells were lysed, immunoprecipitated with FLAG antibodies and then eluted from the FLAG agarose beads with FLAG peptide. Purified SCF E3 ubiquitin ligases were resolved by SDS-PAGE, stained with Coomassie and quantified by densitometry in relation to BSA standards (Figure 3. 8A). Purified ligases were also resolved by SDS-PAGE and immunoblotted for SCF holoenzyme components (Figure 3. 8B). Following purification of equal amounts of Fbxl17 we observed the recruitment of SCF subunits by mutant Fbxl17 proteins was again significantly reduced. For example, Cullin1 binding to Fbxl17 Δ 3LRR was reduced by 81% ($p=4.12\text{E-}04$; $n=4$) and Fbxl17 Δ 10LRR by 82% ($p=1.28\text{E-}06$; $n=4$) relative to WT Fbxl17, while Skp1 binding to Fbxl17 Δ 3LRR was reduced by 77% ($p=5.52\text{E-}05$; $n=5$) and Fbxl17 Δ 10LRR by 67% ($p=2.74\text{E-}05$; $n=4$) relative to WT Fbxl17 (Figure 3. 8C). These data indicate that in addition to the FBD, the LRRs of Fbxl17 facilitate or stabilise the assembly of the SCF^{Fbxl17} ligase. Since the Cullin1 and Rbx1 subunit allow E2 recruitment, these data suggest that the mutant SCF^{Fbxl17} ligases will have reduced activity.

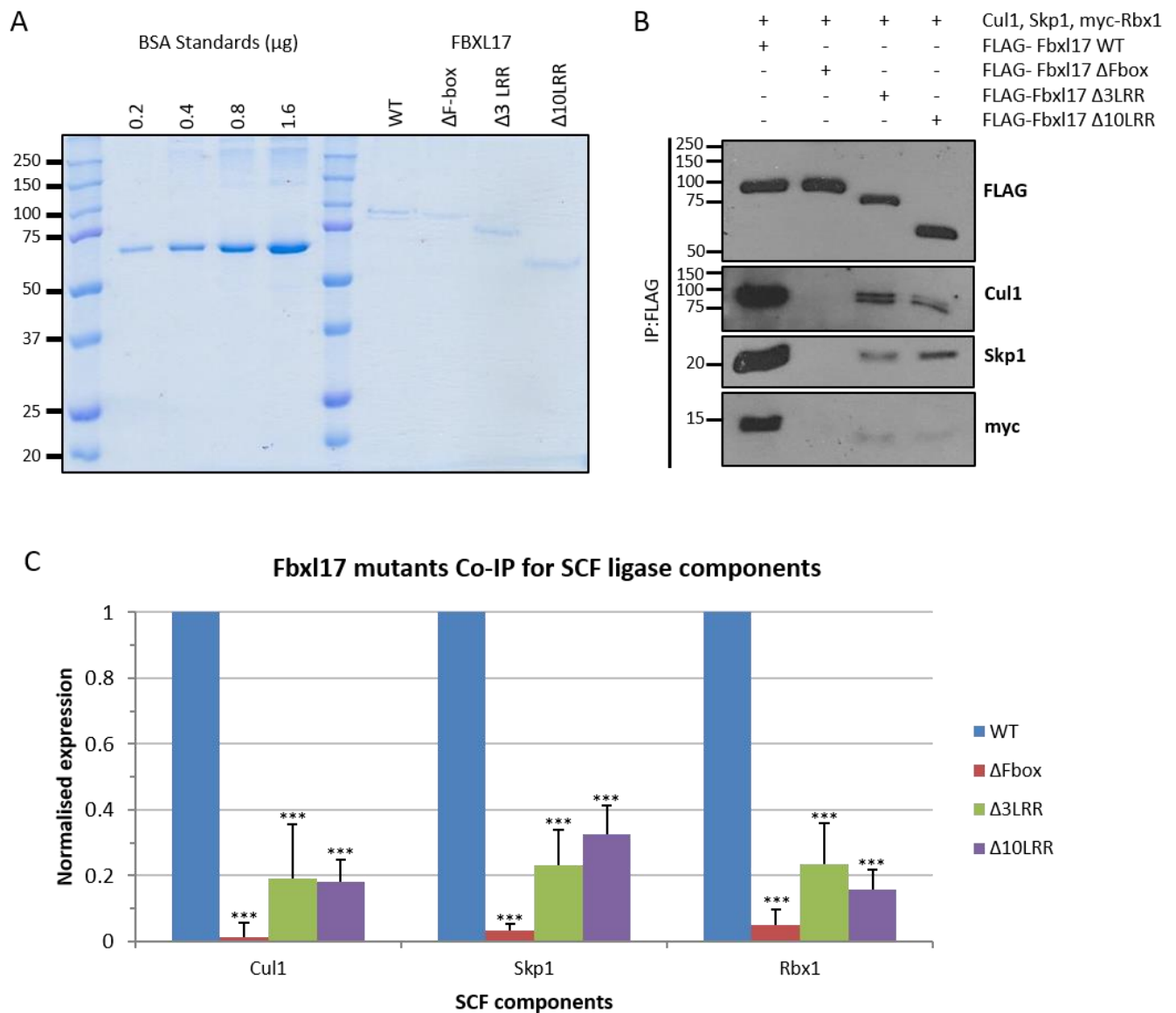


Figure 3. 8 - Loss of Fbx17 LRRs impairs SCF subunit recruitment.

(A) Coomassie gel of purified SCF ligases and BSA standards used for quantification by densitometry. **(B)** Representative immunoblot for SCF holoenzyme components that co-immunoprecipitate with purified FLAG-Fbx17 and mutant Fbx17 constructs; FLAG-Fbx17 ΔFbox, FLAG-Fbx17 Δ3LRR and Fbx17 Δ10LRR. **(C)** Expression of SCF components Cul1, Skp1 and Rbx1 that co-immunoprecipitate with WT and mutant Fbx17 constructs. Normalised to WT expression. Mean ± SEM, $n \geq 3$, *** $p < 0.001$ compared to WT.

3.3.2 Auto-ubiquitination assays

To test the activity of SCF^{Fbxl17} ligases I performed *in vitro* ubiquitination assays of purified SCF complexes, assembled with either WT or LRR-truncated Fbxl17 proteins, in the presence of an E1 and E2 enzyme. To begin with I screened six different E2 enzymes to determine which would have specific ubiquitination activity with SCF^{Fbxl17}. Purified SCF^{Fbxl17} and SCF^{Fbxl17ΔFbox} were added to a ubiquitin mix (ubiquitin buffer, ubiquitin, E1 (UBE1), E2 (various) and ATP) and incubated to allow auto-ubiquitination of Fbxl17. Samples were resolved by SDS-PAGE and immunoblotted for ubiquitin (Figure 3. 9). UbcH2 and UbcH3 showed little to no activity with Fbxl17. UbcH6 showed non-specific ubiquitination activity and residual activity with the negative control SCF^{Fbxl17ΔFbox} (Figure 3. 9, UbcH6 panel, lanes 1 and 5) so was not selected. UbcH5a, 5b and 5c all showed robust ubiquitination activity with SCF^{Fbxl17} and no activity with SCF^{Fbxl17ΔFbox} (Figure 3. 9). UbcH5a was selected for use in all subsequent assays since it demonstrated the highest levels of activity of the three E2 ubiquitin ligases.

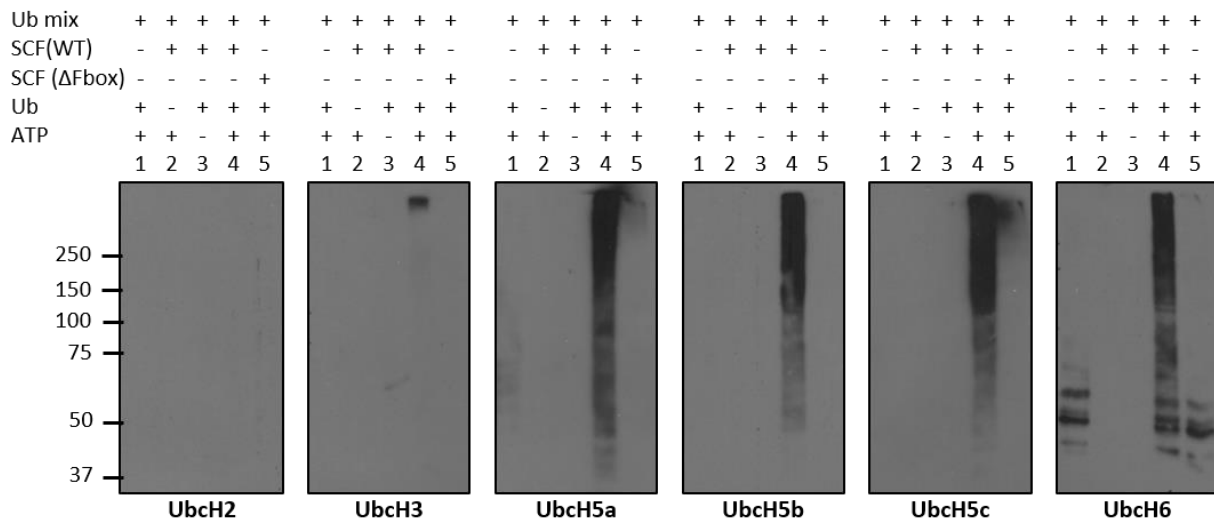


Figure 3. 9 - E2 ligase activity screen for Fbxl17.

Screen of *in vitro* ubiquitination activity of purified SCF^{Fbxl17} complexes with various E2 ligases. Probed with anti-Ub antibody to detect ubiquitinated proteins, n=2.

A

12.5nM							25nM							50nM							100nM						
+							+							+							+						
+							+							+							+						
+							+							+							+						
+							+							+							+						
+							+							+							+						
+							+							+							+						
1	2	3	4	5	6	7	1	2	3	4	5	6	7	1	2	3	4	5	6	7	1	2	3	4	5	6	7

Ubiquitin mix
SCF complex
Ubiquitin
ATP

250
150
100
75
WT
ΔFbox
250
150
100
75
Δ3LRR
Δ10LRR

FLAG

B

12.5nM							25nM							50nM							100nM						
+							+							+							+						
+							+							+							+						
+							+							+							+						
+							+							+							+						
+							+							+							+						
+							+							+							+						
1	2	3	4	5	6	7	1	2	3	4	5	6	7	1	2	3	4	5	6	7	1	2	3	4	5	6	7

Ubiquitin mix
SCF complex
Ubiquitin
ATP

250
150
100
75
WT
ΔFbox
250
150
100
75
Δ3LRR
Δ10LRR

Ubiquitin

(A) Titration of the auto-ubiquitination activity of purified SCF^{Fbx17} ligase complexes. A concentration gradient (12.5nM, 25nM, 50nM, 100nM) of purified SCF^{Fbx17} or mutant complexes SCF^{Fbx17ΔFbox}, SCF^{Fbx17Δ3LRR} or SCF^{Fbx17Δ10LRR} was used in an in vitro ubiquitination assay in the presence of a ubiquitin mix (ubiquitin buffer, UBE1, UbCH5a and ATP). Following SDS-PAGE membranes were probed with anti-FLAG antibody to detect SCF^{Fbx17} ligases, n=2. **(B)** As (A) but probed with anti-ubiquitin antibody, n=2.

3.3.3 Ubiquitination of the Fbxl17 target substrate Sufu

To test whether the ligases made by WT or mutant versions of Fbxl17 could ubiquitinate a heterologous substrate, I performed *in vitro* ubiquitination assays using the published Fbxl17 substrate Sufu (Figure 3. 11) [250]. HA-Sufu was purified from HEK293T cells by immunoprecipitation. High molecular weight smears can be seen after the addition of SCF^{Fbxl17} (Figure 3. 11, lane 4) and to a much lesser extent SCF^{Fbxl17Δ3LRR} (Figure 3. 11, lane 6). Both SCF^{Fbxl17ΔFbox} and SCF^{Fbxl17Δ10LRR} show greatly reduced ubiquitination activity. Together these data indicate the LRRs in Fbxl17 facilitate or stabilise assembly of the SCF E3 ligase and its activity.

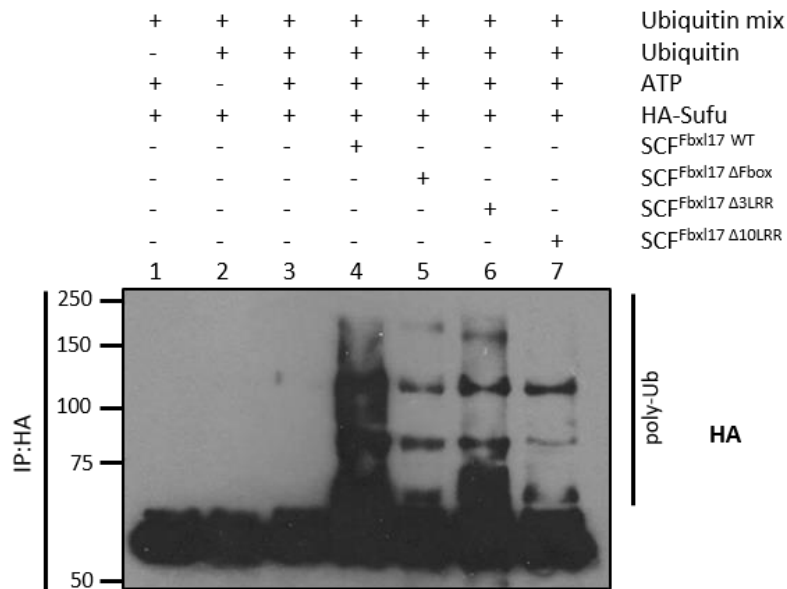


Figure 3. 11 - Loss of Fbxl17 LRRs impairs ubiquitination of the Fbxl17 substrate Sufu.

In vitro ubiquitination assay of SCF^{Fbxl17} and mutant ligase complexes in combination with HA-tagged substrate Sufu in the presence of a ubiquitin mix (ubiquitin buffer, UBE1, UbcH5a and ATP). Proteins resolved by SDS-PAGE and membrane probed with anti-HA antibody, n=3.

3.4 Fbxl17 protein structure prediction

The 3D structure of Fbxl17 is yet to be determined. To better understand how the genomic rearrangements we identified may affect Fbxl17 structure, I used the Robetta protein structure prediction service (<http://new.robetta.org/>) to model the 3D structure of Fbxl17 WT and mutant constructs.

3.4.1 The N-terminus of Fbxl17 is highly disordered

Within the Robetta interface, the DISOPRED3 disorder prediction server estimated that 31% of Fbxl17 is natively unfolded (disordered) (Figure 3. 12). The majority of this disorder occurred at the N-terminus of Fbxl17, which is characterised by low complexity sequence. Disordered regions are usually flexible and dynamic to allow molecular recognition of proteins and nucleic acids [262]. The function of the N-terminus of Fbxl17 is still unknown but it may be important for recruitment of other proteins such as those that regulate Fbxl17 localisation, expression or activity. The nuclear localisation signal (NLS) motif of Fbxl17 is predicted to be at the N-terminus of the protein.

3.4.2 The LRRs of Fbxl17 are highly structured helical repeats

Robetta uses three protein prediction servers to generate secondary structures from protein sequences; Raptor X Property (DeepConcNF) [263], PSIPRED [264] and SPIDER³ [265, 266]. All three approaches show that the LRRs of Fbxl17 are predicted to be a series of helices and β -strands. They show no native disorder suggesting these are highly structured domains (Figure 3. 12).

Comparative modelling by Robetta generated five 3D model predictions for full-length Fbxl17 (1-701aa) (Figure 3. 13A) with a confidence value of 0.50 (scale of 0.0-1.0 where 1.0 is the highest confidence, confidence corresponds to the agreement in structure between the partial threaded models from the top alignment of each independent alignment method). Comparative modelling works on the assumption that proteins with similar sequences that are related evolutionarily will have similar structures [267]. Given that LRRs are a widespread structural motif and the crystal structures for other LRR-family F-box proteins have been resolved [218, 268] it is unsurprising that the prediction error rate for the LRR domains is low compared to the N-terminus of Fbxl17 (Figure 3. 13B). The 3D models for Fbxl17 show a characteristic curved solenoid structure [269]. The concave side of this 'horseshoe' is a series

of parallel β -strands and the convex side is comprised of α -helices. Across all five models, the LRR structure remains largely unchanged but the relative position of the N-terminus varies. This is expected as the N-terminus is natively disordered and therefore predicted to have greater flexibility. Model 5 has the lowest angstrom error estimates across the N-terminus and most of the LRR domains; the lower the angstrom error, the more accurate the 3D position of a particular residue has been predicted, whilst models 1,2 and 4 show a more compact and organised LRR structure with no projecting loops, reflected by low angstrom error estimates across the whole LRR region (Figure 3. 13B). In models 1, 2 and 5 the LRRs of Fbxl17 loop back to remain in close proximity to the N-terminus, which likely offers greater protein stability or may represent an auto-inhibited conformation of Fbxl17 (Figure 3. 13A).

3.4.3 Loss of LRRs changes the predicted 3D structure of Fbxl17

The genomic rearrangements we have observed in Fbxl17 often target the LRRs resulting in complete loss or truncation of this domain. To determine the potential effects of these rearrangements on the 3D structure of Fbxl17, I input the two mutant Fbxl17 sequences into the Robetta prediction server; Fbxl17 Δ 3LRR (1-586aa) and Fbxl17 Δ 10LRR (1-384aa). As with WT Fbxl17, Robetta generated five 3D structure model predictions for Fbxl17 Δ 3LRR and Δ 10LRR with a confidence value of 0.36 and 0.06, respectively (Figure 3. 14 and Figure 3. 15).

All five of the Fbxl17 Δ 3LRR models had similar angstrom error estimate plots, and as with WT Fbxl17 predicted structure, the error estimate was lowest across the F-box domain and LRRs. The eight remaining LRRs of Fbxl17 Δ 3LRR still form the characteristic solenoid shape, but in contrast to WT Fbxl17, the LRRs no longer loop back to remain close to the N-terminus of Fbxl17 (Figure 3. 14). This more open and linear structure may offer less protein stability and may explain the impaired SCF complex assembly observed previously.

The 3D structure of Fbxl17 Δ 10LRR was difficult to model by comparative modelling methods, reflected by the low confidence score (0.06). This is due to a lack of homology of this region to known 3D protein structures. The N-terminus of Fbxl17 is highly disordered, and the five predicted 3D models suggest it contains a number of helices, with model 4 showing the lowest angstrom error estimates across all the models (Figure 3. 15). *Ab initio* modelling was also utilised within the Robetta interface as an alternative to comparative modelling. *Ab initio* or 'from the beginning' methods aim to build 3D models from scratch based on physical principles, such as ensuring hydrophobic residues are buried, rather than making

predictions based on previously solved structures [270]. *Ab initio* modelling improved the confidence score of Fbxl17 Δ 10LRR to 0.12 but the predicted models (not shown) were very similar to those predicted by comparative modelling. It is clear that the structure of Fbxl17 would be drastically altered following loss of 10LRRs. The changes in structure of Fbxl17 caused by loss of LRRs may in part explain the compromised SCF assembly and activity we have observed for the Fbxl17 truncation mutants.

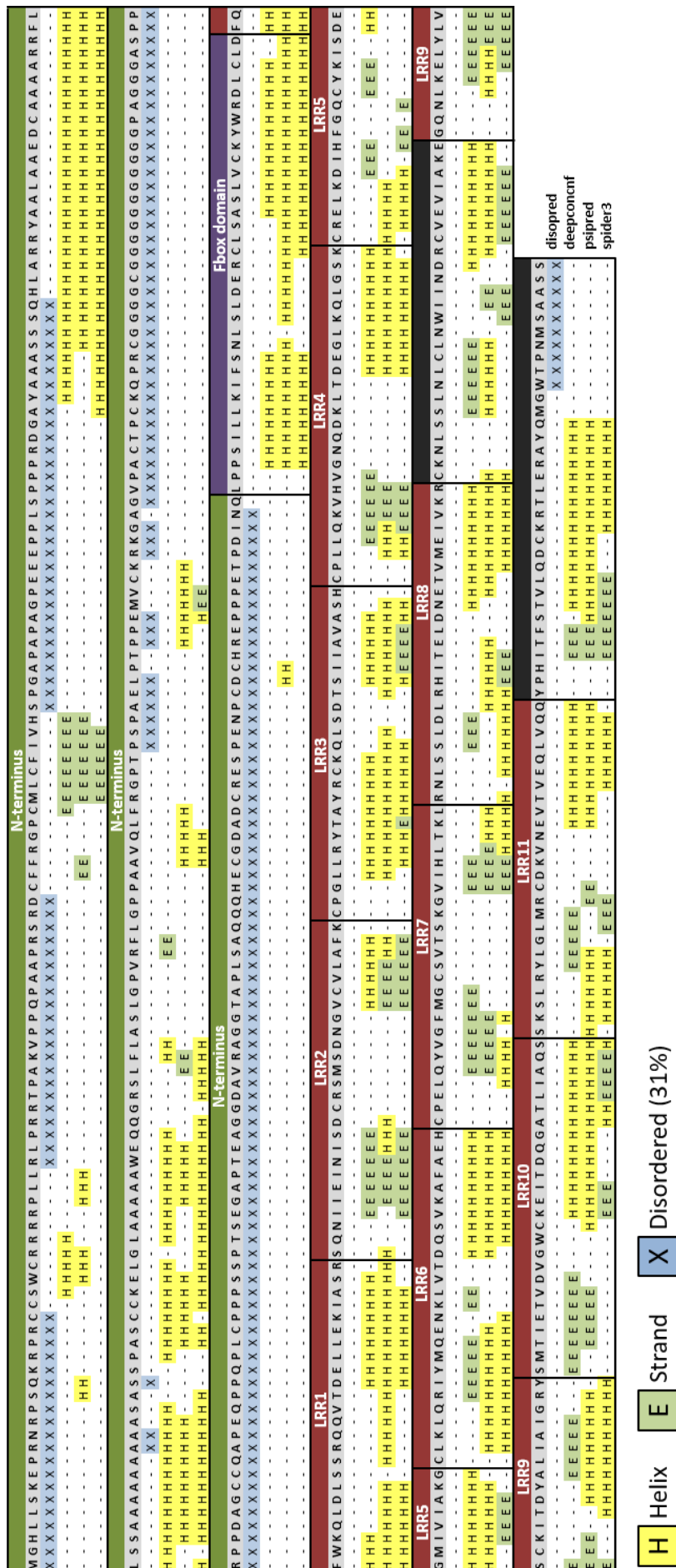
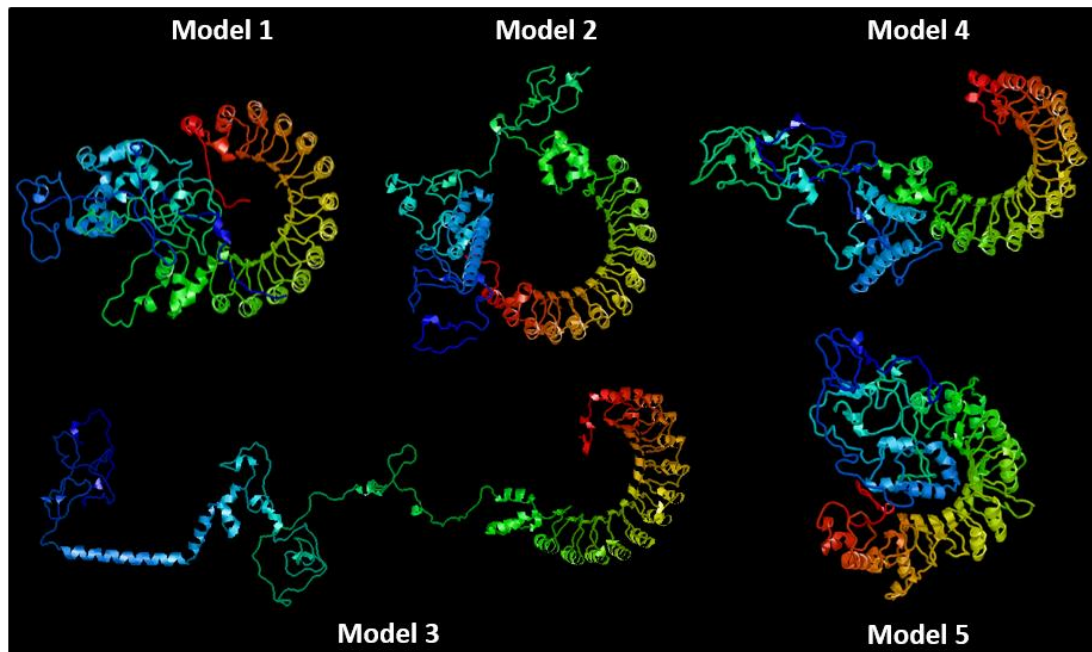


Figure 3. 12 - Fbxl17 secondary structure predictions.

Amino acid sequence for Fbxl17 was submitted to the Robetta protein structure prediction service. The resulting secondary structure predictions from three independent prediction methods have been mapped to Fbxl17 domains. LRR, leucine rich repeat.

A



B

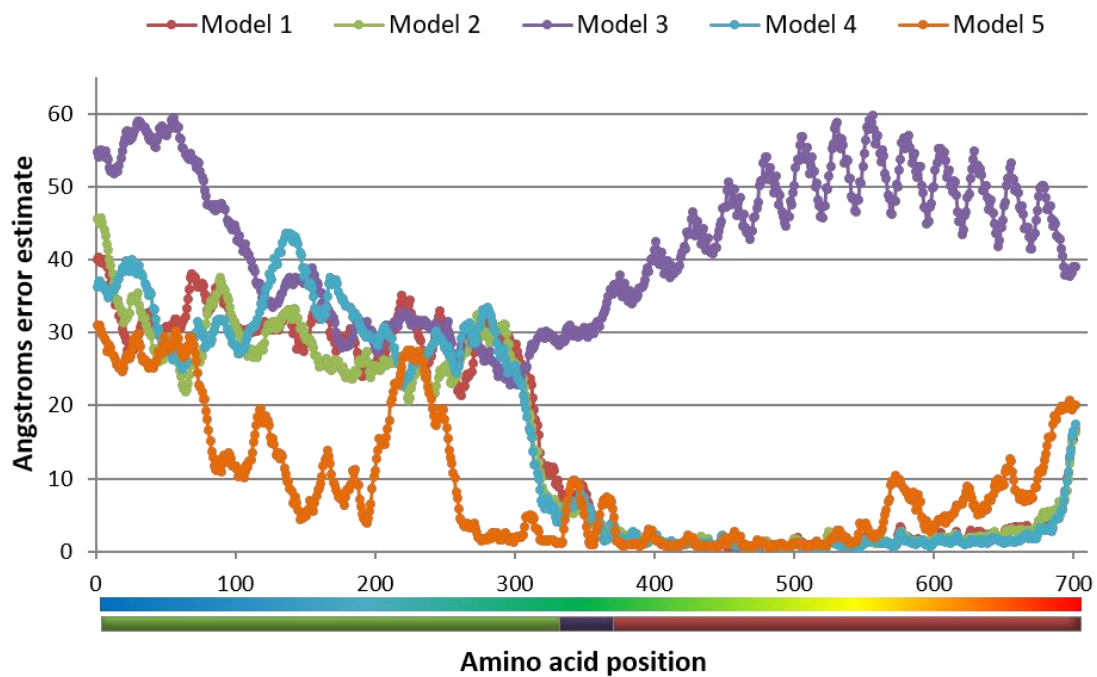
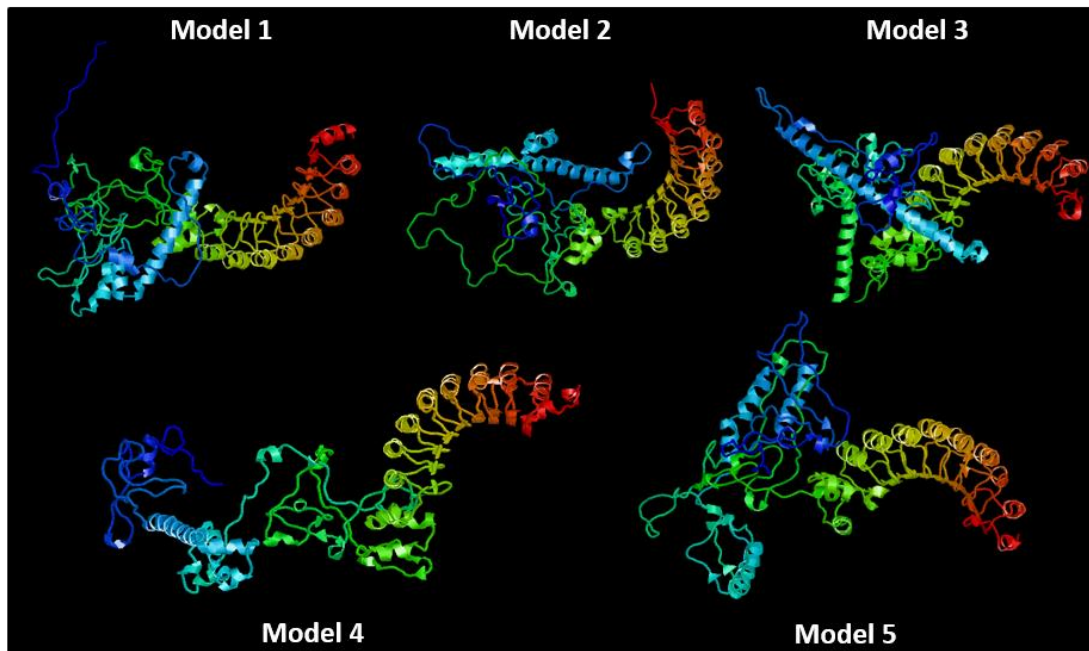


Figure 3. 13 - 3D structure predictions for *Fbxl17* using Robetta protein structure prediction service.

(A) *Fbxl17* 3D structure models generated by comparative modelling. N-terminus, blue; C-terminus, red. **(B)** 3D modelling error in angstroms for each amino acid position of *Fbxl17* for the five Robetta generated 3D models. Schematic underneath represents approximate locations of *Fbxl17* domains (lower rectangle); green, N-terminus; purple, F-box domain; red, leucine rich repeats, mapped to spectrum colouring used in (A) (top rectangle).

A



B

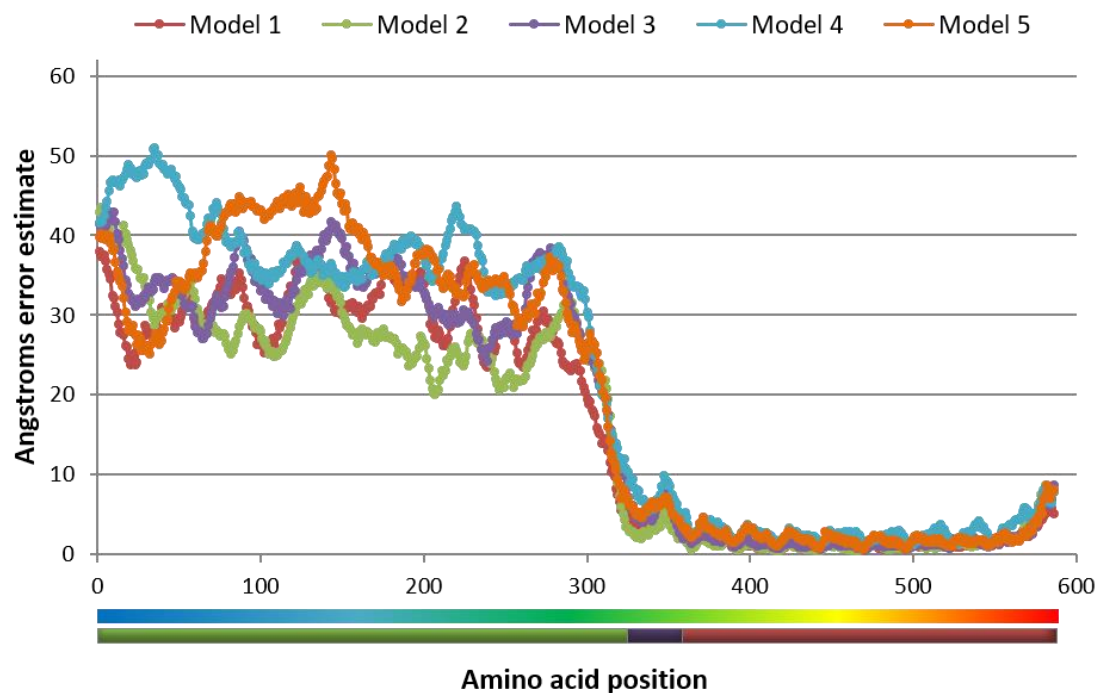
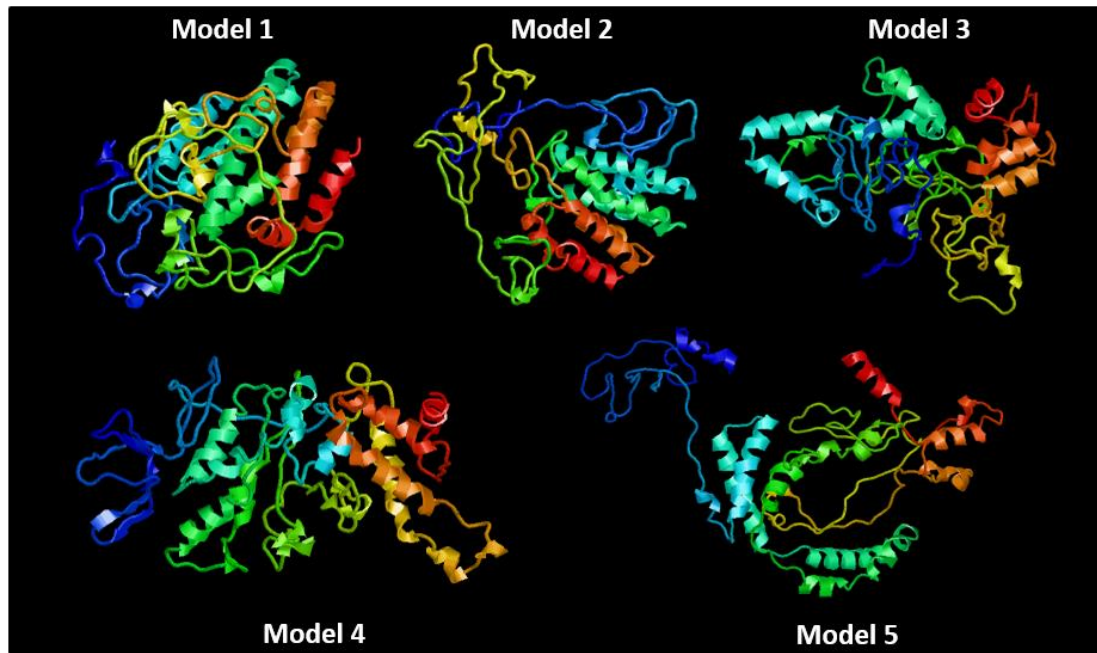


Figure 3. 14 - 3D structure predictions for *Fbxl17*Δ3LRR using Robetta protein structure prediction service.

(A) *Fbxl17*Δ3LRR 3D structure models generated by comparative modelling. N-terminus, blue; C-terminus, red. **(B)** 3D modelling error in angstroms for each amino acid position of *Fbxl17* Δ3LRR for the five Robetta generated 3D models. Schematic underneath represents approximate locations of *Fbxl17* domains (lower rectangle); green, N-terminus; purple, F-box domain; red, leucine rich repeats, mapped to spectrum colouring used in (A) (top rectangle).

A



B

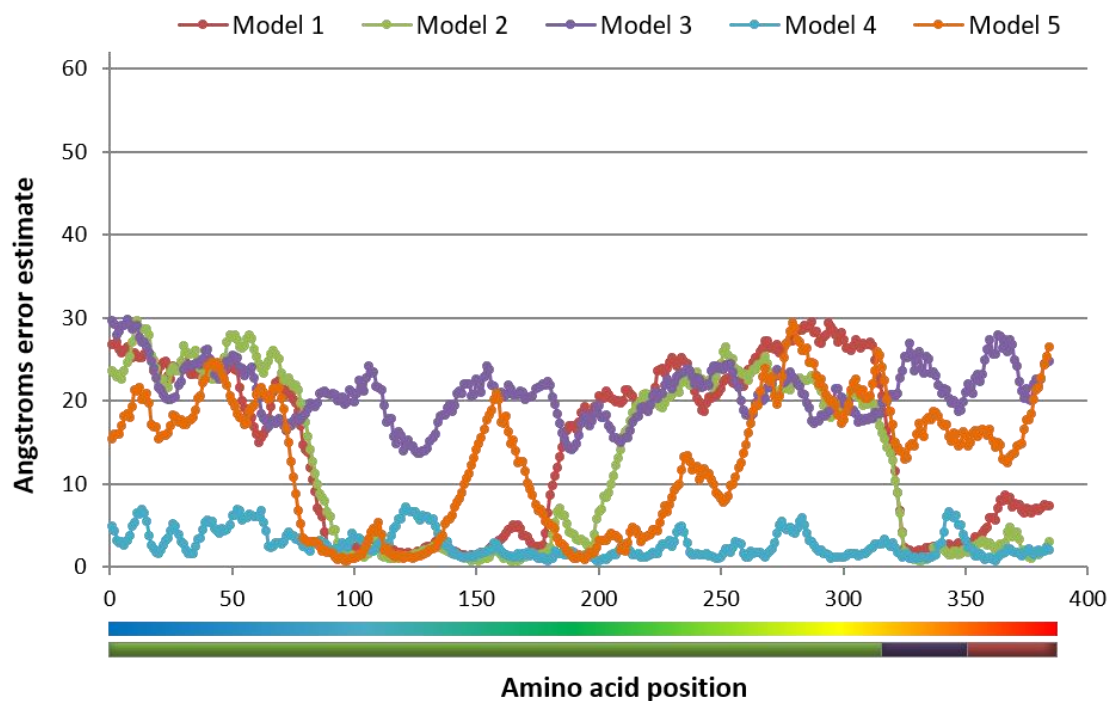


Figure 3. 15 - 3D structure predictions for *Fbxl17*Δ10LRR using Robetta protein structure prediction service.

(A) *Fbxl17*Δ10LRR 3D structure models generated by comparative modelling. N-terminus, blue; C-terminus, red. **(B)** 3D modelling error in angstroms for each amino acid position of *Fbxl17*Δ10LRR for the five Robetta generated 3D models. Schematic underneath represents approximate locations of *Fbxl17* domains (lower rectangle); green, N-terminus; purple, F-box domain; red, leucine rich repeats, mapped to spectrum colouring used in (A) (top rectangle).

3. DISCUSSION

It was previously found that *FBXL17* is rearranged in around 7% of breast cancers according to array-CGH data. Rearrangements of *FBXL17* were also validated in breast and oesophageal cancer cell lines [255]. Independently, analysis of sequence-level mutation data suggested that *FBXL17* behaves like a tumour suppressor gene [271]. My results further indicate that *FBXL17* is frequently mutated in breast cancers and consistently in the genomic regions encoding its LRRs. The incidence of *FBXL17* mutations in the primary breast tumours was 2%, which was lower than predicted from the array-CGH data. However, it has been shown in other cancer types that rare rearrangements can be important. Most notably, the EML4-ALK translocation is present in an estimated 5% of NSCLC cases [39]. Patients with the oncogenic fusion gene respond well to ALK inhibitors and as such discovery of the genomic rearrangement lead to an effective clinical therapy and improved patient outcome [272]. As such, Fbxl17 may also be a suitable therapeutic target in breast cancers rearranged for *FBXL17*.

FBXL17 rearrangements did not cluster with a specific breast cancer subtype; however, the tumours with *FBXL17* mutations may be enriched for *TP53* mutations, given 83% of the *FBXL17*-rearranged tumours were *TP53* mutant, compared to only 40% of the 250 tumours overall. Half of the tumours were assigned to IntClust 10, a high-risk subtype usually presenting clinically at a younger age, with high-grade and poorly differentiated tumours [30]. Furthermore, most (4/6) tumours with *FBXL17* rearrangements were basal-like, which are often aggressive tumours with poor therapeutic responses. Most (but not all) basal-like tumours are characterised by the lack of hormone receptors (ER, PR and HER2, triple-negative cancers) which limits therapeutic targets [273]. Modulating Fbxl17 expression in these tumours may therefore be a viable therapeutic option.

Many point mutations and breaks in *FBXL17* occurred in regions encoding its LRRs. Indeed, the TCGA data mapping somatic point mutations were striking, with only two mutations falling outside the F-box domain or LRR regions. The cancer cell lines and tumour-associated mutations cluster around intron 6. Breaks here would disrupt a short linker region in Fbxl17 that exists between LRR8 and 9 and would truncate Fbxl17 by 3LRRs. The LRR motifs are proposed to be the substrate docking sites within FBXL proteins and are predicted to cause a failure to recruit substrates if lost or mutated. Indeed, Raducu, et al. showed that the LRRs of

Fbxl17 are required for binding to Sufu [250] and the cysteine residue (C627) that is required for binding to BTB-domain containing proteins would be lost in both Fbxl17 Δ 3LRR and Fbxl17 Δ 10LRR [251]. We find that progressive deletion of the LRRs of Fbxl17 also caused decreased auto-ubiquitination and decreased ubiquitination of a substrate, Sufu, by SCF^{Fbxl17}. Auto-ubiquitination is a regulatory feedback mechanism adopted by Fbox proteins to control the pool of free FBPs in a cell in the absence of substrate [208]. As a result, the truncated Fbxl17 protein is likely to be unable to efficiently regulate its own abundance and may sequester Skp1 from other FBPs. This may also explain why we observed more abundant expression of the mutant Fbxl17 constructs in mammalian cells. The ability of SCF^{Fbxl17} to auto-ubiquitinate with several E2 ligases highlights the promiscuity of E2 enzymes and the functional plasticity of the UPS system. It also highlights the potential for Fbxl17 to conjugate different ubiquitin chain linkage types onto substrates. It has already been shown that the E3 ligase BRCA1-BARD1 can assemble both K63-linked chains and K48-linked chains, depending on the E2 enzyme it recruits [193].

Deleting LRRs also impaired the assembly of the E3 ubiquitin-ligase complex, which likely explains the decreased ubiquitination activity we observed. I was able to purify SCF complexes from cells, which were found to be active to varying degrees *in vitro*. Surprisingly both Fbxl17 LRR truncation mutants, Δ 3LRR and Δ 10LRR, bound Skp1 less well compared to WT, despite the presence of a Skp1 binding motif. The C-terminus of an FBP has been shown in specific cases to contact Skp1 to stabilise the ligase [274]. Consistent with this, my data shows that truncating the LRRs of Fbxl17 destabilises the SCF ligase as demonstrated by a lack of SCF subunit recruitment. Reduced interactions with Cul1 and Rbx1 are likely due to less Skp1 binding, since FBPs do not interact directly with Cul1 or Rbx1 [274]. This contrasts BTB-Cul3-Rbx1 E3 ligases, where BTB proteins contact both Cul3 and their substrates directly. The destabilisation caused by loss of LRRs may be due to a change in the 3D structure of Fbxl17, as predicted by Robetta modelling. Robetta models for the Fbxl17 mutants showed that the LRRs of Fbxl17 no longer loop back to remain in close proximity to the N-terminus/F-box domain of Fbxl17, which we propose is important to stabilise Skp1 binding and SCF complex assembly.

Given that the ubiquitination of Sufu was decreased by Fbxl17 LRR-truncated mutants I predict that the pool of substrates ubiquitinated by SCF^{Fbxl17} would be diminished or indeed

altered as a result of loss of LRRs. It is possible that the decreased ubiquitination we observed for Sufu with the truncation mutants is simply due to lack of binding to Fbxl17. However, even if a truncated Fbxl17 were able to recruit some of its substrates, I have shown that it would be less efficient in ubiquitinating them. Thus, in the context of breast cancer, the rearrangements that target the LRRs of *FBXL17* would likely diminish ubiquitination of the network of SCF^{Fbxl17} substrates. The resulting dysregulation of the SCF^{Fbxl17} ubiquinome is likely to have effects on multiple cellular pathways. To fully understand the implications of Fbxl17 mutations in breast cancer, we need to identify its regulatory networks. This may then reveal pathways amenable to therapeutic targeting.

4

FBXL17 AS A REGULATOR OF THE HEXOSAMINE BIOSYNTHETIC PATHWAY

CHAPTER 4 - Fbxl17 as a regulator of the Hexosamine Biosynthetic Pathway

4. Introduction

Ubiquitination controls key cellular processes, including cell cycle progression and inflammatory responses. It is likely that aberrant ubiquitination by mutant SCF^{Fbxl17}, as a consequence of rearrangement, will negatively impact the cellular pathways reliant on Fbxl17 for regulation. We predict that loss of Fbxl17 LRRs will also impede binding to other substrates or diminish substrate ubiquitination where binding to Fbxl17 is still possible. However, the substrates of Fbxl17 remain widely unknown. At the start of this PhD project only two papers reporting binding partners of Fbxl17 had been published. Fbxl17 was first shown to stabilise ribonucleotide reductase subunit M2 (RRM2) promoting its overexpression in breast cancer cells [248] and in 2013, a second substrate of Fbxl17, BACH1, was identified. Turnover of BACH1 by Fbxl17 was important for transcription of the NRF2 target HMOX1, which protects cells from oxidative stress [249]. More recently Fbxl17 has been shown to target Sufu [250] and PRMT1 [212] for proteasomal degradation with implications in medulloblastoma and asthma respectively. In 2018, Mena et al. found that Fbxl17 acts in a quality control capacity to target aberrant BTB heterodimers for degradation, which is required for neural differentiation in *Xenopus laevis* embryos [251]. The range of substrates identified so far highlights the far-reaching effects of the SCF^{Fbxl17} regulatory network in cells.

In order to find substrates of Fbxl17 and therefore identify the regulatory network of Fbxl17 on a wide scale, a yeast two-hybrid (Y2H) screen was performed by Dr Susanne Flach. To focus the screen on LRR-binding partners and therefore potential ubiquitinated substrates of Fbxl17, the bait plasmid contained the F-box domain (FBD) and LRRs (321-701aa) of Fbxl17 but omitted its N-terminus. A normalised human cDNA library fused to a Gal4 activation domain (GAD) was used as prey. Thirty-seven unique prey, cloned in-frame to the GAD, were identified as candidate partners for Fbxl17. More than a third (13/37) of the prey were isolated independently at least twice. The most frequently isolated cDNA encoded GAD fusions to UDP-N-acetylglucosamine pyrophosphorylase 1 (Uap1), which were isolated 26 times [255].

Uap1 is an enzyme required for the synthesis of UDP-GlcNAc, an intermediate utilised in the Hexosamine biosynthetic pathway (HBP), to add *O*-GlcNAc modifications onto serine or threonine residues of target proteins (*O*-GlcNAcylation) (Figure 4. 1). *O*-GlcNAcylation is an important post-translational modification on many intracellular proteins. In this chapter I set out to validate the Y2H results and test whether Uap1 is an interacting partner of Fbxl17. I then investigated the consequences of LRR rearrangements on this interaction and the downstream effects of Fbxl17 activity, or lack thereof, on the HBP and *O*-GlcNAcylation. A manuscript containing some of this work, published in September 2019 in *Cellular and Molecular Life Sciences*, can be found in Appendix B.

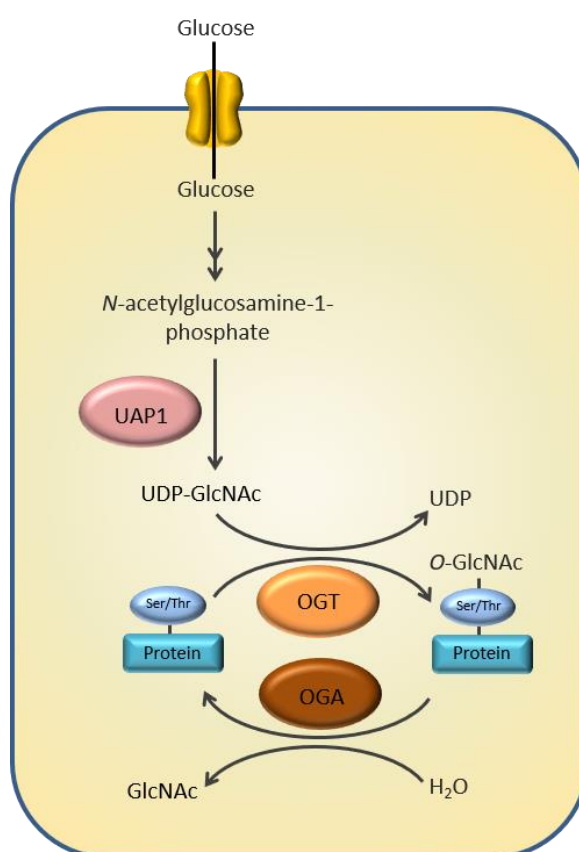


Figure 4. 1 - Downstream steps of the Hexosamine Biosynthetic pathway

When glucose enters the cell, 2-5% is directed to the Hexosamine biosynthetic pathway (HBP). At the downstream steps of the HBP, the enzyme UDP-N-acetylglucosamine pyrophosphorylase 1 (Uap1) converts N-acetylglucosamine-1-phosphate to UDP-GlcNAc. UDP-GlcNAc can then be utilised by OGT for the *O*-GlcNAcylation of nuclear and cytoplasmic proteins. OGT (*O*-GlcNAc transferase) and OGA (*O*-GlcNAcase) catalyse the addition and removal of *O*-GlcNAc respectively.

4. Results

4.1 Fbxl17 interacts with Uap1 in human cells in vivo.

The Y2H results suggested that Uap1 interacts with Fbxl17. To validate this interaction in mammalian cells Dr Flach performed a co-immunoprecipitation assay (Figure 4. 2A). Immunoprecipitates from HEK293T cells expressing N-terminally FLAG-tagged Fbxl17 and HA-tagged Uap1 were isolated using anti-FLAG agarose beads. To test whether the interaction between Fbxl17 and Uap1 is dependent on the LRRs of Fbxl17, the experiment also included the truncated mutants Fbxl17 Δ 3LRR and Fbxl17 Δ 10LRR. Western blotting revealed that Uap1 is co-immunoprecipitated with WT Fbxl17 thus confirming the Y2H results. Uap1 also co-immunoprecipitated with Fbxl17 Δ 3LRR, but truncation of 10LRRs ablated the interaction, indicating that Uap1 binding is dependent on LRRs 2-8 (Figure 4. 2A). In addition to this, I performed a co-immunoprecipitation assay to test Uap1 binding to Fbxl17 Δ Fbox. The Y2H Fbxl17 bait contained the FBD and LRRs, and as such Uap1 may bind to either domain. FLAG-tagged Fbxl17 WT and Δ Fbox were isolated from HEK293T cell lysates, and immunoprecipitates were probed for exogenous HA-tagged Uap1 (Figure 4. 2B). Uap1 can still bind to Fbxl17 Δ Fbox indicating the FBD is not required for the interaction of Fbxl17 with Uap1.

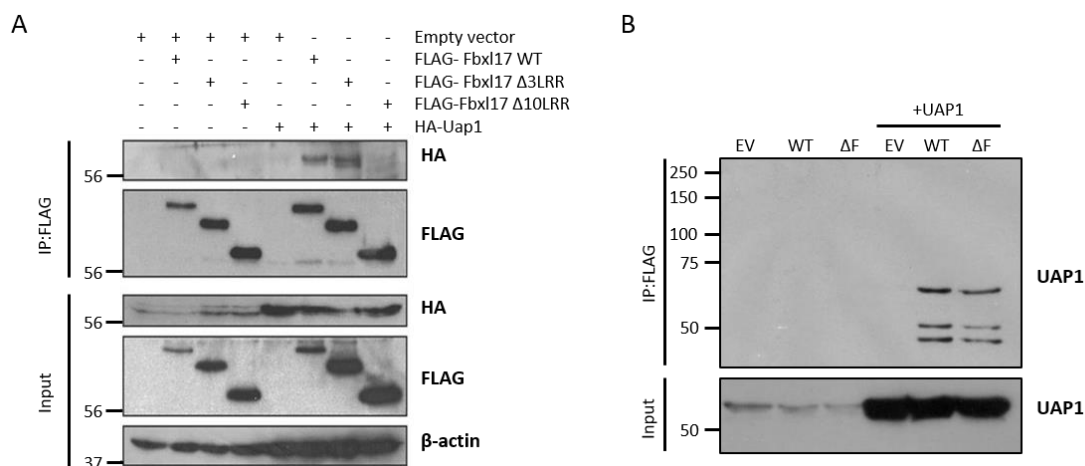


Figure 4. 2 - Deletion of ten LRRs ablates binding of Fbxl17 to Uap1

(A) Immunoprecipitates; using anti-FLAG beads, of HEK293T cells expressing FLAG-Fbxl17, FLAG-Fbxl17 Δ 3LRR or FLAG-Fbxl17 Δ 10LRR, probed for exogenous HA-tagged Uap1. **Experiment performed by Dr. Susanne Flach, reproduced here with permission.** **(B)** As (A) but HEK293T cells expressing FLAG-Fbxl17 or FLAG-Fbxl17 Δ Fbox, and Uap1, probed for Uap1, n=2; EV, empty vector; WT, Fbxl17 WT (1-701aa); Δ Fbox, Fbxl17 Δ Fbox (Δ 324-356).

4.2 Fbxl17 binds Uap1 directly via its LRRs

Interactions in the Y2H screen and in co-immunoprecipitation assays, could arise from proteins bridging the interaction between Fbxl17 and Uap1. Therefore, to test the directness of the interaction between Fbxl17 and Uap1, I performed an *in vitro* GST pull-down assay (Figure 4. 3). I first attempted to express GST-Fbxl17 (321-701aa) and GST-Fbxl17 Δ 10LRR (321-384aa) in bacteria. As with the Y2H, I omitted the N-terminus of Fbxl17 to focus the assay on binding that occurs via the LRRs. Fbxl17 Δ 10LRR was robustly expressed in bacteria as demonstrated by Coomassie staining of proteins immobilised on GST-beads, but we were unable to express GST-Fbxl17 (321-701aa) (data not shown). To try and overcome this issue, I cloned Fbxl17 into a bacterial expression vector that co-expressed Skp1 (Fbxl17_IRES_Skp1), since this has previously been reported to stabilise FBP and their expression in bacteria [275]. Co-expression of GST-Fbxl17 with Skp1 facilitated the expression in bacteria (Figure 4. 3, right panel). The volume of sample loaded to the gel, and

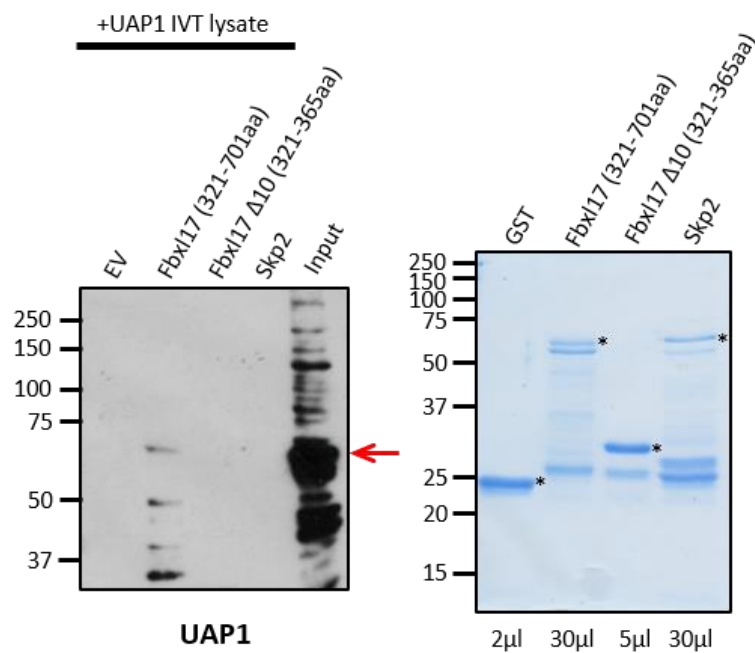


Figure 4. 3 - Fbxl17 binds Uap1 directly.

In vitro GST pull-down assay using bacterially expressed and purified Fbxl17 constructs or Skp2/GST as controls, immobilised on a GST column incubated with rabbit reticulocyte lysate (left panel). Fbxl17 (321-701aa) and Skp2 constructs contained an IRES_Skp1 to aid expression. Input for rabbit reticulocyte lysate= 20%, arrow represents Uap1. Coomassie staining of GST proteins (right panel), volume of sample loaded indicated below lanes * indicates bands relating to expressed proteins, n=2.

subsequently used in the binding assay, was optimised to equalise protein expression (Figure 4. 3, right panel). GST-Fbxl17_IRES_Skp1 and GST-Fbxl17 Δ 10LRR were immobilised on a GST column and incubated with *in vitro* transcribed and translated (IVT) Uap1. GST-Skp2_IRES_Skp1, another LRR containing FBP, and GST alone were included as controls. Following the binding assays, samples were resolved by SDS-PAGE and membranes probed with antibody to Uap1. I observed binding specifically to GST-Fbxl17_IRES_Skp1 (321-701aa) but not to GST only or GST-Skp2_IRES_Skp1. This shows that binding of Uap1 to Fbxl17 is specific and not via an interaction with Skp1. Furthermore, in agreement with the co-immunoprecipitation data, deletion of 10 LRRs abolished Uap1 binding to Fbxl17 (Figure 4. 3, left panel). The folding of GST-Fbxl17 Δ 10LRR is likely to be disrupted (see Chapter 3), which may explain the loss of binding to Uap1. These results indicate Fbxl17 interacts directly with Uap1, and this occurs via its LRRs.

4.3 Overexpression of Fbxl17 does not increase Uap1 turnover

To test the functional significance of Fbxl17 interaction with Uap1, I over-expressed Fbxl17 and monitored the steady state levels of Uap1 by immunoblotting (Figure 4. 4). Fbxl17 Δ Fbox was included as a negative control. Uap1 levels were unchanged in the presence of the proteasome inhibitor MG132 and with increased levels of Fbxl17, which suggests Fbxl17 activity does not promote the proteasomal degradation of Uap1 (Figure 4. 4). However, not all modification of proteins by ubiquitination results in their degradation, and so this does not rule out Uap1 as a substrate of Fbxl17. We also cannot rule out that the cells have adopted a compensatory mechanism, within 48 hours, to counteract any changes to Uap1 levels caused by Fbxl17 overexpression.

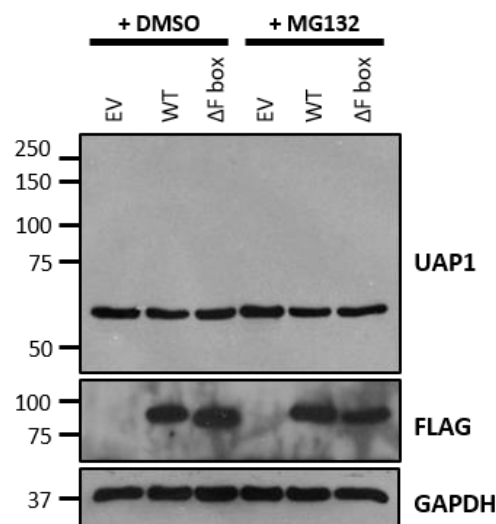


Figure 4. 4 - Fbxl17 does not target Uap1 for proteasomal degradation.

HEK293T cells transfected with Fbxl17 WT, Δ Fbox or empty vector (EV) for 48h, treated with 10 μ M MG132 or DMSO for 4h prior to lysis. Whole cell lysates immunoblotted with the indicated antibodies, n=3.

4.4 Fbxl17 does not ubiquitinate Uap1 *in vitro*

To test whether Uap1 is a substrate of SCF^{Fbxl17} ligase I conducted an *in vitro* ubiquitination assay. Initially, untagged Uap1 was transcribed and translated *in vitro* and added to a ubiquitin mix in the presence of purified SCF^{Fbxl17} ligases. Samples were resolved by SDS-PAGE and immunoblotted for Uap1. No higher molecular weight bands, indicative of modification with ubiquitin, were present in any of the samples suggesting Uap1 is not ubiquitinated by Fbxl17 (Figure 4. 5A). I hypothesised that the concentration of ligases may be too low for robust ligase activity towards Uap1. Alternatively, Uap1 may require additional post-translational modification before it can be recognised as a substrate by Fbxl17, which are not added during IVT preparation of Uap1. To address these concerns, I purified HA-UAP1 from HEK293T cells by immunoprecipitation. I then repeated the *in vitro* ubiquitination assay with 50nM (data not shown) and 100nM of purified SCF ligases. Once again, I did not detect any higher molecular weight bands representing modification of Uap1 (Figure 4. 5B). The absence of a positive control for SCF^{Fbxl17} activity makes it difficult to conclude this with certainty. However, the Fbxl17 SCF ligases samples used in this assay have already been shown to be active *in vitro* (Chapter 3, Figure 3. 11) which suggests the absence of modification of Uap1 is unlikely to be due to lack of SCF^{Fbxl17} ligase activity. Together these data indicate that Fbxl17 cannot ubiquitinate Uap1 *in vitro*.

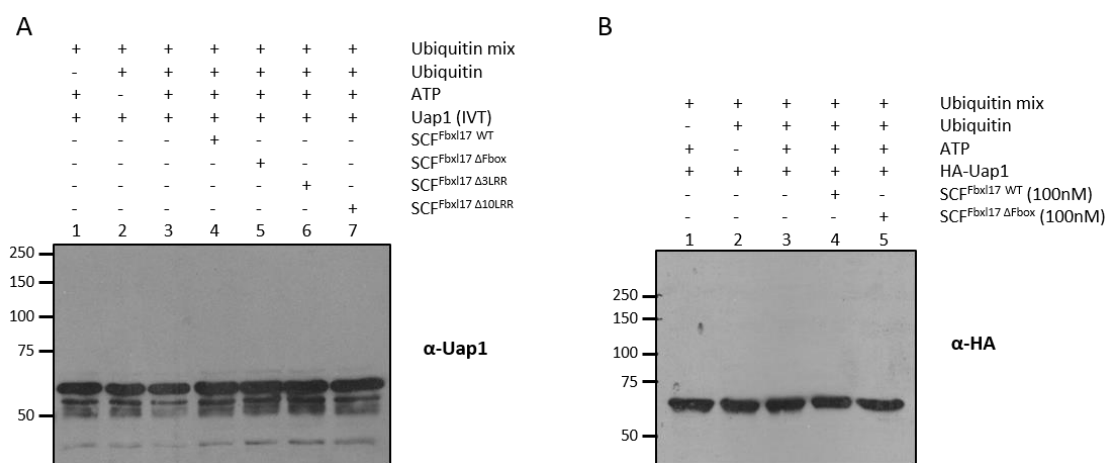


Figure 4. 5 - Fbxl17 does not ubiquitinate Uap1 *in vitro*.

In vitro ubiquitination assay of SCF^{Fbxl17} and mutant ligase complexes in combination with Uap1 (untagged) produced by IVT (**A**) or HA-Uap1 purified from HEK-293T cells (**B**), in the presence of a ubiquitin mix (ubiquitin buffer, UBE1, Ubch5a and ATP). In (**B**) the SCF concentration was increased to 100nM. Proteins resolved by SDS-PAGE and membrane probed with anti-Uap1 or anti-HA antibody as indicated, n=2.

4.5 Fbxl17 inhibits the phosphorylation of Uap1.

Some substrates require co-factors to bind substrates, which could explain why Fbxl17 was unable to ubiquitinate Uap1 *in vitro*. I therefore conducted an *in vivo* ubiquitination assay to see if Fbxl17 could ubiquitinate Uap1 in a cellular setting, where any potential co-factors would be present (Figure 4. 6A). HEK293T cells were co-transfected with HA-Uap1, Myc-ubiquitin and FLAG-Fbxl17 (WT or Δ Fbox) constructs. Following immunoprecipitation of Uap1 with HA antibody immobilised on agarose beads, samples were analysed by immunoblotting. I found no evidence of laddering or smearing of Uap1 indicative of its

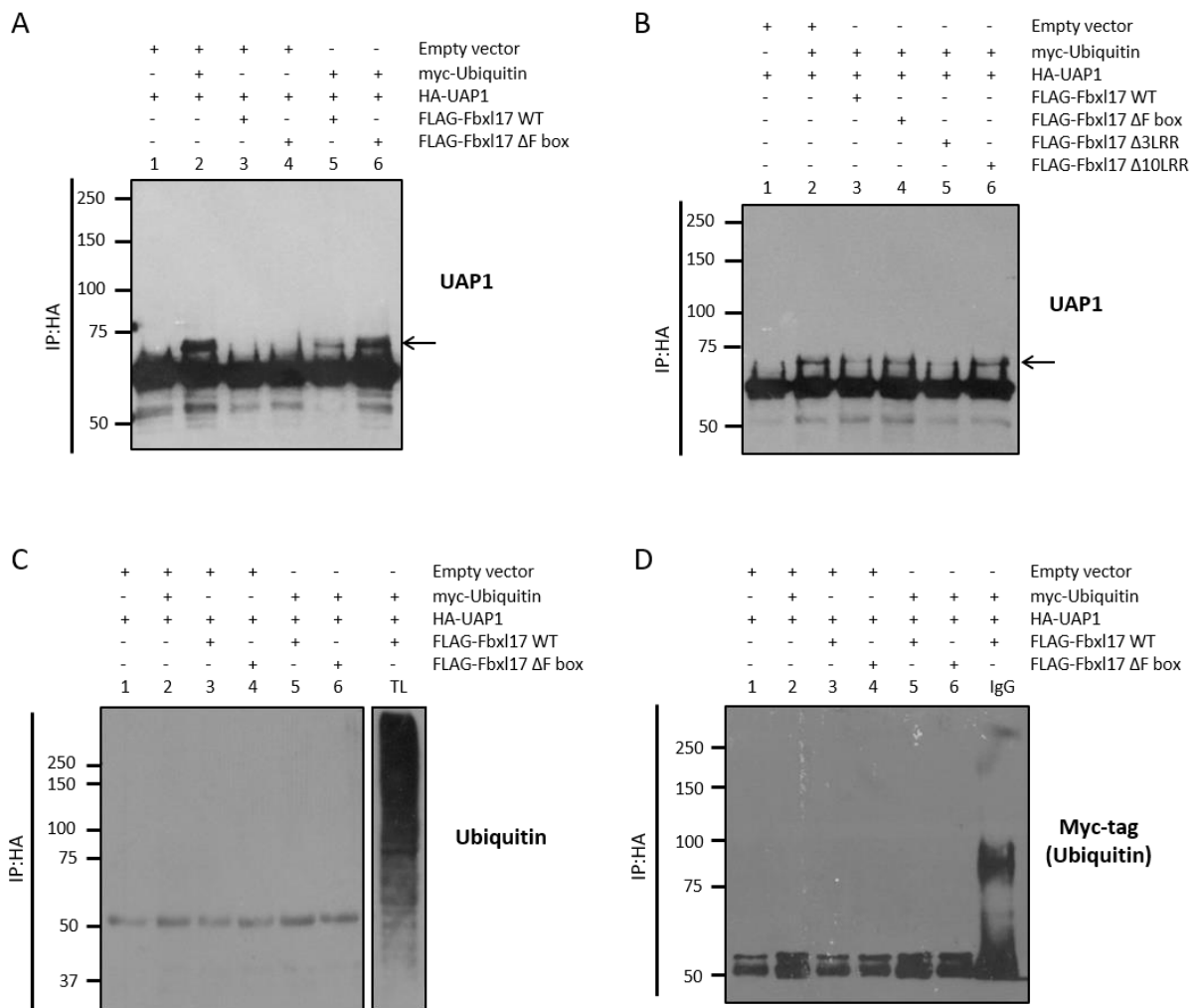


Figure 4. 6 - Fbxl17 does not target Uap1 for ubiquitination.

(A) *In vivo* ubiquitination assay for UAP1. HA-UAP1 immunoprecipitated from HEK293T cells transfected with ubiquitin and indicated Fbxl17 constructs. Membranes probed with anti-UAP1 antibody, arrow indicates modified Uap1, $n=3$. **(B)** as (A) but including mutant Fbxl17 constructs Fbxl17 Δ 3LRR and Fbxl17 Δ 10LRR. **(C-D)** as (A) but probed for ubiquitin (C) and myc-epitope tag (D). TL, total lysate.

polyubiquitination. Instead I detected a discrete, higher molecular weight species of Uap1 upon transfection of Myc-ubiquitin (Figure 4. 6A, lane 2). Moreover, levels of this modified form of Uap1 were reduced when Fbxl17 was overexpressed (Figure 4. 6A, lane 5). Interestingly, this reduction of Uap1 modification was not observed when Fbxl17 Δ Fbox was overexpressed, suggesting this effect was dependent on Skp1 binding and/or the ligase activity of Fbxl17 (Figure 4. 6A, lane 6). I next tested whether the Fbxl17 truncation mutants could also inhibit the modification of Uap1 and repeated the *in vivo* ubiquitination assay in the presence of Fbxl17 Δ 3LRR and Fbxl17 Δ 10LRR. Over-expression of Fbxl17 Δ 3LRR was also able to prevent the modification of Uap1 to a level comparable to WT Fbxl17 (Figure 4. 6B, lane 5) but this effect was lost following deletion of 10LRRs (Figure 4. 6B, lane 6). This suggests that the inhibition of this modification not only requires the F-box domain but also the first eight LRRs of Fbxl17.

To determine the type of modification this higher molecular weight species of Uap1 represented, I immunoblotted with antibodies to ubiquitin and to myc-epitope tag (Myc-ubiquitin) (Figure 4. 6C and D). The modification of Uap1 was only present after overexpression of Myc-ubiquitin and the resulting gel shift, due to a change in molecular

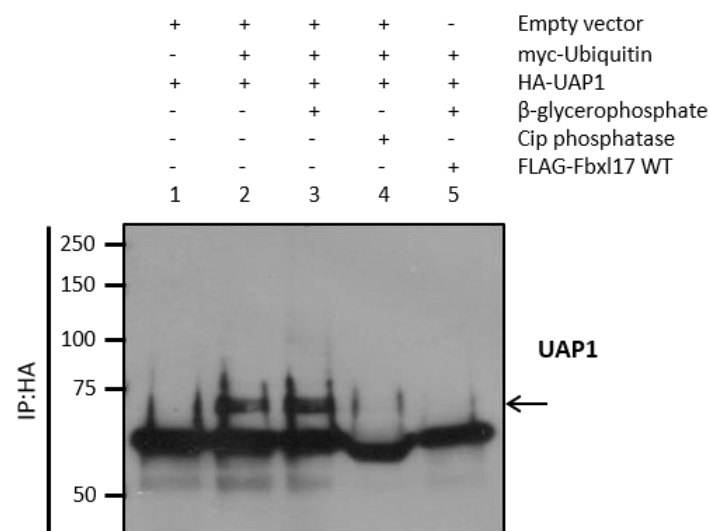


Figure 4. 7 - Fbxl17 inhibits the phosphorylation of Uap1.

(A) *In vivo* ubiquitination assay for UAP1. HA-UAP1 immunoprecipitated from HEK293T cells transfected with ubiquitin and indicated Fbxl17 constructs in the presence of β -Glycerophosphate (lane 3) and Alkaline phosphatase (CIP) (lane 4), Membranes probed with anti-UAP1 antibody, arrow indicates modified Uap1, n=2.

weight, could be accounted for by the addition of a single 8 kDa ubiquitin molecule. I therefore hypothesised that the higher molecular weight band may represent a mono-ubiquitinated form of Uap1. Antibodies to ubiquitin and Myc-tag did not yield any signal in Uap1 immunoprecipitates, only IgG heavy chain, and therefore indicate that the modification present on Uap1 is not ubiquitination.

Data-mining of the PhosphoSitePlus database highlighted multiple studies showing Uap1 is a phosphorylated protein. As such, I tested whether this modified version of Uap1 represented a phosphorylated form of the protein. I repeated the *in vivo* ubiquitination assay in the presence of the phosphatase inhibitor β -glycerophosphate and the alkaline phosphatase (CIP) (Figure 4. 7), which should increase and decrease phosphorylation of proteins, respectively. Strikingly, the levels of modified Uap1 were almost completely ablated following CIP treatment (Figure 4. 7, lane 4), suggesting the higher molecular weight species represented a phosphorylated form of Uap1. There was also a slight increase in modified Uap1 following β -glycerophosphate treatment (Figure 4. 7, lane 3), further suggesting the observed modification of Uap1 is phosphorylation. Overexpression of Myc-ubiquitin seems to promote the phosphorylation of Uap1. In summary, overexpression of ubiquitin increases Uap1 phosphorylation and overexpression of Fbxl17 prevents this modification in an FBD and LRR-dependent manner.

4.6 Fbxl17 knockdown inhibits UDP-GlcNAc production.

Since Fbxl17 overexpression reduced the abundance of phosphorylated Uap1, but not its steady state levels, we reasoned Fbxl17 might regulate endogenous Uap1 activity. Uap1 catalyses the formation of UDP-N-acetylglucosamine (UDP-GlcNAc), an intermediate used by the glycosyltransferase *O*-GlcNAc Transferase (OGT) to add N-acetylglucosamine in *O*-glycosidic linkages to proteins, known as *O*-GlcNAcylation. We hypothesised that the phospho-Uap1 may be an activated form of the enzyme, and our results indicate Fbxl17 acts to suppress this modification. We therefore tested whether reducing Fbxl17 expression would increase endogenous Uap1 activity. Small interfering RNA (siRNA) targeting Fbxl17 were initially tested in HEK293T, U2OS, MCF7 and HB4a cells, with siRNA3, targeting exon 3 of Fbxl17, in U2OS cells found to provide the best knockdown and therefore used in subsequent experiments (Figure 4. 8A). The steady state levels of Uap1 in U2OS cells treated with siRNA3 were monitored by immunoblotting. As with Fbxl17 overexpression, Uap1 levels were unchanged following Fbxl17 knockdown (Figure 4. 8B).

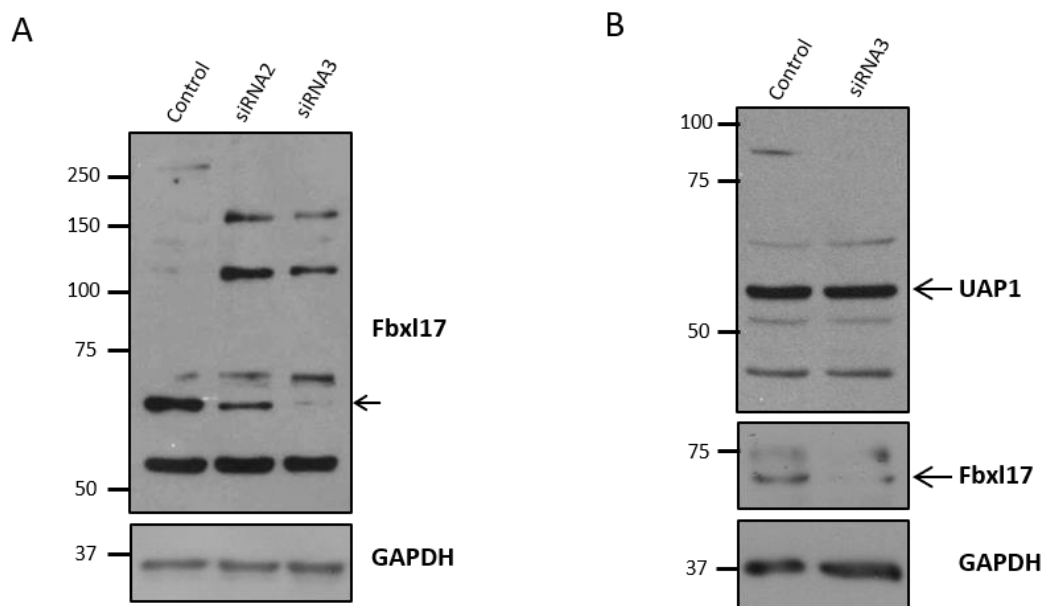


Figure 4. 8 - Uap1 steady state levels are not altered following Fbxl17 knockdown

(A) Expression of Fbxl17 in U2OS cells treated with Fbxl17 targeting siRNA. Immunoblotted with anti-Fbxl17. Arrow represents band corresponding to Fbxl17. **(B)** U2OS cells treated with Fbxl17 targeting siRNA3 or control non-targeting siRNA. Whole cell lysates immunoblotted for indicated proteins, n=2.

If Fbxl17 negatively regulates Uap1 activity, we hypothesised that loss of Fbxl17 should increase Uap1 activity, which should increase the total amount of UDP-GlcNAc, the product of this enzyme. To test if this was the case, U2OS cells were treated with siRNA targeting Fbxl17, metabolites were extracted from cells and UDP-GlcNAc levels were determined by liquid chromatography mass spectrometry (LC-MS) (Figure 4. 9). Surprisingly we observed a 36% decrease ($p=0.013$; $n=5$) in total UDP-GlcNAc levels following Fbxl17 knockdown, which suggests Fbxl17 promotes Uap1 activity.

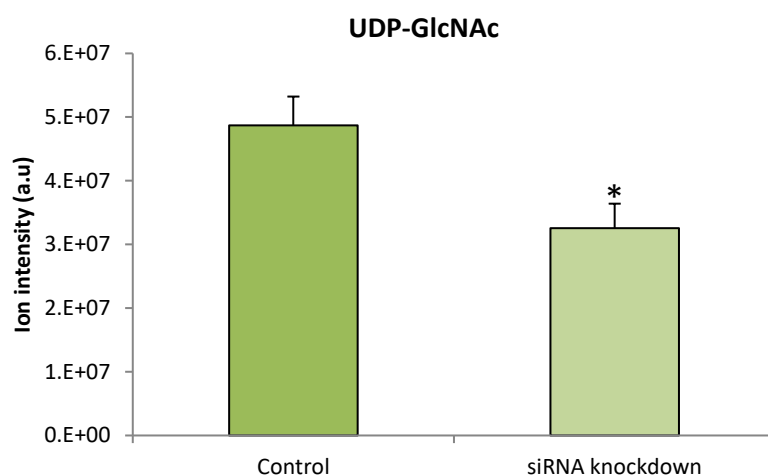


Figure 4. 9 - Knockdown of Fbxl17 inhibits UDP-GlcNAc production.

LC-MS analysis of total UDP-GlcNAc levels in U2OS cells treated with Fbxl17 siRNA3 or control siRNA for 48h. Values are averages from five independent biological repeats \pm SEM, $*=p<0.05$.

4.7 Fbxl17 knockdown results in increased levels of *O*-GlcNAcylation.

To determine the downstream effects of Fbxl17 knockdown on the HBP, we next tested the effect of reduced Fbxl17 expression on global cellular *O*-GlcNAcylation. The activity of OGT is very sensitive to concentrations of UDP-GlcNAc in the cytosol and nucleus; therefore, we would expect the observed decrease in UDP-GlcNAc levels upon reduction of Fbxl17 levels, to affect OGT's ability to add *O*-GlcNAc modifications to proteins. U2OS cells were treated with Fbxl17 siRNA as above and lysates immunoblotted for total *O*-GlcNAc. Although UDP-GlcNAc levels were reduced in Fbxl17 knockdown cells, we observed total *O*-GlcNAc was increased when Fbxl17 was knocked down (Figure 4. 10). Similar results were seen in two breast cell lines, HB4a and MCF7, by expression of shRNA constructs targeting *FBXL17* expression (Figure 4. 11). These data indicate an overall increase in the levels of *O*-GlcNAcylation upon Fbxl17 knockdown in breast cancer cells. This is a surprising result since direct measurement of the Uap1 substrate UDP-GlcNAc indicates that Fbxl17 promotes Uap1 activity. An increase in global *O*-GlcNAc following Fbxl17 knockdown hints at additional downstream regulation of this pathway.

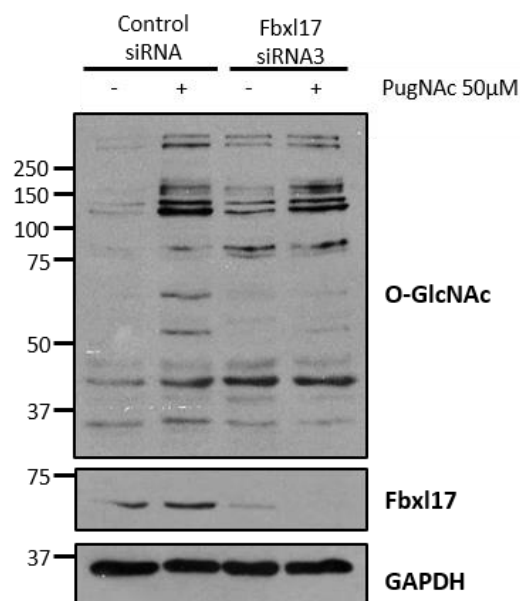


Figure 4. 10 - Knockdown of Fbxl17 increases global *O*-GlcNAcylation.

U2OS cells treated with Fbxl17 siRNA3 or control siRNA for 48h followed by PugNAc treatment; an inhibitor of *O*-GlcNAc- β -N-acetylglucosaminidase (OGA), the enzyme responsible for removing *O*-GlcNAc from proteins, 50 μ M 3h. Whole cell lysates immunoblotted with the indicated antibodies, n=2.

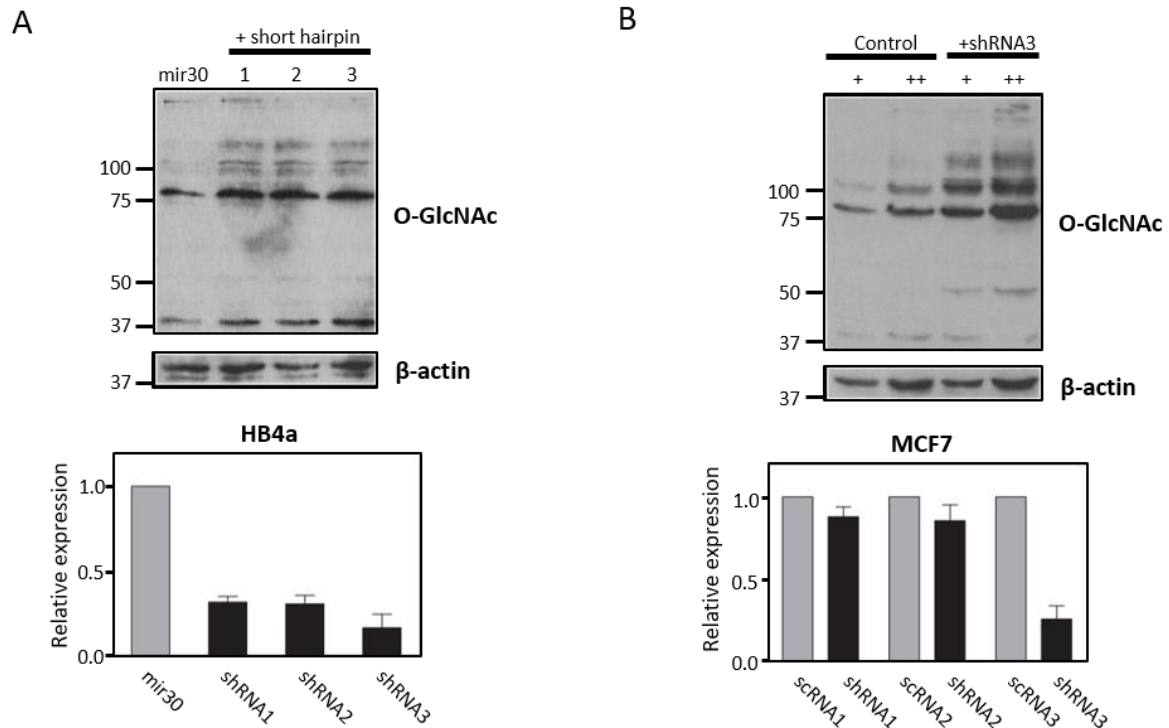


Figure 4. 11 - Knockdown of Fbxl17 increases O-GlcNAcylation in breast cancer cells

(A) FBXL17 mRNA knockdown by shRNA in HB4a immortalised normal breast (bottom panel). Expression normalised to GAPDH and plotted relative to miR30-infected control cells. Mean \pm SEM of at least three independent experiments. O-GlcNAcylation monitored by immunoblotting with anti-O-GlcNAc antibodies (top panel). **(B)** FBXL17 mRNA knockdown by shRNA in MCF7 breast cancer cells (bottom panel). Expression normalised to scrNA-infected cells. Mean \pm SEM of at least three independent experiments. Total O-GlcNAcylation monitored by immunoblotting with anti-O-GlcNAc antibodies. + and ++, 25 or 50 mg of protein lysate (top panel). **Experiments performed by Dr Susanne Flach, reproduced here with permission.**

4.8 Fbxl17 knockdown results in decreased OGA expression

O-GlcNAcylation is tightly regulated in order to maintain *O*-GlcNAcylation homeostasis. The surprising results showing increased *O*-GlcNAcylation following Fbxl17 knockdown, despite a significant decrease in UDP-GlcNAc levels, can therefore only be explained if the expression or activity of the enzymes responsible for adding or removing *O*-GlcNAc is also altered in these cells. I therefore tested whether the expression of OGT and its mechanistic partner OGA; both of which act downstream of Uap1 and UDP-GlcNAc and are responsible for adding and removing *O*-GlcNAc modifications to proteins respectively, were altered following Fbxl17 knockdown. I identified a decrease in OGA levels following Fbxl17 siRNA treatment of U2OS cells, but no change in OGT expression, which strongly suggests the increase in *O*-GlcNAcylated proteins, is the result of decreased OGA expression. In support of this, mass spectrometry analysis of GlcNAc levels, the intermediate produced following hydrolytic cleavage of *O*-GlcNAc modifications from proteins by OGA, were decreased in Fbxl17 knockdown cells indicating decreased OGA activity, although this was not found to be statistically significant.

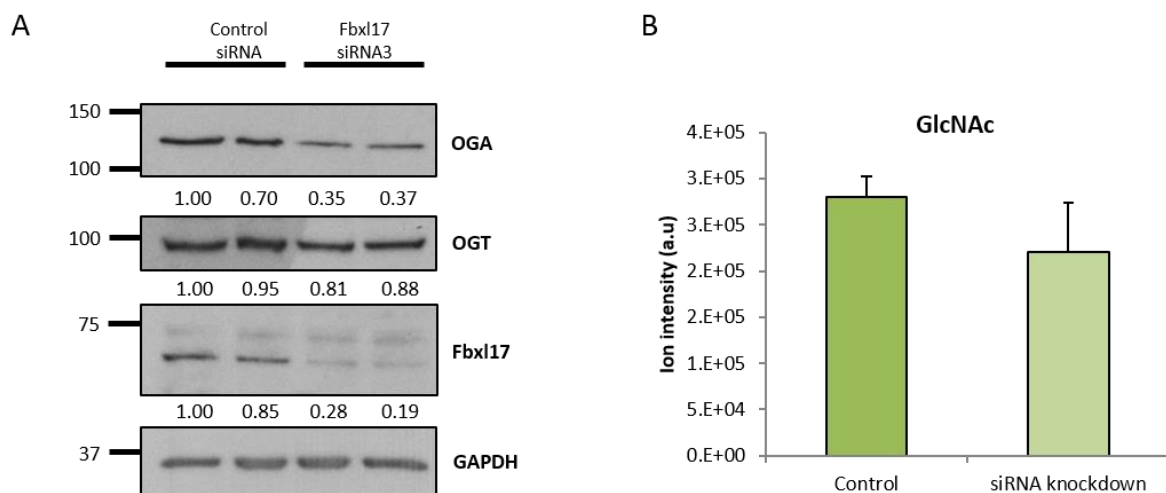


Figure 4. 12 - Knockdown of Fbxl17 results in decreased OGA expression and activity

(A) U2OS cells treated with Fbxl17 siRNA3 or control siRNA for 48h. Whole cell lysates immunoblotted with the indicated antibodies. Band intensities quantified by densitometry and normalised to GAPDH expression (values below blots), $n=3$. **(B)** LC-MS analysis of total GlcNAc levels in U2OS cells treated with Fbxl17 siRNA3 or control siRNA for 48h. Values are averages from five independent biological repeats \pm SEM.

4. Discussion

To investigate the functional consequences of *FBXL17* rearrangements, we screened for proteins interacting with the LRRs of Fbxl17. Our Y2H screen identified 37 novel interacting partners of Fbxl17. A previous survey of Fbxl17 binding proteins performed by Tan, et al. [249] shows partial overlap with the Y2H results. Among their large list of candidates, 7/37 of the proteins identified in the Y2H were also detected. Both screens identified the Kelch-like proteins Khl17 and Khl12, which were later verified as Fbxl17 substrates [251], confirming that the Y2H approach can identify true Fbxl17 interacting partners. However, Uap1, the most frequently recovered cDNA in the Y2H, was not found in either case. One possible explanation for this is that we used a normalised human cDNA library, which screens proteins from all cell types, while Tan, et al. [249] immunoprecipitated Fbxl17 from HEK293 and HCT116 and so required endogenous proteins to bind at a detectable level. Conversely, the Y2H assay requires proteins to form productive interactions for transcription of the reporter gene, and so transient or weak interactions may be lost. Neither approach is likely to capture all interactions and argues for the use of a variety of experimental approaches to discover the regulatory networks of FBPs.

In this chapter I set out to determine if Uap1 is a substrate of Fbxl17. We were able to verify that Fbxl17 and Uap1 interact directly and have shown that Uap1 binding is disrupted only when ten LRRs of Fbxl17 are truncated. This suggests Uap1 can bind to LRR2-8 and as such led to a model whereby, the number of LRRs in Fbxl17, as dictated by the position of a rearrangement within *FBXL17*, would influence its interaction with its repertoire of proteins. As highlighted in Chapter 3, even if binding to LRR-truncated Fbxl17 mutants is still possible, we predict the ubiquitination of these proteins to be diminished.

There is not yet enough data on rearrangement of *FBXL17* in cancers to conclusively identify Fbxl17 inactivation as a driver mutation in cancer. Nonetheless, we were able to show a striking effect of reducing Fbxl17 expression on at least one important cancer relevant pathway, suggesting that inactivation of Fbxl17 would have a major effect on the cancer cell. This was through its regulation of Uap1, which is expressed in many breast cancers and other cancer types [58, 276]. Surprisingly, we did not find Uap1 to be ubiquitinated by Fbxl17, but instead our results showed that increased Fbxl17 expression prevented the phosphorylation of Uap1. In addition, this inhibition of Uap1 phosphorylation was

dependent on the Skp1-binding domain of Fbx17, suggesting that SCF^{Fbx17} ligase activity or complex formation is essential. Fbx17 Δ 3LRR was also able to inhibit the phosphorylation of Uap1 but Fbx17 Δ 10LRR was not, highlighting LRRs 2-8 are also required. This suggests a need for direct binding to Uap1 given that deletion of ten LRRs abolished binding to Uap1. We also note that the phosphorylated form of Uap1 is only observed when we over-express ubiquitin. It is possible that the kinase responsible for phosphorylating Uap1 is activated by ubiquitination or indeed Uap1 is primed for phosphorylation by ubiquitination. The latter would require the Uap1 modification to be subsequently removed, given we could not detect any ubiquitination of Uap1. It is possible the inhibition of Uap1 phosphorylation by Fbx17 overexpression is due to its ability to sequester the ubiquitin in the cell, which prevents it promoting Uap1 phosphorylation. If this holds true, over-expression of any E3 ligase, regardless of Uap1-binding capability, should yield a similar result. We could test this hypothesis by repeating the *in vivo* ubiquitination assay in the presence of an alternative E3

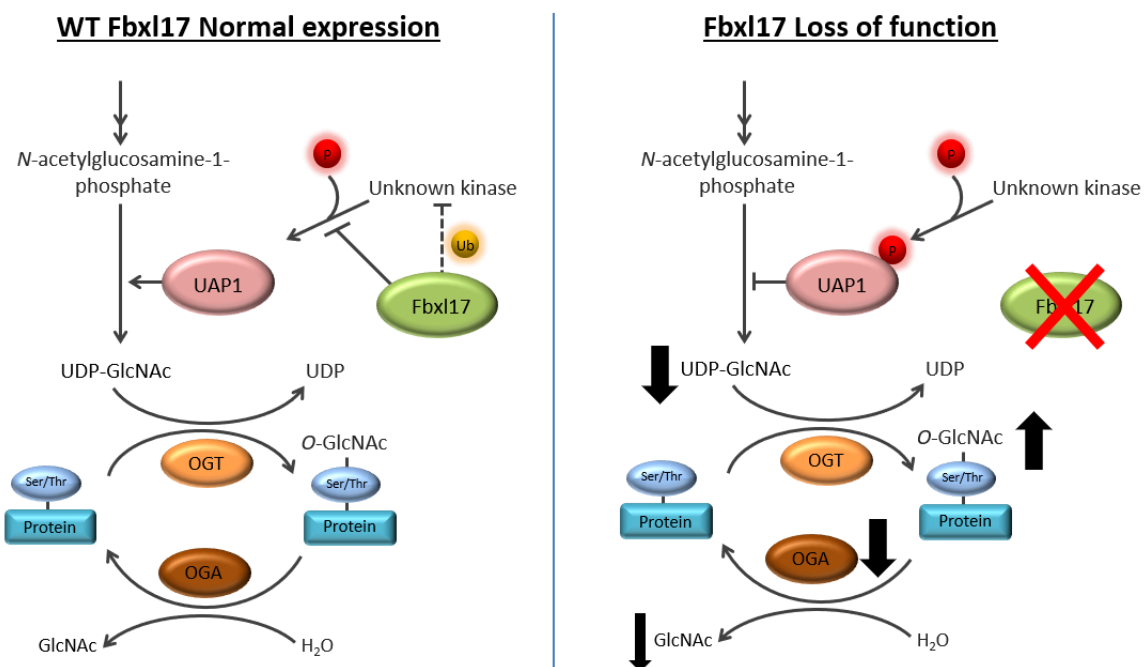


Figure 4. 13 - Model of interaction between Fbx17 and Uap1.

We propose a model whereby the presence of Fbx17 (left panel) inhibits the phosphorylation of Uap1, either by inhibiting a yet unknown kinase or blocking the phosphorylation site by directly binding Uap1. The inhibition of Uap1 phosphorylation requires the F-box domain of Fbx17. In the absence of Fbx17 (right panel), phosphorylation of Uap1 inhibits the activity of Uap1 and therefore the production of UDP-GlcNAc. This is counteracted by a decrease in OGA expression and therefore activity, which results in a global increase in O-GlcNAcylation.

ligase. This would also help determine whether, the ligase activity, the binding to Uap1, or indeed both characteristics, are required for Fbxl17 to inhibit the phosphorylation of Uap1.

In contrast to OGT and OGA [40], little is known about the regulation of Uap1, and my data suggest Fbxl17 positively regulates its activity (Figure 4. 13). UDP-GlcNAc levels are significantly decreased when Fbxl17 is knocked down, indicating reduced Uap1 activity. This is consistent with previous studies showing Uap1 expression is important for UDP-GlcNAc levels [34]. Importantly, this affect was observed in the absence of exogenous ubiquitin expression. Although we have not identified the kinase responsible for phosphorylating Uap1, one possibility is that Fbxl17 ubiquitinates this kinase to inhibit its phosphorylation of Uap1 and promote Uap1 activity. Alternatively, Fbxl17 could shield Uap1 from this kinase, via a direct interaction between Fbxl17 and Uap1 (Figure 4. 13).

We have shown that Fbxl17 regulates the *O*-GlcNAcylation pathway since reducing Fbxl17 expression in three cell lines increased global levels of *O*-GlcNAc-modified proteins. We did not assess glycosylation in the ER or Golgi, so cannot rule out a specific role for Fbxl17 there. However, the increase in global *O*-GlcNAcylation may be the result of greater utilisation of UDP-GlcNAc by OGT, which would explain the lower UDP-GlcNAc levels and higher *O*-GlcNAcylation we observed in Fbxl17 knockdown cells. Although OGT expression levels were unchanged, we cannot eliminate the possibility its activity is increased when Fbxl17 levels are reduced. A more likely reason for the higher levels of *O*-GlcNAc, is due to the observed decrease in OGA expression. It has been proposed that there is an optimal level of global *O*-GlcNAcylation levels for cells to function and this is maintained by mutual regulation and balance of OGT/OGA expression and activity [59, 67]. The decrease in OGA expression may represent a compensatory mechanism adopted by the cell to counteract the decrease in Uap1 activity and UDP-GlcNAc levels. *O*-GlcNAcylation is an important post translational modification on many intracellular proteins—including p53, RNA polymerase II, the polycomb complex and Phosphofructokinase 1 (Pfk1), the main regulator of glycolysis—and is essential for viability of several mammalian cell types [64, 70]. Moreover, there is already considerable evidence that GlcNAcylation is altered in breast cancer and other cancers [81, 82, 277, 278]. Caldwell et al. [77] found that breast cancer cells had increased *O*-GlcNAcylation and elevated OGT. Knocking down OGT inhibited tumour growth, decreased cell cycle progression, increased expression of the cell cycle inhibitor p27Kip1, and decreased

invasiveness [77]. High nuclear and cytoplasmic *O*-GlcNAc was also observed in breast cancer patients with increased relapse rates, increased sites of distant metastases and poor outcome [78]. In breast cancer, low OGA levels are linked to higher grade tumours and metastasis [80]. We have shown that the regulation of Uap1 by Fbxl17 and an unidentified kinase, are factors in determining the levels of the *O*-GlcNAcylated proteome.

In summary, by screening for Fbxl17 interacting proteins we have identified Uap1 as a binding partner, rather than a substrate, of Fbxl17. I have established that Fbxl17, as a positive regulator of Uap1, controls global *O*-linked GlcNAcylation and as such, loss-of-function mutations in *FBXL17*, caused by structural rearrangements in breast cancers, would affect this cancer relevant pathway.

5 | ROLE OF FBXL17 IN DNA DAMAGE REPAIR

CHAPTER 5 - Role of Fbxl17 in DNA damage repair

5. Introduction

In the previous chapter, Uap1 was identified as a binding partner, but not a substrate, of Fbxl17 using a Y2H approach. The results of this assay, and other Fbxl17 substrate screens, highlight the importance of using a variety of experimental approaches to discover the regulatory networks of FBPs. Identifying potential interacting proteins through multiple approaches increases confidence in the interaction and verifies the approach. As such, I next carried out a mass spectrometry analysis of SCF^{Fbxl17} E3 ubiquitin ligases (WT, Δ Fbox and Δ 10LRR) to try and identify the regulatory networks controlled by Fbxl17, the results of which are discussed in this chapter.

Over 830 proteins were identified as potential interacting partners of Fbxl17. All published substrates of Fbxl17, except RRM2, were identified in the mass spectrometry screen, verifying the approach for substrate identification. Interestingly, we also noticed that several proteins involved in the DNA damage response (DDR), were identified as potential interacting partners of Fbxl17. The DDR is frequently dysregulated in breast cancers, and as such represents a cancer-relevant pathway that may be regulated by Fbxl17. As discussed in Chapter 3, *FBXL17* is often rearranged in breast cancers leading to loss of SCF^{Fbxl17} activity, which may therefore contribute to aberrant DDR in breast cancers.

The DNA in our cells continually suffers damage from environmental and endogenous stimuli which can generate a variety of DNA lesions including DNA double-strand breaks (DSBs). DSBs are among the most harmful lesions and failure to accurately repair just one of these breaks can trigger permanent growth arrest and cell death and induce gross chromosomal rearrangements [106]. To cope with the continuous threat to genome integrity posed by DSBs, eukaryotic cells have evolved a complex DDR, which coordinates several DNA repair pathways with cell-cycle checkpoint activation. The two major DNA damage repair pathways, homologous recombination (HR) and non-homologous end-joining (NHEJ), are both tightly regulated by intricate control mechanisms that require the action of many proteins.

In this chapter, I set out to test if Fbxl17 plays a role in the DDR and more specifically, whether Fbxl17 plays a role in HR or NHEJ. Several E3 ubiquitin ligases are already known to be involved in the DDR, such as RNF8, RNF168 and BRCA1 [279]. Through further investigation, I have identified the DNA-damage binding protein 53BP1 as a novel substrate

of SCF^{Fbxl17}. SCF^{Fbxl17} can specifically ubiquitinate the BRCT domain of 53BP1 which I propose targets 53BP1 for degradation. 53BP1 is a well-known tumour suppressor involved in the inhibition of DNA end resectioning at DSBs and a key promoter of NHEJ.

Given that the breast cancer-associated rearrangements in *FBXL17* result in loss of SCF^{Fbxl17} activity (see Chapter 3), I also tested the effect of loss of Fbxl17 on the cellular response to DNA damage-inducing agents. Further understanding the role of Fbxl17 in the DDR will hopefully shed light on how Fbxl17, or indeed the lack thereof, may contribute to breast cancer pathogenesis. This may then identify potential therapeutic vulnerabilities of breast cancers containing *FBXL17* mutations, which can be exploited for a subset of breast cancers.

5. Results

5.1 Identifying Fbxl17 interacting partners by mass spectrometry

To identify interacting partners of Fbxl17, SCF^{Fbxl17} E3 ubiquitin ligases were subjected to mass spectrometry analysis. HEK293T cells were transfected with the SCF subunits Cul1, Skp1 and Rbx1, and then co-transfected with either Fbxl17 WT, Fbxl17 Δ Fbox or Fbxl17 Δ 10LRR. Cells transfected with FLAG empty vector were used as a negative control. Fbxl17 was then immunoprecipitated from cells using α -FLAG agarose beads and eluted with FLAG peptide. Purified SCF ligases were then sent for mass spectrometry analysis.

Mass spectrometry generated a list of 838 proteins, representing potential interacting partners of Fbxl17 and non-specific binding to the EV. The total spectrum counts for Fbxl17 and the SCF subunits Cul1, Skp1 and Rbx1 are shown in Figure 5. 1. The total spectrum count represents the total number of spectra (peaks), within a sample, associated with a single protein/ protein group, including those shared with other proteins. The total spectrum counts for Fbxl17 were highest in the SCF^{Fbxl17 Δ 10LRR} sample (Figure 5. 1), which may reflect the increased expression of Fbxl17 Δ 10LRR we have observed previously (see Chapter 3, Figure 3. 4A). As expected SCF^{Fbxl17 Δ Fbox} had lower spectrum counts for Cul1 and Skp1

		Total spectrum count				
SCF ubiquitin ligase subunits		MW	EV	WT Fbxl17	Fbxl17 Δ Fbox	Fbxl17 Δ 10LRR
FBXL17	F-box/LRR-repeat protein 17	76 kDa	49	304	355	484
CUL1	Cullin-1	90 kDa	20	281	57	293
SKP1	S-phase kinase-associated protein 1	19 kDa	3	31	2	25
RBX1	E3 ubiquitin-protein ligase RBX1	12 kDa	0	12	0	4
Published Fbxl17 substrates						
BACH1	Transcription regulator protein BACH1	82 kDa	0	0	7	0
SUFU	Suppressor of fused homolog	54 kDa	0	4	14	14
PRMT1	Protein arginine N-methyltransferase 1	42 kDa	2	2	6	5
KLHL13	Kelch-like protein 13	74 kDa	0	0	37	0
KLHL9	Kelch-like protein 9	69 kDa	0	0	39	0
KLHL12	Kelch-like protein 12	63 kDa	0	0	18	0
KLHL21	Kelch-like protein 21	67 kDa	0	1	10	0
KLHL20	Kelch-like protein 20	68 kDa	0	0	5	0
KLHL25	Kelch-like protein 25	66 kDa	0	0	5	0
KLHL7	Kelch-like protein 7	66 kDa	0	0	5	0
Hexosamine Biosynthetic Pathway related proteins						
OGT	O-linked N-acetylglucosamine transferase 110 kDa subunit	117 kDa	6	2	13	3

Figure 5. 1 - Total spectrum count of SCF subunits and published Fbxl17 substrates

Total spectrum count represents the total number of spectra associated to a single protein/protein group including those shared with other proteins. Colour scale (Green, high; yellow, medium; red, low) applied to total spectrum count for visualisation.

compared to SCF^{Fbxl17} and SCF^{Fbxl17Δ10LRR}, and no spectra for Rbx1 (Figure 5. 1). However, the spectrum counts for Cul1 in the SCF^{Fbxl17ΔFbox} sample and for Fbxl17 and Cul1 in the EV sample were higher than expected, indicating background in the analysis. The samples were run on a highly sensitive Orbitrap Fusion™ Mass Spectrometer, which can detect peptides that are carried over between sample runs. However, the EV sample was run first to avoid this problem and so is unlikely to be the cause of the background counts in this case. Another possibility is that the EV sample was contaminated with another SCF^{Fbxl17} ligase sample and overexpression of the SCF subunits may have led to off-target binding. SCF^{Fbxl17ΔFbox} may be able to homodimerise with WT Fbxl17 which would explain the slight increase in spectrum counts for Cul1 in the SCF^{Fbxl17ΔFbox} sample compared to the EV sample. Despite the background binding, there is a clear difference in total spectrum counts between the EV and SCF^{Fbxl17} (WT, ΔFbox and Δ10LRR) ligase samples.

The mass spectrometry analysis was carried out to identify novel substrates of Fbxl17. To verify this approach could identify Fbxl17 binding partners, I searched the list of hits for known Fbxl17 substrates and compared the total spectrum counts. The first thing I noted was the spectrum counts for known substrates were much lower than for the SCF subunits. This is as expected, given any co-immunoprecipitated proteins are expressed at endogenous levels in HEK293T cells prior to immunoprecipitation of Fbxl17, whereas Fbxl17 (WT, ΔFbox and Δ10LRR) and the SCF subunits were overexpressed. Manual inspection of the hits showed that the published substrates Sufu and PRMT1 co-immunoprecipitated with all three SCF^{Fbxl17} ligases. This suggests that binding to these substrates does not require LRRs 2-11. The total spectrum count for PRMT1 was the same for EV and SCF^{Fbxl17} samples, which further highlights background in the assay, and makes it difficult to distinguish true hits from background. In contrast, BACH1 and the KLHL proteins 7, 9, 12, 13, 20, 21, 25 and 26 co-immunoprecipitated with SCF^{Fbxl17ΔFbox} only (Figure 5. 1). It may be that the deletion of the FBD stabilises binding to some substrates, as they cannot be subsequently ubiquitinated and targeted for degradation, and so remain bound to the FBP. Fbxl17ΔFbox still contains all 11 LRRs and so we do not expect its ability to bind substrates to differ from WT Fbxl17. However, we do not know what effect loss of the FBD has on the 3D structure of Fbxl17ΔFbox. Uap1, the Fbxl17 interacting partner identified in the previous chapter, was not isolated in the mass spectrometry analysis, but interestingly, we isolated the HBP protein OGT which had the highest total spectrum count with SCF^{Fbxl17ΔFbox} (Figure 5. 1).

5.1.1 Mass spectrometry analysis with DAVID

The Database for Annotation, Visualisation and Integrated Discovery (DAVID) is a comprehensive online bioinformatic tool that serves to extract biological meaning from large lists of genes/proteins, such as those generated by mass spectrometry. DAVID provides a comprehensive set of functional annotation tools that utilise an integrated biological knowledgebase to cluster genes into functionally-related gene groups and pathways [280, 281].

In order to determine which pathways are targeted by Fbxl17, the 838 proteins that co-immunoprecipitated with EV or SCF^{Fbxl17} E3 ubiquitin ligases (WT, Δ Fbox or Δ 10LRR), as identified by mass spectrometry, were uploaded to the DAVID Bioinformatics Resources v6.8 website (<https://david.ncifcrf.gov/tools.jsp>). The Functional Annotation tool was used to perform gene-enrichment analysis, pathway mapping and a gene/term similarity search using DAVID default annotations. The 'Functional Annotation Clustering' function clusters functionally similar terms associated with a gene list into groups. The top five enriched annotation clusters for the 838 proteins identified by mass spectrometry are shown in Figure 5. 2. The ribosome/ribosomal proteins comprised the most enriched cluster with an enrichment score of 67.47 (groups with scores ≥ 1.3 are considered enriched). The group enrichment score represents the geometric mean of members' p-values in a corresponding cluster. The top ranked groups are predicted to have consistently lower p-values for their associated members. Ribosomal proteins are amongst the most abundant proteins in the cell, so may also have a greater chance of being isolated by mass spectrometry. It is therefore unsurprising that the ribosome was the highest ranked cluster.

To focus the DAVID analysis on potential pathways regulated by Fbxl17 I next looked at the Kyoto Encyclopaedia of Genes and Genomes (KEGG) pathway analysis annotation. The KEGG pathway reference database is a collection of pathway maps for major biological processes and highlights the proteins involved in these networks. Of the proteins in my list, 56% were assigned to one or more of 25 different enriched KEGG pathways. The most significantly enriched pathway was the Ribosome with 88 proteins, followed by the Proteasome, another highly abundant protein complex, and Spliceosome, with 30 and 38 proteins respectively (Figure 5. 3). Interestingly, several breast cancer-relevant pathways were identified, including the cell cycle, DNA replication and non-homologous end-joining, all of which are

mis-regulated in cancer. DNA damage repair is often aberrant in breast cancers and leads to the high levels of genomic instability associated with this cancer type [282]. Thus, the involvement of Fbxl17 in NHEJ and in DDR represented an interesting avenue to investigate further.



























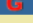


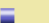





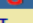
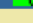






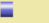


Annotation Cluster 1		Enrichment Score: 67.47			Count	P_Value	Benjamini
<input type="checkbox"/>	UP_KEYWORDS	Ribonucleoprotein	RT		130	2.5E-100	3.3E-98
<input type="checkbox"/>	UP_KEYWORDS	Ribosomal protein	RT		106	3.9E-97	3.8E-95
<input type="checkbox"/>	GOTERM_BP_DIRECT	translation	RT		113	1.4E-79	3.6E-76
<input type="checkbox"/>	GOTERM_MF_DIRECT	structural constituent of ribosome	RT		106	4.1E-78	1.6E-75
<input type="checkbox"/>	GOTERM_CC_DIRECT	ribosome	RT		91	2.5E-76	8.1E-74
<input type="checkbox"/>	KEGG_PATHWAY	Ribosome	RT		88	1.6E-69	3.6E-67
<input type="checkbox"/>	GOTERM_BP_DIRECT	viral transcription	RT		70	4.1E-62	5.4E-59
<input type="checkbox"/>	GOTERM_BP_DIRECT	translational initiation	RT		74	2.9E-59	2.6E-56
<input type="checkbox"/>	GOTERM_BP_DIRECT	nuclear-transcribed mRNA catabolic process, nonsense-mediated decay	RT		68	1.3E-56	8.8E-54
<input type="checkbox"/>	GOTERM_BP_DIRECT	SRP-dependent cotranslational protein targeting to membrane	RT		61	1.9E-55	9.8E-53
<input type="checkbox"/>	GOTERM_BP_DIRECT	rRNA processing	RT		79	1.1E-47	5.0E-45
<input type="checkbox"/>	GOTERM_CC_DIRECT	cytosolic large ribosomal subunit	RT		41	2.8E-36	1.8E-34
Annotation Cluster 2		Enrichment Score: 35.93			Count	P_Value	Benjamini
<input type="checkbox"/>	GOTERM_MF_DIRECT	cadherin binding involved in cell-cell adhesion	RT		80	1.2E-37	2.0E-35
<input type="checkbox"/>	GOTERM_CC_DIRECT	cell-cell adherens junction	RT		81	7.3E-37	5.2E-35
<input type="checkbox"/>	GOTERM_BP_DIRECT	cell-cell adhesion	RT		75	1.8E-35	6.8E-33
Annotation Cluster 3		Enrichment Score: 24.51			Count	P_Value	Benjamini
<input type="checkbox"/>	UP_KEYWORDS	ATP-binding	RT		158	7.1E-33	2.6E-31
<input type="checkbox"/>	UP_KEYWORDS	Nucleotide-binding	RT		182	5.4E-32	1.8E-30
<input type="checkbox"/>	GOTERM_MF_DIRECT	ATP binding	RT		164	8.8E-24	1.2E-21
<input type="checkbox"/>	INTERPRO	P-loop containing nucleoside triphosphate hydrolase	RT		102	7.0E-19	2.5E-16
<input type="checkbox"/>	UP_SEQ_FEATURE	nucleotide phosphate-binding region:ATP	RT		105	1.2E-18	6.6E-16
Annotation Cluster 4		Enrichment Score: 22.98			Count	P_Value	Benjamini
<input type="checkbox"/>	GOTERM_BP_DIRECT	mitochondrial translational elongation	RT		45	2.5E-35	8.3E-33
<input type="checkbox"/>	GOTERM_BP_DIRECT	mitochondrial translational termination	RT		45	5.0E-35	1.4E-32
<input type="checkbox"/>	GOTERM_CC_DIRECT	mitochondrial large ribosomal subunit	RT		33	7.8E-32	3.8E-30
<input type="checkbox"/>	GOTERM_CC_DIRECT	mitochondrial inner membrane	RT		79	1.6E-25	6.3E-24
<input type="checkbox"/>	UP_KEYWORDS	Mitochondrion	RT		101	7.4E-14	1.3E-12
<input type="checkbox"/>	UP_SEQ_FEATURE	transit peptide:Mitochondrion	RT		58	1.1E-12	2.1E-10
<input type="checkbox"/>	UP_KEYWORDS	Transit peptide	RT		59	1.1E-11	2.0E-10
Annotation Cluster 5		Enrichment Score: 15.4			Count	P_Value	Benjamini
<input type="checkbox"/>	UP_KEYWORDS	mRNA splicing	RT		57	3.1E-25	8.1E-24
<input type="checkbox"/>	UP_KEYWORDS	mRNA processing	RT		63	2.7E-24	6.7E-23
<input type="checkbox"/>	GOTERM_BP_DIRECT	mRNA splicing, via spliceosome	RT		50	1.6E-19	2.3E-17
<input type="checkbox"/>	UP_KEYWORDS	Spliceosome	RT		35	5.8E-19	1.3E-17
<input type="checkbox"/>	GOTERM_CC_DIRECT	catalytic step 2 spliceosome	RT		31	3.3E-18	1.1E-16
<input type="checkbox"/>	KEGG_PATHWAY	Spliceosome	RT		38	4.0E-14	3.1E-12
<input type="checkbox"/>	GOTERM_BP_DIRECT	RNA splicing	RT		30	1.8E-9	1.3E-7
<input type="checkbox"/>	GOTERM_CC_DIRECT	spliceosomal complex	RT		21	6.8E-9	1.2E-7
<input type="checkbox"/>	GOTERM_BP_DIRECT	mRNA processing	RT		26	1.9E-6	9.7E-5

Figure 5. 2 - Functional Annotation Clustering Chart

Chart report of annotation terms for all selected annotation categories of the 838 proteins identified by mass spectrometry, grouped into clusters. Top five annotation clusters shown (5/144), classification stringency set to medium. The enrichment score ranks the annotation clusters, using the geometric mean of all the enrichment p-values of each annotation term in the group, the higher, the more enriched. P-value is the significance of the gene-term enrichment calculated with a modified Fisher Exact's test (cutoff 0.1). Count represents the number of genes involved in that term.


























Sublist	Category	Term	RT	Genes	Count	%	P-Value	Benjamini
<input type="checkbox"/>	KEGG_PATHWAY	Ribosome	RT		88	10.5	1.6E-69	3.6E-67
<input type="checkbox"/>	KEGG_PATHWAY	Proteasome	RT		30	3.6	5.2E-24	6.0E-22
<input type="checkbox"/>	KEGG_PATHWAY	Spliceosome	RT		38	4.5	4.0E-14	3.1E-12
<input type="checkbox"/>	KEGG_PATHWAY	RNA transport	RT		43	5.1	1.0E-13	5.8E-12
<input type="checkbox"/>	KEGG_PATHWAY	Epstein-Barr virus infection	RT		27	3.2	1.2E-7	5.5E-6
<input type="checkbox"/>	KEGG_PATHWAY	Pathogenic Escherichia coli infection	RT		15	1.8	4.7E-6	1.8E-4
<input type="checkbox"/>	KEGG_PATHWAY	Protein processing in endoplasmic reticulum	RT		29	3.5	8.3E-6	2.7E-4
<input type="checkbox"/>	KEGG_PATHWAY	Cell cycle	RT		22	2.6	8.1E-5	2.3E-3
<input type="checkbox"/>	KEGG_PATHWAY	Ribosome biogenesis in eukaryotes	RT		16	1.9	6.8E-4	1.7E-2
<input type="checkbox"/>	KEGG_PATHWAY	mRNA surveillance pathway	RT		16	1.9	1.1E-3	2.5E-2
<input type="checkbox"/>	KEGG_PATHWAY	Viral carcinogenesis	RT		27	3.2	1.4E-3	2.9E-2
<input type="checkbox"/>	KEGG_PATHWAY	DNA replication	RT		9	1.1	2.4E-3	4.5E-2
<input type="checkbox"/>	KEGG_PATHWAY	RNA degradation	RT		12	1.4	1.4E-2	2.2E-1
<input type="checkbox"/>	KEGG_PATHWAY	Biosynthesis of antibiotics	RT		24	2.9	1.7E-2	2.4E-1
<input type="checkbox"/>	KEGG_PATHWAY	Carbon metabolism	RT		15	1.8	2.1E-2	2.7E-1
<input type="checkbox"/>	KEGG_PATHWAY	Biosynthesis of amino acids	RT		11	1.3	2.3E-2	2.8E-1
<input type="checkbox"/>	KEGG_PATHWAY	Ubiquitin mediated proteolysis	RT		17	2.0	2.3E-2	2.7E-1
<input type="checkbox"/>	KEGG_PATHWAY	Legionellosis	RT		9	1.1	2.8E-2	3.0E-1
<input type="checkbox"/>	KEGG_PATHWAY	Tight junction	RT		12	1.4	3.3E-2	3.3E-1
<input type="checkbox"/>	KEGG_PATHWAY	Oocyte meiosis	RT		14	1.7	3.8E-2	3.5E-1
<input type="checkbox"/>	KEGG_PATHWAY	Adherens junction	RT		10	1.2	5.0E-2	4.3E-1
<input type="checkbox"/>	KEGG_PATHWAY	Non-homologous end-joining	RT		4	0.5	5.4E-2	4.4E-1
<input type="checkbox"/>	KEGG_PATHWAY	Gap junction	RT		11	1.3	7.4E-2	5.4E-1
<input type="checkbox"/>	KEGG_PATHWAY	Aminoacyl-tRNA biosynthesis	RT		9	1.1	7.8E-2	5.4E-1
<input type="checkbox"/>	KEGG_PATHWAY	NOD-like receptor signaling pathway	RT		8	1.0	8.4E-2	5.5E-1

Figure 5. 3 - KEGG Pathway functional annotation chart

Annotation-term based view of the enriched KEGG pathways associated with the proteins identified in the mass spectrometry analysis for SCF^{Fbxl17} E3 ubiquitin ligases. Count represents the number of genes from the mass spectrometry list associated with each pathway, minimum count threshold set to 2. Percentage (involved genes/total genes in query list). P-value is the significance of the gene-term enrichment calculated with a modified Fisher Exact's test (cutoff 0.1).

5.1.2 Co-immunoprecipitates of SCF^{Fbxl17} ligases are enriched for DNA damage/repair proteins

By surveying the functional annotation clustering, described previously (5.1.1), I found that of the mass spectrometry hits, DNA damage and DNA repair associated-proteins comprised the 19th most enriched cluster with an enrichment score of 5.16 (Figure 5. 4). This was ranked higher than the cluster containing BTB domain-containing proteins (cluster 24, enrichment score 4.24), which are known Fbxl17 substrates (Figure 5. 4).

Annotation Cluster 19		Enrichment Score: 5.16		Count	P_Value	Benjamini
<input type="checkbox"/>	UP_KEYWORDS	DNA damage	RT	35	3.0E-6	2.9E-5
<input type="checkbox"/>	UP_KEYWORDS	DNA repair	RT	31	3.5E-6	3.3E-5
<input type="checkbox"/>	GOTERM_BP_DIRECT	DNA repair	RT	28	3.1E-5	1.2E-3
Annotation Cluster 20		Enrichment Score: 5.1		Count	P_Value	Benjamini
<input type="checkbox"/>	UP_KEYWORDS	Biological rhythms	RT	25	2.0E-10	3.0E-9
<input type="checkbox"/>	GOTERM_BP_DIRECT	rhythmic process	RT	10	1.1E-3	2.8E-2
<input type="checkbox"/>	GOTERM_BP_DIRECT	regulation of circadian rhythm	RT	9	2.3E-3	5.5E-2
Annotation Cluster 21		Enrichment Score: 4.91		Count	P_Value	Benjamini
<input type="checkbox"/>	UP_KEYWORDS	Actin-binding	RT	31	8.8E-7	8.8E-6
<input type="checkbox"/>	GOTERM_MF_DIRECT	actin filament binding	RT	21	6.2E-6	1.8E-4
<input type="checkbox"/>	GOTERM_CC_DIRECT	brush border	RT	11	3.5E-4	3.3E-3
Annotation Cluster 22		Enrichment Score: 4.57		Count	P_Value	Benjamini
<input type="checkbox"/>	INTERPRO	K Homology domain	RT	12	5.2E-7	2.8E-5
<input type="checkbox"/>	GOTERM_MF_DIRECT	mRNA 5'-UTR binding	RT	7	9.8E-7	4.2E-5
<input type="checkbox"/>	SMART	KH	RT	12	1.6E-6	5.7E-5
<input type="checkbox"/>	INTERPRO	K Homology domain, type 1	RT	12	2.6E-6	1.2E-4
<input type="checkbox"/>	UP_SEQ_FEATURE	domain:KH 1	RT	9	3.5E-6	2.4E-4
<input type="checkbox"/>	UP_SEQ_FEATURE	domain:KH 2	RT	9	3.5E-6	2.4E-4
<input type="checkbox"/>	UP_SEQ_FEATURE	domain:KH 3	RT	7	1.8E-5	1.0E-3
<input type="checkbox"/>	GOTERM_MF_DIRECT	translation regulator activity	RT	5	7.8E-5	1.7E-3
<input type="checkbox"/>	GOTERM_BP_DIRECT	mRNA transport	RT	9	1.8E-3	4.4E-2
<input type="checkbox"/>	UP_SEQ_FEATURE	domain:KH 4	RT	4	2.2E-3	7.4E-2
<input type="checkbox"/>	GOTERM_BP_DIRECT	regulation of cytokine biosynthetic process	RT	3	4.2E-2	4.8E-1
Annotation Cluster 23		Enrichment Score: 4.35		Count	P_Value	Benjamini
<input type="checkbox"/>	UP_KEYWORDS	Cell cycle	RT	57	1.0E-7	1.3E-6
<input type="checkbox"/>	UP_KEYWORDS	Mitosis	RT	27	2.7E-5	2.4E-4
<input type="checkbox"/>	UP_KEYWORDS	Cell division	RT	33	1.3E-4	9.1E-4
<input type="checkbox"/>	GOTERM_BP_DIRECT	cell division	RT	34	2.2E-4	6.9E-3
<input type="checkbox"/>	GOTERM_BP_DIRECT	mitotic nuclear division	RT	24	2.3E-3	5.5E-2
Annotation Cluster 24		Enrichment Score: 4.24		Count	P_Value	Benjamini
<input type="checkbox"/>	UP_SEQ_FEATURE	domain:BTB	RT	23	1.3E-7	1.1E-5
<input type="checkbox"/>	GOTERM_CC_DIRECT	Cul3-RING ubiquitin ligase complex	RT	14	8.8E-6	1.1E-4
<input type="checkbox"/>	INTERPRO	Kelch-like protein, gigaaxonin	RT	11	1.2E-5	4.2E-4
<input type="checkbox"/>	INTERPRO	BTB/POZ fold	RT	24	1.4E-5	4.7E-4
<input type="checkbox"/>	UP_SEQ_FEATURE	repeat:Kelch 5	RT	13	1.5E-5	8.7E-4
<input type="checkbox"/>	INTERPRO	BTB/Kelch-associated	RT	13	1.6E-5	5.2E-4
<input type="checkbox"/>	INTERPRO	BTB/POZ-like	RT	23	1.8E-5	5.7E-4
<input type="checkbox"/>	UP_SEQ_FEATURE	repeat:Kelch 4	RT	13	2.8E-5	1.5E-3

Figure 5. 4 - Fbxl17 co-immunoprecipitates are enriched for DNA damage/repair proteins

Chart report of annotation terms for all selected annotation categories for the 838 proteins identified by mass spectrometry grouped into clusters. DNA damage/repair proteins are the 19th most enriched functional annotation cluster, comprising 43 unique proteins. P-value is the significance of the gene-term enrichment calculated with a modified Fisher Exact's test (cutoff 0.1). Count represents the number of genes involved in that term.

In total 43 proteins associated with DNA damage and/or DNA repair were co-immunoprecipitated with Fbxl17 SCF ligases (WT, Δ Fbox or Δ 10LRR) or EV. Among the identified proteins were the NHEJ -associated proteins DNA-PKcs, Ku70 and Ku80 as well the HR and end resection-associated protein Mre11 (Figure 5. 5). Interestingly, the published Fbxl17 substrate BACH1 was also included in this list, suggesting the turnover of BACH1 by Fbxl17 may also have implications in the DDR.

Protein Name	Protein description	MW	Total spectrum count			
			EV	WT Fbxl17	Delta F box	Delta 10LRR
BRCA2	Breast cancer type 2 susceptibility protein	384 kDa	0	0	4	0
BACH1	Transcription regulator protein BACH1	82 kDa	0	0	7	0
POLD1	DNA polymerase delta catalytic subunit POLD1	124 kDa	0	0	3	0
POLE	DNA polymerase epsilon catalytic subunit A	262 kDa	0	1	6	5
E2F7	Transcription factor E2F7	100 kDa	1	1	3	0
FANCD2	Fanconi anemia group D2 protein	164 kDa	0	1	2	1
HUWE1	E3 ubiquitin-protein ligase HUWE1	482 kDa	0	33	28	27
MMS19	MMS19 nucleotide excision repair protein homolog MMS19 1 2	113 kDa	0	0	3	2
MRE11	Double-strand break repair protein MRE11A	81 kDa	0	0	2	0
PDS5A	Sister chromatid cohesion protein PDS5 homolog A	151 kDa	0	1	2	3
RUVBL1	RuvB-like 1	50 kDa	1	3	9	7
RUVBL2	RuvB-like 2	51 kDa	5	6	12	9
SUPT16H	FACT complex subunit SPT16	120 kDa	1	0	3	1
STUB1	E3 ubiquitin-protein ligase CHIP	35 kDa	0	2	7	0
UPF1	Regulator of nonsense transcripts 1	124 kDa	1	0	2	0
XRCC5	X-ray repair cross-complementing protein 5	83 kDa	1	2	14	14
XRCC6	X-ray repair cross-complementing protein 6	70 kDa	4	2	21	19
ASCC3	Activating signal cointegrator 1 complex subunit 3	251 kDa	0	0	2	0
CCAR2	Cell cycle and apoptosis regulator protein 2	103 kDa	2	0	2	0
CDC5L	Cell division cycle 5-like protein	92 kDa	1	3	7	1
DDB1	DNA damage-binding protein 1	127 kDa	0	18	37	18
FMR1	Fragile X mental retardation protein 1	71 kDa	4	2	5	2
MSH6	DNA mismatch repair protein Msh6	153 kDa	0	5	10	7
NONO	Non-POU domain-containing octamer-binding protein	54 kDa	23	10	30	23
NPM1	Nucleophosmin	33 kDa	3	5	12	13
PARP1	Poly [ADP-ribose] polymerase 1	113 kDa	11	10	48	18
PRPF19	Pre-mRNA-processing factor 19	55 kDa	1	2	4	1
PSMD14	26S proteasome non-ATPase regulatory subunit 14	35 kDa	0	4	9	4
PRKDC	DNA-dependent protein kinase catalytic subunit	469 kDa	7	37	49	80
PPP5C	Serine/threonine-protein phosphatase 5	57 kDa	0	3	10	7
RPA1	Replication protein A 70 kDa DNA-binding subunit	68 kDa	0	0	1	2
RIF1	Telomere-associated protein RIF1	274 kDa	0	0	4	2
RPS27L	40S ribosomal protein S27-like	9 kDa	0	1	1	4
RPS3	40S ribosomal protein S3	27 kDa	4	7	19	16
RBX1	E3 ubiquitin-protein ligase RBX1	12 kDa	0	12	0	4
SIRT1	NAD-dependent protein deacetylase sirtuin-1	82 kDa	0	0	3	0
SFPQ	Splicing factor, proline- and glutamine-rich	76 kDa	18	9	29	20
SMC3	Structural maintenance of chromosomes protein 3	142 kDa	1	1	3	1
SSRP1	FACT complex subunit SSRP1 SSRP1 1 1	81 kDa	0	1	11	8
TRIM28	Transcription intermediary factor 1-beta	89 kDa	1	5	37	12
UBR5	E3 ubiquitin-protein ligase UBR5	309 kDa	0	15	31	14
USP7	Ubiquitin carboxyl-terminal hydrolase 7	128 kDa	0	2	3	7
VCP	Transitional endoplasmic reticulum ATPase	89 kDa	0	3	11	1

Figure 5. 5 - Total spectrum counts of DNA damage/repair proteins

Total spectrum counts for Annotation Cluster 19 proteins. Counts represent the total number of spectra associated to a single protein/protein group, including those shared with other proteins. Colour scale (Green; high, yellow; medium, red; low) applied to total spectrum count for visualisation.

Similarly, to the known Fbxl17 substrates, SCF^{Fbxl17ΔFbox} had the highest total spectrum count for most of the DNA damage/repair proteins (35/43) (Figure 5. 5). Over half (24/43) were not detected in the EV sample suggesting they are true interacting partners of the Fbxl17 SCF E3 ubiquitin ligases. The highest spectrum count, across all 43 proteins, was for DNA-PKcs in the SCF^{Fbxl17Δ10LRR} sample (Figure 5. 5).

STRING (Search Tool for the Retrieval of Interacting Genes/Proteins) analysis was also carried out for the 43 DNA damage/repair proteins. STRING is a biological database of known and predicted protein-protein interactions derived from five main sources: genomic context predictions, high-throughput experiments, co-expression, automated text mining and previous knowledge in databases. The DNA damage/repair proteins identified by mass spectrometry were uploaded to the STRING online search tool (<https://string-db.org/>) and a network of protein interactions was generated (Figure 5. 6). A clear cluster of protein-protein interactions can be seen centred around Ku70 (XRCC6) and includes the NHEJ proteins Ku80 (XRCC5) and DNA-PKcs (PRKDC). Several HR-associated proteins are also within this cluster, including RPA and MRE11 which are both involved in DNA end resection. Together these data implicate Fbxl17 is affecting DNA damage and/or DNA repair proteins. I therefore set out to determine whether Fbxl17 plays a role in a specific DDR pathway.

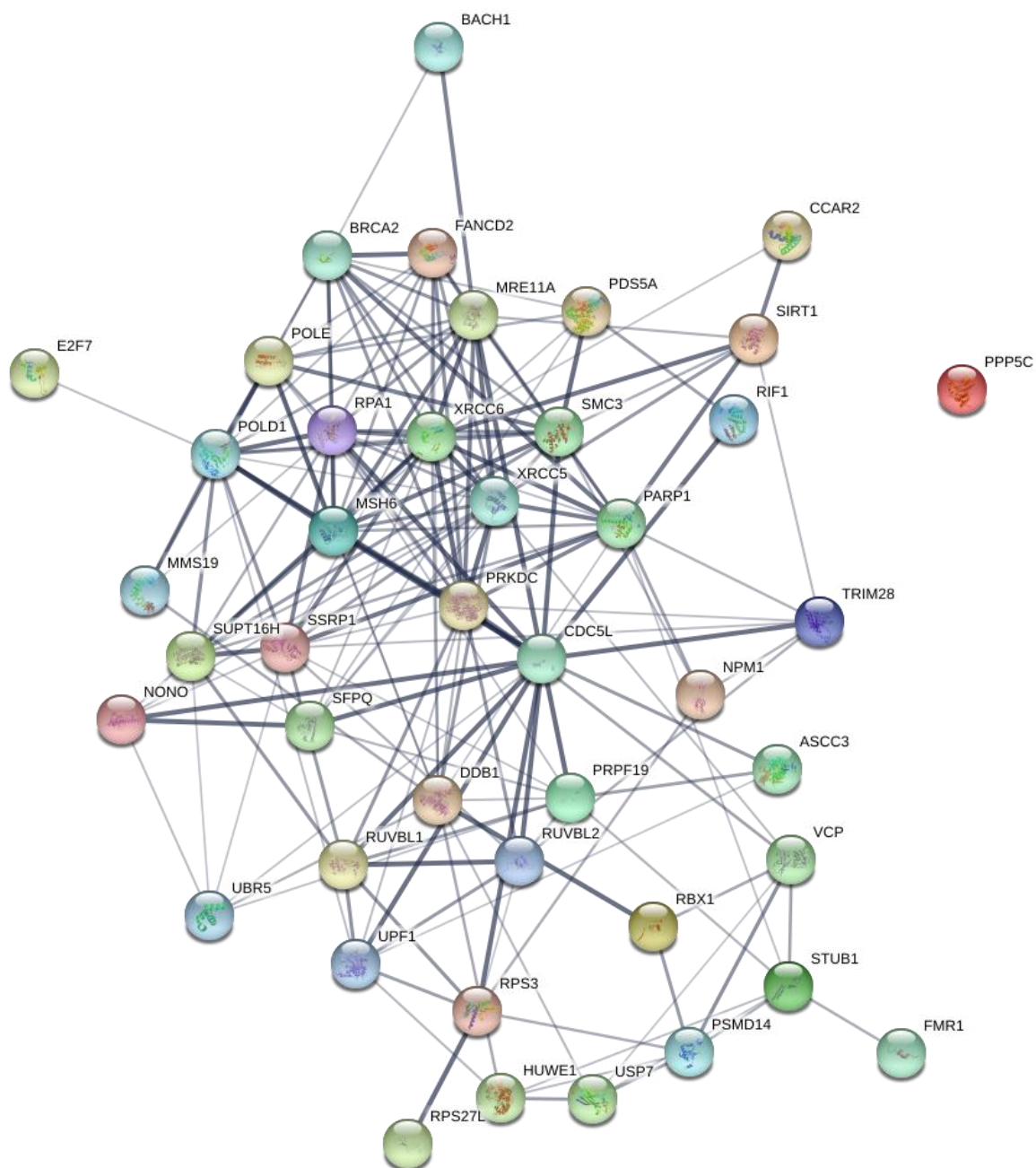


Figure 5. 6 - STRING analysis of DNA damage/ repair proteins identified by DAVID

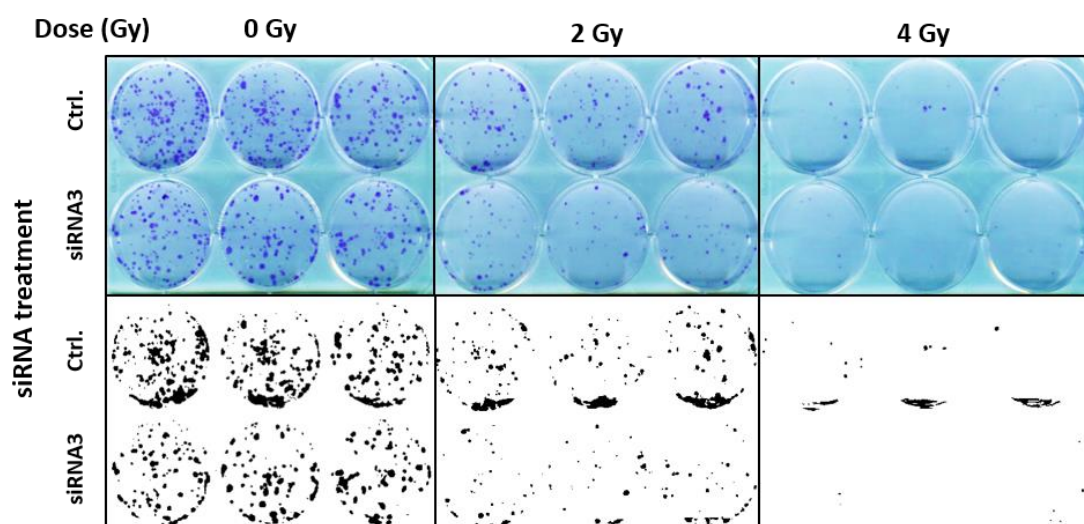
Network of known and predicted protein-protein interactions for the 43 DNA damage/repair proteins identified by mass spectrometry as potential interacting partners of SCF^{Fbx17}. Line thickness indicates the strength of data support, set to medium confidence. Interactions devised from text-mining, high-throughput experiments and co-expression data.

5.2 Fbxl17 knockdown results in a decrease in cell colony size

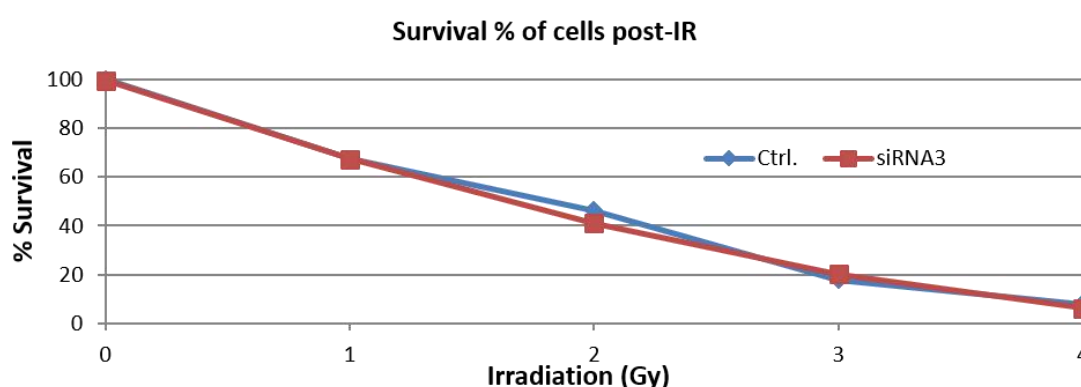
To test whether the presence or absence of Fbxl17 affects the ability of cells to repair and recover from IR-induced DNA damage I performed a colony formation assay. Colony formation or clonogenic assays test the ability of single cells to grow into a colony *in vitro* following insult. U2OS cells were treated with control siRNA or Fbxl17 siRNA3 for 48 hours before plating to 6 well dishes at low density. Cells were then subjected to IR at 1,2,3 and 4 Gy, to induce low levels of DNA damage, and unirradiated cells included as a control. Cells were cultured for ~10 days to allow colonies to form. After crystal violet staining, colonies (>50 cells) were counted and normalised to the unirradiated controls (Figure 5. 7A and B). Increasing the dose of IR consistently decreased cell survival and proliferation, as demonstrated by a reduction in colony formation (Figure 5. 7A and B). Overall, knockdown of Fbxl17 had little effect on colony formation number following IR. siRNA3 treated cells showed the same survival percentages as the control across all IR dosages, except for 2Gy, where siRNA3 cells have a slightly reduced survival (~5%). The experiment would need to be repeated to test if this decrease is significant.

As I identified no difference in total colony number between control and knockdown cells, I next looked to see if there was a difference in colony size. Stained colonies were imaged, magnified 2X and then differentiated into small (<1mm diameter) and large (>1mm) colonies. The number of small colonies was similar, when comparing the controls with Fbxl17 siRNA3 knockdown cells. However, my data shows that there are fewer large colonies in the Fbxl17 knockdown cells, compared to control, after exposure to 1Gy and 2Gy of IR (Figure 5. 7C). One possible explanation for this, is that Fbxl17 knockdown cells take longer to repair the IR-induced damage and so do not form as many large colonies compared to the control cells. Alternatively, knockdown of Fbxl17 may slow the proliferation rate of the cells but have no effect on DNA damage repair. As before, the experiment would need to be repeated to test if the difference in colony size is significant. This suggests that knockdown of Fbxl17 impairs or slows the cells ability to repair and recover from IR-induced DNA damage.

A



B



C

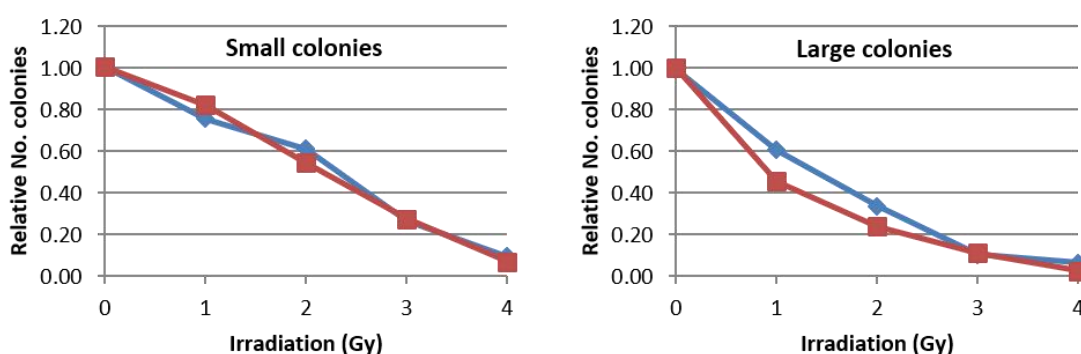


Figure 5. 7 - Fbxl17 knockdown does not affect clonogenic ability of U2OS cells

(A) Representative scanned images (top panel), and corresponding black and white images (bottom panel), of fixed colonies from a clonogenic assay. U2OS cells treated with Fbxl17 siRNA3 or control siRNA and irradiated at the indicated doses (Note: 1Gy and 3Gy images not shown). Colonies formed over 10 days fixed and stained with crystal violet staining solution. **(B)** Graph depicting the survival percentage of plated cells at the indicated IR dosages. Values represent the average number of colonies from 3 biological replicates, relative to unirradiated (0 Gy) cells. **(C)** Graphs representing small and large colonies formed after IR. Values represent mean of three biological replicates, relative to unirradiated cells.

5.3 Cell cycle analysis

The clonogenic assay suggested that knockdown of Fbxl17 slows cell recovery from IR-induced DNA damage. This suggests that Fbxl17 knockdown cells may be less efficient at DNA damage repair. HR and NHEJ operate at different phases of the cell cycle, and so we wanted to test whether this defect could be linked to a certain cell cycle phase, and therefore a certain damage repair pathway. To test this, I performed a cell cycle analysis of Fbxl17 knockdown cells following IR-induced DNA damage. In order to stably knockdown Fbxl17 protein expression, I first designed and constructed three *FBXL17* targeting shRNA plasmids to inhibit Fbxl17 mRNA expression (see section 2.1.6). Fbxl17 shRNA3, which targets the 3' untranslated region (UTR) of *FBXL17*, resulted in an ~80% knockdown of Fbxl17 steady state protein levels in MCF7 (Figure 5. 8) and U2OS cells but had no effect in HEK293T cells (data not shown).

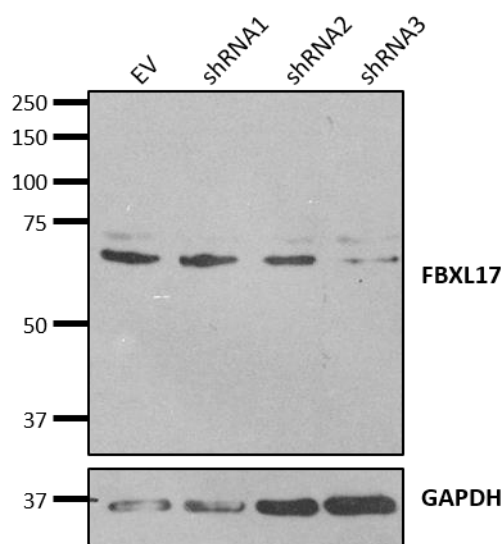


Figure 5. 8 - shRNA knockdown of Fbxl17 expression in MCF7 cells

MCF7 cells infected with Fbxl17 targeting shRNA constructs or empty vector. Whole cell lysates immunoblotted for indicated antibodies.

U2OS cells stably expressing Fbxl17 shRNA3 or mir30 control were irradiated (2Gy) to induce low levels of DNA damage. Cells were then harvested and fixed at 4, 8, 16, 24 and 48h post-irradiation, un-irradiated cells were collected at 4h and 48h as controls. Cells were subsequently stained with propidium iodide (PI), a fluorescent DNA intercalating agent, for flow cytometry analysis. PI stains cells in proportion to the amount of DNA in the cells. Most

cells within a population reside in G1 phase of the cell cycle, as they enter S and G2 phases their DNA content increases, so the DNA stains proportionally more with PI, and therefore the cells fluoresce more brightly (Figure 5. 9A). Both U2OS cells expressing Fbxl17 shRNA3, and those expressing mir30 control, arrested after IR, illustrated by an accumulation of cells in G2/M at 8h and 16h post-irradiation (Figure 5. 9B and C). This suggests that knockdown of Fbxl17 does not affect DNA damage sensing or activation of cell cycle checkpoints. For the most part, the two cell lines behaved the same in response to damage. At 8h and 16h the Fbxl17 knockdown cells have a greater population of cells in G1 than the controls, accompanied by a subtle decrease in cells in S phase. This perhaps suggests the knockdown cells are cycling quicker and proceeding without first repairing damaged DNA or that the cells have arrested in G1 and are unable to recover from the DNA damage as fast. Both cell lines had recovered from IR-induced damage by 24h, with the largest percentage of cells once again in G1.

This preliminary data shows that Fbxl17 knockdown does not have a clear effect on the ability of cells to repair IR-induced DNA damage. The experiment needs to be repeated to determine if the subtle changes observed are significant. It is worth noting that over time, the cell lines expressing Fbxl17 shRNA3 lost their knockdown of Fbxl17 protein expression. This suggests that either the cells with low expression of Fbxl17 are being selected against, or the cells are silencing the shRNA construct to overcome its inhibitory effects. Transient knockdown of Fbxl17 using siRNA would overcome this issue and may also be a better approach given the clonogenic assay results were observed with siRNA-mediated knockdown of Fbxl17 expression. Synchronising the cells at the same cell cycle stage prior to IR may also help to enhance the subtle differences we have observed. DSBs induced by IR can be repaired by both HR and NHEJ and therefore inducing DNA damage by other methods, such as treatment with DNA damaging drugs e.g. Camptothecin, which generates DSBs that can only be repaired by HR, may be a more informative approach.

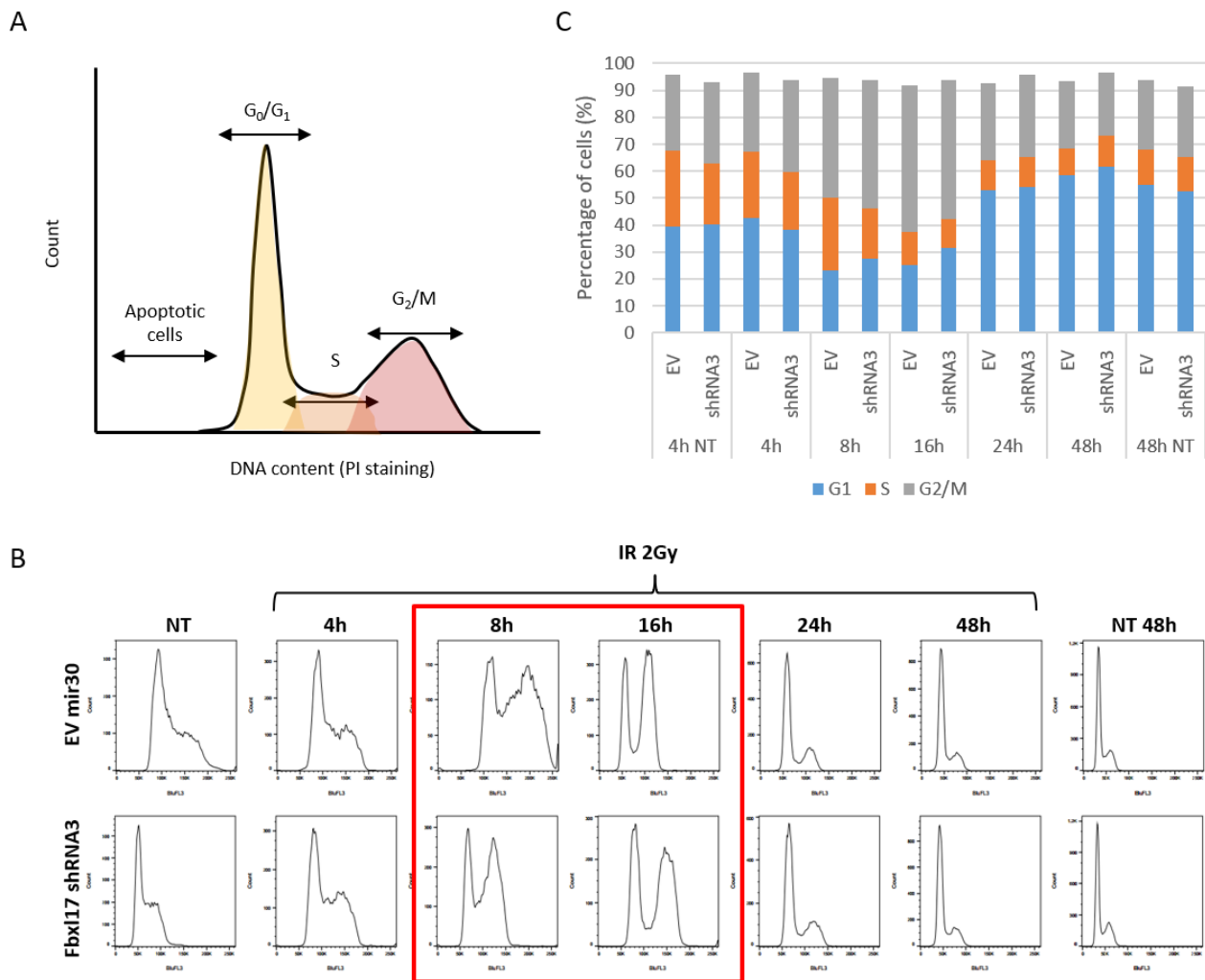


Figure 5. 9 - Cell cycle analysis of Fbxl17 knockdown cells in response to IR

(A) Schematic showing a typical flow cytometry plot for DNA content after PI staining. Labels indicate the cell cycle stages associated with each part of the curve. **(B)** Cell cycle analysis of U2OS cells stably expressing Fbxl17 shRNA3 or mir30 control. Histograms generated by flow cytometry analysis of PI stained cells, fixed at the indicated time points, following IR-induced DNA damage, NT, no treatment/ unirradiated control. **(C)** Quantification of (C) showing the percentage of cells in each stage of the cell cycle at the indicated time points, NT, no treatment/ unirradiated control.

5.4 Loss of Fbxl17 sensitises cells to Camptothecin treatment

The mass spectrometry analysis suggested that Fbxl17 may interact with both HR and NHEJ-associated proteins. To test if either pathway is impaired following Fbxl17 knockdown I treated Fbxl17 knockdown cells with two DNA damaging inducing agents; Camptothecin (CPT), a topoisomerase I inhibitor that induces single-ended DSBs during replication, which requires HR for accurate repair, and etoposide (ETO), a topoisomerase II inhibitor that induces DSBs predominantly repaired by NHEJ. U2OS cells were treated with Fbxl17 siRNA3 or control siRNA for 48h before treatment with 10 μ M CPT or ETO. After 24h of treatment cells were stained with the apoptotic cell marker Annexin V and PI. Flow cytometry analysis was used to determine the percentage of double positive cells as a readout of apoptotic cells (Figure 5. 10 B). Unexpectedly, ETO had no effect on either cell line (data not shown), suggesting the drug concentration was incorrect or the cell line used is resistant to ETO. CPT treatment on the other hand, induced apoptosis in both the control and Fbxl17 knockdown lines, observed as an increase in Annexin V/PI double positive cells. Knockdown of Fbxl17 resulted in a decrease in double Annexin V/PI double positive cells compared to the control, suggesting Fbxl17 affects the cellular response to CPT (Figure 5. 10B).

To test this further, I titrated the concentration of CPT from 0.0625 μ M to 10 μ M and treated the cells as above (Figure 5. 11). As observed previously, at 10 μ M, knockdown of Fbxl17 resulted in a decrease in Annexin V/PI double positive cells. However, at low concentrations of CPT, up to and including 2.5 μ M, knockdown of Fbxl17 expression increased the percentage of apoptotic cells, suggesting cells lacking Fbxl17 are more sensitive to CPT. At 5 μ M the percentage of apoptotic cells was the same between the control and siRNA3 treated cells. Collectively this data suggests that Fbxl17 may be important for DSB repair by HR due to the altered response to CPT in Fbxl17 knockdown cells.

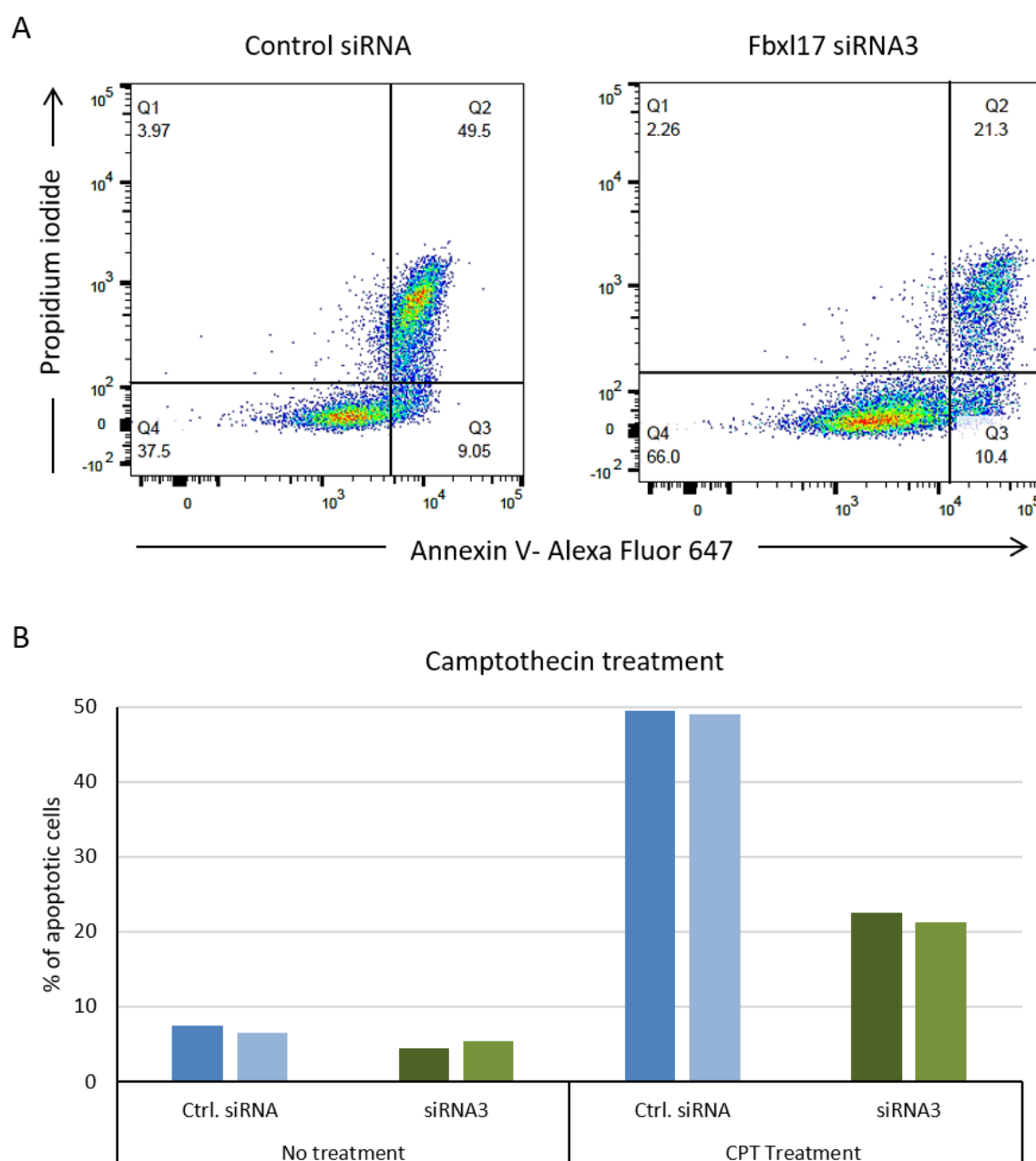


Figure 5. 10 - Knockdown of Fbxl17 protects cells from Camptothecin-induced apoptosis.

(A) A representative Annexin V-Alexa Fluor 647/ propidium iodide staining and flow cytometric analysis of U2OS cells treated with Fbxl17 siRNA3 or control siRNA, undergoing apoptosis following treatment with 10 μ M Camptothecin for 24h, n=2. **(B)** Graphical representation of Annexin V-Alexa Fluor 647/ propidium iodide double positive cells following flow cytometric analysis of U2OS cells treated with Fbxl17 siRNA3 or control siRNA, treated with 10 μ M Camptothecin for 24h, data represents two biological repeats for each condition, both shown side by side.

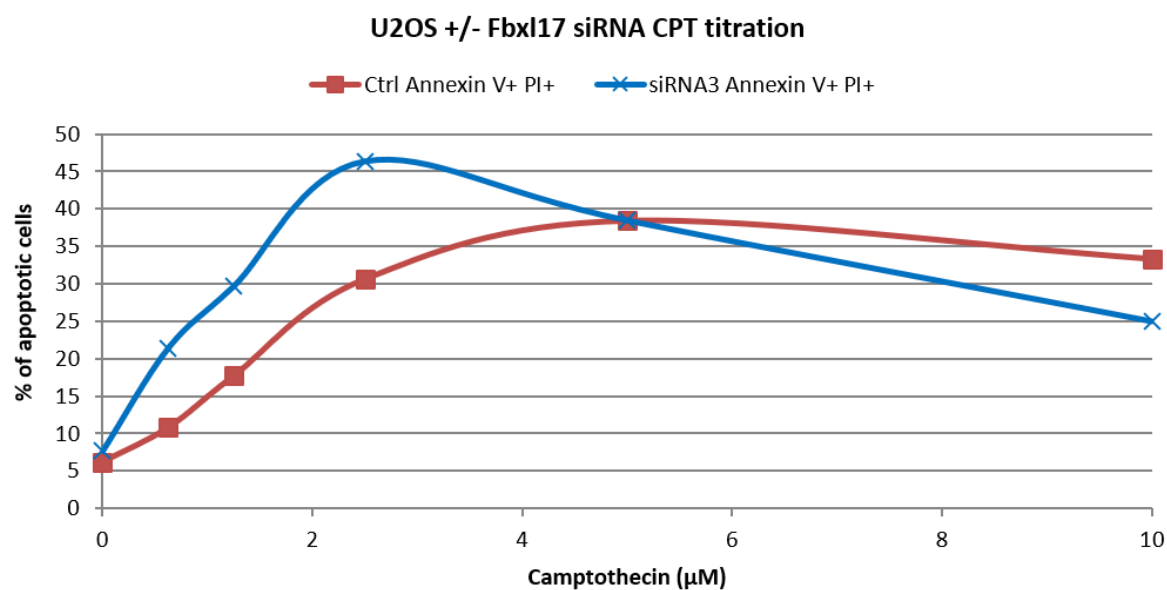


Figure 5. 11 - Fbx17 knockdown sensitises cells to low concentrations of Camptothecin

Graphical representation of Annexin V-Alexa Fluor 647/propidium iodide double positive cells following cytometric analysis of U2OS cells treated with Fbx17 siRNA3 or control siRNA, subjected to increasing concentrations (0.625, 1.25, 2.5, 5 and 10 μM) of Camptothecin for 24h, n=1.

5.5 Fbx17 is recruited to DNA damage sites

DNA damage repair proteins are rapidly recruited to DSBs to ensure rapid and precise repair. Laser micro-irradiation in combination with live cell microscopy can be used to visualise this highly dynamic process in real-time. In short, cells are pre-sensitised with the photosensitiser BrdU which is incorporated into DNA. Upon laser micro-irradiation BrdU forms radicals, which induce DNA breaks specifically in the region of interest that was irradiated. To determine if Fbx17 is recruited to DNA damage sites, U2OS cells stably expressing 53BP1 fused to RFP were transfected with Fbx17 fused to the fluorescent tag Venus at its C-terminus. 53BP1 is a known DNA damage repair protein that has been shown to accumulate at laser-induced DSBs and so acted as a positive control in this experiment [283]. 53BP1 accumulates rapidly at break sites where it inhibits DNA end resection to promote repair by NHEJ. DNA double-strand breaks (DSBs) were induced in the transfected

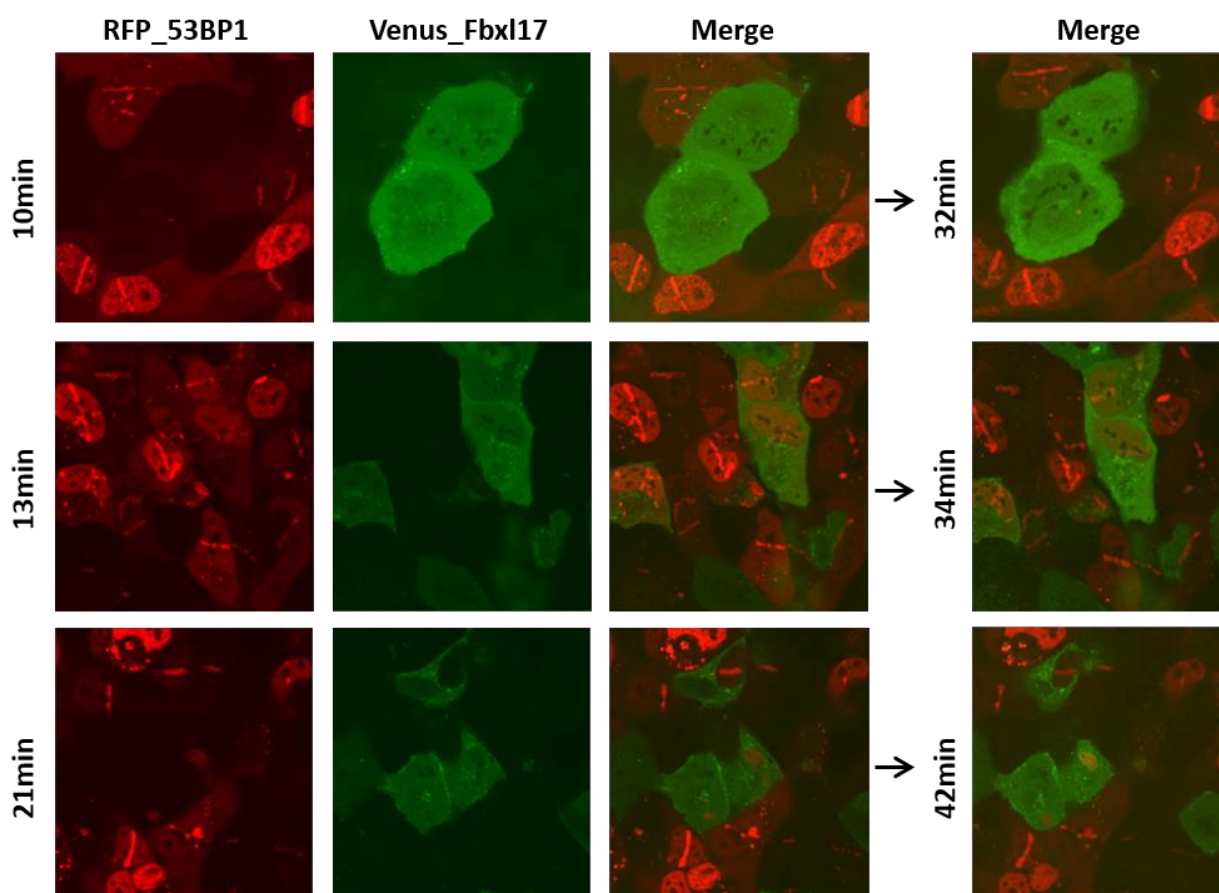


Figure 5. 12 - Fbx17-Venus is not recruited to laser-induced DNA breaks.

Confocal images of live U2OS cells, at indicated time points, after laser micro-irradiation to induce DNA damage. A 405nm laser beam was focused on BrdU-sensitised cells and Venus-tagged Fbx17 (green) was monitored for accumulation. RFP-53BP1 was used as a positive control.

U2OS cells by laser micro-irradiation in lines across the nucleus. Cells were imaged at approximately 10 minutes and 30 minutes post DNA damage induction (Figure 5. 12). RFP-53BP1 showed clear accumulation at the laser induced DSB lines which was maintained throughout, but Fbxl17-Venus showed no accumulation in any cell across the observed time-frame (Figure 5. 12).

During the initial laser lines experiment, we noted that the Fbxl17-Venus construct appeared to show exclusively cytoplasmic localisation which contrasted to what I had previously observed for endogenous Fbxl17 (see section 3.2.3). We proposed that the C-terminal fusion of Venus to Fbxl17 may be interfering with its subcellular localisation. To overcome this, I cloned Fbxl17 into a pEGFP-C1 vector to produce an Fbxl17 construct with GFP fused at the N-terminus of Fbxl17. Confocal microscopy confirmed the C-terminal Fbxl17 fusion protein localised mainly to the nucleus consistent with that of endogenous Fbxl17 (Figure 5. 13).

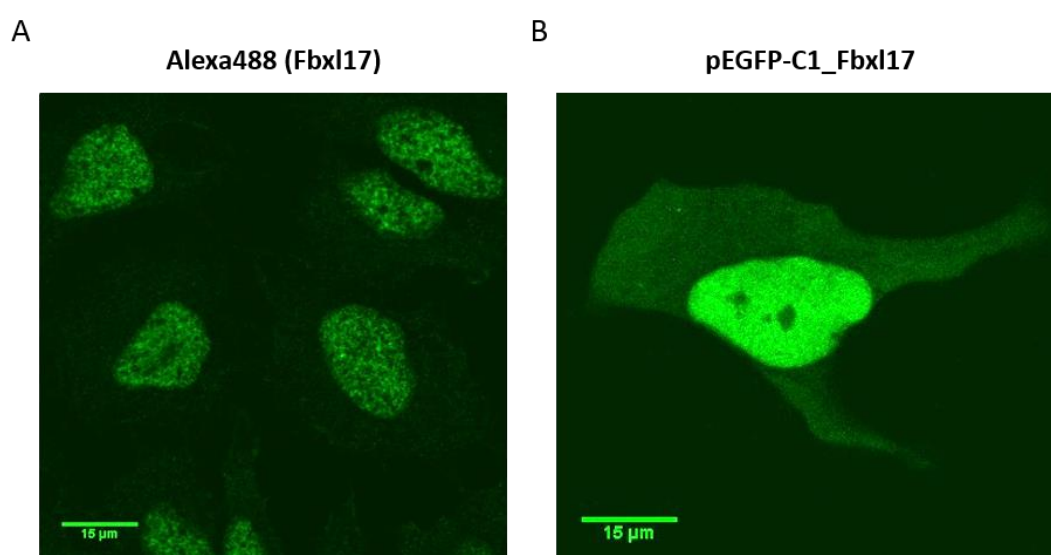


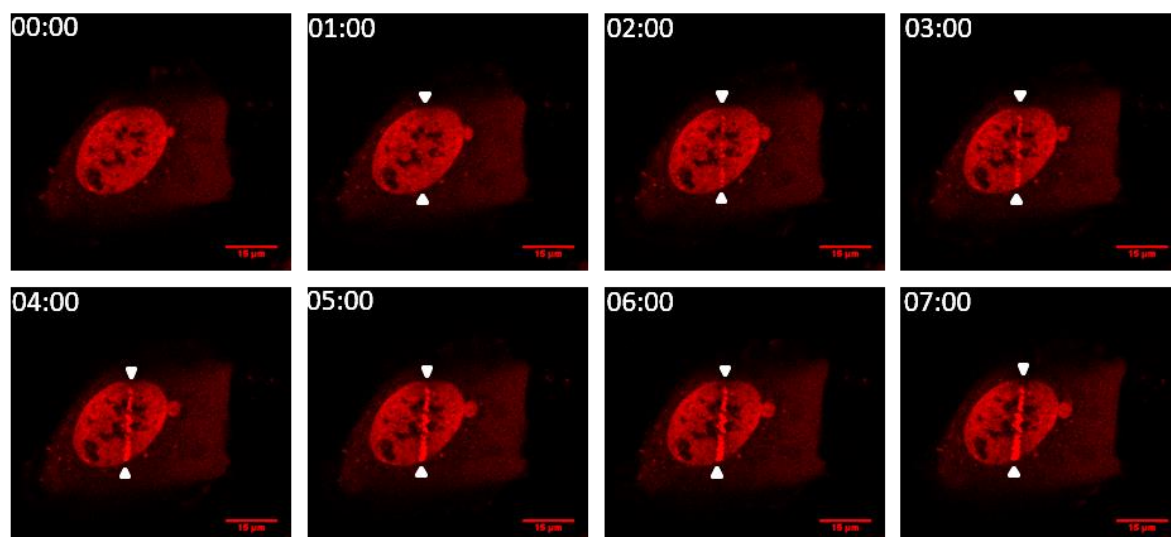
Figure 5. 13 - Localisation of N-terminally GFP-tagged Fbxl17.

(A) Subcellular localisation of endogenous Fbxl17 using immunostaining with FBXL17 antibodies and Alexa Fluor 488. **(B)** Live imaging of a U2OS cell expressing an N-terminally tagged GFP-Fbxl17 construct. Scale bar is 15µm.

The laser micro-irradiation experiments were repeated using GFP-Fbxl17 in U2OS cells expressing RFP-53BP1. We found that Fbxl17 is recruited to the sites of DNA damage, albeit to a lesser extent than the positive control 53BP1. Fbxl17 accumulation could be observed from 2-minutes post-irradiation, coincident with 53BP1, and remained at the DNA damage site for the entire observed time-frame (7 minutes post-irradiation) (Figure 5. 14). Cells

expressing RFP-53BP1 alone were also irradiated to confirm the signal observed in the GFP channel was not bleed-through from the RFP channel; no signal was detected in the GFP channel in this instance (data not shown).

RFP-53BP1



GFP-Fbxl17

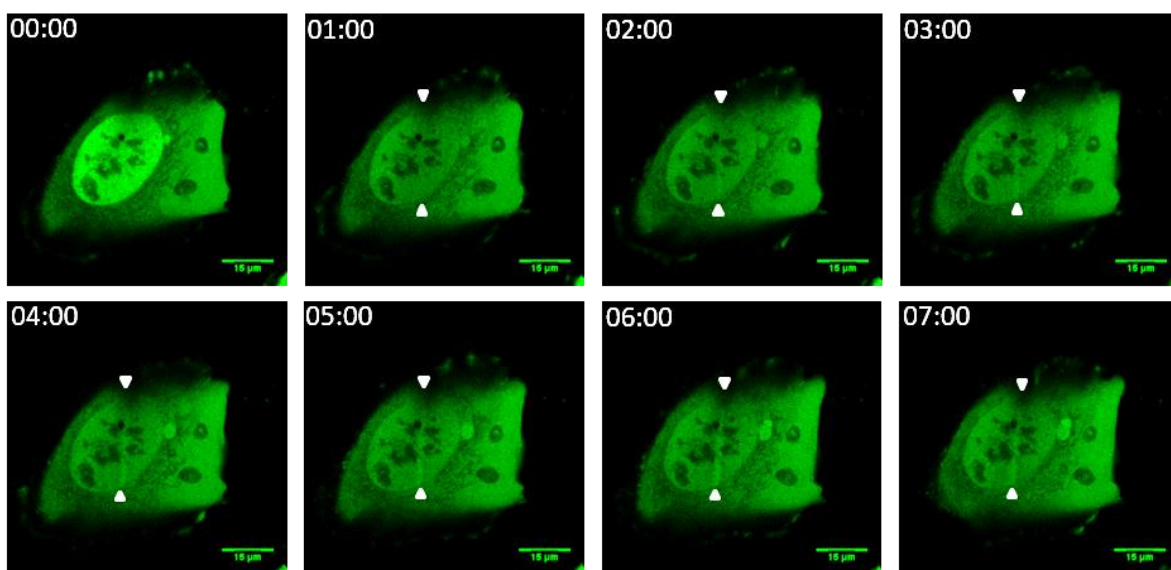


Figure 5. 14 - Fbxl17 is recruited to DNA damage sites

Laser micro-irradiation of U2OS cells stably expressing RFP-53BP1 transfected with GFP-Fbxl17 to determine recruitment of Fbxl17 to double-strand breaks (bottom panel). RFP-53BP1 (top panel) used as a positive control. A 405nm laser beam was focused on BrdU-sensitised cells and live-cell images taken at the indicated time points by confocal microscopy. White triangles indicate site of micro-irradiation across nucleus, images taken at 1 min intervals, scale bar represents 15μm.

5.6 Fbxl17 overexpression decreases 53BP1 expression

After transfecting U2OS cells expressing RFP-53BP1 with GFP-Fbxl17, we were surprised to see, by confocal microscopy, that cells very rarely expressed both proteins at once, inferred by the absence of RFP signal in GFP positive cells. To investigate this further, U2OS cells or U2OS cells stably expressing RFP-53BP1 were transfected with GFP-Fbxl17 or GFP EV control and the steady state levels of 53BP1 were monitored by immunoblotting. Overexpression of Fbxl17 in both cases resulted in decreased 53BP1 protein expression (Figure 5. 15, comparing lane 2 to 3, and 5 to 6). Transfection of GFP-EV unexpectedly increased 53BP1 expression (Figure 5. 15, comparing lane 4 to 5). This may be a cellular response to transfection which is inherently stressful on cells. These data suggest Fbxl17 is targeting 53BP1 for degradation and 53BP1 may therefore be a substrate of SCF^{Fbxl17}.

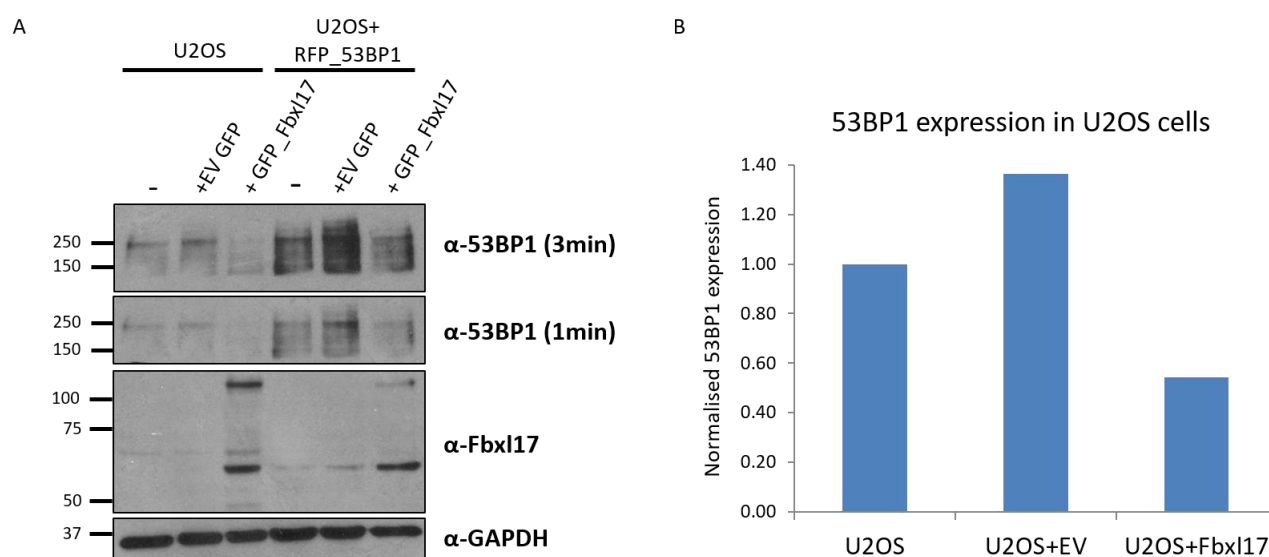


Figure 5. 15 - Fbxl17 overexpression decreases 53BP1 steady state levels.

(A) U2OS or U2OS stably expressing RFP-53BP1 transfected with GFP-Fbxl17 WT or GFP empty vector (EV) for 48h, whole cell lysates immunoblotted with the indicated antibodies, (-) indicates untransfected cells, $n=1$. **(B)** Quantification of the first three lanes in (A) showing endogenous 53BP1 expression in U2OS cells transfected with GFP-Fbxl17 or GFP EV. 53BP1 expression normalised to GAPDH, $n=1$.

5.7 Fbxl17 ubiquitinates the BRCT domain of 53BP1

Fbxl17 ubiquitinates substrates to target them for degradation. We therefore proposed that the decrease in 53BP1 steady state levels is due to ubiquitination by Fbxl17. 53BP1 is a large protein >200kDa and when resolved by SDS-PAGE runs at over 250kDa, therefore observing size shifts in 53BP1 as a result of ubiquitination is difficult to visualise by immunoblotting techniques. Indeed, we did not observe a size shift with 53BP1 fused to RFP which is ~27 kDa, compared to a single ubiquitin molecule which is only 8 kDa. To overcome this, I acquired full-length 53BP1 and five 53BP1 truncated constructs described in [284], from the Jackson lab at the Gurdon Institute, that map the entire length of the protein: full-length 53BP1 (1-1972aa), 53BP1 Δ BRCT (1-1798aa, deletion of tandem BRCT domain), NLS_53BP1_N (1-1052aa with NLS fused to N-terminus), 53BP1_C (1052-1972aa, C-terminal fragment), 53BP1_BRCT (1708-1972aa, NLS and BRCT domain only) and 53BP1_C Δ BRCT (1052-1709aa, C-terminus fragment with deletion of BRCT domain) (Figure 5. 16A). To ensure the constructs could be expressed in mammalian cells, HEK293T cells were transfected with all six constructs. 48h after transfection cells were lysed and resolved on a 4-20% Tris-Glycine gradient gel by SDS-PAGE. All constructs were well expressed, and we noted that higher molecular weight smears characteristic of post-translational modification by ubiquitin were present in two of the lanes, 53BP1_C and 53BP1_BRCT (Figure 5. 16B, lanes 4 and 5). This suggested that the C-terminus of 53BP1 is the acceptor site for this modification. Moreover, given that the higher molecular weight smear was abolished in cells expressing the 53BP1 construct lacking the tandem BRCT domain (Figure 5. 16B, lane 6) we hypothesised that this domain of 53BP1 is ubiquitinated.

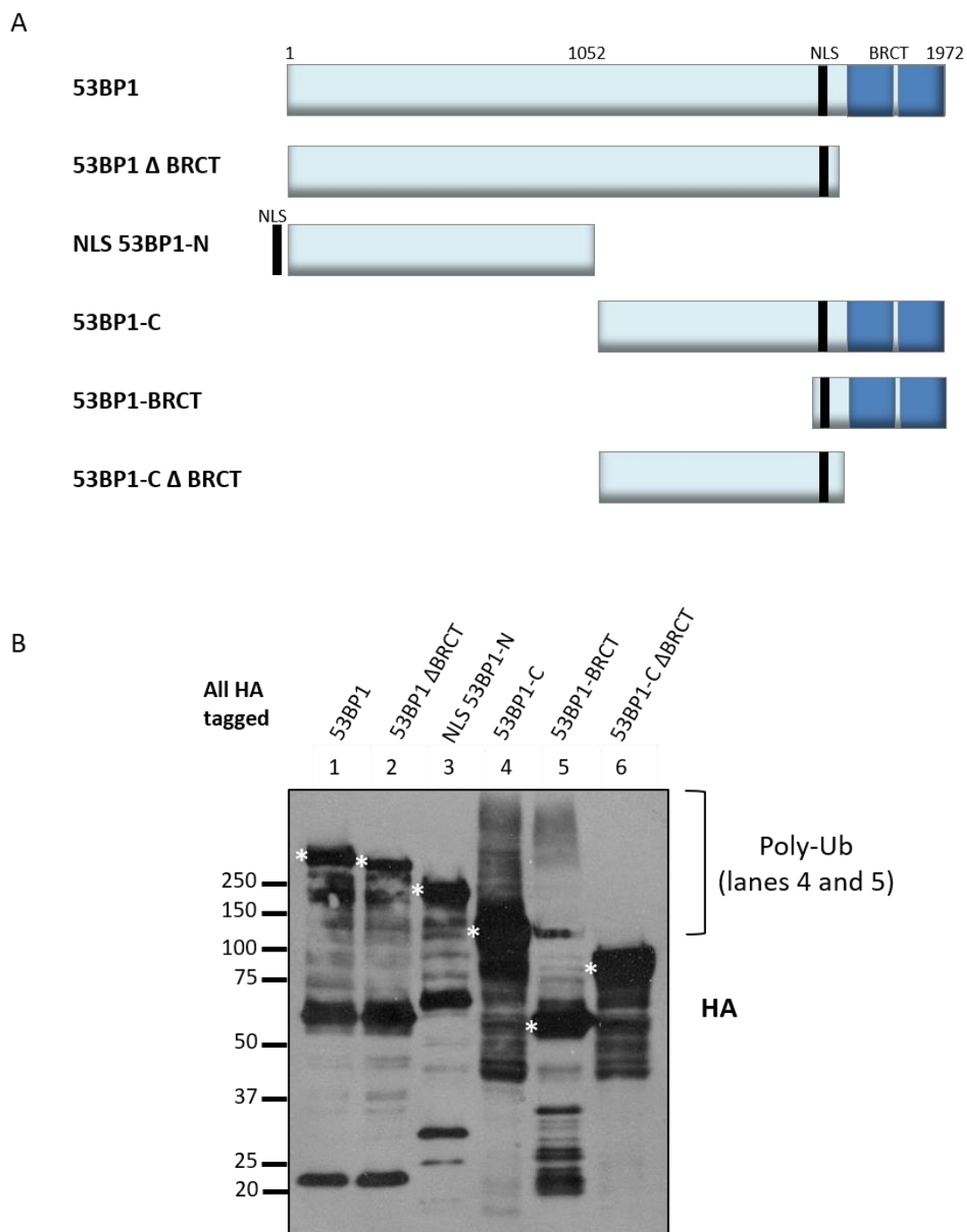


Figure 5. 16 - Schematic of 53BP1 domains and truncated constructs.

(A) Full-length 53BP1 contains a C-terminal nuclear localisation signal (NLS, black line) and tandem BRCT domain (dark blue boxes). All constructs are HA-tagged at the N-terminus. In NLS 53BP1-N the NLS of 53BP1 was fused to the N-terminus of an N-terminal 53BP1 fragment. **(B)** Protein lysates from HEK293T cells transfected with the indicated 53BP1 constructs resolved on a gradient gel by SDS-PAGE and immunoblotted with anti-HA antibody, * indicates band representing 53BP1 fragment, n=2.

To test whether SCF^{Fbxl17} could ubiquitinate the tandem BRCT domain of 53BP1, we conducted an *in vitro* ubiquitination assay. HA-53BP1_BRCT was purified from HEK293T cells by immunoprecipitation and eluted from agarose beads with HA-peptide. HA-Sufu was included as a positive control. Higher molecular weight smears can be seen after the addition of SCF^{Fbxl17} (Figure 5. 17, lane 5). $SCF^{Fbxl17\Delta Fbox}$ shows reduced ubiquitination activity against 53BP1_BRCT compared to SCF^{Fbxl17} (Figure 5. 17, lane 6) suggesting Fbxl17 is capable of ubiquitinating 53BP1_BRCT dependent on its F-box domain. HA-Sufu showed a similar pattern of ubiquitination (Figure 5. 17 , lanes 7 and 8).

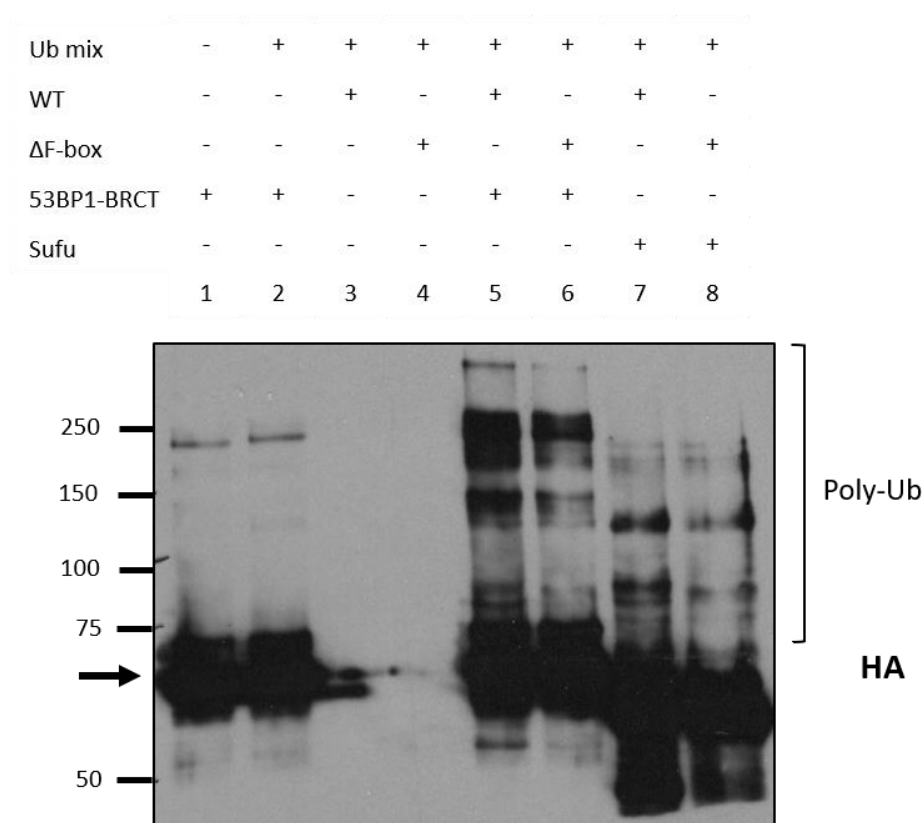


Figure 5. 17 - WT Fbxl17 ubiquitinates the BRCT domain of 53BP1

In vitro ubiquitination assay of SCF^{Fbxl17} and $SCF^{Fbxl17\Delta Fbox}$ ligase complexes in combination with HA-tagged 53BP1_BRCT or HA-tagged Sufu in the presence of a ubiquitin mix (ubiquitin buffer, UBE1, Ubch5a and ATP). Proteins resolved by SDS-PAGE and membrane probed with anti-HA antibody, $n=5$. Arrow indicates position of band representing 53BP1_BRCT (resolves at ~70 kDa). **Experiment done by Gus Rottenberg, reproduced here with permission.**

Despite the increased ubiquitination observed after addition of SCF^{Fbx17}, the assay contained a lot of background ubiquitination. Higher molecular weight smears were observed for 53BP1_BRCT even in the absence of Fbx17 SCF ligases (Figure 5. 17, lanes 1 and 2). This was not due to auto-ubiquitination of SCF^{Fbx17} and SCF^{Fbx17ΔFbox} as the ligases incubated with Ub mix alone did not result in smears (Figure 5. 17, lanes 3 and 4). We hypothesised that the 53BP1_BRCT, which is isolated from HEK293T cells, may already be ubiquitinated before it is used in this assay or that an E3 ubiquitin ligase was being co-immunoprecipitated with 53BP1_BRCT and would therefore be present in 53BP1_BRCT eluates. As SCF^{Fbx17} was shown to increase the ubiquitination of 53BP1_BRCT, we proposed that endogenous Fbx17 may be present in 53BP1_BRCT eluates. To test this, we immunoblotted the 53BP1_BRCT protein purified from HEK293T cells, following lysis with two different lysis buffers, for the presence of Fbx17. Endogenous Fbx17 was identified in both samples suggesting 53BP1 and Fbx17 interact in mammalian cells (Figure 5. 18).

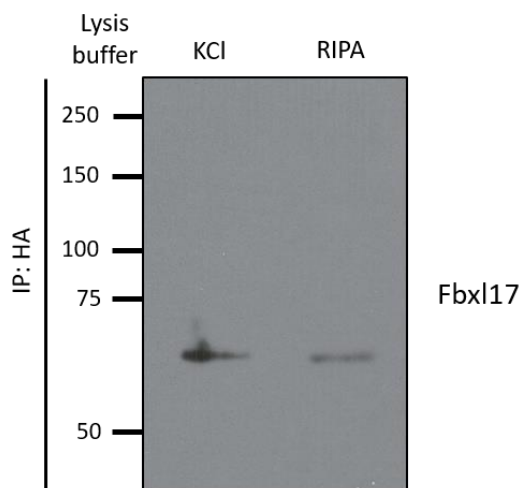


Figure 5. 18 - Endogenous Fbx17 co-immunoprecipitates with HA-53BP1 BRCT.

Immunoprecipitates; using anti-HA beads and elution with HA peptide, of HEK293T cells expressing HA-53BP1 BRCT lysed in KCl or RIPA buffer and probed for endogenous Fbx17. Experiment done by Gus Rottenberg, reproduced here with permission.

Since the data in Figure 5. 18 suggest that Fbxl17 is co-immunoprecipitating with 53BP1 isolated from cells, this might explain the high background seen in the ubiquitination assays. To determine if this was the case and to try to overcome this, 53BP1_BRCT was purified from U2OS cells treated with Fbxl17 siRNA3 to knockdown Fbxl17 expression. This batch of purified 53BP1_BRCT was subsequently used in an *in vitro* ubiquitination assay and 53BP1_BRCT ubiquitination detected by immunoblotting. Remarkably, the high background observed previously was completely abolished (Figure 5. 19, lanes 1 and 2). A higher molecular weight smear was present after the addition of SCF^{Fbxl17} but SCF^{Fbxl17ΔFbox} showed no ubiquitination activity towards 53BP1_BRCT (Figure 5. 19, lanes 5 and 6 respectively). SCF^{Skp2}, another LRR-containing FBP, also showed no ubiquitination activity (Figure 5. 19, lane 7), further highlighting that the ubiquitination of 53BP1_BRCT is specific to the ligase activity of Fbxl17.

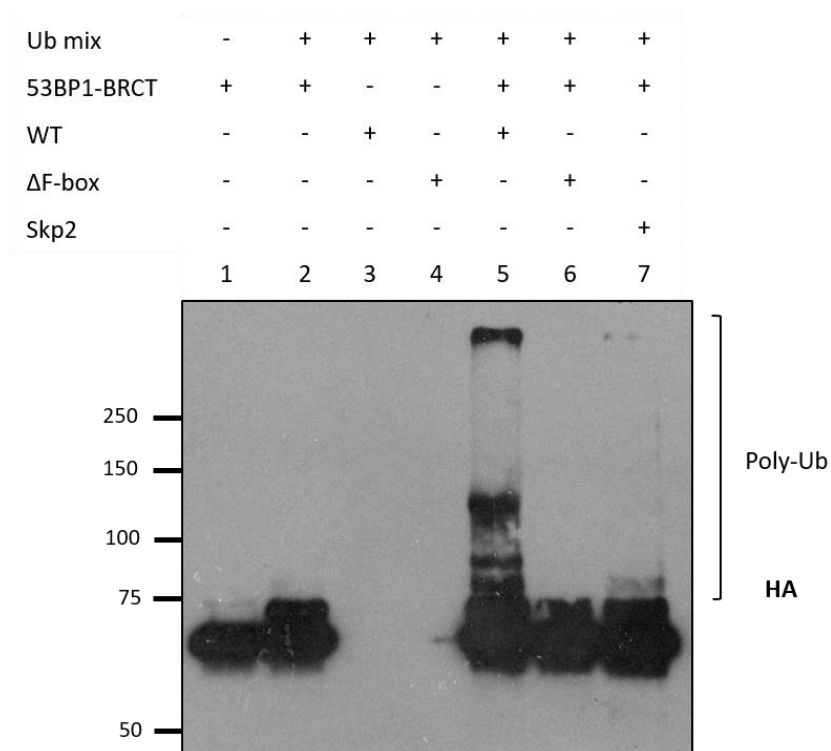


Figure 5. 19 - WT Fbxl17 ubiquitinates the BRCT domain of 53BP1.

In vitro ubiquitination assay of SCF^{Fbxl17} and SCF^{Fbxl17ΔFbox} ligase complexes or the LRR-domain containing FBP Skp2 in combination with HA-tagged 53BP1_BRCT purified from U2OS cells treated with an siRNA targeting Fbxl17. Reaction performed in the presence of a ubiquitin mix (ubiquitin buffer, UBE1, Ubch5a and ATP). Proteins resolved by SDS-PAGE and membrane probed with anti-HA antibody, n=3.

5.8 Loss of Fbxl17 LRRs abolishes ubiquitination of 53BP1

Finally, I tested whether Fbxl17 truncation mutants could ubiquitinate 53BP1_BRCT. I performed an *in vitro* ubiquitination assay with HA-53BP1_BRCT purified from Fbxl17 siRNA-treated U2OS cells, in the presence of SCF^{Fbxl17}, SCF^{Fbxl17ΔFbox}, SCF^{Fbxl17Δ3LRR} or SCF^{Fbxl17Δ10LRR}. Samples were resolved by SDS-PAGE and immunoblotted for the HA-tag on 53BP1_BRCT. As observed previously, a higher molecular weight smear indicative of polyubiquitination was present after the addition of SCF^{Fbxl17} but abolished with SCF^{Fbxl17ΔFbox} (Figure 5. 20, lanes 2 and 3 respectively). Both LRR truncation mutants showed no ubiquitination activity towards 53BP1_BRCT, comparable to SCF^{Fbxl17ΔFbox} (Figure 5. 20, lanes 4 and 5), suggesting the ubiquitination of 53BP1_BRCT by SCF^{Fbxl17} requires LRRs 2-8.

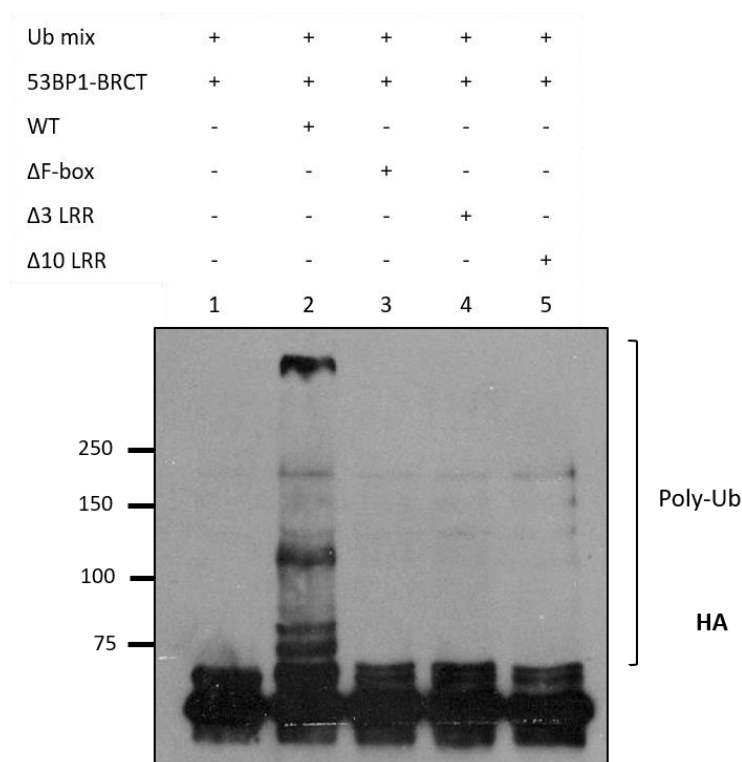


Figure 5. 20 - Loss of Fbxl17 LRRs impairs ubiquitination of 53BP1_BRCT.

In vitro ubiquitination assay of SCF^{Fbxl17} and mutant ligase complexes in combination with HA-tagged 53BP1_BRCT purified from U2OS cells treated with an siRNA targeting Fbxl17, in the presence of a ubiquitin mix (ubiquitin buffer, UBE1, UbcH5a and ATP). Proteins resolved by SDS-PAGE and membrane probed with anti-HA antibody, n=1.

5.9 Fbxl17 interacts with DNA damage response proteins

We serendipitously identified 53BP1 as a substrate of Fbxl17 but note that it was not identified in the Y2H or the mass spectrometry screen. The mass spectrometry results suggested Fbxl17 interacts with other DNA damage response proteins. However, due to high levels of background in the assay it was difficult to identify true interacting partners of Fbxl17. Mammalian expression constructs of three proteins from this list, Ku70, Ku80 and DDB1, were kindly provided by the Jackson and Khoronenkova laboratories. I performed a co-immunoprecipitation assay in mammalian cells to test independently if these were interacting partners of WT Fbxl17. Immunoprecipitates from HEK293T cells expressing either Ku70, Ku80, DDB1, or FLAG EV control, were co-transfected with HA-tagged Fbxl17 (1-701aa). Lysates were immunoprecipitated with anti-FLAG agarose beads and immunoblotted for HA (Fbxl17). Cells were lysed and immunoprecipitated in the presence of the endonuclease benzonase to degrade contaminating DNA/RNA that might potentially bridge, non-specifically, proteins which metabolise DNA. Ku70 and Ku80 were expressed well in HEK293T cells (Figure 5. 21, input) but only weak expression of DDB1 was detected. Fbxl17 expression was low in the Ku70 and Ku80 samples, suggesting an issue with transfection for these samples, as Fbxl17 was detected in the DDB1 and EV lanes (Figure 5. 21, input). Alternatively, overexpression of the Ku proteins may promote Fbxl17 degradation. Western blotting revealed that Fbxl17 co-immunoprecipitates with all three DNA damage/repair proteins (Figure 5. 21). Concurrent with the total spectrum counts (Figure 5. 5), binding of Fbxl17 was strongest with DDB1. However, this most likely reflects the difference in Fbxl17 input, not the binding capacity of Fbxl17. This data verifies that three of the proteins identified by mass spectrometry analysis can co-immunoprecipitate with Fbxl17, suggesting that Fbxl17 may play a role in the DDR by interacting with multiple proteins.

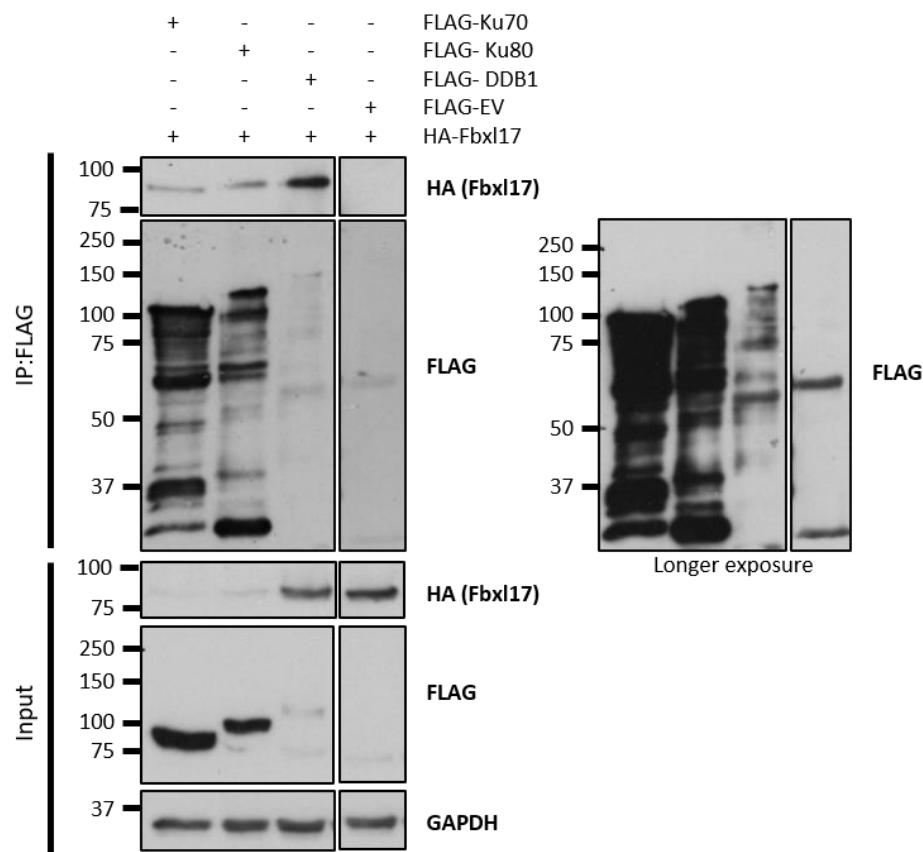


Figure 5. 21 - Co-immunoprecipitation of Fbxl17 with DDR proteins

Immunoprecipitates, using anti-FLAG beads, of HEK293T cells expressing the FLAG-tagged DNA damage/repair proteins Ku70, Ku80 or DDB1, or empty-vector control, co-transfected with HA-tagged Fbxl17, immunoblotted with the indicated antibodies. Right panel represents a longer exposure of the adjacent anti-FLAG blot, n=1.

5. Discussion

To identify further substrates of Fbx17, I performed a mass spectrometry analysis of purified Fbx17 SCF E3 ubiquitin ligases. Over 830 proteins were identified as potential interacting partners of Fbx17. Among these proteins were the known Fbx17 substrates BACH1, Sufu, PRMT1 and several Khl proteins, verifying the mass spectrometry approach for substrate discovery. In addition, no spectra associated with these proteins were isolated in the EV sample, except for PRMT1, for which only 2 counts were recorded in the EV sample. However, many of the known substrates of Fbx17 were only isolated in the SCF^{Fbx17ΔFbox} sample. It may be that the deletion of the FBD stabilises binding to some substrates, as they cannot be subsequently ubiquitinated and targeted for degradation, and so remain bound to the FBP. As a result, the purification conditions for the ligases sent for mass spectrometry analysis may need to be optimised further. It is possible that the wash steps during ligase purification are too stringent and are abolishing the interactions between SCF^{Fbx17} and its substrates. Due to the background observed in the EV sample and the lack of binding of known substrates to SCF^{Fbx17} I did not exclude any proteins for DAVID analysis. A more sophisticated approach is most likely needed to identify potential interacting partners of Fbx17 with some degree of confidence and to test the difference in binding between Fbx17 and the breast cancer-associated truncation mutants.

DAVID analysis of the full list of interacting proteins showed that DNA damage- and DNA repair-associated proteins were enriched, suggesting a role for Fbx17 in the DDR. It is worth noting that the samples prepared for mass spectrometry were not treated with an endonuclease to degrade DNA and RNA in the samples. Therefore, it is possible that contaminating DNA or RNA could have bound non-specifically to the anti-FLAG agarose and resulted in the co-immunoprecipitation of DNA binding proteins. However, this is unlikely to be the case, given over half (24/43) of the DNA damage/repair associated proteins were not detected in the EV sample, and a further 14 recorded total spectrum counts of 4 or less. Furthermore, I verified that Fbx17 can bind to three of the DDR proteins identified by mass spectrometry, Ku70, Ku80 and DDB1, even after benzonase treatment. Fbx17 may be required for the removal of Ku heterodimers from DNA ends, to promote DNA end resection and HR.

The 43 DNA damage/repair proteins identified by mass spectrometry are involved in several repair pathways including HR and NHEJ. In this chapter I set out to determine if Fbxl17 is required for DNA damage repair and whether Fbxl17 plays a role in a specific repair pathway. My preliminary clonogenic assay data suggests that Fbxl17 is required for the repair of and recovery from IR-induced DNA damage, as knockdown of Fbxl17 resulted in decreased colony size. This defect did not seem to be associated with a specific cell cycle stage. However, I have shown that knockdown of Fbxl17 expression changes the response of cells to the DNA damaging agent Camptothecin. Knockdown of Fbxl17 expression sensitised cells to low concentrations of CPT and induced apoptosis. *FBXL17* is frequently rearranged in breast cancers resulting in loss of Fbxl17 activity. As such, CPT treatment may be a useful therapeutic approach for treating tumours with *FBXL17* rearrangements. It would be important to study the relationship between Fbxl17 knockdown and CPT sensitivity in a breast cell line to rule out cell-specific effects.

CPT induces DSBs as a result of replication fork collision during S phase, which can only be repaired efficiently by HR. Therefore, my data suggests Fbxl17 is required for HR. The Traffic light reporter (TLR) assay, which employs a dual fluorescent readout to monitor the efficiency of DNA damage repair by HR and NHEJ simultaneously, could be used to further test this [285]. Although there is not yet enough data to conclusively show Fbxl17 is important for HR, I have been able to show that Fbxl17 is recruited to DNA damage sites. Fbxl17 is recruited to DNA damage sites within 2 minutes of damage induction and is maintained at these sites. It is still unclear how Fbxl17 is recruited to the DNA damage sites and indeed the role it plays there. Fbxl17 may localise independently of other factors or may be brought to break sites via interactions with other DNA damage proteins such as 53BP1. Loss of LRRs reduces Fbxl17 E3 ligase activity and its ability to bind substrates, it would therefore be interesting to test if the Fbxl17 truncation mutants are still recruited to sites of damage and if Fbxl17 can still be recruited in the absence of 53BP1.

Within this chapter I have identified the well-known DNA damage protein, 53BP1, as a novel substrate of Fbxl17. I have shown *in vitro*, that Fbxl17 can ubiquitinate the tandem BRCT domain of 53BP1 and loss of Fbxl17 LRRs abolished this modification. Furthermore, endogenous Fbxl17 co-immunoprecipitates with 53BP1_BRCT. This interaction may be important for the recruitment of Fbxl17 to sites of DNA damage. The tandem BRCT domain

of 53BP1 is an important protein-protein binding domain that facilitates the interaction of 53BP1 with the known tumour suppressor p53 [155]. The chromatin modulator EXPAND1 also binds to the BRCT domain of 53BP1, and relies on this interaction for its accumulation at DSB sites [286]. The ubiquitination of the BRCT domain of 53BP1 by Fbxl17, may facilitate 53BP1 binding to other proteins. Indeed, it has already been shown that the DDR protein MDC1 requires ubiquitination of its tandem BRCT domain to facilitate binding to RAP80, a damage response protein that recruits BRCA1 to sites of damage [287].

A more likely consequence of 53BP1 ubiquitination by Fbxl17, is that it targets 53BP1 for proteasomal degradation. I found that overexpression of Fbxl17 leads to a decrease in 53BP1 steady state protein levels and 53BP1 levels have already been shown to be regulated by ubiquitination. Pozo et al. showed that, under normal growth conditions, 53BP1 exists in three forms; chromatin-bound, lamin A/C-bound and free forms. The free form undergoes Ubch7-dependent proteasomal degradation which maintains a 53BP1 equilibrium [288]. Deletion of Ubch7 stabilised 53BP1 leading to an imbalance in DNA repair pathway choice. Cells favoured NHEJ and, in agreement with what I have observed for Fbxl17 depletion, knockdown of Ubch7 sensitised cells to CPT treatment [288, 289].

53BP1 was not identified as a potential interacting partner of Fbxl17 by mass spectrometry. However, other BRCT domain containing proteins were isolated, including replication factor C subunit 1 (RFC1) and the DNA damage protein PARP1. Mena, et al. have already shown that Fbxl17 can target proteins with shared domains, via its capacity to target BTB domain-containing proteins for degradation [251]. BRCT domain-containing proteins may therefore represent a second group of proteins regulated by Fbxl17. In addition, I have verified that Fbxl17 can co-immunoprecipitate with other DDR proteins that were identified by mass spectrometry, namely Ku70, Ku80 and DDB1. This suggests multiple DDR proteins may be substrates for Fbxl17.

Combining my data, regarding Fbxl17 and 53BP1, I propose a model whereby Fbxl17 regulates the expression of 53BP1 to control DNA damage repair pathway choice. In the presence of Fbxl17, 53BP1 expression is maintained at an equilibrium by the ubiquitination and subsequent degradation of excess/free 53BP1 (Figure 5. 22, left panel), potentially through an interaction with the E2 ubiquitin ligase Ubch7. In the absence of Fbxl17, free 53BP1 accumulates leading to hyper-inhibition of BRCA1 and HR. This leads to the promotion

of NHEJ and a reduced capacity for repair by HR (Figure 5. 22, right panel). This would explain the increased sensitivity to CPT we have observed. Therefore, by identifying the DNA repair pathway regulated by Fbxl17, we can exploit the vulnerabilities caused by Fbxl17 depletion as a therapeutic strategy to treat Fbxl17 deficient tumours in breast cancer.

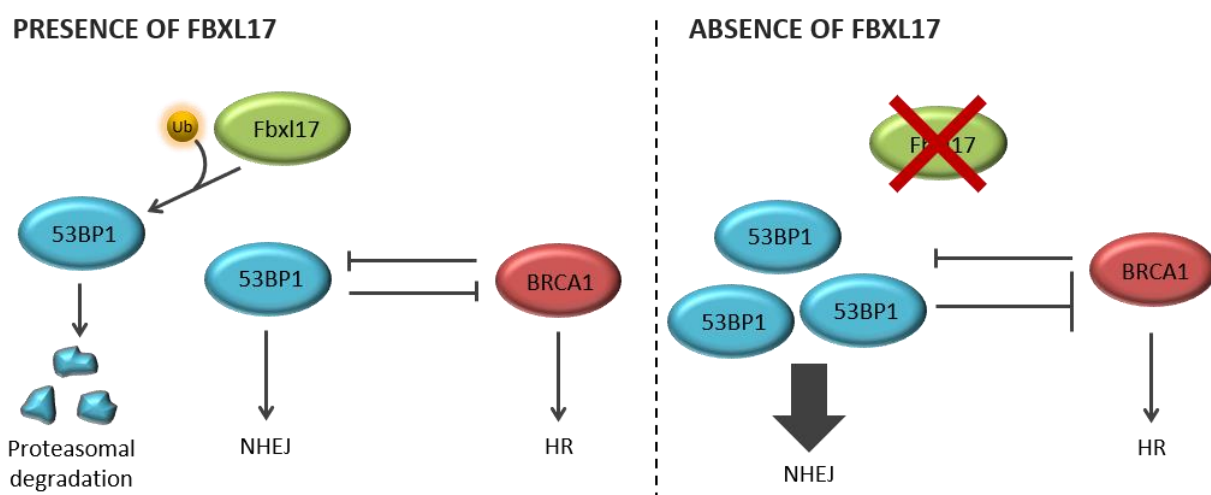


Figure 5. 22 - Proposed model of interaction between Fbxl17 and 53BP1

I propose a model whereby, Fbxl17 ubiquitinates free 53BP1 to target it for proteasomal degradation, to control 53BP1 expression levels. In the absence of Fbxl17, 53BP1 accumulates and hyper-inhibits BRCA1 and therefore HR, leading to the promotion of DNA repair by NHEJ.

6 | GENERAL DISCUSSION

CHAPTER 6 - General Discussion

Breast cancer remains the most common cancer in women globally and is characterised by vast genomic instability and tumour heterogeneity. Increasingly, somatic rearrangements are found to be prevalent in breast cancer and importantly, are proving to be therapeutically significant. By surveying the METABRIC array-CGH copy number data, it was previously shown that the F-box protein encoded by *FBXL17* is rearranged in ~7% of breast cancer cases [255]. In agreement with this, I have observed further examples of *FBXL17* rearrangements in paired-end whole-genome DNA and RNA sequencing data from 250 primary breast tumours, of which ~2% contained rearrangements in *FBXL17*.

What is most striking about *FBXL17* rearrangements, is the consistency with which they target the region of the gene that encodes the substrate-binding leucine rich repeat (LRR) domain of Fbxl17. The rearrangements I observed in primary breast tumours often truncate Fbxl17, removing some or all the LRRs and sometimes also the FBD. The non-synonymous point mutations identified by surveying publicly available TCGA data, also cluster at the FBD and LRRs of *FBXL17*. Truncation rate has previously been utilised as a method to distinguish if a protein is an oncogene (OG) or a tumour suppressor gene (TSG) [290]. By studying the mutational pattern of proteins, it has been shown that TSGs are often enriched in truncation events, suggesting Fbxl17 may therefore be a tumour suppressor. Interestingly, the non-synonymous mutations of the FBP Fbxw7, a well-known tumour suppressor, also occur most frequently within the WD40 domains, the protein-protein interaction domains akin to LRRs in Fbxl17 (Figure 6. 1, middle panel) [291]. In contrast Skp2, an LRR domain-containing protein and known oncogene is mutated across the entire length of the protein (Figure 6. 1, bottom panel) [292]. This data suggests the mutational pattern of FBPs may be useful for determining whether they have oncogenic or tumour suppressive properties in cancer.

TSGs are associated with loss of function (LOF) mutations; therefore, we would expect the loss of Fbxl17 LRRs to be deleterious to its function. Indeed, I have shown that truncating Fbxl17 LRRs impaired its association with the other SCF holoenzyme subunits Skp1, Cul1 and Rbx1, and decreased its ubiquitination activity, despite mutant constructs still containing the characteristic FBD. Loss of the LRRs also affected Fbxl17 binding to its targets, which we propose is due to a change in the 3D structure of Fbxl17. Thus, genomic rearrangements in *FBXL17* have the potential to disrupt SCF^{Fbxl17}-regulated networks in cancer cells.

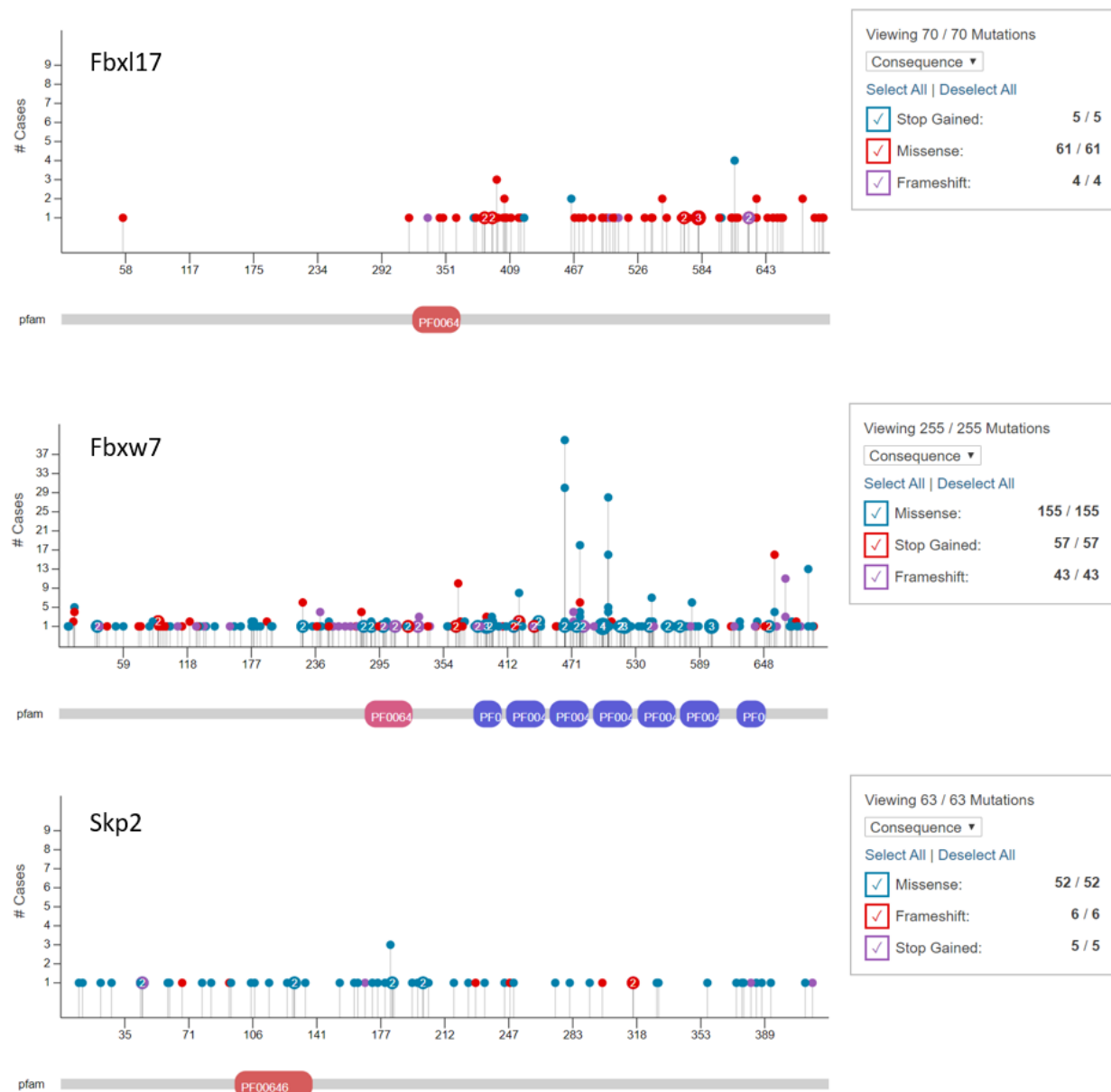


Figure 6. 1 - Mutational patterns of the FBPs Fbxl17, Fbxw7 and Skp2

Non-synonymous somatic mutations mapped to Fbxl17, the known tumours suppressor Fbxw7 and the known oncogene Skp2, as reported by The Cancer Genome Atlas (TCGA), visualised using GDC Data Portal. Pink rectangle below graphs represent the location of the F-box domain, blue rectangles represent WD40 repeats.

To investigate the functional effect of these rearrangements, we performed a yeast two-hybrid screen to identify Fbxl17-interacting proteins. Among the 37 binding partners Uap1, an enzyme involved in O-GlcNAcylation of proteins was identified most frequently. I have

demonstrated that Fbxl17 binds to UAP1 directly and this requires LRRs 2-8. The data published so far for Fbxl17 has exclusively identified typical substrates of SCF^{Fbxl17}. SCF^{Fbxl17} shows a strong preference for K48-linked ubiquitin chains, the linkage type often mediated by SCF-type ubiquitin ligases, and as such the ubiquitination activity of SCF^{Fbxl17} has been shown to target substrates for proteasomal degradation. However, I have identified Uap1 as a binding partner, rather than a substrate, of Fbxl17. The interaction of Uap1 with Fbxl17 does not lead to its ubiquitination and subsequent degradation by the proteasome. Instead, Fbxl17 inhibits the phosphorylation of Uap1, which we propose regulates its activity. This suggests a novel role for Fbxl17 in 'running interference', whereby Fbxl17 can bind to proteins, but instead of ubiquitinating them, regulates their modification by post-translational modifications (PTMs) other than ubiquitin. It has already been shown that FBPs can have SCF-independent roles [198]. However, the inhibition of Uap1 phosphorylation requires the FBD and LRRs of Fbxl17, and so is likely to be an SCF-dependent function of Fbxl17. These data show that not all proteins that bind to the protein-binding domains of FBPs are substrates for ubiquitination. Furthermore, these data highlight an important crosstalk that exists between PTMs. The crosstalk between phosphorylation and ubiquitination is well established [293, 294] but should be considered more frequently in studies of this kind. Loss of Fbxl17 activity will not only affect the ubiquinome of the cell, but will also undoubtedly have consequences for other PTMs, such as phosphorylation, and as I have shown in this dissertation *O*-GlcNAcylation.

As discussed previously, the breast cancer-associated rearrangements in Fbxl17 result in loss of SCF^{Fbxl17} activity. We were able to show a striking effect of reducing Fbxl17 expression on at least one important cancer-relevant pathway, in a relevant cell type. This was through its regulation of Uap1 and the HBP. Knockdown of Fbxl17 resulted in a decrease in UDP-GlcNAc, the intermediate produced by Uap1. Surprisingly, this resulted in elevated *O*-GlcNAcylation, an important PTM for a number of intracellular proteins, arguing for a functional role for Fbxl17 in this pathway. The increase in *O*-GlcNAc modified proteins is most likely due to a compensatory decrease in OGA levels, which I observed following Fbxl17 knockdown. Increased protein *O*-GlcNAcylation and changes in OGT and/or OGA expression have already been reported in breast cancer, where increased global *O*-GlcNAcylation and low OGA levels are linked to higher grade tumours and metastasis [80]. In agreement with this, the majority of primary breast tumours we identified with *FBXL17* rearrangements were basal-like, and

half clustered to IntClust 10, both of which are considered aggressive and high-risk subtypes. Breast tumours containing *FBXL17* mutations may therefore represent a clinically important subset of cancer, that can be targeted therapeutically.

To identify further interacting partners of Fbxl17, we performed a mass spectrometry analysis of purified Fbxl17 SCF E3 ubiquitin ligases. Co-immunoprecipitates were enriched for DNA damage/DNA repair proteins suggesting a novel role for Fbxl17 in the DNA damage response (DDR). In support of this, I have demonstrated that Fbxl17 is rapidly recruited to DNA damage sites upon double-strand break (DSB) induction and loss of Fbxl17 impairs the ability of cells to repair and recover from IR-induced DNA damage.

Unlike the role of Fbxl17 in the HBP, Fbxl17 plays a more classical role in the DDR. I have shown that Fbxl17 can ubiquitinate the tandem BRCT domain of the well-known DDR protein 53BP1, which we propose targets 53BP1 for proteasomal degradation. Studies have already shown that the levels of 53BP1 are controlled by proteasomal degradation, with the E2 ubiquitin-conjugating enzyme Ubch7 implicated in modifying and degrading free forms of 53BP1 under normal growth conditions [288, 289]. This ensures an equilibrium of 53BP1 expression is maintained. Loss of Ubch7 stabilises 53BP1 creating an imbalance in DSB repair pathway choice, forcing cells to adopt NHEJ instead of HR [288, 289]. The E3 ubiquitin ligase responsible for bringing together 53BP1 and Ubch7 remains undiscovered and as such I propose that Fbxl17 is the E3 ligase responsible for dictating the ubiquitination of 53BP1. Auto-ubiquitination assays for Fbxl17 have shown that it is active with several E2 enzymes and therefore could form an active SCF complex with Ubch7. However, perhaps the most compelling evidence that Fbxl17 controls 53BP1 levels is the increased sensitivity to CPT observed following siRNA knockdown of Fbxl17 expression. Han et al. observed increased sensitivity to CPT in Ubch7-depleted cells which they proposed was due to the inability of these cells to promote HR for the repair of CPT-induced DSBs. Therefore, whilst only preliminary, my data suggests that Fbxl17 and its regulation of 53BP1 may also be required for efficient HR. By understanding the vulnerabilities of Fbxl17 deficient tumours we can design suitable therapeutic strategies to effectively treat this subset of breast cancers.

In conclusion, by surveying structural rearrangements in cancer databases, we discovered rearrangements commonly occur in *FBXL17* which affect its ability to bind substrates and assemble as part of a functional SCF ubiquitin ligase complex. By screening for Fbxl17

interacting proteins, we have identified two regulatory networks of Fbxl17 which provide an insight into the role of Fbxl17 in breast cancer pathogenesis. We first discovered Uap1 as a binding partner of Fbxl17 and established that Fbxl17 is a regulator of global O-linked GlcNAcylation. I then identified a novel role for Fbxl17 in the DDR, through its ability to ubiquitinate 53BP1, and propose Fbxl17 is important for HR-mediated DSB repair. These pathways may be amenable to therapeutic targeting in the future for the treatment of breast cancers rearranged in *FBXL17*.

REFERENCES

1. Stratton, M.R., P.J. Campbell, and P.A. Futreal, *The cancer genome*. Nature, 2009. **458**(7239): p. 719-24.
2. Hanahan, D. and R.A. Weinberg, *The hallmarks of cancer*. Cell, 2000. **100**(1): p. 57-70.
3. Hanahan, D. and R.A. Weinberg, *Hallmarks of cancer: the next generation*. Cell, 2011. **144**(5): p. 646-74.
4. Unknown. *Cancer facts & figures- Worldwide data*. 2018 07/11/2019]; Available from: <http://www.wcrf.org/int/cancer-facts-figures/worldwide-data>.
5. CRUK. *The Three Most Common Cancers in Females, Percentages of All Cancer Cases Excluding Non-Melanoma Skin Cancer (C00-C97 excl. C44), UK, 2016*. 2016 07/11/2019]; Available from: <http://www.cancerresearchuk.org/health-professional/cancer-statistics/incidence/common-cancers-compared#ref-2>.
6. CRUK. *Breast cancer mortality statistics*. 2017 07/11/2019]; Available from: <https://www.cancerresearchuk.org/health-professional/cancer-statistics/statistics-by-cancer-type/breast-cancer/mortality#heading-Zero>.
7. Polyak, K., *Heterogeneity in breast cancer*. J Clin Invest, 2011. **121**(10): p. 3786-8.
8. Allison, K.H. and G.W. Sledge, *Heterogeneity and cancer*. Oncology (Williston Park), 2014. **28**(9): p. 772-8.
9. Jordan, V.C., *Tamoxifen: a most unlikely pioneering medicine*. Nat Rev Drug Discov, 2003. **2**(3): p. 205-13.
10. Goldenberg, M.M., *Trastuzumab, a recombinant DNA-derived humanized monoclonal antibody, a novel agent for the treatment of metastatic breast cancer*. Clin Ther, 1999. **21**(2): p. 309-18.
11. Schnitt, S.J., *Classification and prognosis of invasive breast cancer: from morphology to molecular taxonomy*. Mod Pathol, 2010. **23 Suppl 2**: p. S60-4.
12. Perou, C.M., et al., *Molecular portraits of human breast tumours*. Nature, 2000. **406**(6797): p. 747-52.
13. Parker, J.S., et al., *Supervised risk predictor of breast cancer based on intrinsic subtypes*. J Clin Oncol, 2009. **27**(8): p. 1160-7.
14. Chen, J.M., et al., *Genomic rearrangements in inherited disease and cancer*. Semin Cancer Biol, 2010. **20**(4): p. 222-33.
15. Nik-Zainal, S., et al., *Landscape of somatic mutations in 560 breast cancer whole-genome sequences*. Nature, 2016. **534**(7605): p. 47-54.
16. Hasty, P. and C. Montagna, *Chromosomal Rearrangements in Cancer: Detection and potential causal mechanisms*. Mol Cell Oncol, 2014. **1**(1).
17. Nakagawa, H., et al., *Cancer whole-genome sequencing: present and future*. Oncogene, 2015. **34**(49): p. 5943-50.
18. Edwards, P.A. and K.D. Howarth, *Are breast cancers driven by fusion genes?* Breast Cancer Res, 2012. **14**(2): p. 303.
19. Stephens, P.J., et al., *Complex landscapes of somatic rearrangement in human breast cancer genomes*. Nature, 2009. **462**(7276): p. 1005-10.
20. Yoshihara, K., et al., *The landscape and therapeutic relevance of cancer-associated transcript fusions*. Oncogene, 2015. **34**(37): p. 4845-54.
21. Paratala, B.S., et al., *Emerging Role of Genomic Rearrangements in Breast Cancer: Applying Knowledge from Other Cancers*. Biomark Cancer, 2016. **8**(Supple 1): p. 1-14.
22. Gu, W., F. Zhang, and J.R. Lupski, *Mechanisms for human genomic rearrangements*. Pathogenetics, 2008. **1**(1): p. 4.
23. Stephens, P.J., et al., *The landscape of cancer genes and mutational processes in breast cancer*. Nature, 2012. **486**(7403): p. 400-4.

24. Kytölä, S., et al., *Chromosomal alterations in 15 breast cancer cell lines by comparative genomic hybridization and spectral karyotyping*. Genes Chromosomes Cancer, 2000. **28**(3): p. 308-17.
25. Mars, W.M. and G.F. Saunders, *Chromosomal abnormalities in human breast cancer*. Cancer Metastasis Rev, 1990. **9**(1): p. 35-43.
26. Chin, S.F., et al., *High-resolution aCGH and expression profiling identifies a novel genomic subtype of ER negative breast cancer*. Genome Biol, 2007. **8**(10): p. R215.
27. Banerji, S., et al., *Sequence analysis of mutations and translocations across breast cancer subtypes*. Nature, 2012. **486**(7403): p. 405-9.
28. Ellis, M.J., et al., *Whole-genome analysis informs breast cancer response to aromatase inhibition*. Nature, 2012. **486**(7403): p. 353-60.
29. Curtis, C., et al., *The genomic and transcriptomic architecture of 2,000 breast tumours reveals novel subgroups*. Nature, 2012. **486**(7403): p. 346-52.
30. Dawson, S.J., et al., *A new genome-driven integrated classification of breast cancer and its implications*. EMBO J, 2013. **32**(5): p. 617-28.
31. Wood, L.D., et al., *The genomic landscapes of human breast and colorectal cancers*. Science, 2007. **318**(5853): p. 1108-13.
32. Bignell, G.R., et al., *Signatures of mutation and selection in the cancer genome*. Nature, 2010. **463**(7283): p. 893-8.
33. Merid, S.K., D. Goranskaya, and A. Alexeyenko, *Distinguishing between driver and passenger mutations in individual cancer genomes by network enrichment analysis*. BMC Bioinformatics, 2014. **15**: p. 308.
34. Adélaïde, J., et al., *A recurrent chromosome translocation breakpoint in breast and pancreatic cancer cell lines targets the neuregulin/NRG1 gene*. Genes Chromosomes Cancer, 2003. **37**(4): p. 333-45.
35. Baker, S.J., et al., *Chromosome 17 deletions and p53 gene mutations in colorectal carcinomas*. Science, 1989. **244**(4901): p. 217-21.
36. Baker, S.J., et al., *p53 gene mutations occur in combination with 17p allelic deletions as late events in colorectal tumorigenesis*. Cancer Res, 1990. **50**(23): p. 7717-22.
37. Kluth, M., et al., *Deletion of 18q is a strong and independent prognostic feature in prostate cancer*. Oncotarget, 2016. **7**(52): p. 86339-86349.
38. Slamon, D.J., et al., *Studies of the HER-2/neu proto-oncogene in human breast and ovarian cancer*. Science, 1989. **244**(4905): p. 707-12.
39. Sasaki, T., et al., *The biology and treatment of EML4-ALK non-small cell lung cancer*. Eur J Cancer, 2010. **46**(10): p. 1773-80.
40. Pao, W. and N. Girard, *New driver mutations in non-small-cell lung cancer*. Lancet Oncol, 2011. **12**(2): p. 175-80.
41. Jonna, S., et al., *Detection of NRG1 Gene Fusions in Solid Tumors*. Clin Cancer Res, 2019. **25**(16): p. 4966-4972.
42. Adeva-Andany, M.M., et al., *Liver glucose metabolism in humans*. Biosci Rep, 2016. **36**(6).
43. Vander Heiden, M.G., L.C. Cantley, and C.B. Thompson, *Understanding the Warburg effect: the metabolic requirements of cell proliferation*. Science, 2009. **324**(5930): p. 1029-33.
44. Warburg, O., F. Wind, and E. Negelein, *THE METABOLISM OF TUMORS IN THE BODY*. J Gen Physiol, 1927. **8**(6): p. 519-30.
45. WARBURG, O., *On the origin of cancer cells*. Science, 1956. **123**(3191): p. 309-14.

46. Lunt, S.Y. and M.G. Vander Heiden, *Aerobic glycolysis: meeting the metabolic requirements of cell proliferation*. *Annu Rev Cell Dev Biol*, 2011. **27**: p. 441-64.
47. Jones, R.G. and C.B. Thompson, *Tumor suppressors and cell metabolism: a recipe for cancer growth*. *Genes Dev*, 2009. **23**(5): p. 537-48.
48. DeBerardinis, R.J., et al., *The biology of cancer: metabolic reprogramming fuels cell growth and proliferation*. *Cell Metab*, 2008. **7**(1): p. 11-20.
49. Li, Z. and H. Zhang, *Reprogramming of glucose, fatty acid and amino acid metabolism for cancer progression*. *Cell Mol Life Sci*, 2016. **73**(2): p. 377-92.
50. Marshall, S., V. Bacote, and R.R. Traxinger, *Discovery of a metabolic pathway mediating glucose-induced desensitization of the glucose transport system. Role of hexosamine biosynthesis in the induction of insulin resistance*. *J Biol Chem*, 1991. **266**(8): p. 4706-12.
51. Marshall, S., W.T. Garvey, and R.R. Traxinger, *New insights into the metabolic regulation of insulin action and insulin resistance: role of glucose and amino acids*. *FASEB J*, 1991. **5**(15): p. 3031-6.
52. Akella, N.M., L. Ciraku, and M.J. Reginato, *Fueling the fire: emerging role of the hexosamine biosynthetic pathway in cancer*. *BMC Biol*, 2019. **17**(1): p. 52.
53. Chiaradonna, F., F. Ricciardiello, and R. Palorini, *The Nutrient-Sensing Hexosamine Biosynthetic Pathway as the Hub of Cancer Metabolic Rewiring*. *Cells*, 2018. **7**(6).
54. Love, D.C. and J.A. Hanover, *The hexosamine signaling pathway: deciphering the "O-GlcNAc code"*. *Sci STKE*, 2005. **2005**(312): p. re13.
55. Haltiwanger, R.S., G.D. Holt, and G.W. Hart, *Enzymatic addition of O-GlcNAc to nuclear and cytoplasmic proteins. Identification of a uridine diphospho-N-acetylglucosamine:peptide beta-N-acetylglucosaminyltransferase*. *J Biol Chem*, 1990. **265**(5): p. 2563-8.
56. Szumilo, T., et al., *Purification to homogeneity and properties of UDP-GlcNAc (GalNAc) pyrophosphorylase*. *J Biol Chem*, 1996. **271**(22): p. 13147-54.
57. Wang-Gillam, A., I. Pastuszak, and A.D. Elbein, *A 17-amino acid insert changes UDP-N-acetylhexosamine pyrophosphorylase specificity from UDP-GalNAc to UDP-GlcNAc*. *J Biol Chem*, 1998. **273**(42): p. 27055-7.
58. Itkonen, H.M., et al., *UAP1 is overexpressed in prostate cancer and is protective against inhibitors of N-linked glycosylation*. *Oncogene*, 2015. **34**(28): p. 3744-50.
59. Yang, X. and K. Qian, *Protein O-GlcNAcylation: emerging mechanisms and functions*. *Nat Rev Mol Cell Biol*, 2017. **18**(7): p. 452-465.
60. Aebi, M., *N-linked protein glycosylation in the ER*. *Biochim Biophys Acta*, 2013. **1833**(11): p. 2430-7.
61. Van den Steen, P., et al., *Concepts and principles of O-linked glycosylation*. *Crit Rev Biochem Mol Biol*, 1998. **33**(3): p. 151-208.
62. Hanover, J.A., *Glycan-dependent signaling: O-linked N-acetylglucosamine*. *FASEB J*, 2001. **15**(11): p. 1865-76.
63. Issad, T. and M. Kuo, *O-GlcNAc modification of transcription factors, glucose sensing and glucotoxicity*. *Trends Endocrinol Metab*, 2008. **19**(10): p. 380-9.
64. Hart, G.W., M.P. Housley, and C. Slawson, *Cycling of O-linked beta-N-acetylglucosamine on nucleocytoplasmic proteins*. *Nature*, 2007. **446**(7139): p. 1017-22.
65. Jackson, S.P. and R. Tjian, *O-glycosylation of eukaryotic transcription factors: implications for mechanisms of transcriptional regulation*. *Cell*, 1988. **55**(1): p. 125-33.

66. Hart, G.W., et al., *Cross talk between O-GlcNAcylation and phosphorylation: roles in signaling, transcription, and chronic disease*. Annu Rev Biochem, 2011. **80**: p. 825-58.
67. Ong, Q., W. Han, and X. Yang, *O-GlcNAc as an Integrator of Signaling Pathways*. Front Endocrinol (Lausanne), 2018. **9**: p. 599.
68. Kazemi, Z., et al., *O-linked beta-N-acetylglucosamine (O-GlcNAc) regulates stress-induced heat shock protein expression in a GSK-3beta-dependent manner*. J Biol Chem, 2010. **285**(50): p. 39096-107.
69. Qian, K., et al., *Transcriptional regulation of O-GlcNAc homeostasis is disrupted in pancreatic cancer*. J Biol Chem, 2018. **293**(36): p. 13989-14000.
70. Gambetta, M.C., K. Oktaba, and J. Müller, *Essential role of the glycosyltransferase *sxc/Ogt* in polycomb repression*. Science, 2009. **325**(5936): p. 93-6.
71. Slawson, C. and G.W. Hart, *O-GlcNAc signalling: implications for cancer cell biology*. Nat Rev Cancer, 2011. **11**(9): p. 678-84.
72. Liu, F., et al., *O-GlcNAcylation regulates phosphorylation of tau: a mechanism involved in Alzheimer's disease*. Proc Natl Acad Sci U S A, 2004. **101**(29): p. 10804-9.
73. Yuzwa, S.A., et al., *Increasing O-GlcNAc slows neurodegeneration and stabilizes tau against aggregation*. Nat Chem Biol, 2012. **8**(4): p. 393-9.
74. Zhu, Y., et al., *The emerging link between O-GlcNAc and Alzheimer disease*. J Biol Chem, 2014. **289**(50): p. 34472-81.
75. Yang, X., et al., *Phosphoinositide signalling links O-GlcNAc transferase to insulin resistance*. Nature, 2008. **451**(7181): p. 964-9.
76. Fardini, Y., et al., *O-GlcNAcylation: A New Cancer Hallmark?* Front Endocrinol (Lausanne), 2013. **4**: p. 99.
77. Caldwell, S.A., et al., *Nutrient sensor O-GlcNAc transferase regulates breast cancer tumorigenesis through targeting of the oncogenic transcription factor FoxM1*. Oncogene, 2010. **29**(19): p. 2831-42.
78. Tiainen, S., et al., *High extent of O-GlcNAcylation in breast cancer cells correlates with the levels of HAS enzymes, accumulation of hyaluronan, and poor outcome*. Breast Cancer Res Treat, 2016. **160**(2): p. 237-247.
79. Dahl, E., et al., *Systematic identification and molecular characterization of genes differentially expressed in breast and ovarian cancer*. J Pathol, 2005. **205**(1): p. 21-8.
80. Krześlak, A., et al., *Gene expression of O-GlcNAc cycling enzymes in human breast cancers*. Clin Exp Med, 2012. **12**(1): p. 61-5.
81. Sodi, V.L., et al., *mTOR/MYC Axis Regulates O-GlcNAc Transferase Expression and O-GlcNAcylation in Breast Cancer*. Mol Cancer Res, 2015. **13**(5): p. 923-33.
82. Ferrer, C.M., et al., *O-GlcNAcylation regulates cancer metabolism and survival stress signaling via regulation of the HIF-1 pathway*. Mol Cell, 2014. **54**(5): p. 820-31.
83. Zhu, Q., et al., *O-GlcNAcylation plays a role in tumor recurrence of hepatocellular carcinoma following liver transplantation*. Med Oncol, 2012. **29**(2): p. 985-93.
84. Lynch, T.P., et al., *Critical role of O-Linked β-N-acetylglucosamine transferase in prostate cancer invasion, angiogenesis, and metastasis*. J Biol Chem, 2012. **287**(14): p. 11070-81.
85. Itkonen, H.M., et al., *O-GlcNAc transferase integrates metabolic pathways to regulate the stability of c-MYC in human prostate cancer cells*. Cancer Res, 2013. **73**(16): p. 5277-87.
86. Itkonen, H.M., et al., *High OGT activity is essential for MYC-driven proliferation of prostate cancer cells*. Theranostics, 2019. **9**(8): p. 2183-2197.

87. Mi, W., et al., *O-GlcNAcylation is a novel regulator of lung and colon cancer malignancy*. Biochim Biophys Acta, 2011. **1812**(4): p. 514-9.
88. Konopka, J.B., *N-acetylglucosamine (GlcNAc) functions in cell signaling*. Scientifica (Cairo), 2012. **2012**.
89. Olsen, L.R., M.W. Vetting, and S.L. Roderick, *Structure of the E. coli bifunctional GlmU acetyltransferase active site with substrates and products*. Protein Sci, 2007. **16**(6): p. 1230-5.
90. Mio, T., et al., *The eukaryotic UDP-N-acetylglucosamine pyrophosphorylases. Gene cloning, protein expression, and catalytic mechanism*. J Biol Chem, 1998. **273**(23): p. 14392-7.
91. Diekman, A.B. and E. Goldberg, *Characterization of a human antigen with sera from infertile patients*. Biol Reprod, 1994. **50**(5): p. 1087-93.
92. Wang-Gillam, A., et al., *Identification and modification of the uridine-binding site of the UDP-GalNAc (GlcNAc) pyrophosphorylase*. J Biol Chem, 2000. **275**(2): p. 1433-8.
93. Diekman, A.B., G. Olson, and E. Goldberg, *Expression of the human antigen SPAG2 in the testis and localization to the outer dense fibers in spermatozoa*. Mol Reprod Dev, 1998. **50**(3): p. 284-93.
94. Penneff, C., et al., *Crystal structures of two human pyrophosphorylase isoforms in complexes with UDPGlc(Gal)NAc: role of the alternatively spliced insert in the enzyme oligomeric assembly and active site architecture*. EMBO J, 2001. **20**(22): p. 6191-202.
95. Munkley, J., et al., *Glycosylation is an Androgen-Regulated Process Essential for Prostate Cancer Cell Viability*. EBioMedicine, 2016. **8**: p. 103-116.
96. Albitar, M., et al., *Predicting Prostate Biopsy Results Using a Panel of Plasma and Urine Biomarkers Combined in a Scoring System*. J Cancer, 2016. **7**(3): p. 297-303.
97. Gan, B.L., et al., *Downregulation of miR-224-5p in prostate cancer and its relevant molecular mechanism via TCGA, GEO database and in silico analyses*. Oncol Rep, 2018. **40**(6): p. 3171-3188.
98. Mermel, C.H., et al., *GISTIC2.0 facilitates sensitive and confident localization of the targets of focal somatic copy-number alteration in human cancers*. Genome Biol, 2011. **12**(4): p. R41.
99. Kanojia, D., et al., *Genomic landscape of liposarcoma*. Oncotarget, 2015. **6**(40): p. 42429-44.
100. Ricciardiello, F., et al., *Inhibition of the Hexosamine Biosynthetic Pathway by targeting PGM3 causes breast cancer growth arrest and apoptosis*. Cell Death Dis, 2018. **9**(3): p. 377.
101. Nagy, Á., et al., *Validation of miRNA prognostic power in hepatocellular carcinoma using expression data of independent datasets*. Sci Rep, 2018. **8**(1): p. 9227.
102. Lindahl, T., *Instability and decay of the primary structure of DNA*. Nature, 1993. **362**(6422): p. 709-15.
103. Ward, J.F., *DNA damage produced by ionizing radiation in mammalian cells: identities, mechanisms of formation, and reparability*. Prog Nucleic Acid Res Mol Biol, 1988. **35**: p. 95-125.
104. Jackson, S.P. and J. Bartek, *The DNA-damage response in human biology and disease*. Nature, 2009. **461**(7267): p. 1071-8.
105. Pfeiffer, P., et al., *DNA lesions and repair*. Mutat Res, 1996. **366**(2): p. 69-80.
106. van Gent, D.C., J.H. Hoeijmakers, and R. Kanaar, *Chromosomal stability and the DNA double-stranded break connection*. Nat Rev Genet, 2001. **2**(3): p. 196-206.

107. Ranjha, L., S.M. Howard, and P. Cejka, *Main steps in DNA double-strand break repair: an introduction to homologous recombination and related processes*. Chromosoma, 2018. **127**(2): p. 187-214.
108. Symington, L.S., *End resection at double-strand breaks: mechanism and regulation*. Cold Spring Harb Perspect Biol, 2014. **6**(8).
109. Cromie, G.A., J.C. Connelly, and D.R. Leach, *Recombination at double-strand breaks and DNA ends: conserved mechanisms from phage to humans*. Mol Cell, 2001. **8**(6): p. 1163-74.
110. Pâques, F. and J.E. Haber, *Multiple pathways of recombination induced by double-strand breaks in Saccharomyces cerevisiae*. Microbiol Mol Biol Rev, 1999. **63**(2): p. 349-404.
111. Aylon, Y. and M. Kupiec, *New insights into the mechanism of homologous recombination in yeast*. Mutat Res, 2004. **566**(3): p. 231-48.
112. Liang, F., et al., *Homology-directed repair is a major double-strand break repair pathway in mammalian cells*. Proc Natl Acad Sci U S A, 1998. **95**(9): p. 5172-7.
113. Sonoda, E., et al., *Differential usage of non-homologous end-joining and homologous recombination in double strand break repair*. DNA Repair (Amst), 2006. **5**(9-10): p. 1021-9.
114. Lieber, M.R., *The mechanism of double-strand DNA break repair by the nonhomologous DNA end-joining pathway*. Annu Rev Biochem, 2010. **79**: p. 181-211.
115. Chiruvella, K.K., Z. Liang, and T.E. Wilson, *Repair of double-strand breaks by end joining*. Cold Spring Harb Perspect Biol, 2013. **5**(5): p. a012757.
116. Graham, T.G., J.C. Walter, and J.J. Loparo, *Two-Stage Synapsis of DNA Ends during Non-homologous End Joining*. Mol Cell, 2016. **61**(6): p. 850-8.
117. Chang, H.H.Y., et al., *Non-homologous DNA end joining and alternative pathways to double-strand break repair*. Nat Rev Mol Cell Biol, 2017. **18**(8): p. 495-506.
118. Heidenreich, E., et al., *Non-homologous end joining as an important mutagenic process in cell cycle-arrested cells*. EMBO J, 2003. **22**(9): p. 2274-83.
119. Arnoult, N., et al., *Regulation of DNA repair pathway choice in S and G2 phases by the NHEJ inhibitor CYREN*. Nature, 2017. **549**(7673): p. 548-552.
120. Chapman, J.R., M.R. Taylor, and S.J. Boulton, *Playing the end game: DNA double-strand break repair pathway choice*. Mol Cell, 2012. **47**(4): p. 497-510.
121. Ceccaldi, R., B. Rondinelli, and A.D. D'Andrea, *Repair Pathway Choices and Consequences at the Double-Strand Break*. Trends Cell Biol, 2016. **26**(1): p. 52-64.
122. Brandsma, I. and D.C. Gent, *Pathway choice in DNA double strand break repair: observations of a balancing act*. Genome Integr, 2012. **3**(1): p. 9.
123. Huertas, P., *DNA resection in eukaryotes: deciding how to fix the break*. Nat Struct Mol Biol, 2010. **17**(1): p. 11-6.
124. Liu, T. and J. Huang, *DNA End Resection: Facts and Mechanisms*. Genomics Proteomics Bioinformatics, 2016. **14**(3): p. 126-130.
125. Longhese, M.P., et al., *Mechanisms and regulation of DNA end resection*. EMBO J, 2010. **29**(17): p. 2864-74.
126. Symington, L.S. and J. Gautier, *Double-strand break end resection and repair pathway choice*. Annu Rev Genet, 2011. **45**: p. 247-71.
127. Hopfner, K.P., et al., *Structural biochemistry and interaction architecture of the DNA double-strand break repair Mre11 nuclease and Rad50-ATPase*. Cell, 2001. **105**(4): p. 473-85.

128. Stracker, T.H. and J.H. Petrini, *The MRE11 complex: starting from the ends*. Nat Rev Mol Cell Biol, 2011. **12**(2): p. 90-103.
129. Garcia, V., et al., *Bidirectional resection of DNA double-strand breaks by Mre11 and Exo1*. Nature, 2011. **479**(7372): p. 241-4.
130. Mimitou, E.P. and L.S. Symington, *Sae2, Exo1 and Sgs1 collaborate in DNA double-strand break processing*. Nature, 2008. **455**(7214): p. 770-4.
131. Shibata, A., et al., *DNA double-strand break repair pathway choice is directed by distinct MRE11 nuclease activities*. Mol Cell, 2014. **53**(1): p. 7-18.
132. Cannavo, E., P. Cejka, and S.C. Kowalczykowski, *Relationship of DNA degradation by Saccharomyces cerevisiae exonuclease 1 and its stimulation by RPA and Mre11-Rad50-Xrs2 to DNA end resection*. Proc Natl Acad Sci U S A, 2013. **110**(18): p. E1661-8.
133. Wold, M.S., *Replication protein A: a heterotrimeric, single-stranded DNA-binding protein required for eukaryotic DNA metabolism*. Annu Rev Biochem, 1997. **66**: p. 61-92.
134. Sun, J., et al., *Human Ku70/80 protein blocks exonuclease 1-mediated DNA resection in the presence of human Mre11 or Mre11/Rad50 protein complex*. J Biol Chem, 2012. **287**(7): p. 4936-45.
135. Ismail, I.H., et al., *The RNF138 E3 ligase displaces Ku to promote DNA end resection and regulate DNA repair pathway choice*. Nat Cell Biol, 2015. **17**(11): p. 1446-57.
136. Lee, K.J., et al., *Phosphorylation of Ku dictates DNA double-strand break (DSB) repair pathway choice in S phase*. Nucleic Acids Res, 2016. **44**(4): p. 1732-45.
137. Chanut, P., et al., *Coordinated nuclease activities counteract Ku at single-ended DNA double-strand breaks*. Nat Commun, 2016. **7**: p. 12889.
138. Schaeper, U., et al., *Interaction between a cellular protein that binds to the C-terminal region of adenovirus E1A (CtBP) and a novel cellular protein is disrupted by E1A through a conserved PLDLS motif*. J Biol Chem, 1998. **273**(15): p. 8549-52.
139. Ferretti, L.P., L. Lafranchi, and A.A. Sartori, *Controlling DNA-end resection: a new task for CDKs*. Front Genet, 2013. **4**: p. 99.
140. Makharashvili, N., et al., *Catalytic and noncatalytic roles of the CtIP endonuclease in double-strand break end resection*. Mol Cell, 2014. **54**(6): p. 1022-33.
141. Makharashvili, N. and T.T. Paull, *CtIP: A DNA damage response protein at the intersection of DNA metabolism*. DNA Repair (Amst), 2015. **32**: p. 75-81.
142. Sartori, A.A., et al., *Human CtIP promotes DNA end resection*. Nature, 2007. **450**(7169): p. 509-14.
143. Li, X. and W.D. Heyer, *Homologous recombination in DNA repair and DNA damage tolerance*. Cell Res, 2008. **18**(1): p. 99-113.
144. Tarsounas, M., D. Davies, and S.C. West, *BRCA2-dependent and independent formation of RAD51 nuclear foci*. Oncogene, 2003. **22**(8): p. 1115-23.
145. Solinger, J.A., K. Kiianitsa, and W.D. Heyer, *Rad54, a Swi2/Snf2-like recombinational repair protein, disassembles Rad51:dsDNA filaments*. Mol Cell, 2002. **10**(5): p. 1175-88.
146. Li, X. and W.D. Heyer, *RAD54 controls access to the invading 3'-OH end after RAD51-mediated DNA strand invasion in homologous recombination in Saccharomyces cerevisiae*. Nucleic Acids Res, 2009. **37**(2): p. 638-46.
147. Postow, L., *Destroying the ring: Freeing DNA from Ku with ubiquitin*. FEBS Lett, 2011. **585**(18): p. 2876-82.
148. Iwabuchi, K., et al., *Two cellular proteins that bind to wild-type but not mutant p53*. Proc Natl Acad Sci U S A, 1994. **91**(13): p. 6098-102.

149. Iwabuchi, K., et al., *Stimulation of p53-mediated transcriptional activation by the p53-binding proteins, 53BP1 and 53BP2*. J Biol Chem, 1998. **273**(40): p. 26061-8.
150. Cuella-Martin, R., et al., *53BP1 Integrates DNA Repair and p53-Dependent Cell Fate Decisions via Distinct Mechanisms*. Mol Cell, 2016. **64**(1): p. 51-64.
151. Schultz, L.B., et al., *p53 binding protein 1 (53BP1) is an early participant in the cellular response to DNA double-strand breaks*. J Cell Biol, 2000. **151**(7): p. 1381-90.
152. Karanam, K., et al., *Quantitative live cell imaging reveals a gradual shift between DNA repair mechanisms and a maximal use of HR in mid S phase*. Mol Cell, 2012. **47**(2): p. 320-9.
153. Feng, L., et al., *Cell cycle-dependent inhibition of 53BP1 signaling by BRCA1*. Cell Discov, 2015. **1**: p. 15019.
154. Pesavento, J.J., et al., *Certain and progressive methylation of histone H4 at lysine 20 during the cell cycle*. Mol Cell Biol, 2008. **28**(1): p. 468-86.
155. Panier, S. and S.J. Boulton, *Double-strand break repair: 53BP1 comes into focus*. Nat Rev Mol Cell Biol, 2014. **15**(1): p. 7-18.
156. Marcand, S., et al., *Rap1p and telomere length regulation in yeast*. Ciba Found Symp, 1997. **211**: p. 76-93; discussion 93-103.
157. Silverman, J., et al., *Human Rif1, ortholog of a yeast telomeric protein, is regulated by ATM and 53BP1 and functions in the S-phase checkpoint*. Genes Dev, 2004. **18**(17): p. 2108-19.
158. Kumar, R. and C.F. Cheok, *RIF1: a novel regulatory factor for DNA replication and DNA damage response signaling*. DNA Repair (Amst), 2014. **15**: p. 54-9.
159. Chapman, J.R., et al., *RIF1 is essential for 53BP1-dependent nonhomologous end joining and suppression of DNA double-strand break resection*. Mol Cell, 2013. **49**(5): p. 858-71.
160. Drané, P., et al., *TIRR regulates 53BP1 by masking its histone methyl-lysine binding function*. Nature, 2017. **543**(7644): p. 211-216.
161. Ward, I.M., et al., *53BP1 is required for class switch recombination*. J Cell Biol, 2004. **165**(4): p. 459-64.
162. Zimmermann, M., et al., *53BP1 regulates DSB repair using Rif1 to control 5' end resection*. Science, 2013. **339**(6120): p. 700-4.
163. Munoz, I.M., et al., *Phospho-epitope binding by the BRCT domains of hPTIP controls multiple aspects of the cellular response to DNA damage*. Nucleic Acids Res, 2007. **35**(16): p. 5312-22.
164. Callen, E., et al., *53BP1 mediates productive and mutagenic DNA repair through distinct phosphoprotein interactions*. Cell, 2013. **153**(6): p. 1266-80.
165. Beucher, A., et al., *ATM and Artemis promote homologous recombination of radiation-induced DNA double-strand breaks in G2*. EMBO J, 2009. **28**(21): p. 3413-27.
166. Venkitaraman, A.R., *Cancer susceptibility and the functions of BRCA1 and BRCA2*. Cell, 2002. **108**(2): p. 171-82.
167. Bouwman, P., et al., *53BP1 loss rescues BRCA1 deficiency and is associated with triple-negative and BRCA-mutated breast cancers*. Nat Struct Mol Biol, 2010. **17**(6): p. 688-95.
168. Cao, L., et al., *A selective requirement for 53BP1 in the biological response to genomic instability induced by Brca1 deficiency*. Mol Cell, 2009. **35**(4): p. 534-41.
169. Bunting, S.F., et al., *53BP1 inhibits homologous recombination in Brca1-deficient cells by blocking resection of DNA breaks*. Cell, 2010. **141**(2): p. 243-54.

170. Escribano-Díaz, C., et al., *A cell cycle-dependent regulatory circuit composed of 53BP1-RIF1 and BRCA1-CtIP controls DNA repair pathway choice*. Mol Cell, 2013. **49**(5): p. 872-83.
171. Schlegel, B.P., F.M. Jodelka, and R. Nunez, *BRCA1 promotes induction of ssDNA by ionizing radiation*. Cancer Res, 2006. **66**(10): p. 5181-9.
172. Chapman, J.R., et al., *BRCA1-associated exclusion of 53BP1 from DNA damage sites underlies temporal control of DNA repair*. J Cell Sci, 2012. **125**(Pt 15): p. 3529-34.
173. Kakarougkas, A., et al., *Opposing roles for 53BP1 during homologous recombination*. Nucleic Acids Res, 2013. **41**(21): p. 9719-31.
174. Densham, R.M., et al., *Human BRCA1-BARD1 ubiquitin ligase activity counteracts chromatin barriers to DNA resection*. Nat Struct Mol Biol, 2016. **23**(7): p. 647-55.
175. Uckelmann, M., et al., *USP48 restrains resection by site-specific cleavage of the BRCA1 ubiquitin mark from H2A*. Nat Commun, 2018. **9**(1): p. 229.
176. Yu, X. and J. Chen, *DNA damage-induced cell cycle checkpoint control requires CtIP, a phosphorylation-dependent binding partner of BRCA1 C-terminal domains*. Mol Cell Biol, 2004. **24**(21): p. 9478-86.
177. Reczek, C.R., et al., *The interaction between CtIP and BRCA1 is not essential for resection-mediated DNA repair or tumor suppression*. J Cell Biol, 2013. **201**(5): p. 693-707.
178. Nakamura, K., et al., *Collaborative action of Brca1 and CtIP in elimination of covalent modifications from double-strand breaks to facilitate subsequent break repair*. PLoS Genet, 2010. **6**(1): p. e1000828.
179. Polato, F., et al., *CtIP-mediated resection is essential for viability and can operate independently of BRCA1*. J Exp Med, 2014. **211**(6): p. 1027-36.
180. Cruz-García, A., A. López-Saavedra, and P. Huertas, *BRCA1 accelerates CtIP-mediated DNA-end resection*. Cell Rep, 2014. **9**(2): p. 451-9.
181. Aparicio, T., et al., *MRN, CtIP, and BRCA1 mediate repair of topoisomerase II-DNA adducts*. J Cell Biol, 2016. **212**(4): p. 399-408.
182. Vilchez, D., I. Saez, and A. Dillin, *The role of protein clearance mechanisms in organismal ageing and age-related diseases*. Nat Commun, 2014. **5**: p. 5659.
183. Schulman, B.A. and J.W. Harper, *Ubiquitin-like protein activation by E1 enzymes: the apex for downstream signalling pathways*. Nat Rev Mol Cell Biol, 2009. **10**(5): p. 319-31.
184. Metzger, M.B., V.A. Hristova, and A.M. Weissman, *HECT and RING finger families of E3 ubiquitin ligases at a glance*. J Cell Sci, 2012. **125**(Pt 3): p. 531-7.
185. Li, W. and Y. Ye, *Polyubiquitin chains: functions, structures, and mechanisms*. Cell Mol Life Sci, 2008. **65**(15): p. 2397-406.
186. Pickart, C.M. and D. Fushman, *Polyubiquitin chains: polymeric protein signals*. Curr Opin Chem Biol, 2004. **8**(6): p. 610-6.
187. Xu, P., et al., *Quantitative proteomics reveals the function of unconventional ubiquitin chains in proteasomal degradation*. Cell, 2009. **137**(1): p. 133-45.
188. Jin, L., et al., *Mechanism of ubiquitin-chain formation by the human anaphase-promoting complex*. Cell, 2008. **133**(4): p. 653-65.
189. Nishikawa, H., et al., *Mass spectrometric and mutational analyses reveal Lys-6-linked polyubiquitin chains catalyzed by BRCA1-BARD1 ubiquitin ligase*. J Biol Chem, 2004. **279**(6): p. 3916-24.

190. Li, W., et al., *Genome-wide and functional annotation of human E3 ubiquitin ligases identifies MULAN, a mitochondrial E3 that regulates the organelle's dynamics and signaling*. PLoS One, 2008. **3**(1): p. e1487.
191. Ye, Y. and M. Rape, *Building ubiquitin chains: E2 enzymes at work*. Nat Rev Mol Cell Biol, 2009. **10**(11): p. 755-64.
192. Jin, J., et al., *Dual E1 activation systems for ubiquitin differentially regulate E2 enzyme charging*. Nature, 2007. **447**(7148): p. 1135-8.
193. Christensen, D.E., P.S. Brzovic, and R.E. Klevit, *E2-BRCA1 RING interactions dictate synthesis of mono- or specific polyubiquitin chain linkages*. Nat Struct Mol Biol, 2007. **14**(10): p. 941-8.
194. Dove, K.K., et al., *Molecular insights into RBR E3 ligase ubiquitin transfer mechanisms*. EMBO Rep, 2016. **17**(8): p. 1221-35.
195. Berndsen, C.E. and C. Wolberger, *New insights into ubiquitin E3 ligase mechanism*. Nat Struct Mol Biol, 2014. **21**(4): p. 301-7.
196. Petroski, M.D. and R.J. Deshaies, *Function and regulation of cullin-RING ubiquitin ligases*. Nat Rev Mol Cell Biol, 2005. **6**(1): p. 9-20.
197. Reitsma, J.M., et al., *Composition and Regulation of the Cellular Repertoire of SCF Ubiquitin Ligases*. Cell, 2017. **171**(6): p. 1326-1339.e14.
198. Nelson, D.E., S.J. Randle, and H. Laman, *Beyond ubiquitination: the atypical functions of Fbxo7 and other F-box proteins*. Open Biol, 2013. **3**(10): p. 130131.
199. Jonkers, W. and M. Rep, *Lessons from fungal F-box proteins*. Eukaryot Cell, 2009. **8**(5): p. 677-95.
200. Di Fiore, B. and J. Pines, *Defining the role of Emi1 in the DNA replication-segregation cycle*. Chromosoma, 2008. **117**(4): p. 333-8.
201. Miller, J.J., et al., *Emi1 stably binds and inhibits the anaphase-promoting complex/cyclosome as a pseudosubstrate inhibitor*. Genes Dev, 2006. **20**(17): p. 2410-20.
202. Smaldone, S., et al., *Identification of MoKA, a novel F-box protein that modulates Krüppel-like transcription factor 7 activity*. Mol Cell Biol, 2004. **24**(3): p. 1058-69.
203. Lee, J.E., et al., *The steady-state repertoire of human SCF ubiquitin ligase complexes does not require ongoing Nedd8 conjugation*. Mol Cell Proteomics, 2011. **10**(5): p. M110.006460.
204. Ravid, T. and M. Hochstrasser, *Diversity of degradation signals in the ubiquitin-proteasome system*. Nat Rev Mol Cell Biol, 2008. **9**(9): p. 679-90.
205. Holt, L.J., *Regulatory modules: Coupling protein stability to phosphoregulation during cell division*. FEBS Lett, 2012. **586**(17): p. 2773-7.
206. Orlicky, S., et al., *Structural basis for phosphodependent substrate selection and orientation by the SCFCdc4 ubiquitin ligase*. Cell, 2003. **112**(2): p. 243-56.
207. Nash, P., et al., *Multisite phosphorylation of a CDK inhibitor sets a threshold for the onset of DNA replication*. Nature, 2001. **414**(6863): p. 514-21.
208. Skaar, J.R., J.K. Pagan, and M. Pagano, *Mechanisms and function of substrate recruitment by F-box proteins*. Nat Rev Mol Cell Biol, 2013. **14**(6): p. 369-81.
209. Yoshida, Y., et al., *E3 ubiquitin ligase that recognizes sugar chains*. Nature, 2002. **418**(6896): p. 438-42.
210. Glenn, K.A., et al., *Diversity in tissue expression, substrate binding, and SCF complex formation for a lectin family of ubiquitin ligases*. J Biol Chem, 2008. **283**(19): p. 12717-29.

211. Chen, W., et al., *The ubiquitin E3 ligase SCF-FBXO24 recognizes deacetylated nucleoside diphosphate kinase A to enhance its degradation*. Mol Cell Biol, 2015. **35**(6): p. 1001-13.
212. Lai, Y., et al., *Lipopolysaccharide modulates p300 and Sirt1 to promote PRMT1 stability via an SCF*. J Cell Sci, 2017. **130**(20): p. 3578-3587.
213. D'Angiolella, V., et al., *SCF(Cyclin F) controls centrosome homeostasis and mitotic fidelity through CP110 degradation*. Nature, 2010. **466**(7302): p. 138-42.
214. D'Angiolella, V., et al., *Cyclin F-mediated degradation of ribonucleotide reductase M2 controls genome integrity and DNA repair*. Cell, 2012. **149**(5): p. 1023-34.
215. Abbas, T., et al., *CRL1-FBXO11 promotes Cdt2 ubiquitylation and degradation and regulates Pr-Set7/Set8-mediated cellular migration*. Mol Cell, 2013. **49**(6): p. 1147-58.
216. Rossi, M., et al., *Regulation of the CRL4(Cdt2) ubiquitin ligase and cell-cycle exit by the SCF(Fbxo11) ubiquitin ligase*. Mol Cell, 2013. **49**(6): p. 1159-66.
217. Ganoth, D., et al., *The cell-cycle regulatory protein Cks1 is required for SCF(Skp2)-mediated ubiquitinylation of p27*. Nat Cell Biol, 2001. **3**(3): p. 321-4.
218. Hao, B., et al., *Structural basis of the Cks1-dependent recognition of p27(Kip1) by the SCF(Skp2) ubiquitin ligase*. Mol Cell, 2005. **20**(1): p. 9-19.
219. Spruck, C., et al., *A CDK-independent function of mammalian Cks1: targeting of SCF(Skp2) to the CDK inhibitor p27Kip1*. Mol Cell, 2001. **7**(3): p. 639-50.
220. Skaar, J.R., J.K. Pagan, and M. Pagano, *SCF ubiquitin ligase-targeted therapies*. Nat Rev Drug Discov, 2014. **13**(12): p. 889-903.
221. Zhang, W., et al., *Skp2 is over-expressed in breast cancer and promotes breast cancer cell proliferation*. Cell Cycle, 2016. **15**(10): p. 1344-51.
222. Gstaiger, M., et al., *Skp2 is oncogenic and overexpressed in human cancers*. Proc Natl Acad Sci U S A, 2001. **98**(9): p. 5043-8.
223. Frescas, D. and M. Pagano, *Deregulated proteolysis by the F-box proteins SKP2 and beta-TrCP: tipping the scales of cancer*. Nat Rev Cancer, 2008. **8**(6): p. 438-49.
224. Wang, Z., et al., *Roles of F-box proteins in cancer*. Nat Rev Cancer, 2014. **14**(4): p. 233-47.
225. Boichis, O.V., et al., *The role of Skp2 and its substrate CDKN1B (p27) in colorectal cancer*. J Gastrointest Liver Dis, 2015. **24**(2): p. 225-34.
226. Carrano, A.C., et al., *SKP2 is required for ubiquitin-mediated degradation of the CDK inhibitor p27*. Nat Cell Biol, 1999. **1**(4): p. 193-9.
227. Nakayama, K., et al., *Targeted disruption of Skp2 results in accumulation of cyclin E and p27(Kip1), polyploidy and centrosome overduplication*. EMBO J, 2000. **19**(9): p. 2069-81.
228. Latres, E., et al., *Role of the F-box protein Skp2 in lymphomagenesis*. Proc Natl Acad Sci U S A, 2001. **98**(5): p. 2515-20.
229. Zheng, N., Z. Wang, and W. Wei, *Ubiquitination-mediated degradation of cell cycle-related proteins by F-box proteins*. Int J Biochem Cell Biol, 2016. **73**: p. 99-110.
230. Cao, J., M.H. Ge, and Z.Q. Ling, *Fbxw7 Tumor Suppressor: A Vital Regulator Contributes to Human Tumorigenesis*. Medicine (Baltimore), 2016. **95**(7): p. e2496.
231. Mao, J.H., et al., *FBXW7 targets mTOR for degradation and cooperates with PTEN in tumor suppression*. Science, 2008. **321**(5895): p. 1499-502.
232. Akhond, S., et al., *FBXW7/hCDC4 is a general tumor suppressor in human cancer*. Cancer Res, 2007. **67**(19): p. 9006-12.

233. Matsuoka, S., et al., *Fbxw7 acts as a critical fail-safe against premature loss of hematopoietic stem cells and development of T-ALL*. *Genes Dev*, 2008. **22**(8): p. 986-91.
234. Mürköster, S., et al., *Increased expression of the E3-ubiquitin ligase receptor subunit betaTRCP1 relates to constitutive nuclear factor-kappaB activation and chemoresistance in pancreatic carcinoma cells*. *Cancer Res*, 2005. **65**(4): p. 1316-24.
235. Ougolkov, A., et al., *Associations among beta-TrCP, an E3 ubiquitin ligase receptor, beta-catenin, and NF-kappaB in colorectal cancer*. *J Natl Cancer Inst*, 2004. **96**(15): p. 1161-70.
236. Saitoh, T. and M. Katoh, *Expression profiles of betaTRCP1 and betaTRCP2, and mutation analysis of betaTRCP2 in gastric cancer*. *Int J Oncol*, 2001. **18**(5): p. 959-64.
237. Spiegelman, V.S., et al., *Induction of homologue of Slimb ubiquitin ligase receptor by mitogen signaling*. *J Biol Chem*, 2002. **277**(39): p. 36624-30.
238. Kudo, Y., et al., *Role of F-box protein betaTrcp1 in mammary gland development and tumorigenesis*. *Mol Cell Biol*, 2004. **24**(18): p. 8184-94.
239. Kim, C.J., et al., *Somatic mutations of the beta-TrCP gene in gastric cancer*. *APMIS*, 2007. **115**(2): p. 127-33.
240. Randle, S.J. and H. Laman, *F-box protein interactions with the hallmark pathways in cancer*. *Semin Cancer Biol*, 2016. **36**: p. 3-17.
241. Zhang, X., et al., *F-box protein FBXO31 is down-regulated in gastric cancer and negatively regulated by miR-17 and miR-20a*. *Oncotarget*, 2014. **5**(15): p. 6178-90.
242. Zou, S., et al., *FBXO31 Suppresses Gastric Cancer EMT by Targeting Snail1 for Proteasomal Degradation*. *Mol Cancer Res*, 2018. **16**(2): p. 286-295.
243. Gütgemann, I., et al., *Emi1 protein accumulation implicates misregulation of the anaphase promoting complex/cyclosome pathway in ovarian clear cell carcinoma*. *Mod Pathol*, 2008. **21**(4): p. 445-54.
244. Zhao, Y., et al., *Early mitotic inhibitor-1, an anaphase-promoting complex/cyclosome inhibitor, can control tumor cell proliferation in hepatocellular carcinoma: correlation with Skp2 stability and degradation of p27(Kip1)*. *Hum Pathol*, 2013. **44**(3): p. 365-73.
245. Chen, J.Y., M.C. Wang, and W.C. Hung, *Bcr-Abl-induced tyrosine phosphorylation of Emi1 to stabilize Skp2 protein via inhibition of ubiquitination in chronic myeloid leukemia cells*. *J Cell Physiol*, 2011. **226**(2): p. 407-13.
246. Yano, H., et al., *Fbx8 makes Arf6 refractory to function via ubiquitination*. *Mol Biol Cell*, 2008. **19**(3): p. 822-32.
247. Kobe, B. and A.V. Kajava, *The leucine-rich repeat as a protein recognition motif*. *Curr Opin Struct Biol*, 2001. **11**(6): p. 725-32.
248. Xiao, G.G., et al., *Identification of F-box/LLR-repeated protein 17 as potential useful biomarker for breast cancer therapy*. *Cancer Genomics Proteomics*, 2008. **5**(3-4): p. 151-60.
249. Tan, M.K., et al., *Parallel SCF adaptor capture proteomics reveals a role for SCFFBXL17 in NRF2 activation via BACH1 repressor turnover*. *Mol Cell*, 2013. **52**(1): p. 9-24.
250. Raducu, M., et al., *SCF (Fbxl17) ubiquitylation of Sufu regulates Hedgehog signaling and medulloblastoma development*. *EMBO J*, 2016. **35**(13): p. 1400-16.
251. Mena, E.L., et al., *Dimerization quality control ensures neuronal development and survival*. *Science*, 2018. **362**(6411).
252. Flach, S., *PhD Thesis: Structural Variation of the Genome in Breast Cancer*. 2013. p. Susanne Flach.

253. Swift, S., et al., *Rapid production of retroviruses for efficient gene delivery to mammalian cells using 293T cell-based systems*. Curr Protoc Immunol, 2001. **Chapter 10**: p. Unit 10.17C.
254. Olson, A., et al., *RNAi Codex: a portal/database for short-hairpin RNA (shRNA) gene-silencing constructs*. Nucleic Acids Res, 2006. **34**(Database issue): p. D153-7.
255. Mason, B., et al., *Fbxl17 is rearranged in breast cancer and loss of its activity leads to increased global O-GlcNAcylation*. Cell Mol Life Sci, 2019.
256. Robinson, D.R., et al., *Functionally recurrent rearrangements of the MAST kinase and Notch gene families in breast cancer*. Nat Med, 2011. **17**(12): p. 1646-51.
257. Schulte, I., et al., *Structural analysis of the genome of breast cancer cell line ZR-75-30 identifies twelve expressed fusion genes*. BMC Genomics, 2012. **13**: p. 719.
258. Baca, S.C., et al., *Punctuated evolution of prostate cancer genomes*. Cell, 2013. **153**(3): p. 666-77.
259. Dulak, A.M., et al., *Exome and whole-genome sequencing of esophageal adenocarcinoma identifies recurrent driver events and mutational complexity*. Nat Genet, 2013. **45**(5): p. 478-86.
260. Grossman, R.L., et al., *Toward a Shared Vision for Cancer Genomic Data*. N Engl J Med, 2016. **375**(12): p. 1109-12.
261. Institute, N.C. *NCI GDC Data Portal - FBXL17*. [cited 2019 07/12]; Available from: <https://portal.gdc.cancer.gov/genes/ENSG00000145743>.
262. Oldfield, C.J. and A.K. Dunker, *Intrinsically disordered proteins and intrinsically disordered protein regions*. Annu Rev Biochem, 2014. **83**: p. 553-84.
263. Wang, S., et al., *RaptorX-Property: a web server for protein structure property prediction*. Nucleic Acids Res, 2016. **44**(W1): p. W430-5.
264. McGuffin, L.J., K. Bryson, and D.T. Jones, *The PSIPRED protein structure prediction server*. Bioinformatics, 2000. **16**(4): p. 404-5.
265. Heffernan, R., et al., *Highly accurate sequence-based prediction of half-sphere exposures of amino acid residues in proteins*. Bioinformatics, 2016. **32**(6): p. 843-9.
266. Heffernan, R., et al., *Capturing non-local interactions by long short-term memory bidirectional recurrent neural networks for improving prediction of protein secondary structure, backbone angles, contact numbers and solvent accessibility*. Bioinformatics, 2017. **33**(18): p. 2842-2849.
267. Song, Y., et al., *High-resolution comparative modeling with RosettaCM*. Structure, 2013. **21**(10): p. 1735-42.
268. Kuchay, S., et al., *GGTase3 is a newly identified geranylgeranyltransferase targeting a ubiquitin ligase*. Nat Struct Mol Biol, 2019. **26**(7): p. 628-636.
269. Bella, J., et al., *The leucine-rich repeat structure*. Cell Mol Life Sci, 2008. **65**(15): p. 2307-33.
270. Simons, K.T., et al., *Ab initio protein structure prediction of CASP III targets using ROSETTA*. Proteins, 1999. **Suppl 3**: p. 171-6.
271. Davoli, T., et al., *Cumulative haploinsufficiency and triplosensitivity drive aneuploidy patterns and shape the cancer genome*. Cell, 2013. **155**(4): p. 948-62.
272. Shaw, A.T., et al., *Crizotinib versus chemotherapy in advanced ALK-positive lung cancer*. N Engl J Med, 2013. **368**(25): p. 2385-94.
273. Milioli, H.H., et al., *Basal-like breast cancer: molecular profiles, clinical features and survival outcomes*. BMC Med Genomics, 2017. **10**(1): p. 19.
274. Schulman, B.A., et al., *Insights into SCF ubiquitin ligases from the structure of the Skp1-Skp2 complex*. Nature, 2000. **408**(6810): p. 381-6.

275. Yoshida, Y., A. Murakami, and K. Tanaka, *Skp1 stabilizes the conformation of F-box proteins*. Biochem Biophys Res Commun, 2011. **410**(1): p. 24-8.
276. Gao, S., et al., *Reciprocal Regulation Between O-GlcNAcylation and β -Catenin Facilitates Cell Viability and Inhibits Apoptosis in Liver Cancer*. DNA Cell Biol, 2019. **38**(4): p. 286-296.
277. Netsirisawan, P., et al., *Proteomic Analysis Reveals Aberrant O-GlcNAcylation of Extracellular Proteins from Breast Cancer Cell Secretion*. Cancer Genomics Proteomics, 2015. **12**(4): p. 201-9.
278. Huang, X., et al., *O-GlcNAcylation of cofilin promotes breast cancer cell invasion*. J Biol Chem, 2013. **288**(51): p. 36418-25.
279. Schwertman, P., S. Bekker-Jensen, and N. Mailand, *Regulation of DNA double-strand break repair by ubiquitin and ubiquitin-like modifiers*. Nat Rev Mol Cell Biol, 2016. **17**(6): p. 379-94.
280. Huang, d.W., B.T. Sherman, and R.A. Lempicki, *Bioinformatics enrichment tools: paths toward the comprehensive functional analysis of large gene lists*. Nucleic Acids Res, 2009. **37**(1): p. 1-13.
281. Huang, d.W., B.T. Sherman, and R.A. Lempicki, *Systematic and integrative analysis of large gene lists using DAVID bioinformatics resources*. Nat Protoc, 2009. **4**(1): p. 44-57.
282. Duijf, P.H.G., et al., *Mechanisms of Genomic Instability in Breast Cancer*. Trends Mol Med, 2019. **25**(7): p. 595-611.
283. Bekker-Jensen, S., et al., *Dynamic assembly and sustained retention of 53BP1 at the sites of DNA damage are controlled by Mdc1/NFBD1*. J Cell Biol, 2005. **170**(2): p. 201-11.
284. Iwabuchi, K., et al., *Potential role for 53BP1 in DNA end-joining repair through direct interaction with DNA*. J Biol Chem, 2003. **278**(38): p. 36487-95.
285. Wiegman, A., *Monitoring DNA Repair Consequences of ATM Signaling Using Simultaneous Fluorescent Readouts*. Methods Mol Biol, 2017. **1599**: p. 335-346.
286. Huen, M.S., et al., *Regulation of chromatin architecture by the PWWP domain-containing DNA damage-responsive factor EXPAND1/MUM1*. Mol Cell, 2010. **37**(6): p. 854-64.
287. Strauss, C., et al., *MDC1 is ubiquitylated on its tandem BRCT domain and directly binds RAP80 in a UBC13-dependent manner*. DNA Repair (Amst), 2011. **10**(8): p. 806-14.
288. Mayca Pozo, F., et al., *Regulatory cross-talk determines the cellular levels of 53BP1 protein, a critical factor in DNA repair*. J Biol Chem, 2017. **292**(14): p. 5992-6003.
289. Han, X., et al., *Ubch7 regulates 53BP1 stability and DSB repair*. Proc Natl Acad Sci U S A, 2014. **111**(49): p. 17456-61.
290. Kumar, R.D., et al., *Statistically identifying tumor suppressors and oncogenes from pan-cancer genome-sequencing data*. Bioinformatics, 2015. **31**(22): p. 3561-8.
291. Institute, N.C. *NCI GDC Data Portal - FBXW7*. [cited 2019 11/12]; Available from: <https://portal.gdc.cancer.gov/genes/ENSG00000109670>.
292. Institute, N.C. *NCI GDC Data Portal - SKP2*. [cited 2019 11/12]; Available from: <https://portal.gdc.cancer.gov/genes/ENSG00000145604>.
293. Hunter, T., *The age of crosstalk: phosphorylation, ubiquitination, and beyond*. Mol Cell, 2007. **28**(5): p. 730-8.
294. Gao, M. and M. Karin, *Regulating the regulators: control of protein ubiquitination and ubiquitin-like modifications by extracellular stimuli*. Mol Cell, 2005. **19**(5): p. 581-93.

APPENDIX A

FBXL17 structural variants in primary breast tumours

Supplementary Table 1. FBXL17 structural variants from 250 breast cancer cases called by Manta

Case^a	Breakpoint 1 Chromosome	Breakpoint Start	End	Breakpoint 2 Chromosome	Breakpoint Start	End
FBXL17_1	chr5	108049175	108049177	chr7	92973458	92973460
FBXL17_2	chr5	107515003	107515007	chr5	108067751	108067755
FBXL17_3	chr5	107810303	107810306	chr5	107985819	107985822
FBXL17_4	chr5	108177141	108177142	chr5	108186300	108186301
FBXL17_5	chr5	103540026	103540027	chr5	108025458	108025459
FBXL17_6		SV called but failed filtering and rejected on manual review; included in RNA review				

^a Each case is a distinct patient, arbitrarily renumbered for this study

Supplementary Table 2. Aberrant transcript junction sequences from RNA sequencing for *FBXL17* structural variants

Case ^a	Type of SV ^b	Predicted consequences of SV called and possible aberrant transcript(s) of <i>FBXL17</i>	Aberrant transcript sequence found in RNAseq; XX marks splice junction
FBXL17_1	TRA	FBXL17 transcript runs across SV junction into intergenic region on chromosome 7	CGGCCATCTTAGAGCAGGAACGAGCCTTCTTTTAAC XX CTGTCAATTTATGATCCAGTTCAGACAGAGATTGAGAG
FBXL17_2	DUP	FBXL17 exons 7, 8 and 9 duplicated; Fusion, 5' of EFNA5 exon 1 into duplicated exons 7, 8, 9 of FBXL17	Not found
FBXL17_3	DUP	FBXL17 exons 8 and 9 duplicated; Consequences unknown	Not found
FBXL17_4	DUP	Exon 6 duplicated; transcript contains 2 copies of exon 6	6 independent split reads e.g. GTTCAAGTGATATGACGTAGGTCCAAGCTGGAAAGGTTTCTTAG XX CTGTCAATTTATGATCCAGTTCAGACAGAGATTG
FBXL17_5	INV	FBXL17 transcript runs from exon 6 across SV junction into intergenic region	7 independent reads support transcript running from exon 6 into intron 6, without splicing e.g. CTCTAGAAAAGTATTTTAAACAATGTTACAATGGTTAC XX CTGTCAATTTATGATCCAGTTCAGACAGAGATTGAGAG and ACAAATGGTTAC XX CTGTCAATTTATGATCCAGTTCAGACAGAGATTGAGAGAGCTAAGATTTTGCACCTCTTGACAAT
FBXL17_6		SV discarded on manual review. RNA reviewed as negative control	3 independent split reads support a rearrangement splicing exon 6 into exon 4 e.g. GAGATCTTGTAACACTGGCCGAAATGAATACTTTGAGTTCTCTGCATTTTGAGCCCCAG XX CTGTCAATTTATGATCCA and GAGTTCTCTGCATTTTGAGCCCCAG XX CTGTCAATTTATGATCCAGTTCAGACAGAGATTGAGAGAGCTAAGATTTTGG. No reads support normal exon6-exon7 or 8 splicing. No reads for exon 7 splice acceptor

^a Each case is a distinct patient, arbitrarily renumbered for this study^b TRA, inter-chromosome translocation; DUP, junction likely to represent tandem duplication; INV, junction likely to represent inversion

Supplementary Table 3. Molecular classification of tumours with *FBXL17* structural variants

Case ^a	ER	PR	HER2/ERBB2	TP53	IntClust	PAM50
FBXL17_1	neg	wk pos	neg	Gln192Ter	10	basal
FBXL17_2	pos	pos	neg	-	4 (ER+)	luminal A
FBXL17_3	neg	pos	neg	Cys229LeufsTer18	4 (ER-)	basal
FBXL17_4	pos	neg	neg	Tyr220Cys	10	basal
FBXL17_5	pos	pos	pos	Asp281Val	7	luminal A
FBXL17_6	neg	neg	neg	Leu194TyrfsTer14	10	basal

^a Each case is a distinct patient, arbitrarily renumbered for this study

APPENDIX B

Manuscript: Fbxl17 is rearranged in breast cancer and loss of its activity leads to increased global *O*-GlcNAcylation



Fbx17 is rearranged in breast cancer and loss of its activity leads to increased global O-GlcNAcylation

Bethany Mason¹ · Susanne Flach^{2,5} · Felipe R. Teixeira^{1,6} · Raquel Manzano Garcia³ · Oscar M. Rueda³ · Jean E. Abraham^{3,4} · Carlos Caldas^{3,4} · Paul A. W. Edwards^{2,3} · Heike Laman¹

Received: 4 April 2019 / Revised: 5 September 2019 / Accepted: 16 September 2019
© The Author(s) 2019

Abstract

In cancer, many genes are mutated by genome rearrangement, but our understanding of the functional consequences of this remains rudimentary. Here we report the F-box protein encoded by *FBXL17* is disrupted in the region of the gene that encodes its substrate-binding leucine rich repeat (LRR) domain. Truncating Fbx17 LRRs impaired its association with the other SCF holoenzyme subunits Skp1, Cul1 and Rbx1, and decreased ubiquitination activity. Loss of the LRRs also differentially affected Fbx17 binding to its targets. Thus, genomic rearrangements in *FBXL17* are likely to disrupt SCF^{Fbx17}-regulated networks in cancer cells. To investigate the functional effect of these rearrangements, we performed a yeast two-hybrid screen to identify Fbx17-interacting proteins. Among the 37 binding partners Uap1, an enzyme involved in O-GlcNAcylation of proteins was identified most frequently. We demonstrate that Fbx17 binds to UAP1 directly and inhibits its phosphorylation, which we propose regulates UAP1 activity. Knockdown of Fbx17 expression elevated O-GlcNAcylation in breast cancer cells, arguing for a functional role for Fbx17 in this metabolic pathway.

Keywords FBXL17 · Genome rearrangements · O-GlcNAcylation · O-GlcNAc · UAP1 · Ubiquitin · Phosphorylation · Breast cancer

Introduction

The genomes of most common epithelial cancers, such as breast cancer, are highly rearranged, but our knowledge of the rearrangements and the genes they target remains rudimentary [1]. A few common, large-scale rearrangements

have been known for some time, such as loss of the distal arm of 8p, 17p and 18q and the amplification of *ERBB2* in breast cancer, but many more less-frequently occurring aberrations remain to be characterised and may be diagnostically or therapeutically important. For example, the *EML4-ALK* fusion occurs in only approximately 5% of non-small cell lung cancers and is a target for therapy [2]. Genome sequencing has focused on point mutations in exomes, with only a few results for structural mutations reported so far, for limited sets of tumours [3–8]. Array-CGH detects larger scale unbalanced rearrangements and is available for large panels of tumours [9]. If such breaks fall within genes, they

Bethany Mason and Susanne Flach contributed equally to this work.

Electronic supplementary material The online version of this article (<https://doi.org/10.1007/s00018-019-03306-y>) contains supplementary material, which is available to authorized users.

✉ Heike Laman
hl316@cam.ac.uk

- ¹ Department of Pathology at Tennis Court Road, University of Cambridge, Cambridge CB2 1QP, UK
- ² Hutchison-MRC Research Centre, Addenbrooke's Site, Hills Road, Cambridge CB2 0XZ, UK
- ³ Department of Oncology, Cancer Research UK Cambridge Institute and Cancer Centre, Li Ka Shing Centre, University of Cambridge, Cambridge CB2 0RE, UK

- ⁴ Cambridge Breast Unit, NIHR Cambridge Biomedical Research Centre and Cambridge Experimental Cancer Medicine Centre at Cambridge University Hospitals NHS Foundation Trust, Cambridge CB2 2QQ, UK
- ⁵ Present Address: Department of Otolaryngology and Head & Neck Surgery, Hospital of the Ludwig-Maximilians-University, Munich, Germany
- ⁶ Present Address: Department of Genetics and Evolution, Federal University of São Carlos, São Carlos, São Paulo, Brazil

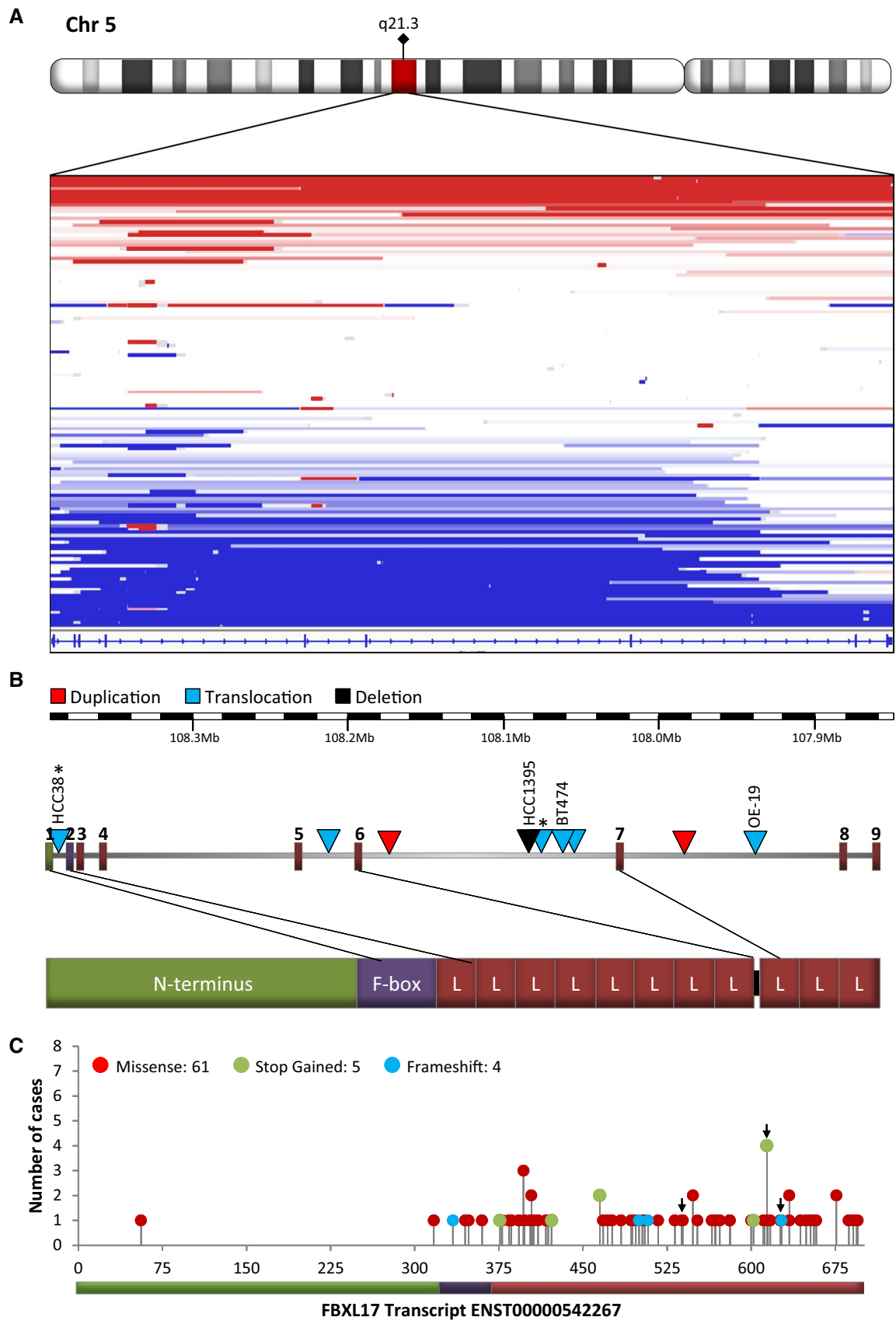


Fig. 1 Breaks in *FBXL17* and the proteins encoded. **a** Breaks in 135/1992 breast tumours [9], detected as copy number steps by array-CGH. X-axis is genomic sequence of *FBXL17*, reversed since *FBXL17* is a negative strand gene. Each horizontal line represents a tumour, with breaks indicated by colour change. Blue, copy number loss; white, no change; red, gain. **b** *FBXL17* exons from Ensembl transcript ENST00000542267.5 (Refseq NM_001163315.2, NP_001156787.2), chr5:107,859,045–108,382,098 in GRCh38/hg38. Triangles indicate breakpoints in *FBXL17* identified in cell lines (as labelled) or primary breast tumours (unlabelled), Asterisk indicates known fusion. Bottom, protein domains of Fbx17 scaled to protein sequence. L, leucine-rich repeat. **c** Non-synonymous somatic mutations mapped to Fbx17 as reported by The Cancer Genome Atlas (TCGA), arrows indicate breast cancer associated mutations. Schematic underneath represents Fbx17 domains, green, N-terminus, purple, F-box domain, red, leucine-rich repeats

must at least inactivate that copy of the gene, and in some cases they will create truncated proteins or gene fusions. Some gene fusion data are also available, from genomic [3–8] or transcript sequencing [10]. From surveying these datasets, we determined that *FBXL17* is among the more frequently rearranged genes in a number of epithelial cancers, including breast, prostate and oesophageal cancers.

FBXL17 encodes a little-studied member of the F-box family of proteins (FBPs). They are components of the ubiquitin conjugation pathway, which, by directing the ubiquitination of target proteins, regulate major cellular processes that require rapid alterations in protein levels, activity and localisation, such as cell cycle progression, cell signalling, and receptor recycling [11]. Ubiquitination of proteins requires an enzymatic cascade involving an E1 ubiquitin-activating enzyme, an E2 ubiquitin-conjugating enzyme, and an E3 ubiquitin ligase [12]. FBPs are subunits of the SCF (Skp1-Cul1-F-box protein)-type E3 ubiquitin ligases, which utilise protein–protein interaction domains, like leucine-rich or WD40 repeats, to recruit substrates to the ligase. FBPs bind an adaptor protein Skp1 through their F-box domains (FBD), and the FBP:Skp1 dimer is a switchable unit that docks with a cullin scaffold and Rbx1 (Ring finger domain containing protein), which in turn recruits a ubiquitin-charged E2 ligase. The Cdh1 protein actively dissociates the pool of FBP:Skp1 dimers from cullin, regulating the levels of active E3 ligases in the cell [13, 14]. FBPs not engaged as part of active E3 ligases also have functions outside of the Ubiquitin Proteasome System (UPS) [15].

Several FBPs have oncogenic and/or tumour suppressive activities [16, 17]. Indeed, the first FBP described, Skp2 (S-phase kinase-associated protein 2, Fbx11) is activated by amplification in several cancers, including breast, lymphoma, non-small cell lung cancer and glioblastoma [18, 19]. Skp2 is thought to have its main oncogenic activity by promoting the degradation of the cyclin-dependent kinase inhibitor, p27 [20–22]. However, loss of *SKP2* also induces senescence in response to oncogenic stimuli, such as Ras

expression or the loss of *Pten* [23]. Fbxw7 is a tumour suppressor, inactivated in approximately 7% cancers [24], which targets the turnover of important oncogenes, such as Myc, cyclin E, and Notch [16]. β -TrCP (*BTRC*, Fbxw11) is also mutated in several cancers, including breast and colorectal cancer and melanoma, potentially stabilising its oncogenic substrate β -catenin [19]. The true extent of FBP dysregulation in cancer, particularly through genomic rearrangements, is unknown. We found *FBXL17* is rearranged in breast cancers, and these rearrangements often disrupt the LRRs of Fbx17. Loss of LRRs leads to a differential loss of interaction with Fbx17 binding partners, and prevents its assembly into a functional SCF complex. We show that Fbx17 interacts with Uap1, UDP-*N*-acetylglucosamine pyrophosphorylase 1, to regulate the overall levels of *N*-acetylglucosamine modification (*O*-GlcNAcylation) of proteins in cells. Our data support a model whereby Fbx17 has tumour suppressor activity in breast cancers.

Results

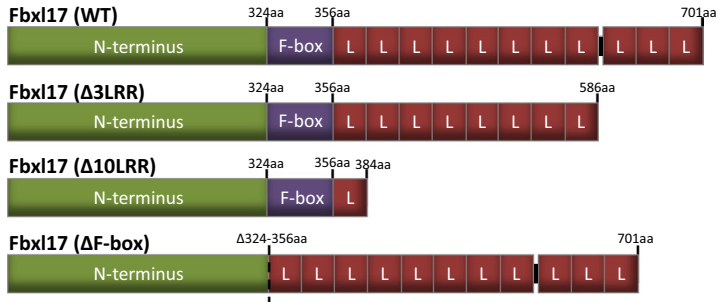
FBXL17 is rearranged in cancer

To identify genes that are rearranged in breast cancers, we scanned segmented array-CGH copy number data for 1992 primary breast tumours [9]. 135 (7%) had at least one genomic break within *FBXL17*, detected as a copy number step, distributed in various ways (Fig. 1a). The majority of these copy number losses or gains occurred at the 3' end of *FBXL17*. Given the LRRs of Fbx17 are encoded from exon 3 onwards it is likely these protein–protein interacting domains are disrupted by such rearrangements.

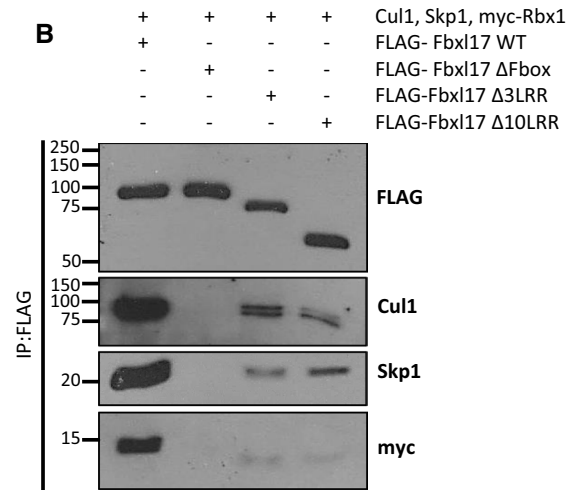
In addition to breaks in tumours, array-CGH data showed breaks in *FBXL17* in four cancer cell lines, the breast carcinoma cell lines, BT-474, HCC38, and HCC1395, and the oesophageal/gastric cardia adenocarcinoma line OE-19 [25]. The breaks were verified by FISH (Figs. 1b and S1). In BT-474, one of three copies of *FBXL17* was broken, with retention of the 3' end, exons 7–9 (Figs. 1b and S1B). Both HCC38 and OE-19 had an extra copy of the 5' end of *FBXL17*, up to intron 1 and intron 7, respectively (Figs. 1b and S1B). In HCC38, this break was confirmed to be the *FBXL17*-*PJA2* fusion transcript reported in [10] (Fig. S1C, S1F and S1G). In HCC1395, both array-CGH (Fig. S1H) and paired-end sequencing showed an internal homozygous deletion in *FBXL17* between exons 6 and 9 [5, 25] verified by RT-PCR and FISH (Fig. S1D, S1E and S1I) which would truncate Fbx17 near its C-terminus and encode a mutant protein lacking approximately three LRRs (Fig. 1b).

Because the cell line examples may not be typical, we looked for examples of *FBXL17* rearrangements in breast cancers, in paired-end whole-genome DNA sequencing

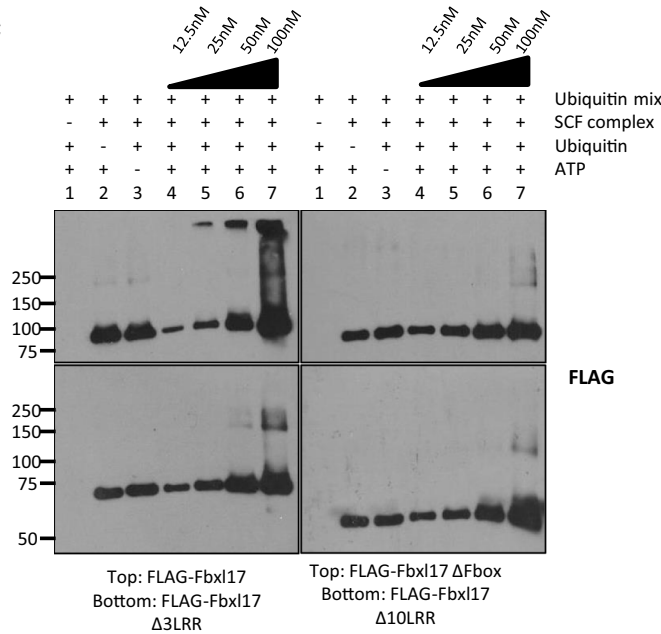
A



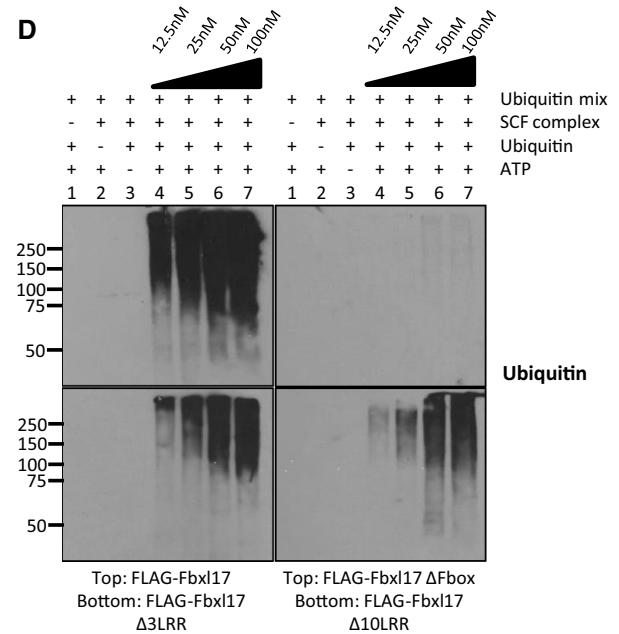
B



C



D



E

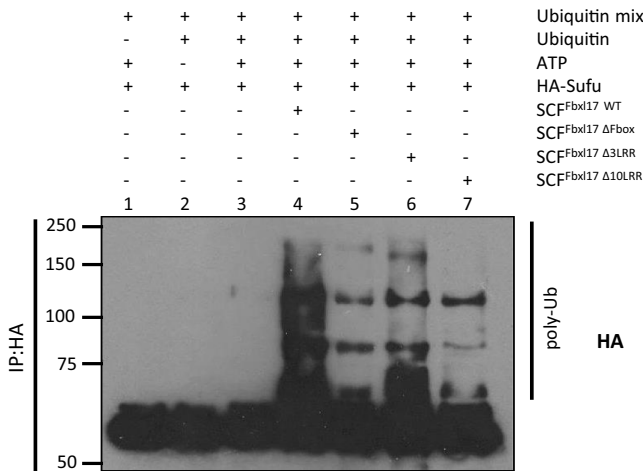


Fig. 2 Loss of Fbxl17 LRRs impairs recruitment of SCF^{Fbxl17} subunits and SCF^{Fbxl17} ligase activity. **a** Schematic showing Fbxl17 constructs used to make SCF ligases, all contain an N-terminal FLAG tag (not shown). L, leucine-rich repeat. **b** A representative immunoblot for SCF holoenzyme components that co-immunoprecipitate with FLAG-Fbxl17 and mutant Fbxl17 constructs FLAG-Fbxl17ΔFbox, FLAG-Fbxl17Δ3LRR and Fbxl17Δ10LRR, $n=4$. **c** Titration of the auto-ubiquitination activity of purified SCF^{Fbxl17} ligase complexes. A concentration gradient (12.5 nM, 25 nM, 50 nM, 100 nM) of purified SCF^{Fbxl17} or mutant complexes SCF^{Fbxl17}ΔFbox, SCF^{Fbxl17}Δ3LRR or SCF^{Fbxl17}Δ10LRR was used in an in vitro ubiquitination assay in the presence of a ubiquitin mix (ubiquitin buffer, UBE1, UbcH5a and ATP). Following SDS-PAGE membranes were probed with anti-FLAG antibody to detect SCF^{Fbxl17} ligases, $n=2$. **d** As (c) but probed with anti-ubiquitin antibody, $n=2$. **e** In vitro ubiquitination assay of SCF^{Fbxl17} and mutant ligase complexes in combination with HA-tagged substrate Sufu in the presence of a ubiquitin mix as in c. Proteins resolved by SDS-PAGE and membrane probed with anti-HA antibody, $n=3$

data from 250 primary breast tumours of the Cambridge Personalised Breast Cancer Programme. Rearrangements ('Structural variants') in *FBXL17* were identified in five of the tumours. Manual inspection of RNA sequences from these five tumours confirmed that two of the rearrangements were transcribed as predicted: a translocation joining exon 6 to an undocumented exon on chromosome 7 and a duplication of exon 6, respectively (Fig. 1b; Supplementary Table 1). A third case with a breakpoint in intron 6 showed unspliced transcription from exon 6 into intron 7; however, we cannot rule out that this was normal unspliced RNA. Serendipitously, a further RNA sample, inspected because it had a rearrangement which did not pass filtering, showed splicing from exon 6 into exon 4. This suggested the presence of a rearrangement which was not detected by DNA sequencing in an additional tumour. The partial agreement we find between RNA and DNA sequencing is expected as both methods lack sensitivity to identify all rearrangements [26]. Thus, consistent with the cell line rearrangements, the breakpoints in the tumours fell within introns that would disrupt the expression of LRRs, with the majority (4/6) occurring in intron 6 (Fig. 1b, Supplementary Table 1). There was no clear relationship between *FBXL17* rearrangement and any molecular classification [27] of the tumours and cell lines, although five of the six tumours and the breast cell lines were *TP53* mutant (Supplementary Table 1). Of the tumours, three were oestrogen receptor (ER) positive, and three were ER-negative. One tumour and one cell line were *ERBB2/HER2* positive. We also classified these tumours into the 11 IntClust sets [27], and they fell into three sets: clusters 4, 7 and 10. In addition, classifying these six cases using PAM50 breast cancer subtyping, gave four basal and two luminal A cases. Although the number of cases is small, these data suggest Fbxl17 is not rearranged in a particular cancer subtype.

Rearrangements of *FBXL17* have also been detected in other epithelial cancers (Supplementary Table 2) including prostate [8] and oesophageal adenocarcinoma [7]. Many of these rearrangements are also predicted to truncate Fbxl17, resulting in loss of LRRs. TCGA (Cancer Genome Atlas project) data was mined for genomic alterations affecting *FBXL17* using cBioPortal (<http://cbioportal.org>) [28]. Perhaps most striking was the TCGA mapping of non-synonymous somatic *FBXL17* mutations. Mutations in *FBXL17* almost exclusively (68/70) target its C-terminus containing the FBD and LRRs (Fig. 1c).

In summary, *FBXL17* is broken in approximately 7% of breast cancers, and additionally rearranged or mutated in other epithelial cancers. At least some of the breaks truncate Fbxl17, removing some or all of the LRRs and sometimes also the FBD. Examples of truncation are present in three cancer cell lines, and rearrangements have been confirmed in primary breast tumours. These genomic alterations suggest the ability of Fbxl17 to recruit substrates for ubiquitination or to form part of an SCF complex may be compromised.

Deletion of LRRs in Fbxl17 compromises ubiquitination activity due to impaired recruitment of SCF subunits

As most of the genomic rearrangements in *FBXL17* are predicted to target its LRRs, we wanted to investigate the effect of their loss on Fbxl17 ligase activity. We used co-immunoprecipitation assays to check the incorporation of Fbxl17 into an SCF E3 ligase. HEK293T cells were co-transfected with the subunits of SCF ligases, Skp1, Cullin1, Rbx1, and various N-terminally FLAG-tagged Fbxl17 constructs (full-length Fbxl17 (1-701aa), an internal FBD deletion, Fbxl17ΔFbox (Δ324-358aa) and two LRR-truncation constructs Fbxl17Δ3LRR (1-586aa), and Fbxl17Δ10LRR (1-384aa) (Fig. 2a). 48 h post transfection, cells were lysed, immunoprecipitated with FLAG antibodies, and blotted for the associated SCF subunits (Figs. 2b and S2B). While Skp1, Rbx1 and Cullin1 co-immunoprecipitated efficiently with WT Fbxl17, these components were reduced in the immunoprecipitates of the truncation mutants. For example, Cullin1 binding to Fbxl17Δ3LRR was reduced by 81% ($p=4.12E-04$; $n=4$) and Fbxl17Δ10LRR by 82% ($p=1.28E-06$; $n=4$) relative to WT Fbxl17, while Skp1 binding to Fbxl17Δ3LRR was reduced by 77% ($p=5.52E-05$; $n=5$) and Fbxl17Δ10LRR by 67% ($p=2.74E-05$; $n=4$) relative to WT Fbxl17, despite these truncations having intact FBDs (Figs. 2b and S2B). As expected, when the FBD was deleted in Fbxl17ΔFbox, none of the subunits were co-immunoprecipitated. These data indicate that in addition to the FBD, the LRRs of Fbxl17 facilitate the assembly of the SCF^{Fbxl17} ligase.

Since the Cullin1 and Rbx1 subunit allow E2 recruitment, these data suggest that the mutant SCF^{Fbx117} ligases will have reduced activity. We tested this by performing in vitro ubiquitination assays of purified SCF complexes, assembled with either WT or LRR-truncated Fbx117 proteins, in the presence of an E1 and E2 enzyme. We first tested the ability of the mutant Fbx117 proteins to promote auto-ubiquitination as part of an SCF E3 ligase (Figs. 2c, d and S2A). We observed higher molecular weight bands using an antibody raised against Fbx117 using 25 nM of SCF^{Fbx117} in in vitro ubiquitination reactions, and the signal intensified with increasing concentrations of the WT ligase. In parallel assays, 50 nM of mutant SCF^{Fbx117Δ3LRR} ligase showed residual activity which increased at 100 nM, but it was considerably less than WT SCF^{Fbx117} ligase. SCF^{Fbx117Δ10LRR} ligase showed the greatest reduction in activity (Fig. 2c), comparable to the inactive SCF^{Fbx117ΔFbox} mutant. The difference in activity of the SCF complexes was even more apparent when the membranes were probed for ubiquitin (Fig. 2d). SCF^{Fbx117ΔFbox} had no ligase activity, while E3 ubiquitin ligases made with the LRR-truncated Fbx117 mutants had reduced ligase activity compared to WT Fbx117.

To test whether the ligases made by WT or mutant versions of Fbx117 could ubiquitinate a heterologous substrate, we performed in vitro ubiquitination assays using Sufu (Fig. 2e) [29]. HA-Sufu was purified from HEK293T cells by immunoprecipitation. High molecular weight smears can be seen after the addition of SCF^{Fbx117} (Fig. 2e, lane 4) and to a much lesser extent SCF^{Fbx117Δ3LRR} (Fig. 2e, lane 6). Both SCF^{Fbx117ΔFbox} and SCF^{Fbx117Δ10LRR} show greatly reduced ubiquitination activity. Together these data indicate that the LRRs in Fbx117 contribute to assembly of the SCF E3 ligase and its ligase activity.

Fbx117 interacting proteins identified by yeast-two hybrid screening

Our data suggest that if Fbx117 is mutated in the LRR-encoding region, the proteins interacting with them will be mis-regulated as a result of aberrant SCF assembly and its effects on ligase activity. We performed a yeast two-hybrid screen to identify Fbx117 interacting partners. To focus the screen on LRR-binding partners, we engineered the bait plasmid to contain the FBD and LRRs (321-701aa) of Fbx117 but omitted its N-terminus. 37 unique prey, cloned in-frame to the Gal4 activation domain (GAD), were identified as candidate partners for Fbx117 (Table 1; Fig. S3A). More than a third (13/37) of the prey were isolated independently at least twice. The most common prey plasmids isolated encoded GAD fusions to UDP-*N*-acetylglucosamine pyrophosphorylase 1 (Uap1) and to ubiquitin-fold modifier conjugating enzyme 1 (Ufc1), which were isolated 26 and 13 times, respectively. Moreover, since multiple, non-identical

plasmids were isolated, a minimal common region defined a likely interacting domain within it, e.g. aa 357-505 at the C-terminus of Uap1 (Table 1). Additionally, Khlh12 and Khlh17, two members of the Kelch-like family of proteins, casein kinase 2b (Csnk2B), rearranged L-Myc fusion (Rlf), and C21orf91 were repeatedly isolated. To test whether the interaction between Fbx117 and its prey was dependent on its LRRs, three LRRs (Δ3LRR) were deleted from the bait plasmid. Although this truncation did not affect Fbx117 expression (Fig. S3B), none of the yeast co-transformed with the Δ3LRR bait plasmid and the various prey grew under the selective conditions requiring a bait-prey interaction. These results indicated Fbx117 interaction with its prey was dependent on its three C-terminal LRRs (Fig. S3A).

Fbx117 interacts with Uap1, Ufc1, Khlh12 and Csnk2B in human cells in vivo

To validate the yeast two-hybrid results, we tested Uap1, Ufc1, Csnk2B and Khlh12 for their interaction with Fbx117 in human cells, using co-immunoprecipitation assays. All four proteins tested were detected in immunoprecipitates of FLAG-tagged Fbx117 (Fig. 3a–d). We noted truncation of LRRs resulted in increased expression of mutant Fbx117 (Fig. 2b–d). Despite their enhanced expression, Khlh12 did not interact with either the Δ3LRR or Δ10LRR mutants, indicating its interaction with Fbx117 was dependent on the LRRs (Fig. 3a). Uap1 and Ufc1 both co-immunoprecipitated with WT and Δ3LRR Fbx117, but truncation of 10 LRRs ablated their interaction (Fig. 3b, c). Uap1 was also present in immunoprecipitates of the mutant FLAG-Fbx117ΔFbox indicating that Uap1 binding is dependent on LRR2-8 in Fbx117 (Fig. S3C). In contrast to the other partner proteins, HA-Csnk2B co-immunoprecipitated roughly equivalently with WT, Δ3LRR, and Δ10LRR constructs, suggesting that their interaction does not rely on the LRRs and thus may interact via the FBD or N-terminus of Fbx117 in human cells (Fig. 3d).

The diminished interactions of truncated Fbx117 with some of its binding partners could be caused by a change in its subcellular distribution. Cellular fractionation and immunofluorescence assays were conducted in parallel to determine the distribution of the WT and mutant proteins in cells. Endogenous Fbx117 was present in both cytoplasmic and nuclear fractions (Figs. S3D, S4A). Immunofluorescence showed all transfected Fbx117 constructs showed a predominantly nuclear localisation and also weaker cytoplasmic staining (Fig. S4A). This argues against an altered localisation preventing the mutant forms from interacting with its binding partners.

In sum, these data validate results from the yeast two-hybrid screen since the binding partners identified also interact in human cells with the full length Fbx117 protein.

Table 1 Fbxl17 interacting proteins

Gene symbol	Full name	isolates	Minimal region (aa)	Full-length size (aa)	Modified
<i>UAP1</i>	UDP- <i>N</i> -acetylglucosamine pyrophosphorylase 1	26	357–505	505	Ub
<i>UFC1</i>	Ubiquitin-fold modifier conjugating enzyme 1	13	12–95	167	Ub
<i>CSNK2B</i>	Casein kinase 2, beta polypeptide	4	1–123	215	Ub
<i>KLHL12</i>	Kelch-like 12 (<i>Drosophila</i>)	4	1–162	568	
<i>RLF</i>	Rearranged L-myc fusion	4	1670–1914	1914	
<i>C21orf91</i>	EURL/Chromosome 21 open reading frame 91	4	1–178	296	
<i>ACSBG2</i>	Acyl-CoA synthetase bubblegum family member 2	3	528–666	666	
<i>ETFA</i>	Electron-transfer-flavoprotein, alpha polypeptide	3	103–284	333	Ub
<i>METAP2</i>	Methionyl aminopeptidase 2	3	323–342	478	Ub
<i>AKD1</i>	Adenylate kinase domain containing 1	2	415–624	1911	
<i>SCG5</i>	Secretogranin V (7B2 protein)	2	1–188	212	
<i>TASP1</i>	Taspase, threonine aspartase, 1	2	135–318	420	
<i>KLHL7</i>	Kelch-like 7 (<i>Drosophila</i>)	2	37–240	586	Ub
<i>PHF7</i>	PHD finger protein 7	1	50–236	381	
<i>ZMYM2</i>	Zinc finger, MYM-type 2	1	141–390	1377	
<i>IDO1</i>	Indoleamine 2,3-dioxygenase 1	1	14–128	403	
<i>PSME4</i>	Proteasome (prosome, macropain) activator subunit 4	1	367–420	1843	Ub
<i>PPP3CB</i>	Protein phosphatase 3, catalytic subunit, beta isozyme	1	381–496	524	Ub
<i>ZNF350</i>	Zinc finger protein 350	1	310–532	532	
<i>TGFBI</i>	Transforming growth factor, beta-induced, 68 kDa	1	115–326	683	
<i>SCPEP1</i>	Serine carboxypeptidase 1	1	273–452	452	Ub
<i>FILIP1L</i>	Filamin A interacting protein 1-like	1	508–705	1135	
<i>ACPL2</i>	Acid phosphatase-like 2	1	266–464	480	
<i>TPP2</i>	Tripeptidyl peptidase II	1	879–1141	1249	Ub
<i>OLR1</i>	Oxidized low density lipoprotein (lectin-like) receptor 1	1	124–273	273	
<i>USP25</i>	Ubiquitin specific peptidase 25	1	323–450	1055	Ub
<i>FAM190A</i>	Family with sequence similarity 190, member A	1	555–726	900	
<i>PCCB</i>	Propionyl CoA carboxylase, beta polypeptide	1	172–468	539	
<i>TMOD1</i>	Tropomodulin 1	1	66–334	359	
<i>IFT46</i>	Intraflagellar transport 46 homolog (<i>Chlamydomonas</i>)	1	1–216	304	
<i>SRBD1</i>	S1 RNA binding domain 1	1	260–491	995	
<i>MED14</i>	Mediator complex subunit 14	1	1053–1282	1454	Ub
<i>CCDC147</i>	Coiled-coil domain containing 147	1	478–684	872	
<i>HADH</i>	Hydroxyacyl-CoA dehydrogenase	1	112–261	261	Ub
<i>CLPX</i>	ClpX caseinolytic peptidase × homolog (<i>E. coli</i>)	1	42–341	633	
<i>COG2</i>	Component of oligomeric golgi complex 2	1	457–534	738	Ub
<i>TMEM126A</i>	Transmembrane protein 126A	1	89–195	195	Ub

Minimal region denotes the amino acids present in all interacting cDNA clones; full-length size is the predicted size of the protein. Ub denotes protein is ubiquitinated in [39]

Furthermore, the association of Khl12, Ufc1, and Uap1 with Fbxl17 was dependent on its LRRs, as truncation of this region weakened or ablated their interaction.

To test the directness of the interaction between Fbxl17 and one of its interacting proteins, we performed a GST pull-down assay using Uap1. We tested GST-Fbxl17(321–701aa), GST-Fbxl17Δ10LRR(321–383aa), and GST-Skp2,

another LRR-containing FBP, and GST only were used as controls. GST-FBP proteins were co-expressed with an IRES-Skp1 to facilitate expression in bacteria, with the exception of Fbxl17Δ10LRR, which was robustly expressed. GST-FBPs were immobilised on a GST column and incubated with in vitro transcribed and translated Uap1. Following binding assays, samples were resolved by SDS-PAGE, and membranes probed with antibodies

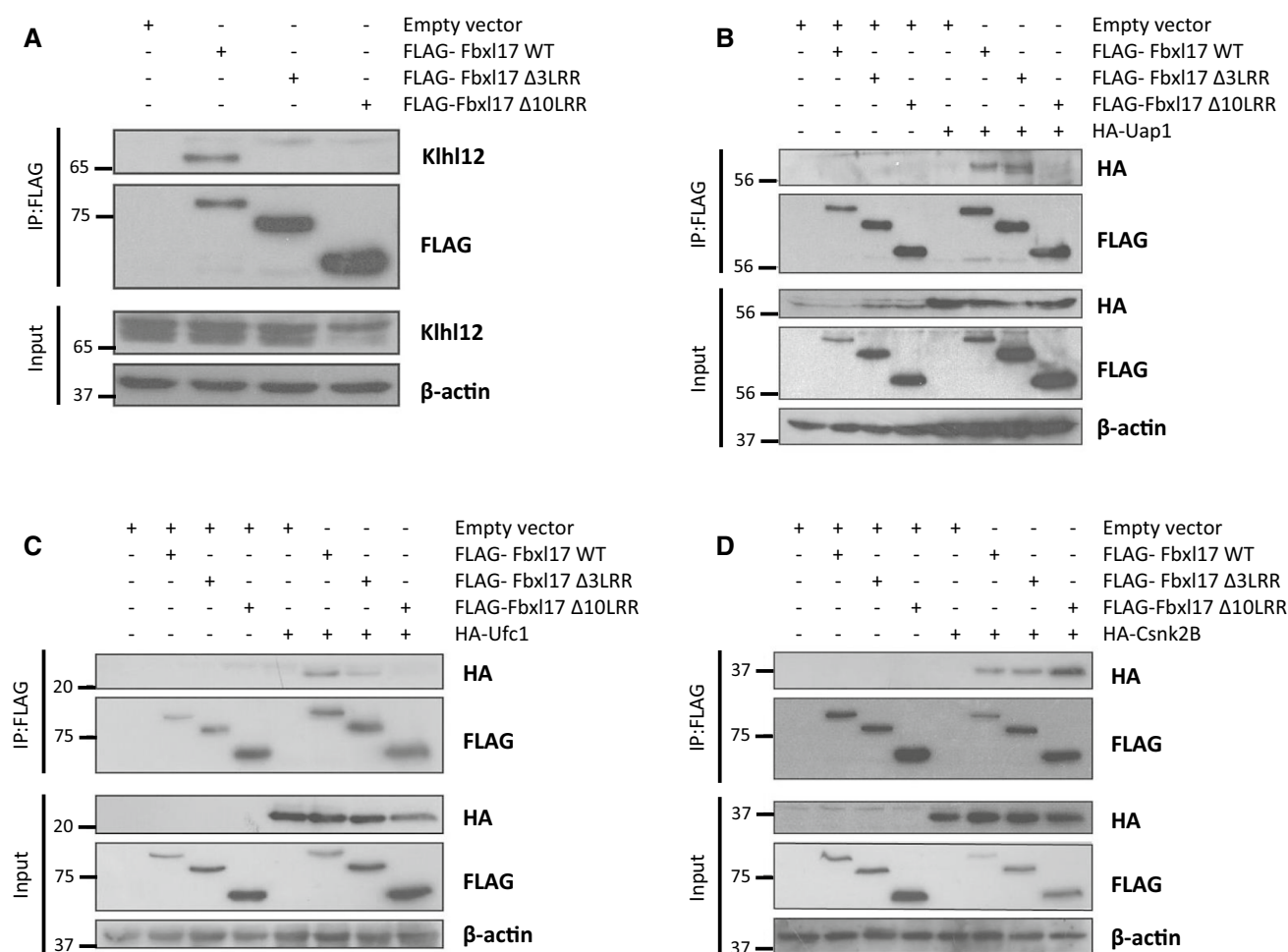


Fig. 3 Deletion of the LRRs of Fbx117 affects its binding to different proteins to different extents. **a** Immunoprecipitates; using anti-FLAG beads, of HEK293T cells expressing FLAG-Fbx117, FLAG-

Fbx117Δ3LRR or FLAG-Fbx117Δ10LRR, probed for endogenous Khl12. **b–d** As (**a**), but with co-expression of exogenous HA-tagged Uap1 (**b**), Ufc1 (**c**), or Csnk2B (**d**) and probed with anti-HA antibody

to Uap1. We observed Uap1 binding specifically to GST-Fbx117(321–701aa), but not to GST only or to GST-Skp2. Moreover, deletion of 10 LRRs abolished Uap1 binding to Fbx117 (Fig. 4a). These results indicate Fbx117 interacts directly with Uap1, and this occurs via its LRRs.

Fbx117 inhibits the phosphorylation of Uap1

To test the functional significance of Fbx117 interaction with Uap1, we over-expressed Fbx117 and monitored the steady state levels of Uap1 by immunoblotting. We found Uap1 levels were unchanged in the presence of MG132 or with increased levels of Fbx117 (Fig. 4b), which suggests it does not promote the proteasomal degradation of Uap1. We next tested whether Uap1 was a substrate of SCF^{Fbx117} ligase in vivo, by co-transfecting cells with HA-Uap1, Myc-ubiquitin, and FLAG-Fbx117 (WT or ΔF-box domain) constructs. However, we found no evidence of laddering or smearing

of Uap1, indicative of its poly-ubiquitination. Instead, we detected a discrete, higher molecular weight species of Uap1 upon transfection of Myc-ubiquitin (Fig. 4c, lane 2). Moreover, levels of this modified form of Uap1 were reduced when Fbx117 was overexpressed (Fig. 4c, lane 5), indicating Fbx117 opposed this modification of Uap1. Interestingly, this reduction of Uap1 modification was not observed when Fbx117ΔFbox was overexpressed, (Fig. 4c, lane 6) suggesting this effect was dependent on Skp1 binding and/or the ligase activity of Fbx117.

To determine the type of modification this higher molecular weight species of Uap1 represented, we immunoblotted with antibodies to ubiquitin and to Myc-epitope tag (Myc-ubiquitin). Surprisingly, these antibodies did not yield any signal in Uap1 immunoprecipitates, despite the overexpression of ubiquitin (S2C and S2D). These results indicated that the post-translational modification present on Uap1 was not ubiquitination. Based on the PhosphoSitePlus database,

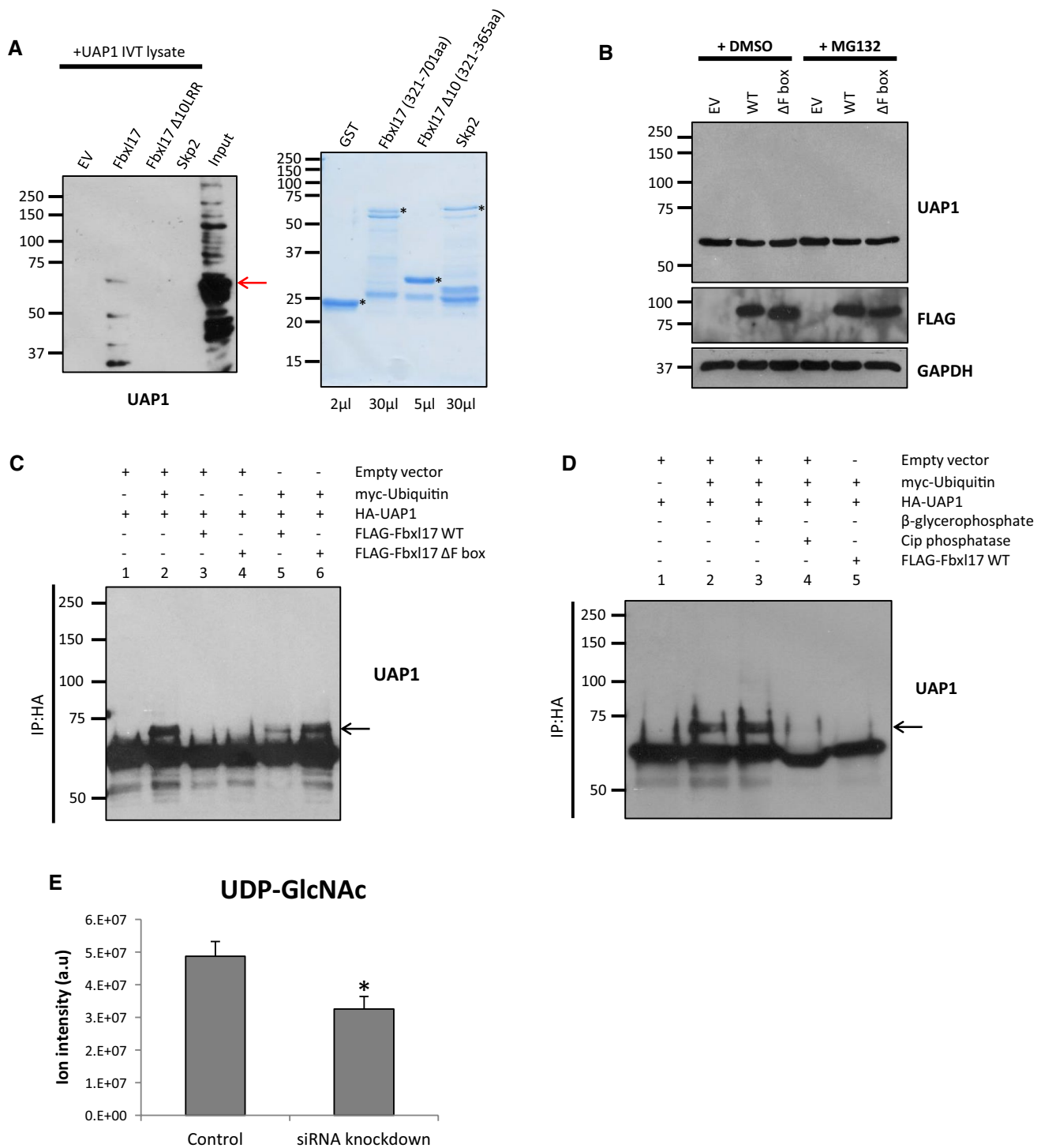


Fig. 4 Fbxl17 inhibits the phosphorylation of UAP1. **a** In vitro GST pull-down assay using bacterially expressed and purified Fbxl17 constructs or Skp2/GST as controls immobilised on a GST column incubated with rabbit reticulocyte lysate (left panel). Fbxl17(321-701aa) and Skp2 constructs contained an IRES_Skp1 to aid expression. Input for rabbit reticulocyte lysate=20%. Coomassie staining of GST proteins, volume of sample loaded indicated below lanes (right panel) * indicates bands relating to expressed proteins, arrow represents Uap1, $n=2$. **b** HEK293T cells transfected with Fbxl17WT, Δ Fbox or empty vector (EV) for 48 h then treated with 10 μ M MG132 or DMSO for

4 h. Whole cell lysates immunoblotted with the indicated antibodies, $n=3$. **c** In vivo ubiquitination assay for UAP1. HA-UAP1 immunoprecipitated from HEK293T cells transfected with ubiquitin and indicated Fbxl17 constructs. Membranes probed with anti-UAP1 antibody, arrow indicates modified Uap1, $n=3$. **d** In vivo ubiquitination assay for UAP1 as in **c** in the presence of β -glycerophosphate (lane 3) and alkaline phosphatase (CIP) (lane 4), $n=2$. **e** LC-MS analysis of total UDP-GlcNAc levels in U2OS cells treated with Fbxl17 siRNA3 or control siRNA for 48 h. Mean \pm SEM for five biological replicates, $*p<0.05$

where multiple studies report Uap1 to be a phosphorylated protein, we tested whether this modified form of Uap1 represented a phosphorylated form. We conducted the *in vivo* ubiquitination assay in the presence of the phosphatase inhibitor β -glycerophosphate and alkaline phosphatase (CIP). Strikingly, the levels of modified Uap1 were almost completely absent following CIP treatment, suggesting the higher molecular weight species represented a phosphorylated form of Uap1 (Fig. 4d, lane 4). In sum, these data show that the overexpression of ubiquitin increases Uap1 phosphorylation, and Fbx17 overexpression prevents this modification, and this function is dependent on its FBD.

FBXL17 knockdown results in increased levels of O-GlcNAcylation

Since Fbx17 overexpression reduced the abundance of a phosphorylated Uap1, but not Uap1 steady state levels, we reasoned Fbx17 might regulate Uap1 activity. Uap1 catalyses the formation of UDP-*N*-acetylglucosamine (UDP-GlcNAc), which is used by the glycosyltransferase *O*-GlcNAc Transferase (OGT) to add *N*-acetylglucosamine in *O*-glycosidic linkages to nuclear and cytosolic proteins. UAP1 is the main enzyme synthesizing UDP-GlcNAc [30–34]. Since our results indicate Fbx17 opposes Uap1 phosphorylation, we tested whether reducing Fbx17 expression would affect the amount of UDP-GlcNAc in the cell. U2OS cells were transfected with an siRNA targeting Fbx17 (Fig. S4B), metabolites were extracted from these cells and UDP-GlcNAc levels were determined by mass spectrometry. We observed a 36% decrease ($p = 0.013$; $n = 5$) in total UDP-GlcNAc levels in Fbx17 knockdown cells (Fig. 4e), which suggests that Fbx17 promotes Uap1 activity.

To determine the downstream effects of Fbx17 on this pathway, we next tested the effect of reduced Fbx17 expression on the levels of *O*-GlcNAc modified cellular proteins. U2OS cells were treated with Fbx17 siRNA as above, and cell lysates were immunoblotted for *O*-GlcNAc. Although UDP-GlcNAc levels were reduced in Fbx17 KD cells (Fig. 4e), we observed increased levels of *O*-GlcNAc-modified proteins in Fbx17 knockdown cells (Fig. 5a). This was also shown in two breast cell lines, HB4a and MCF7, by expression of shRNA constructs targeting *FBXL17* expression (Figs. 5b, c; S4C). This increase in *O*-GlcNAc modified proteins, despite reduced levels of UDP-GlcNAc, may be a result of changes in the expression or activity of the enzymes responsible for adding or removing *O*-GlcNAc, namely Ogt and Oga, which act downstream of Uap1 and UDP-GlcNAc. We therefore determined whether Ogt and Oga were changed following knockdown of Fbx17. Although Ogt levels were unchanged, Oga levels were reduced which suggests the increased *O*-GlcNAcylated proteins is due to decreased Oga levels (Fig. 5d). Consistent with reduced Oga levels,

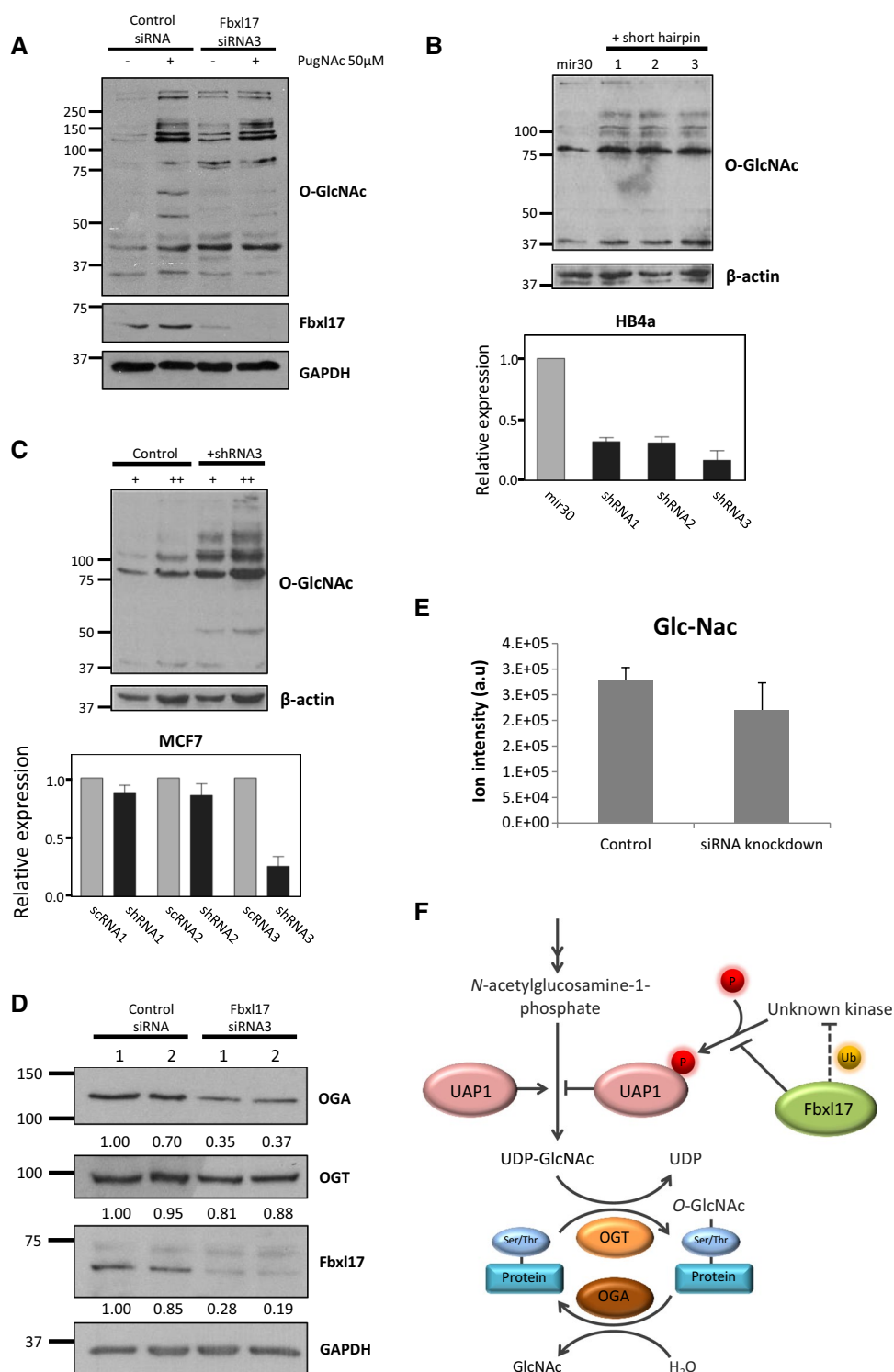
mass spectrometry analysis of levels of GlcNAc, the product of Oga-mediated cleavage of *O*-GlcNAc modifications from proteins, were reduced by 18%, although this was not significant, in cells treated with Fbx17 siRNA (Fig. 5e). Finally, we surveyed the expression of Fbx17 and Uap1 expression in breast cancer datasets using the R2 platform (<http://www.r2.amc.nl>). Kaplan–Meier analysis for these genes revealed that breast tumours with either low Fbx17 expression, or high Uap1 expression were associated with poorer survival in patients (Fig. S5).

Discussion

Our results collectively indicate that *FBXL17* is frequently mutated in epithelial cancers in the genomic regions encoding its LRRs. We found *FBXL17* was rearranged in around 7% of breast cancers according to array-CGH, and also in cancer cell lines. Independently, analysis of sequence-level mutation data also suggested that *FBXL17* behaves like a tumour suppressor gene [35]. Many point mutations and breaks in *FBXL17* occurred in regions encoding its LRRs. These motifs are proposed to be the substrate docking sites within FBXL proteins, and are predicted to cause a failure to recruit substrates. Indeed, we find that progressive deletion of its LRRs caused decreased auto-ubiquitination and ubiquitination of a substrate, Sufu, by SCF^{Fbx17}. However, we also discovered that deleting LRRs impaired the assembly of the E3 ubiquitin-ligase complex. Both of the Fbx17 LRR truncation mutants, $\Delta 3\text{LRR}$ and $\Delta 10\text{LRR}$, bound Skp1 less well compared to WT, despite them containing the Skp1 binding motif. Reduced interactions with Cul1 and Rbx1 are likely due to less Skp1 binding, since FBPs do not interact directly with Cul1 or Rbx1 [36]. The C-terminus of an FBP has been shown in specific cases to contact Skp1 to stabilise the ligase [36], and our data show that truncating the LRRs of Fbx17 also destabilises the SCF ligase. We predict that even if a truncated Fbx17 were able to recruit some of its substrates, it would be less efficient in ubiquitinating them. Thus in the context of breast cancer, the rearrangements that target the LRRs of *FBXL17* would likely diminish ubiquitination of the network of SCF^{Fbx17} substrates.

To investigate functional consequences of these rearrangements, we screened for proteins interacting with the LRR of Fbx17. Our yeast two-hybrid screen identified 37 novel interactions, which was found to only minimally overlap with previous studies reporting Fbx17 interacting proteins [37, 38]. Only eight proteins, Khlh12, Khlh17, Zmym2, Hadh, Clpx, Ppp3cb, Pccb, Srbd1 also appeared in these other studies. However, Uap1 and Ufc1, the most frequently recovered cDNAs in our screen, were not identified by either. The varied findings by different screening methodologies, indicates they identify distinct partner proteins

Fig. 5 Knockdown of Fbxl17 increases total *O*-GlcNAcylation. **a** U2OS cells treated with Fbxl17 siRNA3 or control siRNA for 48 h followed by PugNAc treatment, 50 μ M 3 h. Whole cell lysates immunoblotted with the indicated antibodies, $n=2$. **b** *FBXL17* mRNA knockdown by shRNA in HB4a immortalised normal breast cells (bottom panel). Expression normalised to GAPDH and plotted relative to miR30-infected control cells. Mean \pm SEM of at least three independent experiments. *O*-GlcNAcylation monitored by immunoblotting with anti-*O*-GlcNAc antibodies (top panel). **c** *FBXL17* mRNA knockdown by shRNA in MCF7 breast cancer cells (bottom panel). Expression normalised to scRNA-infected cells. Mean \pm SEM of at least three independent experiments. Total *O*-GlcNAcylation monitored by immunoblotting with anti-*O*-GlcNAc antibodies. + and ++, 25 or 50 μ g of protein lysate (top panel). **d** U2OS cells treated with Fbxl17 siRNA3 or control siRNA for 48 h. Whole cell lysates immunoblotted with the indicated antibodies. Band intensities quantified by densitometry and normalised to GAPDH expression (values below blots), $n=3$. **e** LC-MS analysis of total GlcNAc levels in U2OS cells treated with Fbxl17 siRNA3 or control siRNA for 48 h. Mean \pm SEM for five biological replicates. **f** Model of interaction between Fbxl17 and Uap1



and argues for a variety of experimental approaches to discovering protein interaction networks. Screens for interacting partners may identify substrates or regulators of FBPs. When validating four of the most repeatedly isolated prey cDNAs in mammalian cells, we noted differential binding (Csnk2B > Uap1 > Ufc1 > Klhl12) depending on the deletion

of 3 or 10 LRRs. Notably, the Casein Kinase 2 subunit, Csnk2B, remained bound to Fbxl17 after deletion of 10 LRRs, suggesting that it binds to another region of Fbxl17, or other E3 ubiquitin ligase components, and may be a regulator of the ligase. Among the other interactors, Fbxl17 binding to Klhl12 or Ufc1 was decreased when the last three

LRRs were truncated. However, Uap1 binding was disrupted only when ten LRRs were truncated suggesting Uap1 can bind to LRR2-8. These data led us to a model whereby the number of LRRs in Fbx117, as dictated by the position of a rearrangement within *FBXL17*, would influence its interaction with its repertoire of partners. However, due to inefficient ligase assembly by LRR-truncated Fbx117 mutants, we predict the ubiquitination of these proteins would be diminished. We note that 15 of the 37 proteins identified in the yeast two-hybrid screen are listed as being ubiquitinated proteins in a whole proteomic analysis of HEK293 cells (Table 1) [39].

There are not yet enough data on rearrangement of *FBXL17* in cancers to conclusively identify *FBXL17* inactivation as a driver mutation in cancer. Nonetheless, we were able to show a striking effect of reducing Fbx117 expression on at least one important cancer-relevant pathway, in a relevant cell type, suggesting that inactivation of Fbx117 would have a major effect on the cancer cell. This was through its regulation of Uap1, which is expressed in many breast cancers (Figs. S4D, S5D) and other cancer types [34, 40]. Surprisingly, we did not find Uap1 to be ubiquitinated by Fbx117, but instead our results showed that increased Fbx117 expression prevented the phosphorylation of Uap1. In addition, this inhibition of Uap1 phosphorylation was dependent on the Skp1-binding domain of Fbx117, suggesting that SCF^{Fbx117} ligase activity is essential. In contrast to Ogt and Oga [41], little is known about the regulation of Uap1, and our data suggest Fbx117 positively regulates its activity (Fig. 5f). UDP-GlcNAc levels are significantly decreased when Fbx117 is knocked down suggesting reduced Uap1 activity which is consistent with previous studies showing Uap1 expression is important for UDP-GlcNAc levels [34]. Although we have not identified the kinase responsible for phosphorylating Uap1, one possibility is that Fbx117 ubiquitinates this kinase to inhibit its phosphorylation of Uap1 and promote Uap1 activity. Alternatively, Fbx117 could shield Uap1 from this kinase, via a direct interaction between Fbx117 and Uap1 (Figs. 4a, 5f).

We have shown that Fbx117 regulates the *O*-GlcNAcylation pathway since reducing *FBXL17* expression in three cell lines increased global levels of *O*-GlcNAc-modified proteins. We did not assess glycosylation in the ER or Golgi, so cannot rule out a specific role for Fbx117 there. However, the increase in global *O*-GlcNAcylation may be the result of greater utilisation of UDP-GlcNAc by Ogt, which would explain the lower UDP-GlcNAc levels and higher *O*-GlcNAcylation we observed in Fbx117 knockdown cells. Although Ogt expression levels were unchanged, we cannot rule out that its activity is increased when Fbx117 levels are reduced. However, the higher levels of *O*-GlcNAc modified proteins are likely due to the observed decrease in Oga expression. It has been proposed that there is an optimal

level of global *O*-GlcNAcylation levels for cells to function and this is maintained by mutual regulation and balance of Ogt/Oga expression and activity [41, 42]. The decrease in Oga expression may represent a compensatory mechanism adopted by the cell to counteract the decrease in Uap1 activity and UDP-GlcNAc levels. *O*-GlcNAcylation is an important post-translational modification on many intracellular proteins—including p53, RNA polymerase II, the polycomb complex and Phosphofructokinase 1 (Pfk1), the main regulator of glycolysis—and is essential for viability of several mammalian cell types [43, 44]. Moreover, there is already considerable evidence that GlcNAcylation is altered in breast cancer and other cancers [45–48]. Caldwell et al. [49] found that breast cancer cells had increased *O*-GlcNAcylation and elevated OGT. Knocking down *OGT* inhibited tumour growth, decreased cell cycle progression, increased expression of the cell cycle inhibitor p27Kip1, and decreased invasiveness [49]. High nuclear and cytoplasmic *O*-GlcNAc was also observed in breast cancer patients with increased relapse rates, increased sites of distant metastases and poor outcome [50]. In breast cancer, low OGA levels are linked to higher grade tumours and metastasis [51]. We have shown that the regulation of Uap1 by Fbx117 and an unidentified kinase, are factors in determining the levels of the *O*-GlcNAcylated proteome.

In conclusion, by surveying structural rearrangements in cancer databases, we discovered rearrangements commonly occur in *FBXL17* which affect its ability to bind substrates and also assemble as part of a functional SCF ubiquitin ligase complex. By screening for Fbx117 interacting proteins, we discovered Uap1 as a binding partner, but not a substrate of Fbx117, and established that Fbx117 is a negative regulator of global *O*-linked GlcNAcylation. The loss-of-function mutations in *FBXL17* caused by structural rearrangements could have additional effects on the cell, since the targets of Fbx117 are involved in major, cancer-relevant cellular processes.

Materials and methods

Yeast two-hybrid assay

The matchmaker gold yeast two-hybrid system (Clontech) was used to screen a human cDNA library (Mate & Plate™ Library—Normalized, Universal Human (Clontech)). Fbx117 aa 321 to 701 was PCR amplified and subcloned into pGBKT7 (Clontech). aa 321 to 586 was amplified from pGBKT7-FBXL17 plasmid and subcloned into pGBKT7 to create the (Δ3LRR) bait construct.

Purification of SCF^{Fbxl17} complexes

HEK293T cells were transfected with SCF components (Skp1, Cul1, Myc-Rbx1) and FLAG-Fbxl17 constructs. After 48 h, cells were resuspended in lysis buffer (LB) (25 mM Tris-HCl, pH 7.5, 225 mM KCl, 1% NP-40) with a protease inhibitor cocktail (Sigma-Aldrich) and phosphatase inhibitors (10 mM NaF, 1 mM PMSF, 1 mM Na₃VO₄). Lysates were incubated with Anti-FLAG[®] M2 Affinity Gel (Sigma-Aldrich) for 5 h at 4 °C with rotation. Beads were washed in LB and eluted in 300 µg/mL FLAG peptide (Sigma-Aldrich) in elution buffer (10 mM HEPES, pH 7.9, 225 mM KCl, 1.5 mM MgCl₂, 0.1% NP-40) for 1 h at 4 °C with rotation. Purified SCF complexes were stored in 15% glycerol.

In vitro ubiquitination assays

A screen of 10 different E2 enzymes determined that E2 UbcH5a enabled the most specific SCF^{Fbxl17} activity and was used in subsequent experiments. Purified SCF complexes at 12.5, 25, 50 and 100 nM were tested in the presence of a ubiquitin-mix (ubiquitin buffer, ubiquitin (20 µM) E1 (UBE1, 100 nM), E2 (UbcH5a, 500 nM) and Mg-ATP (2 mM) (Boston Biochem)) incubated at 30 °C for 90 min to determine ligase activity by auto ubiquitination. 50 nM of the SCF was sufficient for ligase activity and used in subsequent experiments. To test substrate ubiquitination substrates were transfected into HEK293T cells and immunoprecipitated using their indicated epitope tags conjugated to agarose beads. The purified substrate was then eluted from the beads and added as a component of the ubiquitin-mix. HA-Sufu was kindly provided by Vincenzo D'Angiolella (CRUK/MRC Oxford Institute for Radiation Oncology, Oxford, UK). Ubiquitination was detected by probing for the substrate or HA tag.

In vivo ubiquitination assays

HEK293T cells were transfected with expression constructs of interest, including myc-ubiquitin, and treated with 10 µM MG132 (Sigma-Aldrich) 5 h prior to lysis. UAP1 was then immunoprecipitated with Monoclonal Anti-HA-Agarose antibody (Sigma-Aldrich). Modified UAP1 was detected with an endogenous UAP1 antibody. To test for phosphorylation 10 mM β-glycerophosphate or alkaline phosphatase (CIP) was added to the LB where indicated. LB containing CIP did not contain phosphatase inhibitors (NaF, Na₃VO₄).

DNA constructs

Coordinates and exon numbers for the *FBXL17* gene are from Ensembl transcript ENST00000542267.5 (Fig. 1).

Human *FBXL17* cDNA (GenScript) was subcloned into pcDNA3 and pcDNA3-FLAG. Truncation (Δ3LRR) and (Δ10LRR) and deletion constructs (ΔFbox) were constructed by amplification or two-step PCR mutagenesis. Human Ufc1 and Uap1 cDNAs were obtained from GeneArt. pcDNA3.1-FLAG-hKLHL12 was kindly provided by S. Angers (University of Toronto, Canada). pCK2_V2N1_Venus2-HA-CSNK2B_N1 was kindly provided by A. Beck-Sickinger (Leipzig University, Germany).

Antibodies

The following antibodies were purchased anti-β-actin (Abcam, ab8227), anti-Cul1 (Santa Cruz, sc-11384), anti-Fbxl17 (Genetex, GTX119211), anti-FLAG[®] M2 (Sigma-Aldrich, F3165), anti-Gal4 DBD (Santa Cruz, sc-510), anti-GAPDH (Sigma, G9545), anti-HA (Abcam, ab9110), anti-HA (C29F4) (Cell Signalling, 3724S), anti-Histone H1 (Santa Cruz, sc-8030), anti-Klhl12 (Abcam, ab14233), anti-myc tag (Cell Signalling, 2272), anti-*O*-GlcNAc (Covance, MMS-248R), anti-p19 (Skp1) (BD Biosciences, 610530), anti-UAP1 (Abcam, ab95949), anti-Ub (Santa Cruz, sc-8017), HRP-conjugated antibodies to mouse or rabbit IgG (Santa Cruz Biotechnology, sc-2055, sc-2313) or chicken IgY (Abcam, ab97135), Donkey anti-Rabbit and anti-Mouse IgG conjugated to Alexa Fluor 488 (Invitrogen). Signal detection was by enhanced chemiluminescence (ECL) (GE Healthcare).

Cell culture, plasmids and transfection

HB4a is an immortalised normal breast epithelial cell line from M.J. O'Hare [52]. Cell lines were maintained in DMEM supplemented with 10% foetal bovine serum (ThermoFisher), 2 mM glutamine, 100 U/mL penicillin and streptomycin at 37 °C in a humidified 5% CO₂ atmosphere. Where indicated, cells were treated with (50 µM) PugNAc, an inhibitor of *O*-GlcNAc-β-*N*-acetylglucosaminidase (Oga), for 3 h prior to cell lysis.

Immunoblotting and immunoprecipitation analysis

Cells were lysed in protein extraction buffer (20 mM Tris-HCl pH 7.4, 1% IGEPAL, 1% Triton X-100, 50 mM NaCl, 2 mM EDTA pH 8, 30 mM NaP₂O₇ and protease inhibitor cocktail (Roche)). For the analysis of *O*-GlcNAcylated proteins, cells were lysed in RIPA buffer plus protease inhibitors.

For immunoprecipitation (IP) experiments, cells were lysed in hypotonic lysis buffer (10 mM Tris-HCl pH 7.5, 10 mM NaCl, 2 mM EDTA, 0.5% Triton X-100 and protease

inhibitors) and immunoprecipitated with agarose-anti-HA (Sigma) or agarose-anti-FLAG (Anti-FLAG[®] M2 Affinity Gel, Sigma-Aldrich) for 3.5 h. Beads were pelleted and washed four times in 1×NET2 wash buffer (50 mM Tris-HCl pH7.5, 150 mM NaCl, 0.05% Triton X-100). Bound proteins were eluted by addition of 40 µL 2×Laemmli sample buffer and incubation at 60 °C for 3 min.

siRNA and shRNA expression

siRNAs were purchased from Eurofins genomics and transfected at a final concentration of ~60 nM using Lipofectamine[™] RNAiMAX (ThermoFisher). Sequences for the siRNAs were as follows:

siRNA2: GCAGAGAACTCAAAGATAT
siRNA3: GGACAACTCACTGATGAA

4×10⁶ ψNx cells were calcium phosphate transfected with shRNA or scRNA retroviral expression constructs with 25 µM chloroquine (Sigma-Aldrich). 2 days post-transfection, 2×10⁶ of target cells were infected with retroviruses in the presence of polybrene (Sigma-Aldrich).

Sequences for the shRNAs were as follows:

shRNA 1: GGACAACTCACTGATGAAGG (targets exon 3 of *FBXL17*);
shRNA 2: GCTTGGACCTACGTCATATCA (targets exon 6 of *FBXL17*);
shRNA 3: AGGCATGATCGTCATAGCTAA (targets exon 4 of *FBXL17*).

The following day, cells were selected using 1.7 µg/mL of puromycin. After selection, RNA was extracted, reverse transcribed and quantified by qPCR. Expression level was normalised to *GAPDH* expression and was plotted relative to the expression of *FBXL17* in the relevant control. Values represent mean ± SEM of at least three independent experiments.

Metabolites extraction and LC–MS analysis

Cells were washed three times with PBS prior the extraction and 1 ml of extraction buffer (50% LC–MS grade methanol and 30% acetonitrile, 20% ultrapure water) was added per 1×10⁶ cells. Cell were then incubated on dry ice for 15 min, collected, kept under vigorous shaking for 15 min at 4 °C, and left for 1 h incubation at 20 °C. Samples were centrifuged at 13,000 rpm and supernatants were transferred to autosampler vials for LC–MS analysis. To avoid bias due to machine drift and processed blindly, samples were randomized. Q Exactive mass spectrometer (Thermo Fisher Scientific) coupled to a Dionex U3000 UHPLC (Thermo Fisher

Scientific) system was used to perform the LC–MS analysis. Sequant ZIC-pHILIC column (150mm 3 2.1 mm) and guard column (20 mm 3 2.1 mm) (Merck Millipore) were utilized for the chromatographic separation and the column oven temperature was maintained at 40 °C. The mobile phase was composed of 20 mM ammonium carbonate and 0.1% ammonium hydroxide in water (solvent A), and acetonitrile (solvent B). The flow rate was set at 200 mL/min with the gradient was programmed as follows: initially stayed at 20% of A and 80% of B for 2 min, then subjected to a linear increase to 80% of A and decrease to 20% of B in 15 min. Both solvents were then brought back to initial condition and staid for 8 min. The mass spectrometer was operated in full MS and tSIM (targeted Single Ion Monitoring), in positive and negative mode. XCalibur Qual Browser and XCalibur Quan Browser software (Thermo Fisher Scientific) were used to acquire the spectra and analyse the data.

Quantitative PCR

All qPCR reactions were performed in triplicates using LightCycler[®] 480 SYBR Green Master Mix (Roche) according to manufacturer's instructions. The relative expression ratio of a target gene in comparison to a reference gene in a cDNA panel was quantified [53]. *GAPDH* was used as an endogenous housekeeping transcript. The relative expression level was based on the difference in Ct values between a control cell line such as HB4a and a sample cell line in the cDNA panel.

Acknowledgements Funding was provided by Breast Cancer Now (2013NovPhD172) to BM and HL and PAWE, and Cancer Research UK (C1023/A14545 and C1023/A9140) to PAWE; SF was supported by a Wildy Studentship from Gonville & Caius College, and the Department of Pathology, University of Cambridge. FRT was funded by a BEPE-FAPESP fellowship (2012/09241-8). The Personalised Breast Cancer Program is funded by Addenbrookes Charitable Trust, the Mark Foundation and Cancer Research UK grants to CC and JEA. We thank the patients and staff of the Cambridge Breast Unit for providing and collecting tumours for sequencing. We also thank Christian Frezza, Efterpi Nikitopoulou and Laura Tronci for their LC–MS expertise.

Author contributions BM, SF, FRT, PAWE, and HL designed and conducted experiments, and interpreted results. RMG, OMR, JEA and CC provided and analysed genomics data. BM, PAWE and HL wrote the manuscript.

Open Access This article is distributed under the terms of the Creative Commons Attribution 4.0 International License (<http://creativecommons.org/licenses/by/4.0/>), which permits unrestricted use, distribution, and reproduction in any medium, provided you give appropriate credit to the original author(s) and the source, provide a link to the Creative Commons license, and indicate if changes were made.

References

- Edwards PA (2010) Fusion genes and chromosome translocations in the common epithelial cancers. *J Pathol* 220(2):244–254
- Pao W, Girard N (2011) New driver mutations in non-small-cell lung cancer. *Lancet Oncol* 12(2):175–180
- Bass AJ et al (2011) Genomic sequencing of colorectal adenocarcinomas identifies a recurrent VTI1A-TCF7L2 fusion. *Nat Genet* 43(10):964–968
- Banerji S et al (2012) Sequence analysis of mutations and translocations across breast cancer subtypes. *Nature* 486(7403):405–409
- Stephens PJ et al (2009) Complex landscapes of somatic rearrangement in human breast cancer genomes. *Nature* 462(7276):1005–1010
- Nik-Zainal S et al (2012) Mutational processes molding the genomes of 21 breast cancers. *Cell* 149(5):979–993
- Dulak AM et al (2013) Exome and whole-genome sequencing of esophageal adenocarcinoma identifies recurrent driver events and mutational complexity. *Nat Genet* 45(5):478–486
- Baca SC et al (2013) Punctuated evolution of prostate cancer genomes. *Cell* 153(3):666–677
- Curtis C et al (2012) The genomic and transcriptomic architecture of 2,000 breast tumours reveals novel subgroups. *Nature* 486(7403):346–352
- Robinson DR et al (2011) Functionally recurrent rearrangements of the MAST kinase and Notch gene families in breast cancer. *Nat Med* 17(12):1646–1651
- Skaar JR, Pagan JK, Pagano M (2013) Mechanisms and function of substrate recruitment by F-box proteins. *Nat Rev Mol Cell Biol* 14(6):369–381
- Hershko A, Ciechanover A (1998) The ubiquitin system. *Annu Rev Biochem* 67:425–479
- Wu S et al (2013) CAND1 controls in vivo dynamics of the cullin 1-RING ubiquitin ligase repertoire. *Nat Commun* 4:1642
- Pierce NW et al (2013) Cand1 promotes assembly of new SCF complexes through dynamic exchange of F box proteins. *Cell* 153(1):206–215
- Nelson DE, Randle SJ, Laman H (2013) Beyond ubiquitination: the atypical functions of Fbxo7 and other F-box proteins. *Open Biol* 3(10):130131
- Lipkowitz S, Weissman AM (2011) RINGs of good and evil: RING finger ubiquitin ligases at the crossroads of tumour suppression and oncogenesis. *Nat Rev Cancer* 11(9):629–643
- Randle SJ, Laman H (2016) F-box protein interactions with the hallmark pathways in cancer. *Semin Cancer Biol* 36:3–17
- Gstaiger M et al (2001) Skp2 is oncogenic and overexpressed in human cancers. *Proc Natl Acad Sci U S A* 98(9):5043–5048
- Frescas D, Pagano M (2008) Deregulated proteolysis by the F-box proteins SKP2 and beta-TrCP: tipping the scales of cancer. *Nat Rev Cancer* 8(6):438–449
- Carrano AC et al (1999) SKP2 is required for ubiquitin-mediated degradation of the CDK inhibitor p27. *Nat Cell Biol* 1(4):193–199
- Nakayama K et al (2000) Targeted disruption of Skp2 results in accumulation of cyclin E and p27(Kip1), polyploidy and centrosome overduplication. *EMBO J* 19(9):2069–2081
- Latres E et al (2001) Role of the F-box protein Skp2 in lymphomagenesis. *Proc Natl Acad Sci USA* 98(5):2515–2520
- Lin HK et al (2010) Skp2 targeting suppresses tumorigenesis by Arf-p53-independent cellular senescence. *Nature* 464(7287):374–379
- Akhoondi S et al (2007) FBXW7/hCDC4 is a general tumor suppressor in human cancer. *Cancer Res* 67(19):9006–9012
- Bignell GR et al (2010) Signatures of mutation and selection in the cancer genome. *Nature* 463(7283):893–898
- Schulte I et al (2012) Structural analysis of the genome of breast cancer cell line ZR-75-30 identifies twelve expressed fusion genes. *BMC Genomics* 13:719
- Dawson SJ et al (2013) A new genome-driven integrated classification of breast cancer and its implications. *EMBO J* 32(5):617–628
- Cerami E et al (2012) The cBio cancer genomics portal: an open platform for exploring multidimensional cancer genomics data. *Cancer Discov* 2(5):401–404
- Raducu M et al (2016) SCF (Fbxl17) ubiquitylation of Sufu regulates Hedgehog signaling and medulloblastoma development. *EMBO J* 35(13):1400–1416
- Haltiwanger RS, Holt GD, Hart GW (1990) Enzymatic addition of O-GlcNAc to nuclear and cytoplasmic proteins. Identification of a uridine diphospho-N-acetylglucosamine:peptide beta-N-acetylglucosaminyltransferase. *J Biol Chem* 265(5):2563–2568
- Szumilo T et al (1996) Purification to homogeneity and properties of UDP-GlcNAc (GalNAc) pyrophosphorylase. *J Biol Chem* 271(22):13147–13154
- Wang-Gillam A, Pastuszak I, Elbein AD (1998) A 17-amino acid insert changes UDP-N-acetylhexosamine pyrophosphorylase specificity from UDP-GalNAc to UDP-GlcNAc. *J Biol Chem* 273(42):27055–27057
- Kreppel LK, Hart GW (1999) Regulation of a cytosolic and nuclear O-GlcNAc transferase. Role of the tetratricopeptide repeats. *J Biol Chem* 274(45):32015–32022
- Ikonen HM et al (2015) UAP1 is overexpressed in prostate cancer and is protective against inhibitors of N-linked glycosylation. *Oncogene* 34(28):3744–3750
- Davoli T et al (2013) Cumulative haploinsufficiency and triplosensitivity drive aneuploidy patterns and shape the cancer genome. *Cell* 155(4):948–962
- Schulman BA et al (2000) Insights into SCF ubiquitin ligases from the structure of the Skp1-Skp2 complex. *Nature* 408(6810):381–386
- Tan MK et al (2013) Parallel SCF adaptor capture proteomics reveals a role for SCFFBXL17 in NRF2 activation via BACH1 repressor turnover. *Mol Cell* 52(1):9–24
- Mena EL et al (2018) Dimerization quality control ensures neuronal development and survival. *Science* 362:6411
- Wagner SA et al (2011) A proteome-wide, quantitative survey of in vivo ubiquitylation sites reveals widespread regulatory roles. *Mol Cell Proteomics* 10(10):M111.013284
- Gao S et al (2019) Reciprocal regulation between O-GlcNAcylation and β -catenin facilitates cell viability and inhibits apoptosis in liver cancer. *DNA Cell Biol* 38(4):286–296
- Ong Q, Han W, Yang X (2018) O-GlcNAc as an integrator of signaling pathways. *Front Endocrinol (Lausanne)* 9:599
- Yang X, Qian K (2017) Protein O-GlcNAcylation: emerging mechanisms and functions. *Nat Rev Mol Cell Biol* 18(7):452–465
- Hart GW, Housley MP, Slawson C (2007) Cycling of O-linked beta-N-acetylglucosamine on nucleocytoplasmic proteins. *Nature* 446(7139):1017–1022
- Gambetta MC, Oktaba K, Müller J (2009) Essential role of the glycosyltransferase xsc/Ogt in polycomb repression. *Science* 325(5936):93–96
- Netsirisawan P et al (2015) Proteomic analysis reveals aberrant O-GlcNAcylation of extracellular proteins from breast cancer cell secretion. *Cancer Genomics Proteomics* 12(4):201–209
- Ferrer CM et al (2014) O-GlcNAcylation regulates cancer metabolism and survival stress signaling via regulation of the HIF-1 pathway. *Mol Cell* 54(5):820–831

47. Sodi VL et al (2015) mTOR/MYC axis regulates O-GlcNAc transferase expression and O-GlcNAcylation in breast cancer. *Mol Cancer Res* 13(5):923–933
48. Huang X et al (2013) O-GlcNAcylation of cofilin promotes breast cancer cell invasion. *J Biol Chem* 288(51):36418–36425
49. Caldwell SA et al (2010) Nutrient sensor O-GlcNAc transferase regulates breast cancer tumorigenesis through targeting of the oncogenic transcription factor FoxM1. *Oncogene* 29(19):2831–2842
50. Tiainen S et al (2016) High extent of O-GlcNAcylation in breast cancer cells correlates with the levels of HAS enzymes, accumulation of hyaluronan, and poor outcome. *Breast Cancer Res Treat* 160(2):237–247
51. Krześlak A et al (2012) Gene expression of O-GlcNAc cycling enzymes in human breast cancers. *Clin Exp Med* 12(1):61–65
52. Stamps AC et al (1994) Analysis of proviral integration in human mammary epithelial cell lines immortalized by retroviral infection with a temperature-sensitive SV40 T-antigen construct. *Int J Cancer* 57(6):865–874
53. Pfaffl MW (2001) A new mathematical model for relative quantification in real-time RT-PCR. *Nucleic Acids Res* 29(9):e45

Publisher's Note Springer Nature remains neutral with regard to jurisdictional claims in published maps and institutional affiliations.